PRIFYSGOL ABERYSTWYTH UNIVERSITY

This summary sheet should be completed after you have read the guidance notes. The completed sheet should be submitted by you to your Department/School/Institute at the time of submission of your work and the supporting documentation.

Candidate's Surname/Family Name: *Souness*

Candidate's Forenames: *Colin James*

Candidate for the Degree of: *PhD*

Full title of thesis: *Distribution and character of mid-latitude glacier-like forms on Mars.*

Summary:

This thesis presents glacial geomorphological work undertaken on the planet Mars. This work was performed using remotely-sensed data, primarily from the Mars Reconnaissance Orbiter (MRO), to better understand 'glacier-like forms' (GLFs) which have been observed in Mars' mid-latitudes.

Up until now most of the work conducted in this field has been undertaken by geologists and non-glacial specialists. Therefore, the material contained within this volume represents one of the first sizeable contributions to the area made from a glacial standpoint.

Using satellite imagery (in conjunction with various image analysis and geographic information system packages) Mars' global population of GLFs was mapped, morphometrically characterised and analysed. These investigations provided insights into how GLFs formed, why they are found in their present-day locations and whether they continue to develop under present-day environmental conditions.

Overall, to quote the abstract of this thesis (page 1), we find that:

"GLFs, observed ubiquitously in Mars' mid-latitudes, are all composed of a similar material and were formed in a similar way, most likely under Earth-like 'mass-balance' conditions whereby ice accumulated at altitude and subsequently flowed, under its own weight, downhill and into an ablation zone where GLFs experienced net mass loss.

"it would appear that those GLFs that remain on Mars today are relict deposits that have survived where local conditions impair ablation, and that these residual GLFs appear currently to flow under the influence of local relief and gravity. From the examination of crevasse patterns it appears that this flow occurs under an englacial strain regime similar to that which commonly defines spatial flow patterns in terrestrial glaciers."

DECLARATION

This work has not previously been accepted in substance for any degree and is not being concurrently submitted in candidature for any degree.

Signed ..... (candidate)

Date .....

STATEMENT 1

This thesis is the result of my own investigations, except where otherwise stated.

Other sources are acknowledged by footnotes giving explicit references.
A bibliography is appended.

Signed ..... (candidate)

Date .....

STATEMENT 2

I hereby give consent for my thesis, if accepted, to be available for photocopying and for inter-library loan, and for the title and summary to be made available to outside organisations.

Signed ..... (candidate)

Date .....

Table of contents:

List of figures:

Preface to Chapter 2:

Chapter 2:

Chapter 3:

Chapter 4:

List of tables:

Chapter 3:

Chapter 4:

Abstract

Mars' mid-latitudes host a range of apparently flow-related landforms that strongly resemble terrestrial glaciers. Such 'glacier-like forms' (GLFs) are strikingly similar to alpine valley glaciers found on Earth. These martian GLFs are believed to be composed of massive water ice but little is known about how they formed, how they evolve, and how they interact with the martian surface. This thesis presents various studies of Mars' mid-latitude GLFs that were designed to address some of these issues. New observations and new results were obtained using survey and mapping techniques.

The findings presented in this thesis suggest that GLFs, observed ubiquitously in Mars' mid-latitudes, are all composed of a similar material and were formed in a similar way, most likely under Earth-like 'mass-balance' conditions whereby ice accumulated at altitude and subsequently flowed, under its own weight, downhill and into an ablation zone where GLFs experienced net mass loss. It is likely these conditions existed on Mars during a past martian ice age.

From their geographical distribution (relative to latitude, elevation and relief) it would appear that those GLFs that remain on Mars today are relict deposits that have survived where local conditions impair ablation, and that these residual GLFs appear currently to flow under the influence of local relief and gravity. From the examination of crevasse patterns it appears that this flow occurs under an englacial strain regime similar to that which commonly defines spatial flow patterns in terrestrial glaciers. This thesis also observes and identifies various small-scale features and textures that suggest that the evolution and subsequent flow of GLFs has been (or may currently be) sensitive to many environmental factors common on Earth, such as the agency of liquid water. This suggests that GLFs (and possibly other associated ice masses) may have been significant movers and shapers of Mars' surface sediments and structures, contributing widely to the evolution of Mars' present-day surface.

Acknowledgements:

The author would like to acknowledge the support of various bodies and individuals whom have contributed either financial assistance or personal and professional support over the course of this research undertaking.

Thanks go to the National Environmental Research Council for funding the author throughout the duration of the project. Also, we acknowledge contributions which were made to help cover fieldwork costs by The Mount Everest Foundation and the Earth and Space Foundation. Equipment support was accepted from DMM Climbing Wales and Kahtoola crampon manufacturers.

Acknowledgement is due to The California Institute of Technology in Pasadena, CA, and the University of Notre Dame in South Bend, IN, who hosted the candidate for research training in November 2009 and March 2011 respectively.

Many thanks go to Professor Bryn Hubbard (Aberystwyth University) and Dr Duncan Quincey (Leeds University) who provided seemingly inexhaustible professional support to the author throughout this project. Also, thanks go to Professors Neil Glasser (Aberystwyth University), Mike Hambrey (Aberystwyth University) and Ralph Milliken (Brown University) for their advice on project-related matters, and to Dr Alun Hubbard (Aberystwyth University) for the loan of essential fieldwork equipment.

On a personal note, I would like to thank my family, friends and girlfriend for supporting me during what has (at times) been a very demanding undertaking, and also Dr Daniel Clewley and Mr Andrew Fitzpatrick for being great office-mates over the last 3 years.

Colin Souness

Introduction

Large deposits of H_2O ice exist in the near-surface layers of Mars' mid-latitudes (e.g. Forget et al., 2006; Dundas and Byrne, 2010). Many of the ice masses visible in these regions today appear to have undergone some amount of viscous flow or local deformation. In many cases, these 'viscous flow features' (VFFs) strongly resemble glaciers found on Earth. However, little is known about how these VFFs formed or how they have evolved since their initial deposition.

Research published on Mars' ice masses to date has been undertaken primarily by geologists and planetary scientists; very few studies have been attempted by trained glaciologists or glacial geomorphologists. A niche therefore exists for research conducted from a glaciological standpoint. Certain details and nuances of martian glaciation, details which could easily be overlooked by specialists from other disciplines but which may, nonetheless have great significance for our understanding of Mars' cryosphere, may be picked up in work conducted from a glaciological perspective. The work contained within this thesis aims to provide that perspective.

It seems that Mars' mid-latitude H_2O ice is all that remains of what may once have been a much larger body of ice that existed during a geologically recent martian ice age (e.g. Head et al., 2003; Forget et al., 2006). Now only residual deposits remain, some of which, as discussed, strongly resemble terrestrial glaciers. Their existence poses several interesting questions about Mars' recent geological and geomorphological history. The work contained within this thesis seeks answers to these questions predominantly by studying a specific type of martian H_2O ice flow which has been described as a 'glacier-like form', or GLF (e.g. Hubbard et al., 2011; Souness et al., 2012). These GLFs are, amongst the suite of icy VFFs identified in the literature, the sub-class which bears the closest similarity to terrestrial glaciers. Thus, by identifying and studying GLFs we isolate a population of features that maximises the applicability and value of the terrestrial glacier analogue as a tool in better understanding the cryospheric processes that currently operate on Mars.

We perceive the most pressing questions surrounding the existence of martian GLFs as follows:

1: Mars' present-day climate prohibits the accumulation of water ice at the surface everywhere out-with the polar regions. Therefore, conditions must have been markedly different in the recent geological past in order for these GLFs to have developed. Massive changes have occurred in Mars' climate. Therefore, we ask, what factors are responsible for the present-day distribution of glacier-like forms on Mars and what can these forms tell us about the nature of Mars' geologically recent climate and the ways in which it has changed over time?

2: Liquid water has not been observed on Mars' contemporary surface. Extensive evidence has, however, been documented which suggests that liquid water has been a major contributor to Mars' surface development in the past, particularly during Mars' early 'Noachian' geological epoch but also, perhaps, during the more recent 'Amazonian' epoch. If Mars' cryospheric landscapes have been active in recent geological time then liquid water may have been present. This could be important to any life that has ever existed on Mars, or to any life that we may hope to establish there in the future. Therefore, we ask: what role has (or does) liquid water played in the recent glacial history of Mars?

3: Glaciation and cryospheric processes have been (and continue to be) an extremely important factor contributing to the evolution of the Earth's surface. Glaciations would appear to have been (or perhaps *be*) an active process on Mars, therefore the possibility exists that ice has played an equally important role in the shaping of Mars' surface. Very little evidence has, however, been uncovered to quantify this contribution or to constrain the mechanisms by which ice has altered Mars' surface. This thesis investigates the mode and mechanisms of geologically recent glaciation on Mars in order to better understand how and to what extent flowing ice has shaped Mars' contemporary surface.

This thesis consists of an introduction (this section), 4 results chapters, a discussion chapter (Chapter 5), recommendations for further work (Chapter 6) and a chapter for conclusions and final comments (Chapter 7). All 4 results chapters (chapters 1-4)

constitute original research and are presented as separate papers. These papers have been formatted for inclusion in this thesis and are preceded in each case by a preface which outlines the over-arching motivation behind each chapter and specifically addresses how the material in each fits into the methodological and scientific framework of the thesis as a whole. This framework is arranged as follows:

After performing a detailed review of the related literature published to date (Chapter 1) we utilise recently acquired satellite imagery from the Mars Reconnaissance Orbiter (MRO), the JMars martian GIS package provided online by Arizona State University, image analysis software such as ITT ENVI and GIS platforms such as ESRI's ArcMap, to conduct a detailed population-wide survey of glacier-like form distribution, morphometry and geographical context (Chapter 2). This survey provides insights into the population-scale origins of glacier-like forms and the mechanisms responsible for their observed emplacement and geologically recent flow. Subsequent detailed inspection of glacier-like forms, informed by observations of texture, morphology and landscape association (made and recorded during the initial survey) led to the identification of crevasse fields. In Chapter 3 we examine these crevasse fields and compare them to their terrestrial counterparts in an effort to better understand the flow regimes which shape Mars' glacier-like forms. Finally, in Chapter 4 we look at VFF flow at a catchment scale and bring the cumulative experience and results from previous chapters to bear on a particular issue within the literature, testing an established hypothesis relating to the interpretation of a specific landform in the Protonilus Mensae / Coloe Fossae area of Mars' northern mid latitudes. Simultaneously, we evaluate the current state of our collective knowledge of ice flow characteristics on Mars. Chapter 5 provides an overview and discussion of what has been gained through the studies presented in chapters 1-4, examining how this thesis has contributed to science, before Chapter 6 looks at further work that could be done and Chapter 7 presents conclusions and final comments.

During the course of this research project, contributions were also made to work carried out by other affiliated parties. These contributions included data, analyses and figures from the paper by Hubbard et al. (2011), published in *Icarus*. This paper, on which the author of this thesis is duly featured, is attached in Appendix 1.

A. Preface to Chapter 1

A1. Introduction to Chapter 1

The planetary sciences as a whole and, specifically, investigations into the nature of Mars' surface evolution, have traditionally been the territory of geologists, physicists and planetary geophysicists. Literature on the subject of martian surface processes contributed from the physical geography community has been sparse. In particular, there has been a paucity of published material relating to Mars' varied glacial-type landforms from a 'traditional' glaciological or geomorphological stand-point.

This potentially means that although extensive work has already been done characterising the distribution, appearance, morphometry and viable mechanics of Mars' various H_2O ice-related landforms, no definitive analogue-based comparisons have yet been made of Mars' ice masses to those on Earth. Consequently, the extensive (and ever-growing) pool of knowledge and archived material relating to Earth-based glaciation, and the existing skills-base offered by trained and experienced glaciologists and geomorphologists, have not yet been fully utilised. There is therefore great potential to bring new expertise to bear on existing martian problems.

Chapter 1 of this thesis is designed to provide a review of martian glaciological literature as it existed in the early and 'design' stages of this research. It is structured to provide geological context for Mars' recent glaciations and thereafter to describe the range of cryospheric landforms found in Mars' mid-latitudes, finally highlighting key areas where our understanding of the underlying processes is still limited and where researchers with a glacial geomorphological background might best contribute to ongoing international research efforts.

Chapter 1 of this thesis has now been published as a review paper in *Progress in Physical Geography* (Souness and Hubbard, 2012). As such, it is strictly a review, and does not give detailed descriptions of many of the fundamental issues associated with Earth-analogue-based extra-terrestrial geomorphological studies, or

the sensors and Mars-orbital platforms used in the research contained within this thesis. Therefore, these details are included below in Sections A.2. and A.3. respectively.

A2. Challenges associated with extra-terrestrial geomorphological investigation

Ice, and thus glaciation, has made (and in many areas continues to make) an extremely important contribution to the evolution of Earth's surface. Therefore, it might seem natural to assume that if Mars has experienced one or more glacial periods in its recent geological past, the resulting ice masses will have left a strong geomorphological signature, potentially playing an important role in shaping Mars' contemporary surface. However, although Mars and Earth share many characteristics, such as a solid, rocky crust, an atmosphere, similar atmospheric circulation and wind patterns and even a similarly-timed diurnal cycle, certain differences in their respective structural and atmospheric compositions preclude the drawing of such direct parallels. For example, Mars' gravity is only 38% of Earth's (Howard, 2009), its atmosphere is only 0.6% the density of Earth's and drier than Earth's by a factor of ~1000, and the average atmospheric temperature on Mars is ~ -60º C (Read and Lewis, 2004) (see Table 1 for further key parameters). As a result, research into landform origins on planets other than our own face some problems, especially where the bulk of the available information is in the form of remotely sensed data and not from direct observation or sampling (sample return missions have, to date, been achieved only as far afield as the Moon). Many of these problems revolve around some of geomorphology's most basic scientific principles and the issue of how those basic principles can be applied to other planets. Can extra-terrestrial landscapes always be interpreted within the context of terrestrial knowledge?

All processes in geomorphology operate within a context determined by several basic parameters. These parameters are often known as boundary or base conditions and include environmentally fundamental factors such as local gravity, temperature and atmospheric density. Alterations to these base conditions can dramatically change the way in which processes occur, impacting heavily on rates of

Table 1: Key planetary and atmospheric parameters for Earth and Mars		
	Earth	Mars
Mean orbital radius (10^{11} m)	1.50	2.28
Distance from Sun (AU)	0.98-1.02	1.38-1.67
Orbital eccentricity	0.017	0.093
L_s of perihelion	281°	251°
Planetary obliquity	23.93°	25.19°
Rotation rate, Ω (10^{-5} s^{-1})	7.294	7.088
Solar day, sol (s)	86,400	88,775
Year length (sol)	365.24	668.6
Year length (Earth days)	365.24	686.98
Equatorial radius (10^6 m)	6.378	3.396
Surface gravity, g (m s^{-2})	9.81	3.72
Surface pressure (Pa)	101,300	600 (variable)
Atmospheric constituents (molar ratio)	N_2 (77%)	CO_2 (95%)
	O_2 (21%)	N_2 (2.7%)
	H_2O (1%)	Ar (1.6%)
	Ar (0.9%)	O_2 (0.13%)
Bond Albedo	0.306	0.25
Equilibrium temperature, T_e (K)	256	210
Scale height, $H_p = RT_e/g$ (km)	7.5	10.8
Surface temperature (K)	230-315	140-300
Dry adiabatic lapse rate (K km^{-1})	9.8	4.5
Buoyancy frequency, N (10^{-2} s^{-1})	1.1	0.6
Deformation radius, $L = NH_p / \Omega$ (km)	1100	920

Table 1: Adapted from Read and Lewis (2004). AU = astronomical units (where 1 AU = Earth's mean distance from the Sun), L_s = Areocentric longitude, sol = solar day, K = degrees Kelvin.

change, the scale on which changes occur and on the operation of many finer mechanical aspects of those changes.

As previously mentioned, gravity, temperature and atmospheric density all present striking differences between Earth and Mars. These factors combine to ensure that processes operate differently on Mars from on our own planet. For geomorphologists, this means that very often the processes and principles that we have studied, modelled and broadly understand on Earth cannot always be applied directly to Mars, or at least we must adjust our perceptions to accommodate vastly different, and sometimes unknown, boundary conditions. For example, although glaciers on Earth can flow and move as much as several metres per day in some areas, on Mars it is likely that icy landforms move at speeds as low as centimetres per thousands of years, or perhaps even slower. This is on account of low gravity, very low temperatures, and the very thin atmosphere (which leads to a very low likelihood of ice accumulating to thicknesses sufficient to initiate pronounced glacial flow). This makes it a very challenging task to understand how Mars' surface has developed, when the importance of moving ice, flowing water and even wind is so difficult to quantify. Due attention must therefore be paid to the effects of base conditions that are often hugely removed from our own.

A good example of how Mars' base conditions may have influenced glacial activity can be seen in the spacing of suspected formerly glacierized valleys around the edges of the Argyre and Hellas impact basins in Mars' southern hemisphere (see Figure 1 in Chapter 1 of this volume). Here, valleys are spaced 10 – 30 km apart, whereas on Earth glacial valleys in mountainous areas tend to be separated by only 1 – 3 km. This tenfold difference in scale is thought to have been caused by Mars' low temperatures, extreme cold increasing the viscosity of ice and reducing its susceptibility to deformation under pressure (Pelletier et al., 2010). This reduced susceptibility to deformation would retard flow in more confined areas such as in narrow valleys. According to Pelletier (2010) this means that when glaciation first began on Mars, ice masses in wider alcoves may have flowed more readily than in narrower basins. Therefore over time these wider flows would most likely have become the more dominant erosive force, slowly carving a landscape of valleys on a scale much larger than we see on Earth (Pelletier et al., 2010).

Another principle of geomorphology that can be especially problematic in planetary landscape analyses is equifinality. This refers to the phenomenon of multiple distinct, possibly starkly dissimilar, processes generating similar end product landforms. This makes it difficult in such cases to infer the origins of particular landscapes on a purely visual basis, presenting problems for the use of satellite imagery as a means of studying martian GLFs. Thus, to maximise possible landform discrimination, interpretations should be based on the analysis of multiple, independent properties. Unfortunately it has not yet been possible to sample many martian glacial landforms directly, making visual analysis the best available option for interpretation. This method alone is a fairly blunt instrument and is particularly susceptible to equifinality.

An example of one case of equifinality is the observed similarity between channels incised by running water and those cut by flowing lava. Channels which look fluvial in nature, but which are believed to have been cut by lava, have also been identified on the surface of the Moon and on Venus (Figure 1). Lava channels similar to these can be observed on the flanks of many terrestrial volcanoes and it is possible that the river-like channels that have often been interpreted as evidence for plentiful water flowing across the surface of Mars are in fact remnants of the volcanic episodes that Mars is known to have undergone. Similar suggestions have been made for the glacier-like flows observed on Mars. Could they in fact be long-since cooled rivers of molten rock rather than slowly creeping ice masses? Most of the available evidence, including data from orbital radar soundings, suggests that this is unlikely. However, as it has not yet been possible to sample martian GLFs directly, uncertainty still exists regarding their material composition and all possibilities should be considered, requiring a full appreciation of equifinality.

A3. Available data sources

Over recent years the martian surface has come under increased scrutiny by geoscientists from various disciplines. This is due primarily to the unprecedented volume and quality of imagery that has become available thanks, most recently, to

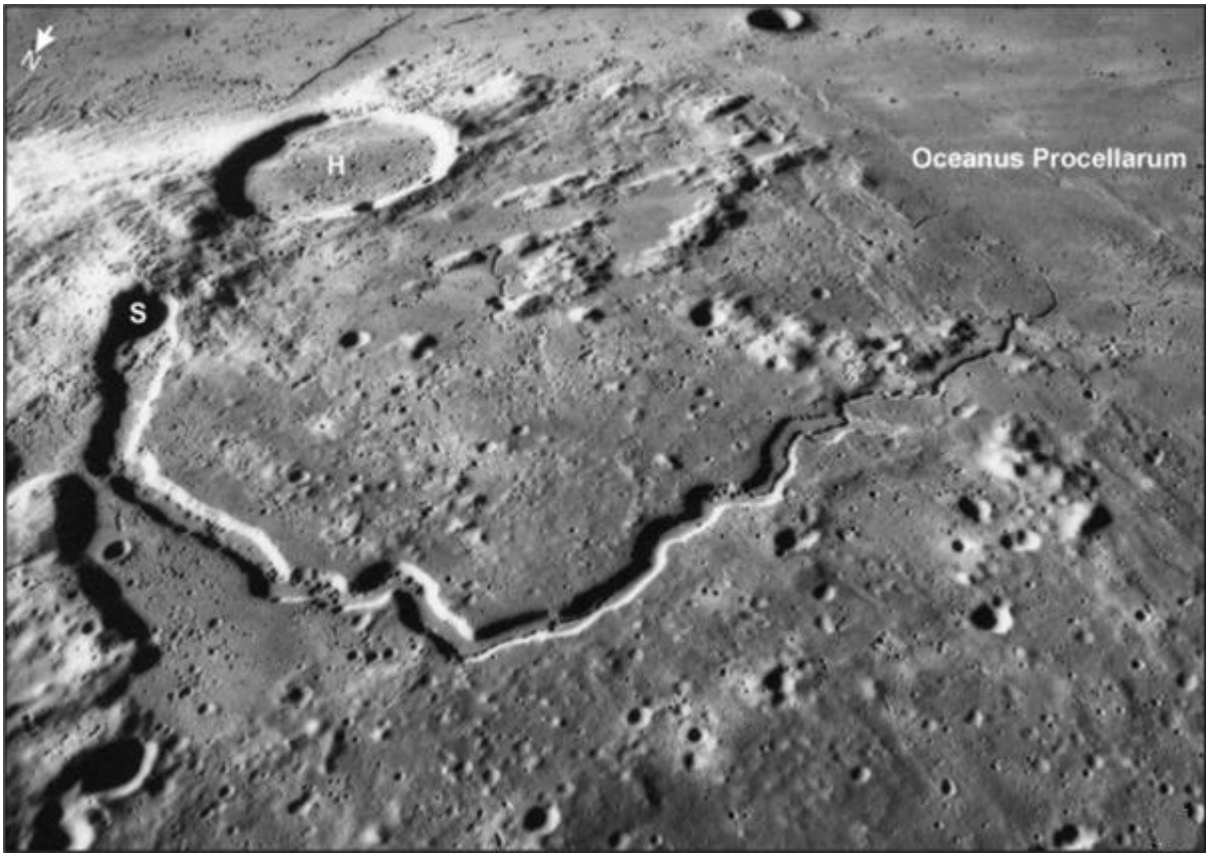

Fig. 1: An example of river-like channels believed to have been carved by flowing lava on the Moon (figure adapted from Leverington, 2011). This image (AS15-M-2612) is from the Apollo 15 Metric camera, and shows an oblique view of the Vallis Schröteri channel system. The head depression of this system (S) is located near crater Herodotus (H), which is 35 km in diameter (Leverington, 2011).

the 2006 activation of the Mars Reconnaissance Orbiter (MRO) which has since been returning images at a spatial resolution as high as 30 cm per pixel (from the High Resolution Imaging Science Experiment / HiRISE camera), and a spectral resolution comprising 560 continuous bands (using the Compact Reconnaissance Imaging Spectrometer for Mars / CRISM instrument).

The major aim of this thesis is to expand the scientific community's understanding of Mars mid-latitude glacial landforms by applying Earth analogue-based techniques. As the only reliably 'repeatable' sampling technique common to both Earth and Mars was (and still is) the acquisition of remotely-sensed satellite imagery, this thesis

relies exclusively on this as its data source. Below an overview is provided of martian satellite imagery and the various platforms that provide it.

A3.1. Mars' space-borne sensor platforms

Since the 1960s thirty nine Mars missions have been undertaken. Of these, one was Japanese, one was conducted by the European Space Agency (ESA), eighteen were conducted by the former Soviet Union, and the remaining nineteen were conducted by the USA's National Aeronautical and Space Administration (NASA) (nssdc.gsfc.nasa.gov; marsprogram.jpl.nasa.gov). Twenty two of these missions were outright failures, returning no data. The remaining seventeen however were, to varying degrees, fruitful. An account of the platforms involved in these successful missions is given for reference in tables 2-5. These include a list of the sensors carried by each platform and a limited synopsis of each sensor's technical specifications. Data from nearly all of these platforms are freely accessible to the present-day researcher, but by far the most comprehensive and most detailed datasets available are those from the relatively recent Mars Global Surveyor, Mars Odyssey, Mars Express and Mars Reconnaissance Orbiter.

Table 2: NASA-operated Mars imaging platforms (successful missions) (nssdc.gsfc.nasa.gov; marsprogram.jpl.nasa.gov)

Name	Mission	Designation	Launch	Arr. date	Imaging equipment carried	Status
Mariner 4	Flyby	MM64	28/11/64	14/07/65	1 x Television Subsystem (TVS) vidicon camera	Complete
Mariner 6	Flyby	MM69A	24/02/69	31/07/69	2 x TVS vidicon cameras	Complete
Mariner 7	Flyby	MM69	27/03/69	05/08/69	2 x TVS vidicon cameras	Complete
Mariner 9	Orbiter	MM71	30/05/71	13/11/71	1 x TVS vidicon camera	End: 1972
Viking 1	Orbiter	Viking-B Orbiter	20/08/75	19/06/76	Twin (stereo) television framing (TVF) vidicon cameras	End: 1980
Viking 2	Orbiter	Viking-A Orbiter	09/09/75	07/08/76	Twin (stereo) television framing (TVF) vidicon cameras	End: 1978
Mars Global Surveyor	Orbiter	MGS	07/11/96	12/09/97	Mars Orbiter Camera (Narrow and wide angle assemblies)	End: 2007
Mars Odyssey	Orbiter	Mars Surveyor 2001 Orbiter	07/04/01	24/10/01	Thermal Emission Imaging System (THEMIS)	Operating
Mars Reconnaissance Orbiter	Orbiter	MRO	12/08/05	10/03/06	High Resolution Imaging Science Experiment (HiRISE) camera. Compact Reconnaissance Imaging Spectrometer for Mars (CRISM) Mars Colour Imager (MARCI) Context Imager (CTX)	Operating

Table 3: Mars space-borne platform imaging device specifics (nssdc.gsfc.nasa.gov; marsprogram.jpl.nasa.gov)		
Name	**Camera**	**Specifics**
Mariner 4	TVS vidicon	1.05 x 1.05 degree field of view (FOV). 1 band. 200 x 200 pixel resolution (res.). 6 bits per pixel.
Mariners 6 and 7	TVS vidicon A	Wide angle camera. 1 band. 9 degree FOV. 704 x 945 pixel resolution.
	TVS vidicon B	Narrow angle. 1 band. 0.9 degree FOV. 704 x 945 pixel res.
Mariner 9	TVS vidicon	Selectively filtered mode: 500 m/TV line res. 11 x 14 deg. FOV.
		Unfiltered mode: 50 m/TV line res. 1.1 x 1.4 deg. FOV.
Viking 1	Twin TVF vidicon cameras	Selectively filtered; blue, green, red, violet and clear. 475 mm focal length (FL). 1.54 x 1.69 deg. FOV.
Viking 2	Twin TVF vidicon cameras	Selectively filtered; blue, green, red, violet and clear. 1 band. 475 mm focal length (FL). 1.54 x 1.69 deg. FOV.
Mars Global Surveyor	Mars Orbiter Camera	Narrow angle assembly: 3.5 m FL. 0.4 deg. FOV. ~ 1.5 m/pixel res.
		Wide angle assembly: dual blue (11.4 mm FL) and red (11.0 mm FL) band cameras. Both cameras have 140 deg. FOV. 280 m/pixel res. (at nadir).
Mars Odyssey	THEMIS	Infrared imager: Anastigmatic telescope. 9 infrared bands imaged between 6.6 – 15.0 micrometers. 100 m/pixel res.
		Visible imager: 5 colour bands imaged at 0.423, 0.553, 0.652, 0.751 and 0.870 micrometers. 2.9 deg. FOV. 18 m/pixel res.
Mars Reconnaissance Orbiter	HiRISE	Blue-green, red, NIR filters. 12 m FL. 1.14 x 0.18 FOV. 30 cm/pixel res.
	CRISM	560 WL. imaged from 400-4050 nanometres. 18 m FOV. 18 m/pixel res.
	MARCI	Atmospheric imager. 7 bands imaged. 5 visible and 2 UV.
	CTX	Wide-angle, low res. Context images. 5.7 deg FOV. 6 m/pixel res.

Table 4: Mars imaging platforms operated by non-US nations or organisations (successful missions) (nssdc.gsfc.nasa.gov; marsprogram.jpl.nasa.gov)						
Name	**Mission**	**Nationality**	**Launch**	**Arr.**	**Imaging equipment carried**	**Status**
Mars 3	Orbiter	USSR	28/05/71	02/12/71	Vega phototelevision camera Zulfar phototelevision camera	End: 1972
Mars 5	Orbiter	USSR	25/07/73	12/02/74	Vega phototelevision camera Zulfar phototelevision camera	End: 1974
Mars Express	Orbiter	European Space Agency (ESA)	02/06/03	25/12/03	Super/High-Resolution Stereo Colour Imager (HRSC) Infrared Mineralogical Mapping Spectrometer (OMEGA)	Operating

Table 5: Mars space-borne platform (non-US nations or organisations) imaging device specifics (nssdc.gsfc.nasa.gov; www.mentallandscape.com)			
Name	**Nationality**	**Camera**	**Specifics**
Mars 3	USSR	Vega	Red, green or blue colour filters. 52mm lens
		Zulfar	Telescopic. Orange colour filtered. 350mm lens
Mars 5	USSR	Vega	Red, green or blue colour filters. 52mm lens
		Zulfar	Telescopic. Orange colour filtered. 350mm lens
Mars Express	ESA	HRSC	Pushbroom scanner. 4 band imager (R, G, B, NIR). 2.35 km swath-width. Dual lens, 10 m/pixel / 2.3 m/pixel res.
		OMEGA	2 independent channels: Visible channel: Pushbroom sensor. 8.8 deg. FOV. 350 m – 10 km swath width. 4.1 arcmin instantaneous field of view (IFOV).
			NIR channel: Whiskbroom sensor. 13 – 20 nanometers spectral res. IFOV of 16, 32, 64 or 128.

Chapter 1:

Mid-latitude glaciation on Mars: A review of the current literature

1. Introduction

Over recent years there has been a dramatic increase in both the quality and quantity of remotely-sensed images recovered of the surface of Mars. Much of this imagery is freely available to researchers and the public. With platforms like the Mars Reconnaissance Orbiter (MRO) returning data at a resolution as high as 30 cm / pixel (from the High Resolution Imaging Science Experiment [HiRISE] camera) and wider-angle images at a resolution of ~6 m / pixel (from the Context [CTX] imager), the immediate result has been a widespread boom in scientific interest and research into Mars' surface properties and the processes that have shaped the planet's surface, both in the past and at present.

One aspect of Mars' surface that has seen particular attention is the assemblage of landforms and formations related to the presence and/or influence of water ice. This interest is to a large degree attributable to the fact that a better understanding of where water lies on Mars, and the quantities in which it exists, will have a considerable impact on both future plans for manned exploration and our continued research into the possibility of life having existed on Mars in the past or, indeed, the chances of establishing it there in the future. Additionally, research into glacial landforms on Mars – the present climate of which is widely considered to preclude precipitation and thus the accumulation of snow and/or ice in a manner conducive to the formation of terrestrial-style glacial features – may enhance our understanding of how climate can change on planetary scales, both extra-terrestrially and, by analogy, on Earth.

This chapter aims to provide a synopsis of mid-latitude glaciation on Mars, summarising our understanding of this field at a level suitable for a non-specialist physical-geography-based audience and, simultaneously, reviewing the existing literature. Ultimately, we identify areas where further work and contributions from geographers with expertise outside the traditional planetary sciences would be most valuable in contributing to advances in this area.

In Section 1 we provide a long-term geological and environmental context for Mars' current landscape. In Section 2 we summarise theories relating to the origin of

martian water ice deposits, and in Section 3 we summarise observations of glacial-type features and their role within the martian cryosphere. Research investigating the mechanical properties of these glacial formations is summarised in Section 4 and Section 5 highlights areas where further study would be most valuable. In this review we do not consider Mars' polar caps in any detail as these have been reviewed fully elsewhere (e.g., Fishbaugh and Head, 2001).

1.1. Geological and climatic context

Much like the Earth and the other planets of the solar system, Mars is thought to be some 4.65 Gyr old. Although relatively little is known about martian geological history compared to that of Earth, repeated visual analyses of Mars' crustal surfaces have led to the identification of three dominant epochs of surface evolution (Tanaka, 1986). These were established by Scott and Carr (1978) and are defined as (from oldest to youngest): the Noachian (~4.65 - 3.7 Gyr), the Hesperian (~3.7 – 3.0 Gyr) and the Amazonian (~3.0 Gyr to present) (Malin and Edgett, 2000; Hartmann and Neukem, 2001; Head, 2007). Although not precise, these ages do provide a useful chronological guide to the sequence of events responsible for landscaping the surface of Mars. The key features of these periods are outlined below, with particular attention paid to the Amazonian epoch, when valley-style glaciation and associated cryospheric processes are widely believed to have gained geomorphological prevalence (e.g. Baker et al., 2010).

1.1.1. Pre-Amazonian Mars

1.1.1.1. The Noachian epoch (~4.65 - 3.7 Gyr)

The earliest epoch of Mars' geological history is known as the Noachian. Evidence suggests that this was a time characterised by intense meteorite bombardment and extensive volcanic activity (Cattermole, 1992). The oldest rocks visible on present-day Mars date to the early Noachian epoch and many of these now comprise the rim material of large impact basins that were formed by meteoroid strikes during that

time (Cattermole, 1992). Isidis, Hellas and Argyre represent well-known examples of such craters (Figure 1). The surfaces within and around such large crater basins are comprised of younger material derived from processes and events that post-date the impacts themselves. Image-based studies of these surfaces have led some to suggest that they are sedimentary in origin and that they could have been deposited either subaerially or subaqueously, in the case of the latter possibly at the bed of large lakes (e.g. Malin and Edgett, 2000; Fassett and Head, 2005). These observations suggest that Mars' surface during the late Noachian epoch was exposed to intense aeolian and fluvial reworking, implying both that the atmosphere was considerably denser during the late Noachian epoch than it is today, and that liquid water was far more abundant at that time (Malin and Edgett, 2000; Fassett and Head, 2005). This interpretation is supported by analyses of fragments of Mars' crust transported to Earth as meteorites, revealing evidence of aqueous weathering and carbonate deposits that have been dated to 4×10^6 yrs bp (Hartmann and Neukem, 2001; Fassett and Head, 2005). However, the stability of this surface liquid water has been questioned on the basis of data gathered by the Observatoire pour la Minéralogie, l'Eau, les Glaces et l'Activité (OMEGA) sensor, which indicate that CO_2 did not form a major constituent of Mars' early atmosphere, interpreted by Bibring et al. (2005) as evidence against atmospheric temperatures having been high enough to permit the presence of stable liquid water at the planet's surface. However, irrespective of its medium-term stability, it is clear that liquid water played a significant role in landscaping the surface of Noachian Mars.

As well as extensive fluvial activity, the Noachian epoch saw the activation of considerable tectonic forces as many of the major topographic features visible on Mars today began to form (Figure 1), e.g., the Tharsis Montes region (Mutch et al., 1976; Johnson and Phillips, 2005) and the martian global dichotomy. The term 'global dichotomy' describes the topographical boundary that separates the older, heavily cratered and predominantly raised highland topography of the southern two thirds of the planet from the younger, resurfaced and subdued lowland plains in the

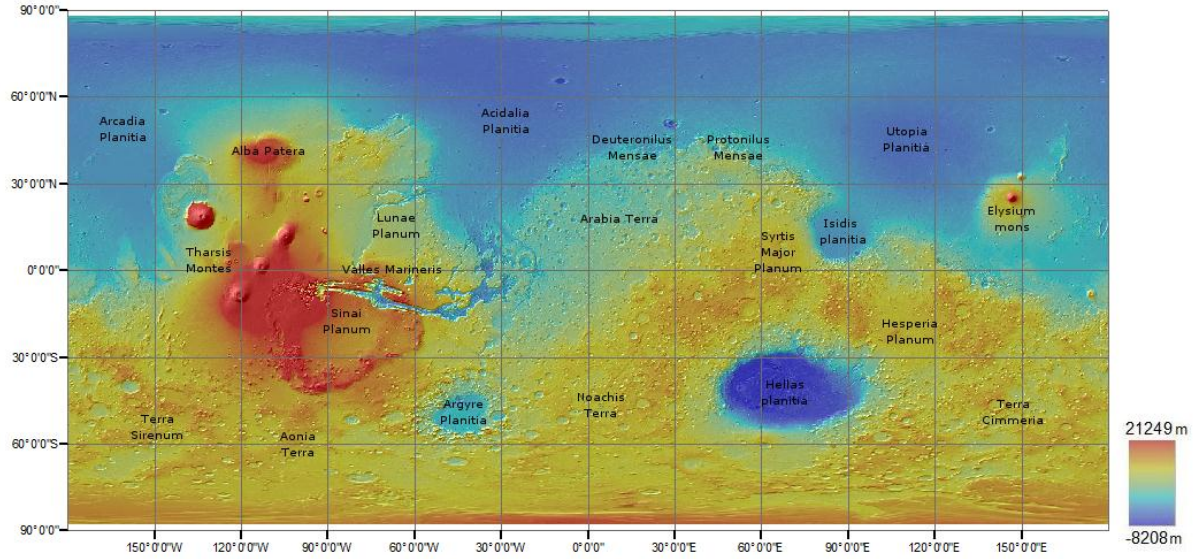

Figure 1: A global map of Mars [colourised using Mars Orbiter Laser Altimeter (MOLA) elevation data].

northern sector of the northern hemisphere. This global dichotomy encircles the planet presenting a sudden change in elevation between north and south and running through a range of latitudes from just south of the equator to around 50°N (Smrekar et al., 2004) (Figure 1).

1.1.1.2. The Hesperian epoch (~3.7 – 3.0 Gyr)

By the end of the Noachian epoch meteoroid flux in the vicinity of Mars (and thus the rate of impact events) had decreased markedly to a level comparable to the modern day (Mutch et al., 1976). Thus martian surface alteration became more heavily dominated by fluvial activity, which continued into the Hesperian epoch (~3.7 – 3.0 Gyr) (Head, 2007).

Around the onset of the Hesperian epoch Mars also experienced increased planetary heat loss associated with a peak in surface igneous activity (Cattermole, 1992). Thus began a period of intense volcanism, leading to the emplacement of vast plains of flood lava deposits. Examples of such plains can be seen in elevated areas such as

Lunae Planum, Sinai Planum, Syrtis Major, Hesperia Planum and Malea Plani (Cattermole, 1992) (Figure 1). Uplift also persisted in the Tharsis region leading to crustal extension which at this time is thought to have caused the formation of the Valles Marineris canyon system (Mutch et al., 1976) (Figure 1).

1.1.2. The Amazonian epoch (~3.0 Gyr – present)

The Amazonian epoch is difficult to characterise succinctly because so many different processes have played important roles in shaping the planet's surface over the past ~3 x 10^9 years. However, as an awareness of the martian environment during this time is crucial to placing the contribution of martian glaciation and other cryospheric processes to the planet's development in context, we summarize below the major geological, geomorphological, climatic and cryospheric changes that are believed to have influenced Mars during the Amazonian epoch.

1.1.2.1. Mars' Amazonian geomorphology

With the decline in volcanic activity that had occurred by the middle of the Amazonian epoch, other processes gained prevalence. Key amongst these were aeolian activity (defined predominantly by dust storms and related events [Leovy, 2001; Lorenz, 2009]), fluvial processes on both a meso (Fairén et al., 2008) and a mega (Zealey, 2008) scale, and glacial activity (Kargel and Strom, 1992; Madeleine et al., 2009; Soare and Osinski, 2009; Morgan et al., 2009). Evidence of all three process sets can be seen across the surface of Mars, although apparent glacial activity is particularly pronounced toward the polar regions and in Mars' mid-latitudes (Milliken et al., 2003; Madeleine et al., 2009).

The relative dominance of aeolian, fluvial and glacial processes as modes of surface alteration would appear to have shifted considerably over the course of the Amazonian epoch. However, in recent geological time it would seem that ice-related processes have become particularly dominant (e.g. Baker et al., 2010), and evidence drawn from both surface mapping and climate modelling (e.g. Forget et al., 2006)

suggests that Mars has experienced relatively recent ice ages, almost certainly during the past few million years (e.g. Head et al., 2003; Schon et al., 2009).

1.1.2.2. Mars' contemporary climate

The surface of present-day Mars is both extremely cold and extremely dry. Average surface temperature is -60º C, ranging between +27 ºC and -133 °C (Read and Lewis, 2004). In terms of atmospheric moisture content, readings made by landing craft have shown an H_2O partial pressure of 1 microbar, or 160 ppm (Clark, 1997, in: DeVincensi et al., 1999). This equates to an atmosphere that is drier than Earth's by a factor of ~1000 (Read and Lewis, 2004).

Despite the differences in thermal and hydrological characteristics observed between Earth and Mars, atmospheric circulation and weather patterns display marked similarities. In both cases, the dominant pattern of circulation is driven by the differential heating (through incoming solar radiation) experienced between the equatorial latitudes and the polar regions. Mars experiences 'trade winds' associated with Hadley circulation, just as occur on Earth, and also cyclonic and anti-cyclonic weather systems driven by convection and by the rotation of the planet (Leovy, 2001).

One of the most notable peculiarities of the martian climate relates to the planet's polar ice caps. The larger of these is the northern polar cap (Figure 2). Every northern winter the north polar cap expands dramatically as temperatures drop below the point at which CO_2 freezes on Mars, and up to 30% of Mars' atmosphere (which is ~95% CO_2 by volume) solidifies (in a layer up to 2 m thick) at the northern pole during this period (Read and Lewis, 2004; Forget, 2009). This kind of atmospheric condensation can also be seen in lower latitudes where thin layers of CO_2 frost periodically form on the ground overnight (Figure 2). Thus, for some time it was believed that Mars' polar caps were composed entirely of CO_2. However, measurements of surface temperature over Mars' northern polar ice cap taken in the 1970s by the Viking 'infrared thermal mapper' (IRTM) indicated that this cap was

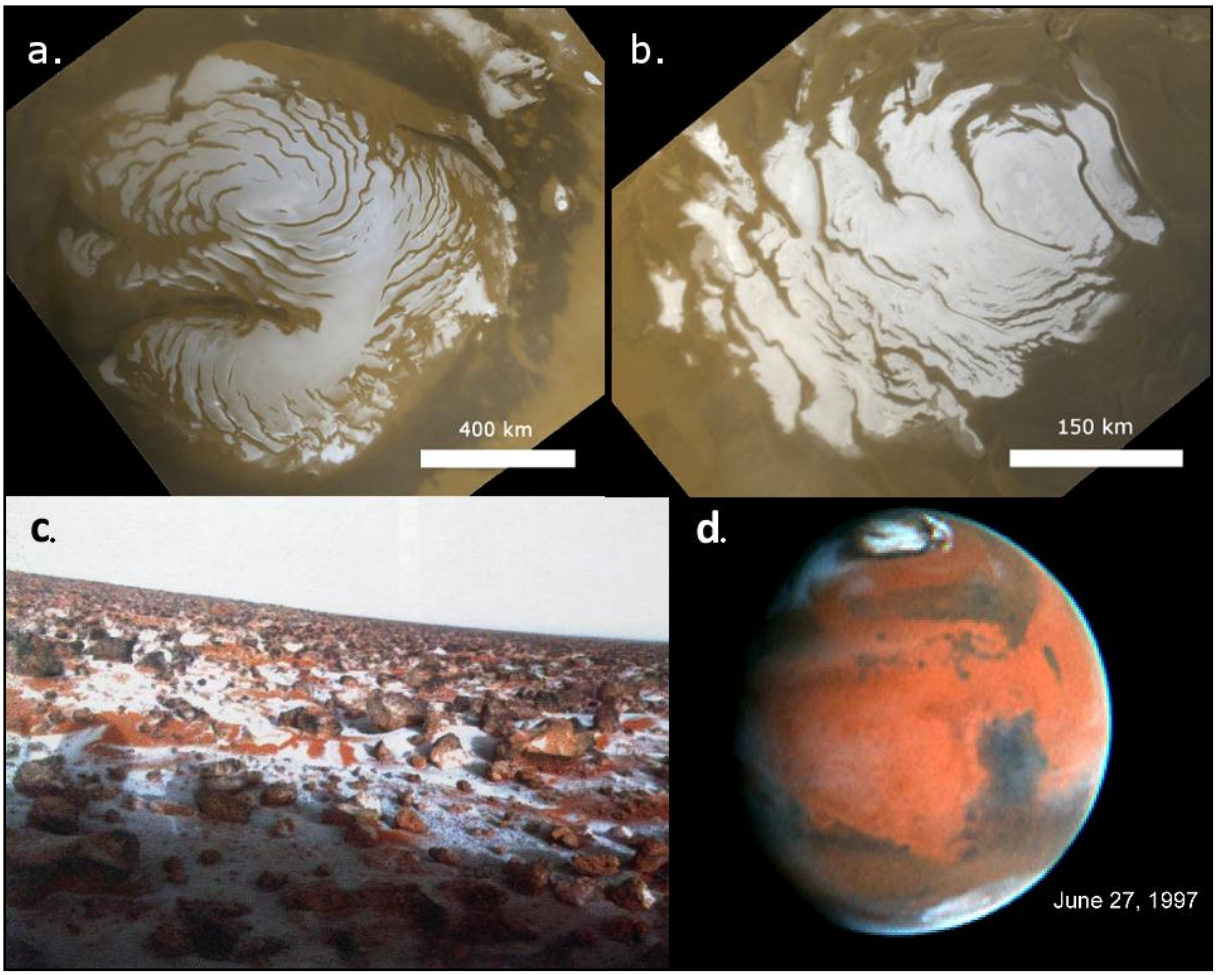

Figure 2: A collection of images describing the behaviour of ice and water vapour on Mars: Mars' northern polar cap shown as a mosaic of MOC images (www.msss.com) (a); Mars' southern polar cap shown as a mosaic of MOC images (www.msss.com) (b); A photo taken by the Viking 1 Lander showing early-morning CO_2 ground frost in the western Chryse Planitia area (adapted from Read and Lewis, 2004) (c); An image of Mars taken by the Hubble space telescope on June 27, 1997, showing white H_2O vapour clouds at various latitudes (www.nasaimages.org) (d). Note, in (a) and (b) images are oriented 'north' up, as per conventional map projections.

composed of H_2O ice (and not CO_2 ice) during the northern hemispheric spring and summer when the transient layer of CO_2 ice had sublimated as ambient temperatures rise above 150 K (-123°c) (Kieffer et al., 1976). The findings of this study were reinforced by the Viking's 'Mars atmospheric water detector' (MAWD), which detected relatively high concentrations of atmospheric H_2O over both of Mars' polar caps (Farmer et al., 1976), and were later confirmed by Earth-based spectroscopic analysis (Clark and McCord, 1982).

Subsequent studies have shown that small quantities of atmospheric H_2O vapour circulate between the northern and southern polar caps in the high atmosphere (Forget, 2009), where clouds of water-ice particles can sometimes be seen to condense, particularly during the northern hemispheric summer (Smith, 2008) (Figure 2). This coincides with the strong release of water vapour that MAWD observed in the higher northern latitudes during northern summers (Read and Lewis, 2004; Madeleine et al., 2009). Recent measurements made by the Phoenix lander suggest that, although these clouds are very thin, some (similar in appearance to cirrus clouds on Earth) occasionally generate frozen precipitation at very high altitudes (Whiteway et al., 2009). However, it is not thought that this precipitation could reach the martian surface under current climatic conditions.

1.1.2.3. Martian climate change and Ice Ages during the Amazonian epoch

As discussed above, current conditions on Mars are cold and dry relative to Earth. This makes water ice unstable when exposed at the planet's surface anywhere except at the poles (Forget et al., 2006). However, although the Amazonian epoch appears to have been cold and dry throughout, possibly not too dissimilar from Earth's Antarctic Dry Valleys (Marchant and Head, 2007), a wealth of evidence exists to suggest that ice-related processes have played a major role in shaping surfaces on Mars during the (geologically very recent) late Amazonian epoch, particularly in middle and higher latitudes (Forget et al., 2006; Levy et al., 2009; Page et al., 2009). Atmospheric modelling studies have suggested that some of these apparently ice-related landforms formed through precipitation of water ice from the atmosphere (Forget et al., 2006) thus implying that the climate of Mars has undergone considerable change, perhaps even repeated or cyclical change, during its recent geological history. Some researchers have theorised that such climatic changes precipitated one or more 'Ice Ages' during the Amazonian epoch (Kargel, 2004).

Ice Ages on Earth are widely believed to be precipitated by changes in our planet's rotational obliquity, and the same is thought to be true for Mars. On Earth cyclical

periods of lower obliquity contribute to periods of relatively low temperatures at high latitudes, inducing or sustaining glaciation (Imbrie and Imbrie, 1986). On Mars, however, glacial periods are thought to occur during periods of higher obliquity. Under such conditions Mars' polar regions would have been exposed to higher levels of solar radiation which would have increased the ablation of the perennial H_2O polar ice caps, thus permitting a rise in atmospheric moisture levels and an increase in equatorward movement of atmospheric H_2O (Head et al., 2003). This atmospheric water could then condense either into or onto the ground around the mid-latitudes, thus initiating surface modification and the development of periglacial and / or permafrost landforms (Forget et al., 2006; Schon et al., 2009) (See Section 2.2 for further development of ice precipitation and deposition).

The timing and magnitude of Mars' obliquity shifts have been calculated from known perturbations in Mars' motion caused by other planets in the solar system (Ward, 1992; Read and Lewis, 2004). These analyses revealed that Mars' obliquity has ranged between 15° and >45° in the last 10 x 10^6 yrs (Figure 3), quite probably driving climatic and environmental changes at corresponding timescales. This range contrasts markedly with the obliquity range of Earth, which has varied only between 22.0º and 24.5º over the last 18 x 10^6 years (Laskar et al., 1993). The last major shift in martian obliquity (from 35º to 25º) appears to have occurred between approximately four and five million years ago (Touma and Wisdom, 1993). It is thought that this last major fall in obliquity (and thus polar temperatures, sublimation, atmospheric moisture and mid-latitude precipitation) may have brought about the end of the last major glacial period or 'ice age' on Mars. Ice deposits would therefore have been left to ablate in Mars' now drier atmosphere, shrinking away without any new mass supply. The ice deposits and landforms seen on Mars today therefore most likely represent the diminished remains (shielded beneath a layer of dust and debris) of what may once have been a much larger ice mass or series of ice masses.

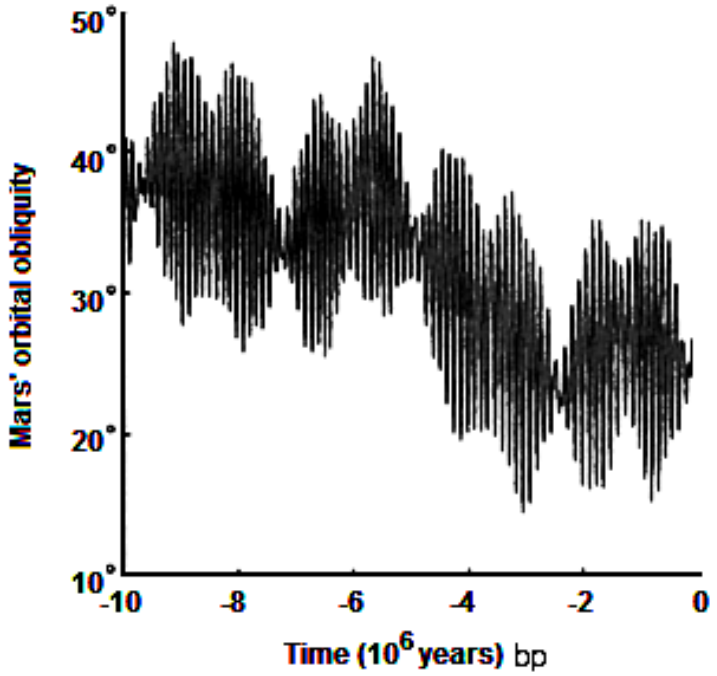

Figure 3: A line graph (adapted from Touma and Wisdom, 1993) showing calculated changes in Mars rotational obliquity over the last 10 x 10^6 yrs. Note the well-defined transition from a higher (~37º) to a lower (~25º) mean obliquity that occurs between ~4 x 10^6 yrs bp and ~5 x 10^6 yrs bp.

2. Water ice on present-day Mars

The polar and mid-latitudes of present-day Mars support a range of what are believed to be glacial or ice-related features and landforms. Some of these bear a striking resemblance to terrestrial valley glaciers (e.g. Marchant and Head, 2003; Head et al, 2005; Forget, 2006), as expanded upon below (Section 3). However, it is important to note that H_2O ice is likely to be the primary agent in the formation of many martian features, surface textures and formations other than apparent valley glaciers. Examples of some such ice formations are pedestal craters (Kadish et al., 2008), surface polygons and other textured or patterned ground types of probable periglacial origins (e.g. Mangold 2005; Burr et al., 2005; Soare et al., 2008; Levy et al., 2010), and possible pingos (e.g. Dundas and McEwan, 2010). However, exposed ice is only rarely seen in martian imagery, because it sublimates quickly in Mars' cold and hyper-arid atmosphere. Repeated HiRISE observations and subsequent

numerical modelling of previously buried ground ice exposed by fresh mid-latitude impact craters showed that such ice fades completely from image series over a few months (Dundas and Byrne, 2010). From observations made using repeat imagery at various sites and under a range of local conditions Dundas and Byrne (2010) were able to measure rates of ice loss through sublimation occurring over the several month-long study period. These were found to occur at a rate of between 1.3 – 9.8 mm over the course of the study for ejecta ice and 0.88 – 2.6 mm for cases where the ground ice table was exposed (Dundas and Byrne, 2010).

2.1. Mars' dissected mantle terrain

Observations of transient ice exposures such as those described above, along with the visual identification and interpretation of certain landforms (apparently glacial in nature; see Section 4 below) have led to speculation that large quantities of H_2O ice may be present in Mars' sub-polar latitudes, buried beneath a layer of dust or regolith and thus shielded from the atmosphere. Forget et al. (2006) used high-resolution climate modelling to show that during a past martian ice age, most probably caused by a high-obliquity event (see Section 1.1.2.3. above), H_2O ice would likely have accumulated at the surface in considerable quantities well into Mars' mid-latitudes, i.e. as low as 30º north and south. Modelled predictions such as these are supported by the observation of a unique, apparently geologically recent mantle-like formation which appears to be extensively present between the latitudes of ~30º and ~60º in both of Mars' hemispheres. This formation appears to be draped over most other surfaces, effectively smoothing smaller-scale topography (Kreslavsky and Head, 2002). It has been identified by various studies through inspection of many different image sets, and from the statistical analysis of surface roughness sampled from Mars Orbiter Laser Altimeter (MOLA) elevation data (Kreslavsky and Head, 2000).

This mid-latitude mantle appears to be several metres thick and sedimentary in structure, exhibiting strong layering in places (Schon et al., 2009). It also exhibits evidence of successive disaggregation and dissection events, followed by phases of re-accumulation/deposition, often building a complicated stratigraphy and resulting in

a pitted or ‘dissected’ appearance visible in higher-resolution images such as those captured by the HiRISE camera (Figure 4). These characteristics have led to the surface being named the ‘dissected mantle terrain’ (e.g. Searls et al., 2008). Mustard et al. (2001) interpreted this mantle deposit as most likely being composed of successive layers of ice-cemented dust, with each layer representing an independent ice accumulation event - formed during the martian equivalent of a glacial phase. Each such event was interceded by an interglacial phase during which the recently-accumulated mantle surface was subjected to ablation and disaggregation, resulting in the characteristic layered and pitted appearance of the dissected mantle terrain. Another explanation for the dissected mantle, explored by Mustard et al. (2001), was that this layered deposit could be dust cemented through chemical processes rather than by ice, but no strong subsequent support for this model has been forthcoming.

2.2. Origins of Mars’ contemporary mid-latitude ice deposits

The dissected mantle terrain discussed above covers approximately 23% of the martian surface (Kreslavsky and Head, 2002). It could therefore constitute a considerable reservoir of H_2O. Unfortunately, as there have been very few opportunities to observe or sample the fabric of this mantled deposit directly, its precise composition, origin and mode of deposition are still contested issues.

Since direct internal sampling has not been possible, most genetic interpretations of both the mantle itself and the various icy formations that are found in association with it (see Section 3) have focussed on observations of structure and morphology. A composition of predominantly H_2O ice has been fairly well established from studies of mantle-associated deposits (e.g. Holt et al., 2008; Plaut et al., 2009) (see below; this Section) and is now widely acknowledged (e.g. Head et al., 2010). However, both the mode of ice deposition and the relative proportions of ice and rock within mid-latitude ice formations (the two issues being inextricably linked) remain a serious point of contention.

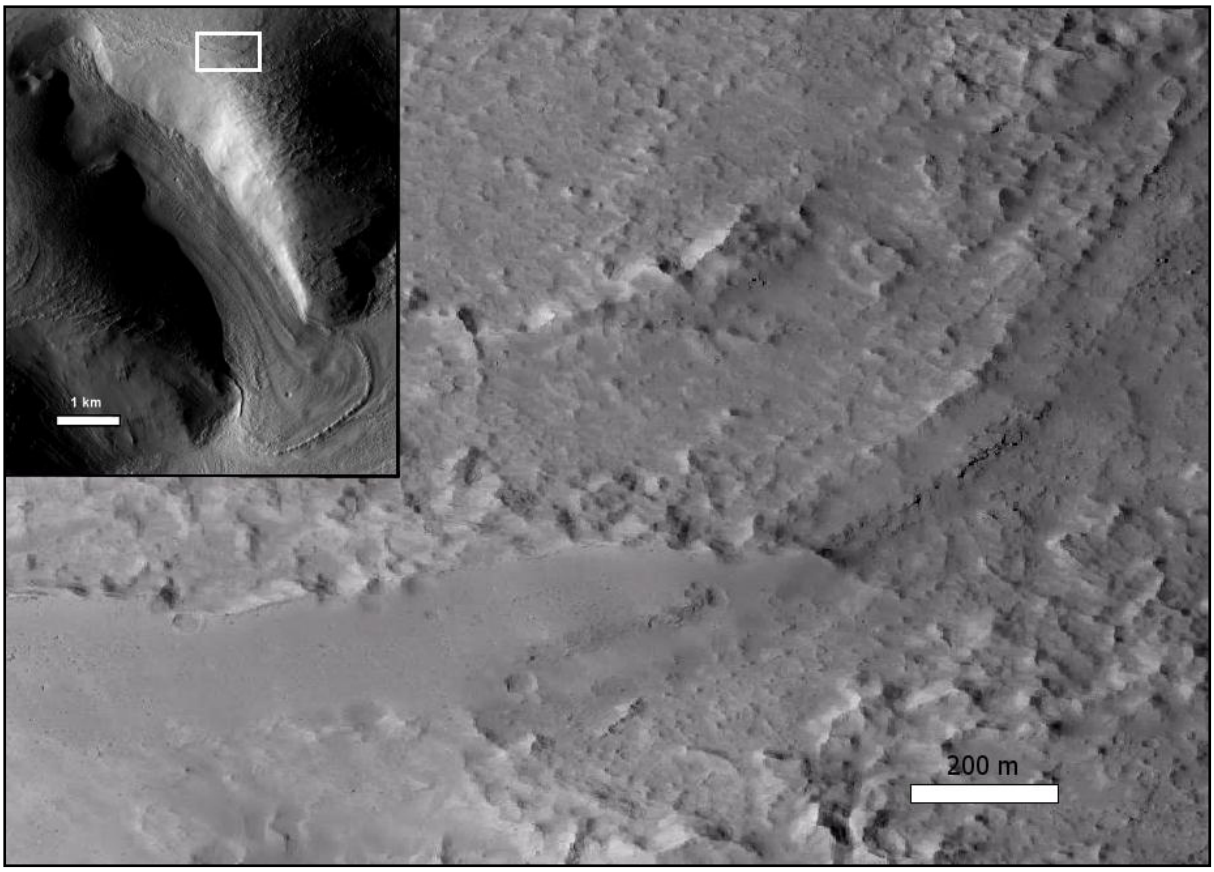

Figure 4: Detail of dissected mantle terrain featured in HiRISE image PSP_008809_2215. The location of this exploded HiRISE section (relative to a nearby GLF in eastern Protonilus Mensae) is shown in the inset (subset from CTX image P22_009455_2214_XN_41N305W, detail centred at 54.728 E, 41.313 N). Clear variation in texture is evident between the smooth surface in the lower left of the image and the weathered, pitted surfaces in the rest of the frame. Pronounced stratification is also visible running through the scene, but particularly in the top right of the image. Both images are oriented north-up and illumination is from the left.

Two dominant theories have been proposed to explain the depositional origins of the dissected mantle terrain: one via atmospheric airfall precipitation of snow or ice (which has subsequently become mixed into, or buried by, dust and / or regolith [e.g. Schon et al., 2009]), and the other via the condensation of atmospheric water vapour directly into the void spaces between regolith clasts within surface sediments (e.g. Mellon and Jakosky, 1995; Mustard et. al., 2001). The latter hypothesis is attractive in that it overcomes the need for airfall deposition of snow or ice, a phenomenon that is considered to be highly unlikely on Mars under its current climatic regime (Read and Lewis, 2004). However, the inter-granular condensation hypothesis requires that Mars' surface ice deposits are composed predominantly, or at least substantially, of

rocky debris or dust – a requirement that appears to be at odds with recent shallow sub-surface radar (SHARAD) - based studies which indicate that at least some glacial landforms in Mars mid-latitudes appear to be predominantly composed of ice (e.g. Holt et al., 2008; Plaut et al., 2009). The SHARAD profiles gathered provided conclusive evidence that the features under scrutiny, namely Lobate Debris Aprons, or LDA (see Section 3.2.1 for definition), were indeed composed of a material distinct from the underlying bedrock. The SHARAD data also indicate that the internal fabric of the observed LDA is different from the dust and debris that was visible on the surface. This layer of debris is between 0.5 and 10 m thick. Furthermore, the dielectric properties of these Lobate Debris Aprons' internal mass were consistent with a composition of almost pure water ice with minimal lithic content. These observations strongly suggest that the features under investigation (and thus possibly, by extension, icy deposits in general) are composed of massive ice, further supporting an 'airfall' explanation for initial accumulation.

It should be noted that the observations of Holt et al. (2008) and Plaut et al. (2009) were made in only one region of Mars, whereas ice deposits occur throughout Mars' mid-latitudes. Until recently, no evidence has been published to support the assumption that all dissected mantle deposits and ice-associated flow formations formed in the same way and at the same time. However, Souness et al. (2012) recently reported a comprehensive survey of glacier-like forms, or 'GLFs' (see Section 3.2.3) within Mars' mid-latitudes, identifying 1309 individual GLFs. The survey and accompanying inventory revealed population-wide similarities in both GLF distribution (including latitude and elevation) and GLF morphometry (including length, width and orientation) which suggest that all GLFs share a common origin and composition.

Head et al. (2005) argued for a high ice-debris ratio in many mid-latitude icy forms (see Section 3), citing their overall morphology and specifically their tendency to flow around obstacles even on a local scale as being evidence of sufficiently low material viscosity to preclude high debris concentrations. Bryson et al. (2008) also later supported this interpretation, arguing for high ice concentrations in the surface layers of Mars' mid-latitudes on the basis that the lag between ice being exposed by recent impacts and this ice sublimating to the point at which the site becomes opaque once

again (i.e. obscured by re-accumulated dust) is in most cases too long and the volume of lost ice too high for dust to have constituted more than a small proportion of the surface material. These observations, together with the observation of sedimentary-style structures within icy deposits (Schon et al., 2009), and the body of work which exists to suggest that snowfall may indeed have been possible on Mars during its recent geological history (e.g. Forget et al., 2006; Levy et al., 2009; Page et al., 2009; Kite et al., in press), would seem to favour the airfall mode of deposition.

Uncertainty still exists regarding the particulars of where and how ice deposits have survived over geological time (e.g. Souness et al., 2012). Various studies however, utilising both laboratory–based tests and numerical modelling techniques, have yielded results which suggest that a thick (>1 m) layer of ice, if buried beneath a layer of fine-grained basaltic regolith >1.5 cm in thickness, could survive (under present conditions) in Mars' mid-latitudes, possibly having lain preserved in such a state since the last martian glacial period (Fanale et al., 1986; Bryson et al., 2008). Just such a glacial period is thought to have ended between approximately 4^6 and 5^6 yrs bp (Touma and Wisdom, 1993; Head et al., 2003) (see Section 1.1.2.3).

3. Viscous Flow Features (VFFs)

The icy dissected mantle terrain deposits discussed above (see Section 2.1) cover extensive areas of Mars' mid-latitudes and available evidence indicates that they are long-lived, stable and static. The dissected mantle terrain does not therefore appear to have transported or reworked significant quantities of material on Mars' surface. In contrast, a localized sub-set of mantled terrain features shows evidence of flow (or of having flowed) in a manner similar to glaciers or rock glaciers on Earth. Squyres (1978) first reported such forms upon inspection of imagery from the Mariner 9 probe which showed features characterized by surface lineations, compressional ridges and convex topography in certain areas of Mars' mid-latitudes. Subsequent observations of these apparently mobilized deposits suggest viscous flow of ice-rich sediments capable of transporting significant volumes of surface material.

Since the advent of the Mariner 9 imagery, benefiting from the ever-increasing coverage and resolution of available data, many studies have remarked upon the presence of concentrically ridged, lobate features in the martian mid-latitudes, many of which share visible characteristics with terrestrial glaciers (e.g. Marchant and Head, 2003; Head et al, 2005; Forget, 2006). These landforms often appear on the slopes of high-relief landscapes and exhibit morphologies indicative of viscous flow. The observation of flow-like attributes in these lobes has led to the name 'viscous flow feature' (VFF) (e.g. Milliken et al, 2003). However, in no instance has flow yet been measured directly, even through use of repeat imaging. Indeed, given that rates of flow in terrestrial cold-based rock glaciers (where temperatures are higher than those on Mars) can be as little as < 1 mm yr (Rignot et al., 2002), it is unlikely that it will ever be possible to make reliable statements on the presence or absence of flow in martian VFFs based solely on remotely sensed data. Current thinking therefore favours the explanation that, similarly to the dissected mantle terrain discussed above (Section 2.2.1), these landforms are icy relics from a geologically recent, high planetary obliquity, glacial period, possibly a few million years ago (Forget et al., 2006; Levy et al., 2009; Page et al., 2009). This interpretation of VFFs is supported by their apparent preference for poleward-facing alcoves and valleys in both hemispheres (Milliken et al., 2003; Berman et al., 2009; Souness et al., 2012), suggesting the persistence of icy deposits in areas that receive relatively low levels of insolation. However, it should be noted that no evidence has yet been presented to suggest that VFFs have preferentially formed in poleward-facing alcoves, merely that they have *survived* in these niches since formation, whenever and however that occurred.

3.1. Distribution and classification of VFFs

Utilising 13,000 globally distributed Mars Orbiter Camera (MOC) images with a resolution of <10 m/pixel, Milliken et al. (2003) identified 146 images that contained VFFs. These 146 images were found to have been captured almost exclusively (97%) between the latitudes of 30 and 50º in both hemispheres (Milliken et al., 2003) (Figure 5). This distribution is consistent with climatic models of historic ice precipitation and subsequent ice preservation on Mars' surface (Section 2.1 above)

(Fanale et al., 1986; Bryson et al., 2008; Forget et al., 2006; Schon et al., 2009), and corresponds to the regions of dissected mantle terrain mapped by Kreslavsky and Head (2000). A planetary-scale survey of several thousand CTX images has also identified several populations of VFFs overwhelmingly located in the mid-latitudes (Souness et al., 2012). In the northern hemisphere, concentrations of VFFs were observed to occur in the so-called 'fretted terrains' (Sharp, 1973) of Mars' dichotomy escarpment, characterised by extensively incised landscapes of interlinking valleys and raised, cliff-encircled mesas. These fretted terrains include areas such as Deuteronilus Mensae and Protonilus Mensae (Figure 1). In the southern hemisphere particularly high VFF populations were observed in the region east of the large Hellas Planitia impact basin, and in the cratered highlands of Terra Sirenum (Milliken et al., 2003).

In their survey, Milliken et al. (2003) defined certain morphologic criteria which were used to isolate VFFs from a host of other enigmatic martian landforms. These criteria include the presence of: (i) primary or secondary lobate features (typically in alcoves), (ii) lineations on the surface (both parallel and transverse to the slope on which the material flows), (iii) compressional ridges or extensional troughs, (iv) ridges at the flow front or base of the slope, and (v) other general evidence that the material flowed around or over obstacles such as craters or mounds (Milliken et al., 2003). The lateral margins and lower extents of VFFs are also commonly defined by unbroken, raised ridges (Berman et al., 2009) which are often arranged as a nested series of multiple ridges aligned parallel to each other (Figure 6). This apparent nesting has been observed on both flat surfaces and on adjacent valley walls (Marchant and Head, 2003). Ridges of this type have been described by Arfstrom and Hartmann (2004) as being moraine-like in appearance, and these authors concluded that such 'moraine-like ridges' are formed by sediment deposition or re-working by flowing ice masses. The observation of nested moraine-like sequences has been discussed by Arfstrom and Hartmann (2004) as being evidence of

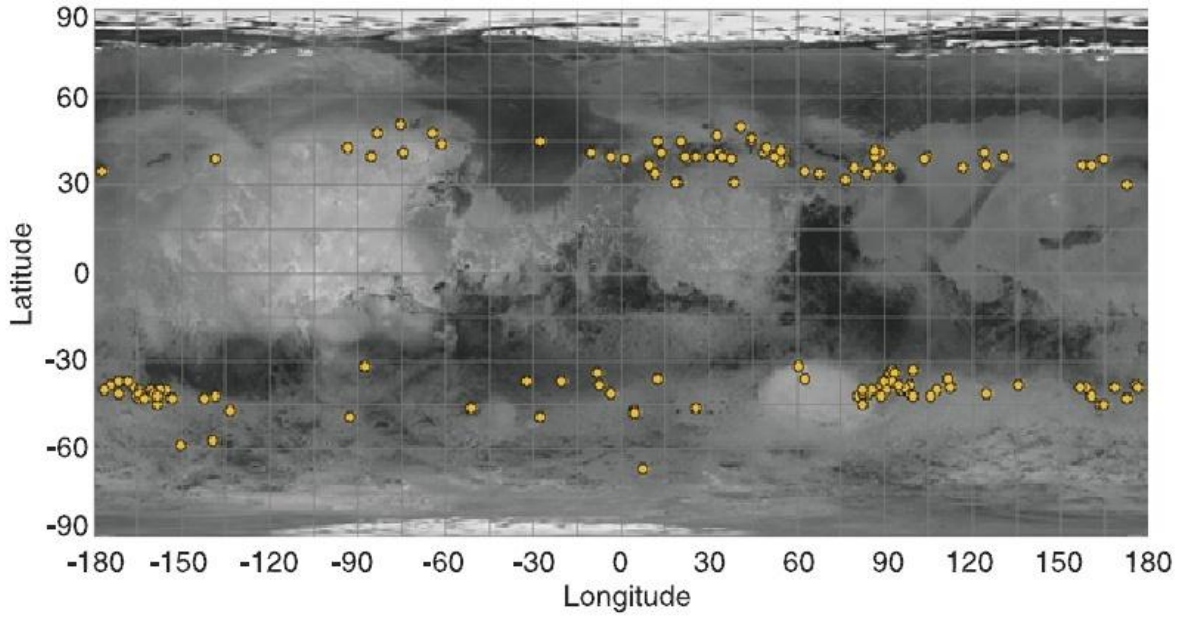

Figure 5: A global map of Mars showing the distribution of VFFs as surveyed by Milliken et al (2003).

successive flow events which could have been driven by climatic fluctuations. Protalus ramparts have also been considered as a terrestrial analogue for martian moraine-like ridges, suggesting that they could have formed through the accumulation of rockfall and avalanche debris (Arfstrom, 2003; Howard, 2003). However, Arfstrom and Hartmann (2004) argued that the observed distances between many martian moraine-like ridges and their respective possible debris source areas are too high for the protalus rampart mechanism to apply, some martian examples sitting kilometres away from possible debris sources.

The broad VFF classification utilised by Milliken et al. (2003) encompasses a range of similar (and in many cases apparently inter-related) landforms that are widely interpreted as being of a glacial origin. Although a range of other debris and mass-movement forms occur in Mars' mid-latitudes, VFFs can be distinguished from debris flows and landslides because the latter tend to be raised above the surrounding landscape and tend to have visible material source hollows in their respective headwalls. VFFs on the other hand rarely rise substantially above the adjacent

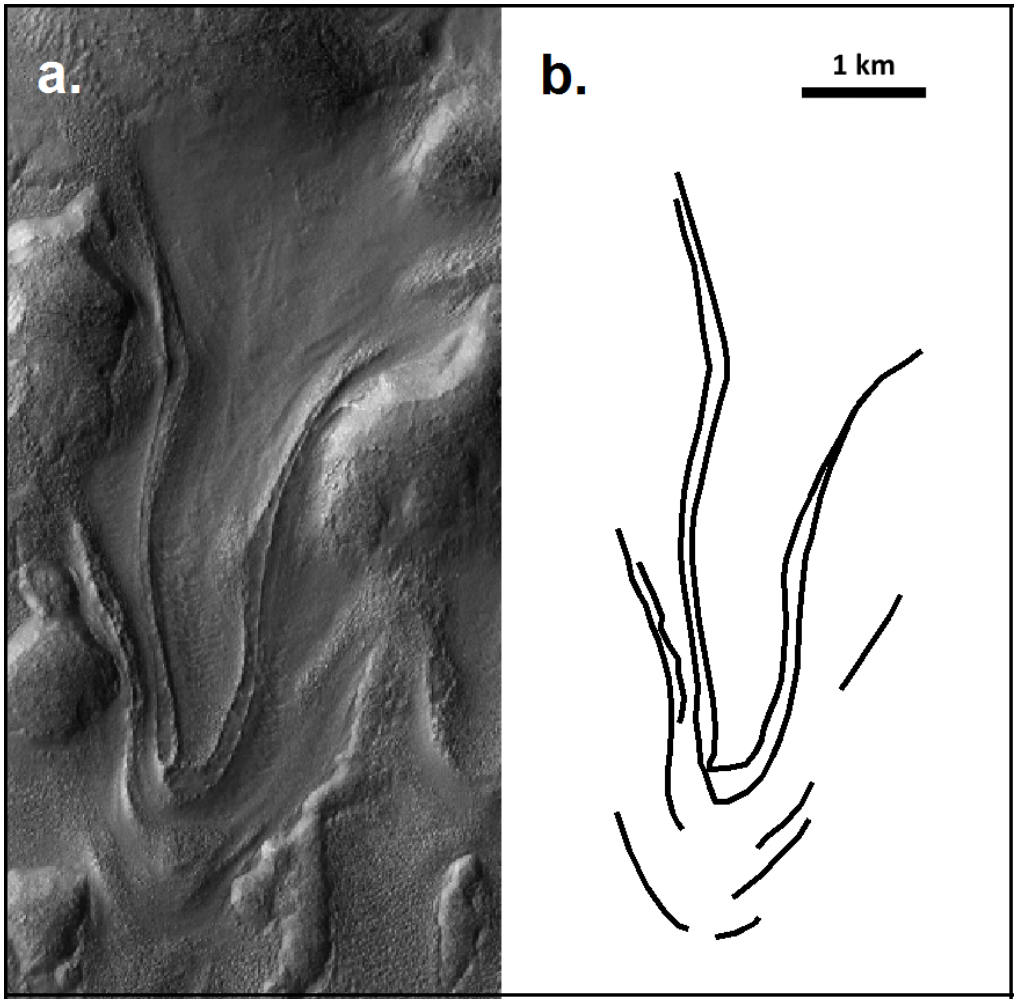

Figure 6: A subset of HiRISE image PSP_002320_1415 (detail centred at 113.160 E, -38.132 N) showing a GLF situated in Greg crater, Eastern Hellas (a). Well-formed moraine-like ridges are visible parallel to the flanks and nested around the terminus of this GLF. A diagram highlighting these moraine-like ridges is shown (b). The image is oriented north-up and illumination is from the left.

topography and have no such corresponding mass-source hollow (e.g. Van Gasselt et al., 2010).

Flow modelling (Milliken et al., 2003; Turtle et al., 2001) and investigations of surface crater densities (e.g. Hartmann, 2005) indicate that VFFs are geologically recent and almost certainly younger than 10^7 years. However, both of these dating techniques (flow modelling being used retrospectively to infer GLF formation times) are subject to potentially significant error due to a number of poorly understood variables that need to be approximated in these investigations. These variables include the 3-d

geometry of VFFs (for modelling), the physical and hence rheological composition of VFFs (for modelling) and the rates at which craters on the surface of VFFs are obscured by sublimation, dissection, and possibly viscous relaxation of the icy material below (Pathare et al., 2004). Recent work by Hartmann and Werner (2010) has shown that counting smaller craters on VFFs (craters with a diameter < ~90 m) can give a reliable indication of long-term VFF re-surfacing rates because they survive only ~10% as long on VFFs as they do on nearby plains (a few 10^6 years on VFFs compared to 10^7 years on the plains). However, definitive ages for VFFs are still elusive.

Different types of VFF are considered to form separate components of what Head et al. (2010) describe as an integrated glacial landsystem (Figure 7). VFF morphology can vary widely within such landsystems, even within dense local populations, yielding at least three common VFF sub-types. These are lobate debris aprons (LDAs) (Squyres, 1979), lineated valley fill (LVF) (Squyres, 1979), and glacier-like forms (GLFs) (Hartmann et al., 2003; Hubbard et al, 2011; Souness et al., 2012).

3.2. Sub-classifications of VFFs

3.2.1. Lobate Debris Aprons (LDAs)

LDAs are laterally elongated ramparts of icy material that appear to accumulate at the base of, and to flow away from, cliffs (Squyres, 1978, 1979) (Figure 8). They are typically very thick [several hundreds of metres (Holt et al., 2008; Plaut et al., 2009)], run parallel to the adjacent escarpment and terminate at lobate margins (Head et al., 2005). Head et al. (2010) observed that LDAs, as well as being linear features, also occur circumferentially, in some cases completely encircling isolated mesas of the kind often observed in Protonilus Mensae and Deuteronilus Mensae (Figure 1).

LDAs are generally heavily textured by flow-related ridges and troughs and have a convex down-slope profile. This convexity indicates that flow does indeed occur throughout the mass, the textures and patterning observable in remotely-sensed

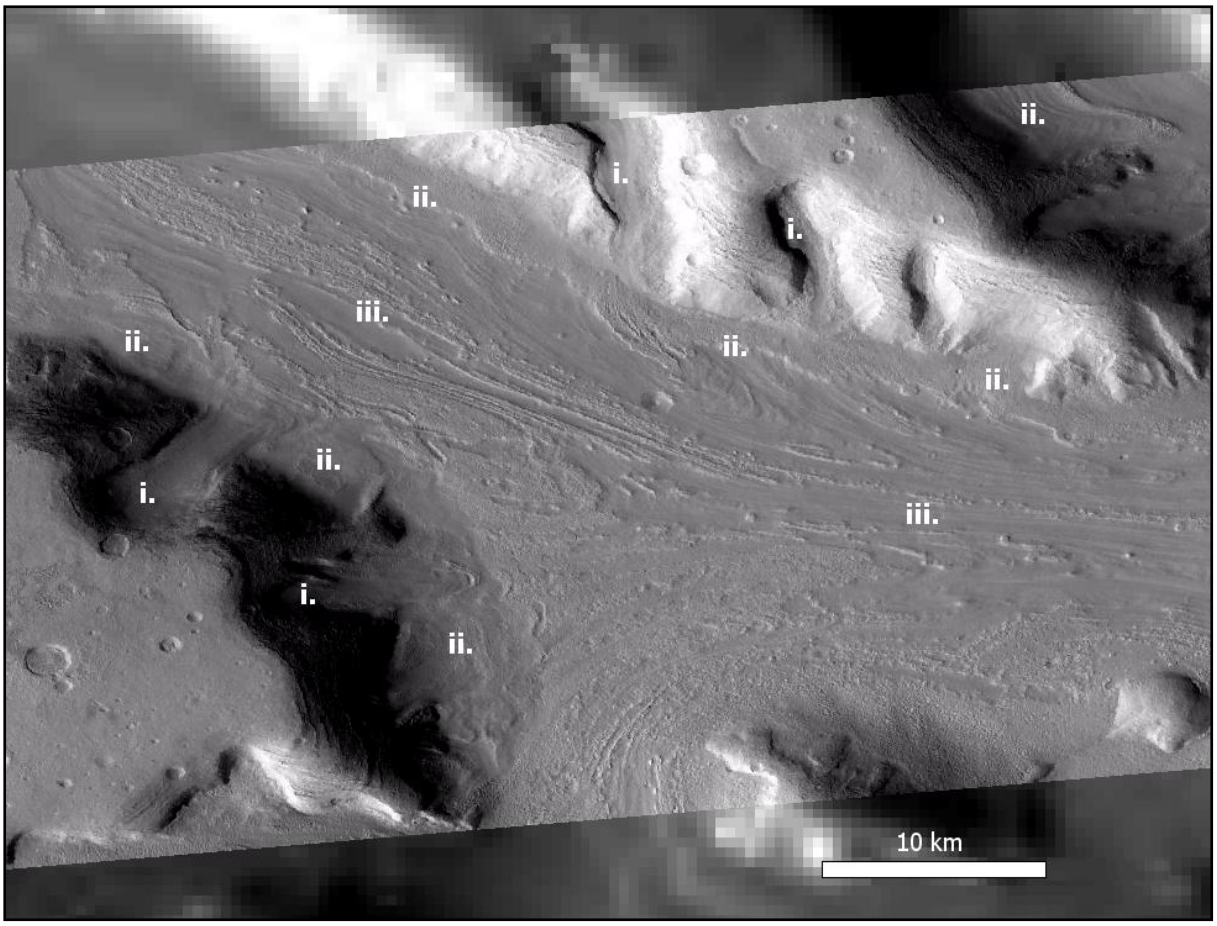

Figure 7: An integrated glacial landsystem on Mars of the type described by Head et al. (2010). Different components of this system are annotated as follows: GLFs (i.); LDA (ii.); LVF (iii.). GLFs (i.) can be seen flowing from cirque-like alcoves (in the bottom left and top right of the frame) and contributing to the laterally-extensive LDA (ii.) which line the valley. This LDA then converges in the valley centre to form LVF (iii.). This scene is a subset of CTX image P17_007715_2232_XN43N312W (detail centred at 47.477 E, 44.213 N), projected on a backdrop of THEMIS daytime Infra-red (IR) imagery. The image is oriented north-up and illumination is from the left.

imagery being only the surface expression of this flow (Squyres, 1978, 1979). Such convexity and 'deep' flow in martian LDAs was initially interpreted as evidence of interstitial ice deposits which 'lubricate' debris throughout the vertical profile (Head et al., 2005). This suggests that VFFs may move under the pressure of their own weight in a manner comparable to terrestrial glaciers, which flow down-slope under the forces created by ice overburden.

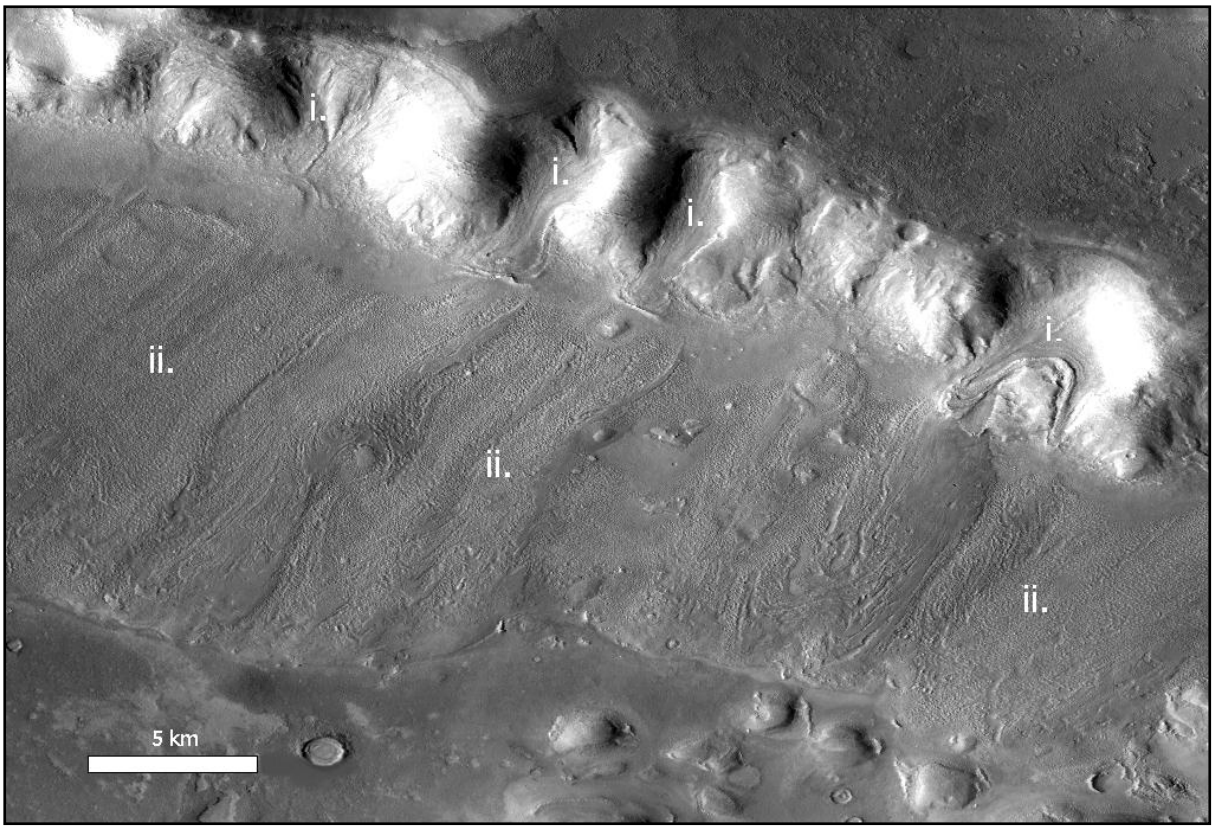

Figure 8: A subset of CTX image P20_008770_2240_XN_44N322W (detail centred at 37.348 E, 44.984 N) showing a well developed LDA flowing away from a raised mesa in western Protonilus Mensae. The LDA (ii.) is flowing from the top right of the frame to the bottom left. In this case it is being fed from above by numerous GLFs (i.). The image is oriented north-up and the illumination is from the left.

Definitive evidence demonstrating the exact composition of LDAs remains elusive. Early hypotheses suggested that viscous interstitial ice may have been gradually incorporated into LDAs, possibly in association with rockfall debris from adjacent cliffs (which may either have brought ice with it (Head et al., 2005), or may have fallen onto small amounts of H_2O frost which seasonally accumulated on talus slopes below) (Squyres, 1979). However, recent research (e.g. Holt et al., 2008; Plaut et al., 2009) has, as discussed in Section 2.2, lent credence to an airfall origin and thus a predominantly ice-based composition. Unfortunately, a comprehensive SHARAD survey has yet to be performed for all VFFs and therefore the possibility exists that compositions could vary among LDAs and other VFFs. However, morphometric analyses of GLFs (see Section 3.2.3) by Souness et al (2012) indicate some level of

homogeneity in the origins and structural and compositional characteristics of VFFs. Debate however still persists on the subject.

3.2.2. Lineated Valley Fill (LVF)

Lineated valley fill (LVF) forms on valley floors from the convergence of two or more LDA-type flows (Squyres, 1979; Lucchitta, 1984). This convergence of opposing LDAs can produce a diverse range of complex patterns and contorted surfaces (Figure 9). These regularly appear to be enhanced and dissected by processes of sublimation and disaggregation, forming what is often referred to as thermokarst (e.g. Van Gasselt et al., 2010), this name specifically implying melting and thermal weathering of interstitial ice deposits. This thermokarstic surface is interpreted by some as evidence for an episodic climatic history, a changeable environment having led to the repeated contribution and subsequent removal of mass from the LVF, in a manner similar to that which is proposed for the evolution of the dissected mantle terrain (e.g. Van Gasselt et al., 2010) (Section 2.1 above). In all likelihood a combination of flow-related strain and thermokarstic re-working is responsible for the present-day morphology of LVF, the flow component being exemplified by occasional complex arcuate patterning and the apparent tendency of lineations to orientate parallel to the valley walls. Where two or more large valleys converge it is not uncommon for LVF to be quite chaotic in appearance (Figure 9).

3.2.3 Glacier-Like Forms (GLFs)

Glacier-like forms (GLFs) represent the most morphologically and visually distinctive sub-type of VFF. Broadly speaking, GLFs (Hartmann et al., 2003, Hubbard et al., 2011) are similar in appearance to terrestrial valley glaciers, generally forming in small cirque-like alcoves or valleys from which they often appear to flow (Figure 10), apparently transporting mass and debris derived from the valley walls (Head et al., 2010) and possibly depositing it in the lower reaches of the basin. Most have a broad upper basin that merges gradually with the surrounding topography, and an elongate

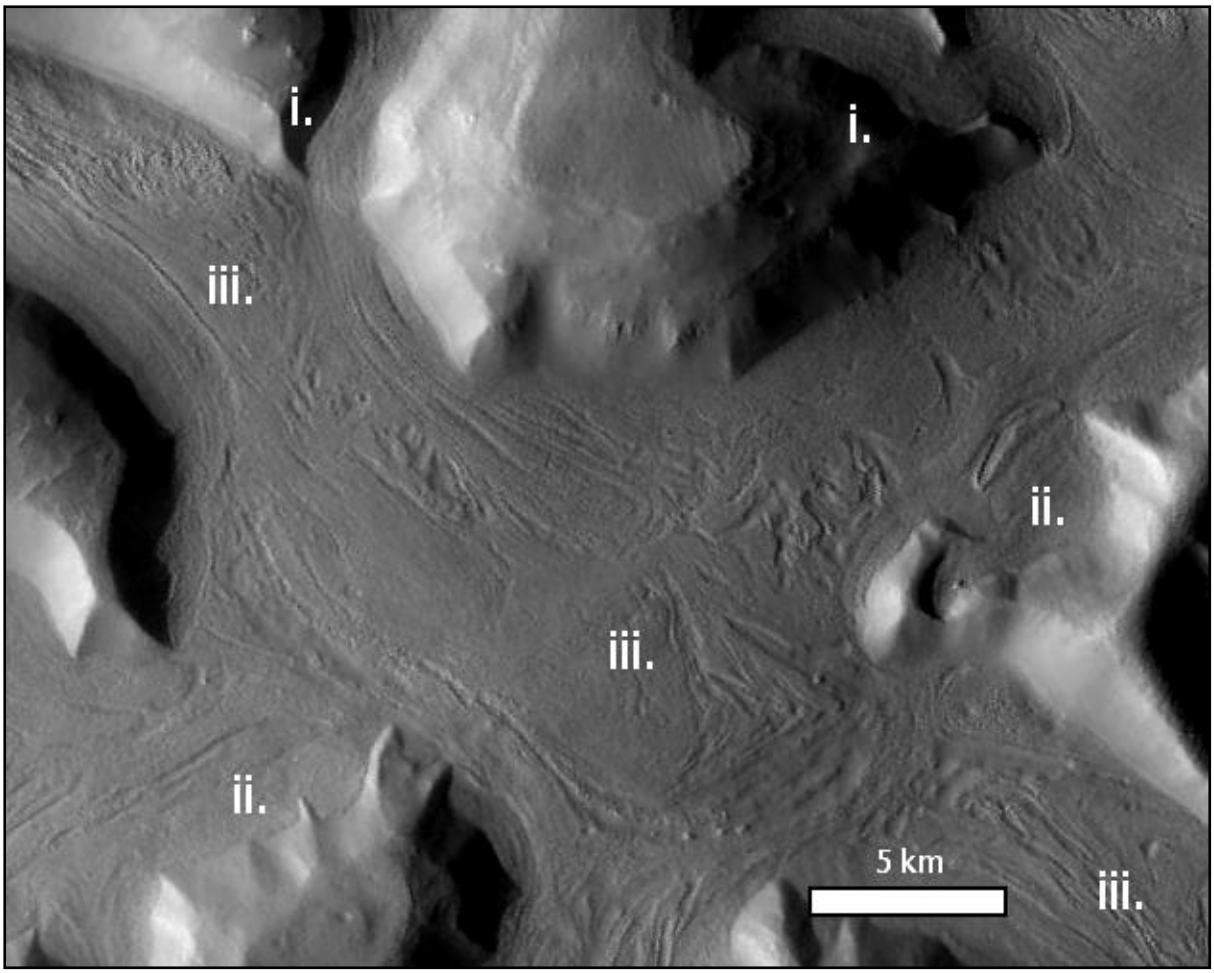

Figure 9: A subset of CTX image P02_001768_2160_XI_36N303W (detail centred at 56.650 E, 35.543 N) showing complex patterning of LVF in Coloe Fossae. In this image LVF from 5 independent valleys appears to converge in a central basin, resulting in extensive compression and deformation of the icy material. Various components of the integrated glacial landsystem (Head et al., 2010) are shown and annotated: GLF (i.), LDA (ii.) and LVF (iii.). This image is oriented north-up and illumination is from the left.

tongue that is typically confined by raised bounding ridges (Arfstrom and Hartmann, 2004; Hubbard et al., 2010), broadly consistent with terrestrial valley glaciers. Although GLFs commonly occur in isolation and need not necessarily be part of an integrated glacial landsystem, it is often the case that GLFs appear in association with other sub-types of VFF. There are many instances where GLFs can be seen to flow from their cirque-like alcoves and merge into the upper reaches of LDAs (Figures 7 and 8). This phenomenon is particularly common in Protonilus Mensae and Deuteronilus Mensae (Figure 1). Indeed, in some cases LDAs include mass

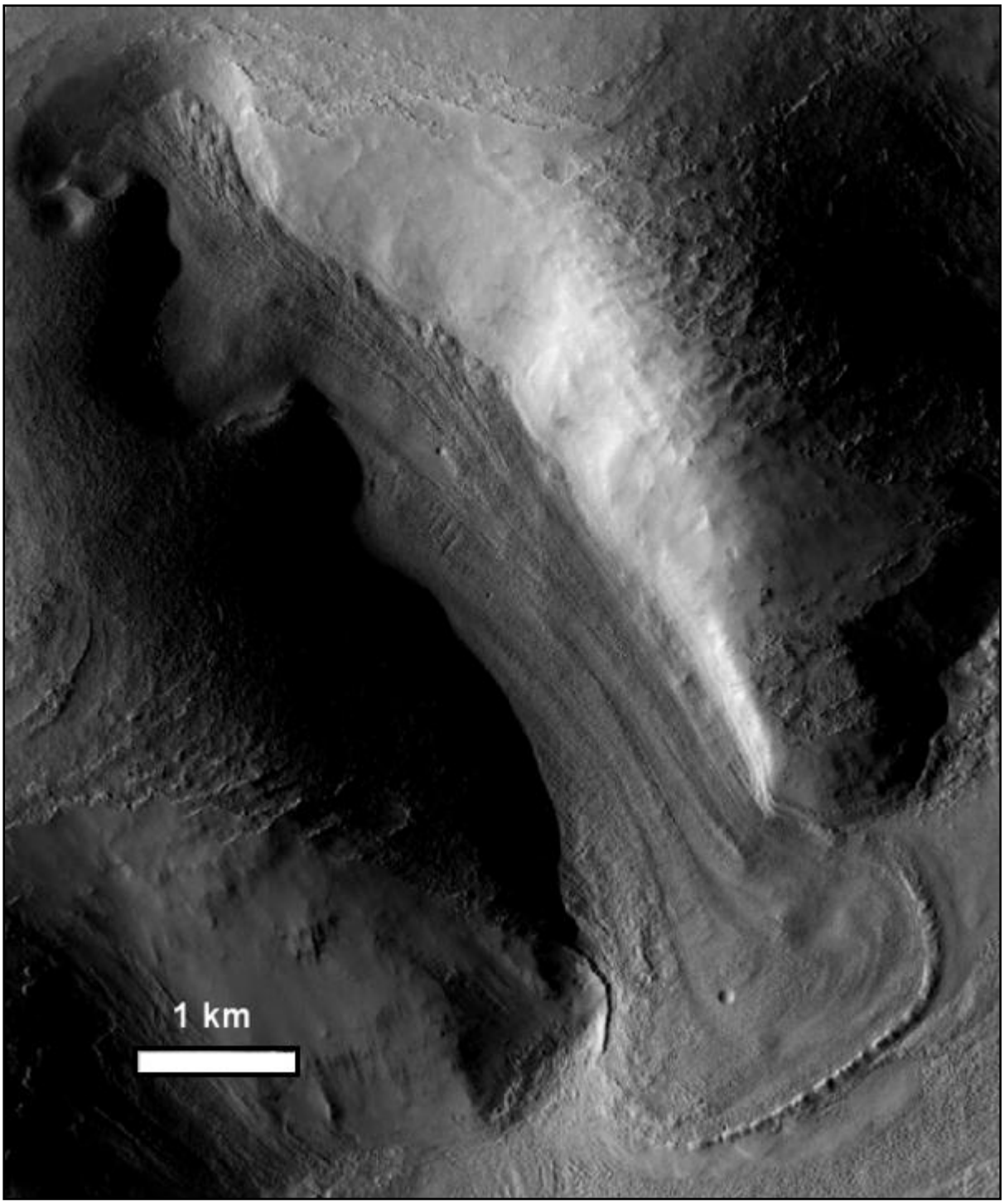

Figure 10: This subset of CTX image P22_009455_2214_XN_41N305W (detail centred at 54.711 E, 41.241 N) shows a well-formed GLF in eastern Protonilus Mensae, similar in overall morphology to a terrestrial valley glacier. Mass appears to flow from cirque-like alcoves from whence it is channelled down-valley toward the terminus. Longitudinal foliation similar to medial moraines appears where these flows converge. MLRs are also visible around the feature's terminus (see also figure 8). Rifts resembling crevasses, as seen on many terrestrial glaciers, can be distinguished on the left (true right) of the GLF. This image is oriented north-up and illumination is from the left.

solely derived from several GLFs. In most cases, however, LDAs appear to have formed without the inclusion of any well-developed GLF-type flows. However, if Mars' integrated glacial landsystems were to be viewed from the perspective of catchment hydrology, GLFs could be described as the lowest-order component of the system, commonly occurring at the highest elevations and representing the source of initial ice mass input to VFFs more generally.

A detailed geomorphological and glaciological analysis of a single GLF (located in Crater Greg in the eastern Hellas region) was reported by Hubbard et al. (2011), who identified and characterized a range of distinctive terrain types located on and adjacent to the GLF's surface and within the confines of the pronounced moraine-like ridges that enclose the GLF (see Figure 6). Analysis of these terrains in the context of the local geomorphology and overall GLF appearance led Hubbard et al (2011) to conclude that this GLF has, since reaching its maximal extent, experienced an extended period of recession, interspersed by several episodes of still-stand or re-advance. Furthermore, the landforms preserved in the pro-glacial area (possibly a former glacier bed) have led to speculation that this GLF may have been wet-based (i.e. featured an active sub-glacial hydrological component) at some point in its recent geological history, a possibility that could have important implications for our understanding of Mars' climate during the Amazonian epoch.

4. Fabric and mechanical properties of VFFs

VFFs on Mars have been compared to terrestrial rock glaciers (e.g. Squyres, 1989; Colaprete and Jakosky, 1998; Milliken et al., 2003), the term referring to a loosely-classified (and relatively poorly understood) suite of lobate rock debris masses, cemented by a deforming matrix of inter-granular ice or frozen sediment, which flow down-slope in a manner similar to glaciers (Washburn, 1979). The tendency for terrestrial rock glaciers to develop clear, arcuate, concentric supraglacial flow structures makes them a very tempting analogue for many martian VFFs, which commonly display similar morphologies (Figure 11). However, while evidence has

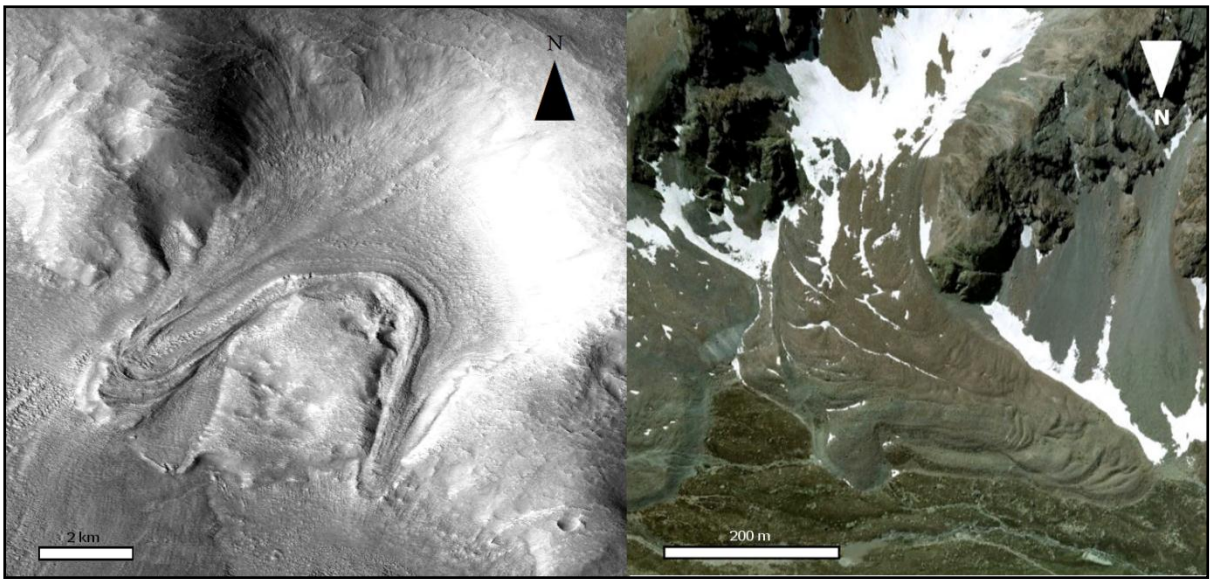

Figure 11: A comparison of a martian GLF (left) (featured in CTX image P20_008770_2240_XN_44N322W and situated at 37.545 E, 45.026 N in western Protonilus Mensae) to a terrestrial rock glacier as described by Washburn (1979). This rock glacier is located at 9.929 E, 46.504 N in the Val Muragl, near Pontresina, Switzerland (image from Google Earth^{TM}). The two features share various characteristics, including multiple flow units, complex lobate morphologies and mid-channel chevrons.

recently been published which favours an ice-rich rather than debris-rich VFF composition (e.g. Holt et al., 2008; Plaut et al., 2009) (see Section 2.2), relatively little is known about the internal structure of most VFFs (or indeed of rock glaciers on Earth) so it is arguable that the analogue has yet to be fully explored.

Understanding the rheology of VFFs still presents many problems as there are still many aspects of VFF structure that are not yet fully understood. Milliken et al. (2003) modelled the stress-strain rate within observed VFFs using a flow-line application of the shallow ice approximation commonly (at that time) applied to glaciers on Earth (Paterson, 1981). Although subject to potentially large errors - particularly since VFF density and thickness were (and indeed remain) unknown - Milliken et al. (2003) calculated basal shear stresses ~10^{-2} MPa for VFFs estimated to be 10 m thick, and ~10^{-1} MPa for VFFs estimated to be 100 m thick.

Another obstacle to reliable estimates of VFF flow rate, either at present or in the past, is the unknown nature of conditions at the bed of VFFs. There has been a

general consensus that VFFs are ‘cold-based’, i.e. they are frozen to the underlying surface (Head and Marchant, 2003; Shean et al., 2005). This conclusion is based on the absence of substantive evidence for wet-based glaciation (e.g. proglacial or lateral meltwater streams which visibly drain the bed of VFFs) and on the prevailing low atmospheric temperatures that occur ubiquitously on Mars at present (Read and Lewis, 2004). Thus, theoretical flow models typically assume that VFFs have been frozen to their bed and that most flow occurs as ductile deformation within the basal layers of the feature, although not at the ice-bed interface. Consequently, driven by terrestrial analogues, it is assumed that VFFs have exerted minimal erosion on underlying bedrock or sediments in accordance with the dominant understanding of cold-based glaciation on Earth (e.g. Jansson and Glasser, 2005). However, a number of recent investigations of VFF morphology and associated landforms suggest that martian glaciation may, during some period in the past at least, have been at least partially wet-based (Arfstrom and Hartmann, 2005; Hubbard et al., 2011). Hubbard et al (2011) identified textures and landforms in the pro-glacial area of one feature in Crater Greg (eastern Hellas) which suggest that some re-working of basal sediments by glacial action has taken place. This would appear to preclude a purely ‘cold based’ scenario as some basal sliding would have been necessary in order to produce such re-worked deposits. Also, features similar to eskers (a glacio-fluvial landform found in terrestrial de-glaciated areas) were observed in proximity to the GLF investigated (Hubbard et al., 2011). At the very least, liquid water does appear to have been an active geomorphological agent at the surface and in the vicinity of some VFFs. A survey of CTX imagery conducted by Fassett et al. (2010) revealed many examples of small supraglacial and proglacial valleys situated atop or in association with martian mid-latitude VFFs. These were observed to be qualitatively similar to terrestrial meltwater channels (Fassett et al., 2010).

If GLFs and other VFFs have indeed been wet-based at some point in their existence, the extent to which VFFs are credited with shaping Mars’ landscape would require considerable re-evaluation since wet-based glaciers are a far more potent agent of erosion, deposition and landscape change than their ‘protective’ cold-based counterparts (e.g. Sugden, 1978).

5. Summary and avenues for future research

5.1. Summary

A varied suite of broadly glacial landforms has been described (e.g. Marchant and Head, 2007; Milliken et al., 2003; Head et al., 2010) and mapped (e.g. Milliken et al., 2003; Souness et al., 2012) in Mars' mid-latitude regions. This suite includes the widespread dissected mantle terrain as described by Kreslavsky and Head (2000; 2002), rampart-like LDAs (e.g. Squyres, 1978, 1979), complexly-patterned LVF (e.g. Squyres, 1979; Lucchitta, 1984) and the low-order, topographically constrained and linear GLFs (as described by Hubbard et al., 2011 and Souness et al., 2012). LDAs, LVF and GLFs are all sub-types of VFF and are described by Head et al. (2010) as individual components of an integrated martian glacial landsystem (Figures 7 and 9). Compelling evidence exists to suggest that all VFFs are composed predominantly of massive water ice (Holt et al., 2008; Plaut et al., 2009), and that they are relict features from a geologically recent martian glacial period (e.g. Forget et al., 2006; Schon et al., 2009) that have lain preserved until the present day beneath a thin layer of sediment (e.g. Fanale et al., 1986; Bryson et al., 2008).

5.2. Avenues for future research

5.2.1. VFF origin and evolution

Many aspects relating to both the origin and mechanics of martian VFFs remain poorly understood (for example see Section 2.2 which outlines the debate over mechanisms of initial ice deposition), leaving substantial scope for future work. According to prevailing planetary-scale system models cryospheric processes are closely linked to climate on a global scale, and climate is, in turn, recognised as playing a key role in the development of both the planet's surface structures and its capacity for supporting life. Therefore developments in our understanding of VFFs could have wide-ranging ramifications for our understanding of Mars' climate and the chronology and mechanics of the planet's surface-forming events.

Most work to date that has been directed at expanding our understanding of martian VFFs has revolved around the use of terrestrial analogues, with Earth's glaciers and glacial processes providing theoretical models of accumulation, flow, landscape modification and climatic interaction. However, it is still unknown whether some of even the most fundamental aspects of the terrestrial glacial model apply to Mars. For example, the links between climate, topography, ice accumulation and landscape evolution are poorly understood. On Earth, the locations and rates at which glaciers grow and flow are primarily determined by mass inputs and mass outputs. The relationship between a glacier's mechanical evolution and these factors (primarily a function of temperature and precipitation) is known as its mass-balance regime. It is generally assumed that a mass-balance regime either operates on Mars, or at least has operated in the past when Mars' VFFs were active. However, whether this regime (or at least its systematic variation with elevation) is/was comparable to that on Earth is still unknown. Indeed, this seems highly improbable given the likelihood that temperatures on Mars have been ubiquitously below the H_2O freezing point across Mars' full altitudinal range. With such different base conditions on Mars, these differences including lower temperatures, gravity and atmospheric density, it seems inevitable that profound contrasts exist in the manner in which common mechanisms will express themselves on the two planets, a problem explored to some extent by Howard (2009) and Pelletier et al. (2010). These factors make it difficult to hypothesise with confidence regarding even the fundamentals of VFF initiation and the spatial expression of mass accumulation responsible for driving the flow which has been so well documented from geomorphological evidence. Some work has already been produced pursuing this line of inquiry, including observations of the apparent altitude dependence of landforms apparently relict from 'tropical mountain glaciers' in Mars' Tharsis volcanic region (Fastook et al., 2008). Several studies also exist describing the apparent latitude dependence of ice deposits on Mars (e.g. Kreslavsky and Head, 2002; Milliken et al., 2003; Forget et al., 2006) (see Section 2). However, further research into where VFFs occur, both presently and in the past (from residual trace landforms), along with further detailed analyses into VFF population characteristics such as that conducted by Souness et al (2012), who examined the distribution of GLFs and how it relates to geographical factors such as latitude, elevation, aspect and local topography, could help shed light on the question of how mass balance operates on Mars and help ascertain the validity of

the terrestrial model in a martian context. Development of this model for application to Mars could in turn permit the development of high resolution numerical models of past martian glacial episodes and, by extension, Mars' past climate.

5.2.2. VFFs and liquid water

Whether martian VFFs have always been cold-based or if they have experienced warm-based or thermally-mixed (polythermal) conditions also has importance for on-going attempts to understand Mars' past climate and its relationship with cryospheric processes. Furthermore, as polythermal or warm-based glaciation requires the presence of liquid water within the glacial system, a more developed understanding of VFF thermodynamics, particularly in the basal zone, could have widespread implications for the way we think about water on Mars. Not only would this impact upon theories relating to the presence or establishment of life on Mars, but it would markedly alter the extent to which Mars' surface evolution could be attributed to glacial processes, warm-based ice being a far more effective agent of erosion than cold-based ice (see Section 4). The thermal characteristics of a glacier's bed and the interaction of liquid water and flowing ice have large and, broadly speaking, well-understood impacts on terrestrial glacial processes and thus glacier morphology. It therefore follows that, using terrestrial analogues, further analyses of the various features found on, and in association with, martian VFFs that are possibly of fluvial origin, such as those previously performed by Fassett et al. (2010) and Hubbard et al. (2011), in conjunction with more developed studies of martian VFF structure (made with a view to assessing the likelihood of liquid water's involvement either basally, interstitially, englacially or supraglacially) could prove most informative. This issue also dovetails directly into questions of VFF structure. Existing works investigating the phenomenon of liquid water in conjunction with VFFs and tackling the possibility of polythermal glaciation on contemporary or geologically recent Mars include Fassett et al. (2010) and Hubbard et al. (2011).

5.2.3. VFF composition and structure

Although recent evidence describing the internal structure of VFFs points to a composition of predominantly H_2O ice and thus an airfall-driven mode of accumulation (Holt et al., 2008; Plaut et al., 2009), the available data on VFF composition is still extremely limited, being confined to observations made at only a small number of sites. A more detailed database of VFF internal structure including SHARAD data for a wider range of VFFs across Mars, describing variations in structure between landforms and within local populations would greatly enhance our understanding of VFF mechanical properties, helping us to more accurately model both (i) spatially-variable accumulation patterns and (ii) general ice flow rates. This in turn could help to further refine our ability to constrain the age of Mars' glacial features and thus assist in better mapping the chronology of Mars' geomorphological and climatic evolution. Although the inaccessible nature of martian field sites and limitations in the available technology seriously inhibit the feasibility of taking more direct, surface samples, such a study would be valuable. Insights into the composition of Mars' dissected mantle terrain have been gleaned from direct observation of ice deposits in impact-generated exposures and dissected sedimentary structures (e.g. Schon et al., 2009; Dundas and Byrne, 2010), but no such discoveries have yet been made on VFFs.

5.2.4. VFF activity and mechanical history

The extent to which VFFs and associated landforms are relict or whether they continue to undergo change and development remains uncertain. Even the generalised pattern of flow (historic and / or contemporary) within VFFs is poorly understood. Attempts to quantify stress and strain patterns more accurately within VFF sub-types could prove extremely valuable, especially to the ice flow modelling and palaeo-ice sheet reconstruction communities. Studies of the interrelationships between the various, previously classified (see Section 3), types of feature (beyond what has already been attempted) could also prove most enlightening. In this context, a more developed understanding of the rate at which VFFs are re-surfaced by processes such as sublimation, dissection and viscous relaxation could also aid in

the development of new and more reliable dating techniques and flow models. Some studies already tackling this issue, both on VFFs and in other icy martian environments, include those by Mangold (2003), Levy et al. (2009) who have investigated the modification of LVF and LDA surfaces in the time elapsed since their deposition / formation, and Van Gasselt et al. (2010) who have attempted to quantify the rate of viscous relaxation and thus crater annealing in ice deposits at the martian dichotomy boundary.

B. Preface to Chapter 2

B1. Introduction to Chapter 2

As discussed in Chapter 1 (Section 5.2), many aspects relating to both the origin and mechanics of martian VFFs remain poorly understood.

Chapter 2 of this thesis (now published in *Icarus* [Souness et al., 2012]) provides an empirical overview of glacier-like forms (GLFs [see Hubbard et al., 2011; also Section 3.2.3]), presenting broad initial observations on feature distribution and morphology, as well as contextual information and interpretations at a planetary and hemispheric scale. These analyses contribute new data in themselves, but were primarily designed to facilitate more detailed, higher spatial resolution investigations such as those presented in subsequent chapters.

In the remainder of this preface we set out the justification for the work presented in Chapter 2 and the architecture of the survey that was undertaken, as well as presenting some discussion of biases in the data.

B2. Study of GLFs

Offering a glaciological perspective to martian cryospheric studies involved using Earth's glaciers as analogues, drawing from terrestrial glaciological literature. Therefore, we saw it as prudent to concentrate on investigating a sub-class of viscous flow feature (VFF [see Chapter 1, Section 2.3]) that provides the best potential for effective inter-planetary glaciological comparison. Accordingly, the investigations undertaken and discussed in Chapter 2 concentrate exclusively on GLFs. We clarify this point here as it is not underwritten specifically in Chapter 2. By excluding lobate debris aprons (LDA [see Chapter 1, Section 3.2.1]) and lineated valley fill (LVF [see Chapter 1, Section 3.2.2]) we do not suggest that these other VFF sub-types necessarily formed in a different way from GLFs, or that they are compositionally different.

At the time the work presented in Chapter 2 was initially undertaken, GLFs had not specifically been described or classified in the literature. A detailed description of one GLF in Mars' eastern Hellas region (See Figure 1, Chapter 1) has subsequently been published by Hubbard et al. (2011). However, prior to conducting the work in Chapter 2 it was still necessary to devise a set of criteria that would facilitate the repeatable discrimination of GLFs from other associated VFFs. Drawing on criteria previously used for identifying VFFs by Milliken at al. (2003) and on material within the body of terrestrial glacial literature, the following criteria were devised, stating that in order to qualify as a GLF, a feature must:

(i) be surrounded and constrained by higher topography and show general evidence of flow over or around obstacles.
(ii) be distinct from the surrounding landscape, exhibiting a texture or colour different from adjacent terrains.
(iii) display surface foliation indicative of down-slope flow; e.g. compressional / extensional ridges, surface lineations or arcuate surface morphologies or surface crevassing.
(iv) have a length to width ratio > 1 (i.e. be longer than it is wide), and thus be distinct from the apron-like LDA class of feature.
(v) have either a discernable 'head' or a discernable 'terminus' indicating a compositional boundary or process threshold.
(vi) appear to contain a volume of ice (or some other viscous substance), having a relatively flat 'valley fill' surface (Figure 1b), thus differentiating it from an assemblage of post-glacial type landforms.

These criteria are reiterated in Chapter 2, Section 2.2.

B3. Initial GLF survey design

The first component of the research presented in Chapter 2 is a survey of Mars' mid-latitudes, undertaken in order to count, isolate and characterise Mars' GLFs. This survey was conducted using Context Camera (CTX) images (~6 m/pixel resolution). Prior to undertaking this research (presented concisely in Chapter 2), some

preliminary steps were taken and initial analyses of the available data performed to ascertain that: (i) the correct approach was being taken to the survey; (ii) the appropriate dataset was being used; (iii) this dataset was being sampled in the correct manner. The preliminary measures taken to satisfy these initial concerns are described here for completeness.

B3.1. Survey necessity check

Our GLF survey was based on the earlier survey of VFF distribution conducted by Milliken et al. (2003). This previous survey was carried out using data from the high resolution but narrow swath-width (see Preface to Chapter 1, Section A3.1) Mars Orbiter Camera (MOC). Prior to designing and conducting our own survey (using more recent, more abundant and higher swath width, albeit lower resolution, CTX data [Preface to Chapter 1, section A3.1]) those MOC images identified as containing VFFs by Milliken et al. (2003) were re-visited in order firstly to apply and test the criteria devised to isolate GLFs from the wider population of VFFs (Section B.2), and secondly to confirm that a comprehensive (and labour-intensive) survey of the available CTX data was indeed necessary. This check of Milliken et al's (2003) output data would also help to constrain the format that this new survey, if deemed necessary, should take.

Milliken et al. (2003) originally identified 146 images from a sample of over 13,000 that contained one or more VFFs. We revisited these 146 images, checking them specifically for GLFs. This produced the map shown at Figure 1. Only a very small proportion (14 images / ~10 %) of this MOC imagery sample contained features that qualifed under our criteria as being GLFs. A concentration of positive images is apparent in the eastern Hellas area of Mars' southern mid-latitudes (Figure 1) and a handful of others are scattered around this latitudinal zone. However, in the northern hemisphere only a single image was recognised as containing GLFs.

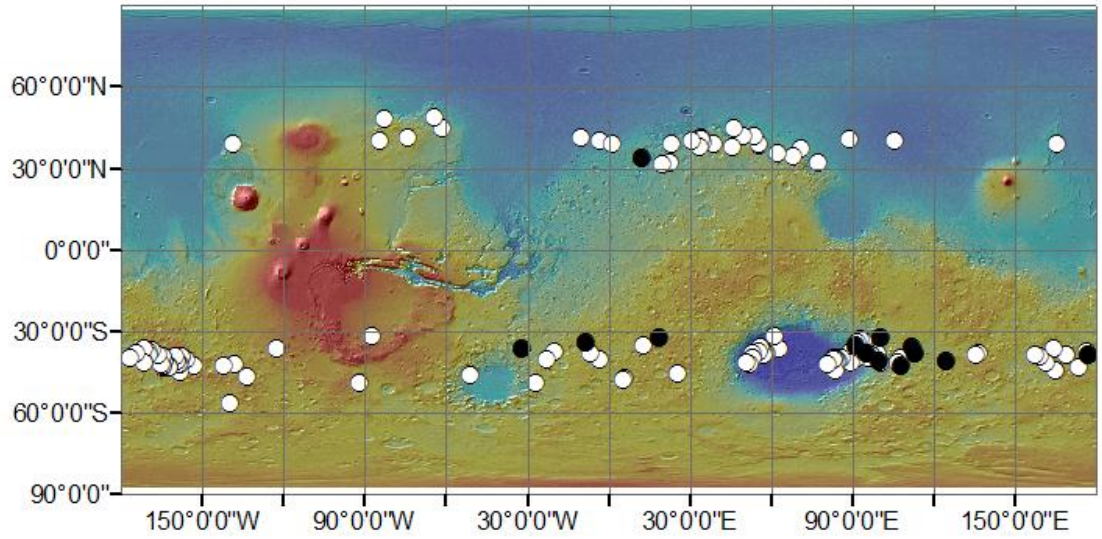

Figure 1: Mars Orbiter Laser Altimeter colourized grid showing the distribution of MOC images identified by Milliken et al. (2003) as containing VFFs (white spots), and those identified in this study as containing GLFs (black spots).

The small number of GLFs identified in this analysis of Milliken et al's inventory highlighted the necessity of undertaking a new survey using the lower-resolution, but wider swath-width and more spatially comprehensive, CTX imagery.

B3.2. Defining the geographical limits of the survey

Although the surface coverage provided by the narrow-angle MOC imagery used by Milliken et al. (2003) proved insufficient for mapping GLFs, the distribution map of miscellaneous VFFs produced by Milliken et al. (2003) (Figure 1) showed compelling evidence that glacial landforms on Mars are presently found almost exclusively in the mid latitude regions between the 30th and 60th parallels of both hemispheres. Therefore, using this prior survey as a guide, it was decided to target the secondary survey upon these areas, thereby saving undue effort surveying non-glacierised latitudes and maximising the practicable spatial resolution of the survey. However, to ensure comprehensive inclusion, it was decided to expand the latitudes identified by Milliken et al. (2003) by 5º on either side of each hemispheric range. The regions of

interest (ROI) for the new survey were therefore finally defined as the latitudes lying between 25º and 65º north and south.

B3.3. Familiarisation with the subject matter and methods

B3.3.1. Trial run survey

Imagery data were acquired during a 3 week orientation and research visit to the California Institute of Technology (Caltech) in November 2009. During this period the opportunity was also taken to conduct a trial-run survey under the guidance of Dr Ralph Milliken. This survey was conducted over two weeks using 1600 images captured over Mars' northern mid-latitudes. It was possible to explore the various image viewing methods available, become familiar with the range of landforms present in Mars' mid-latitudes, get a fuller picture of dominant landscape trends, atmospheric conditions (relating to visibility), nuances of the viewing technique and, importantly, to 'get an eye' for perspective and relief in single band, monochrome imagery. This enabled us to mitigate against error due to variable camera perspective and inexperience during the early stages of the subsequent main survey.

B3.3.2. CTX survey technique

During the trial-run survey a survey technique was developed which maximised efficiency and minimised the risk of double-counting individual GLFs. Individual images were tabulated in Microsoft Excel and their image IDs hyperlinked to their respective online viewing page (Figure 2.). These pages are maintained by the School of Earth and Space Exploration within Arizona State University (http://viewer.mars.asu.edu/planetview/). Using these hyperlinks, images can be viewed quickly and at full resolution without downloading any data directly, a process that can be extremely lengthy. The individual images were also ordered sequentially

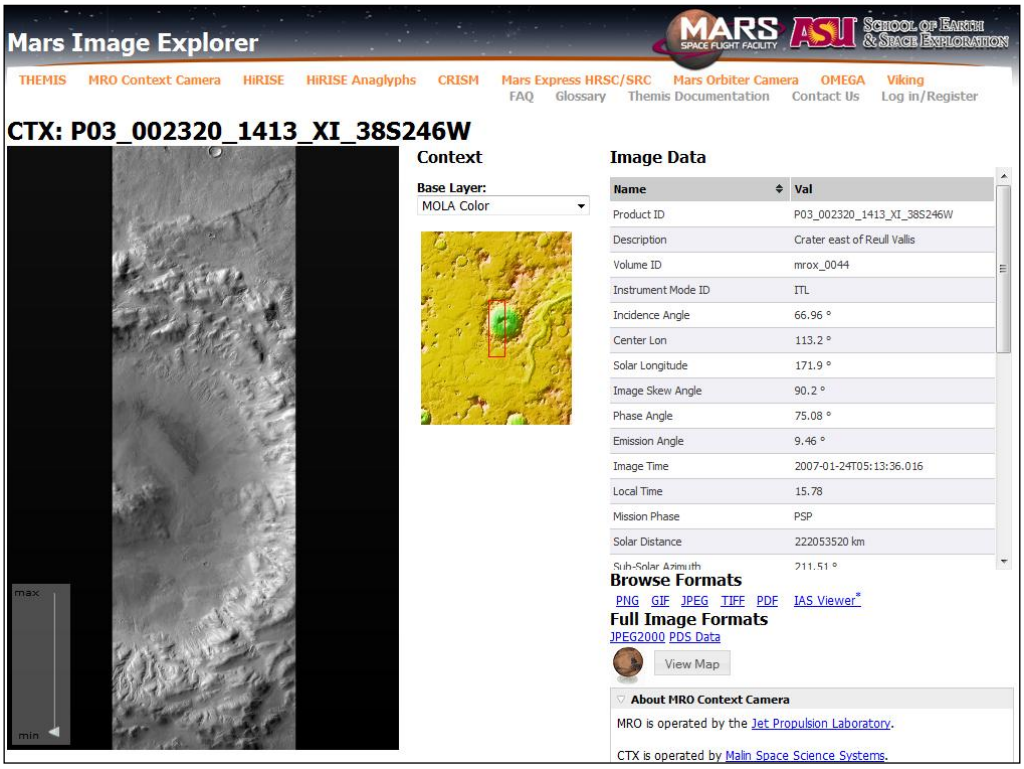

Figure 2: The Arizona State University 'Mars Image Explorer viewing page for CTX image P03_002320_1413. A zoomable and manually navigable version of the complete image is featured to the left. On the right of this is a small MOLA context image, displaying a shapefile outlining the exact location of the main featured CTX image on the martian surface. This feature was extremely useful in that it permitted the viewer to keep track of context when inspecting CTX images, reducing the chances of accidental result duplication or 'double head-counting' in the GLF census. The only complication is that, as can be seen, the MOLA context image is inverted (rotated 180 degrees rather than flipped) for reasons unknown to the author.

by longitude, information on which was contained within the image IDs. This permitted the systematic survey of the ROIs, observations progressing westwards consecutively.

B4. Data acquisition

A spreadsheet containing the image I.D. codes and locator coordinates for every CTX image captured from the time of initial MRO Mars orbital insertion to November 2009 was attained from Caltech. From this initial image set, only those images

centred in Mars' mid-latitudes (25º - 65º north and south) were required. Therefore, the files were sorted by latitude and were divided into hemispheres before extracting all those with locator coordinate latitude values within the defined ROI. The end result was a dataset consisting of 8058 images (see Figure 2.3. in Chapter 2 for a map of CTX image distribution).

B4.1. Assessing bias in the dataset

The MRO platform is pointable, permitting images to be specifically and accurately targeted. Therefore, the distribution of the CTX images used in the research presented in Chapter 2 represents the scientific objectives and changing priorities of the various research teams involved with the MRO program at the time of survey design. Consequently, it was expected that the spatial distribution of the image data (drawn as it was from the complete cache, and not from a specifically designed survey set) would contain spatial bias. Prior to beginning a systematic survey of the images this bias was assessed to remove, or compensate for, any gaps or dis-proportionate spatial weightings in the dataset. Note that this analysis was conducted before the decision was made to expand the survey ROIs by 5º north and south. Therefore, the following paragraphs describe measures taken using only 6578 CTX images lying between 30º and 60º north and south.

B4.2. Characterising bias

The distribution of images was mapped by longitude and latitude (Figure 3).

The MRO occupies a polar orbit, therefore its imagery, including that from the CTX, covers swaths that extend roughly north to south. This means there is more overlapping in the latitudinal domain, the image targeting co-ordinates used to plot distribution representing only the centre point of the imaged area. Therefore,

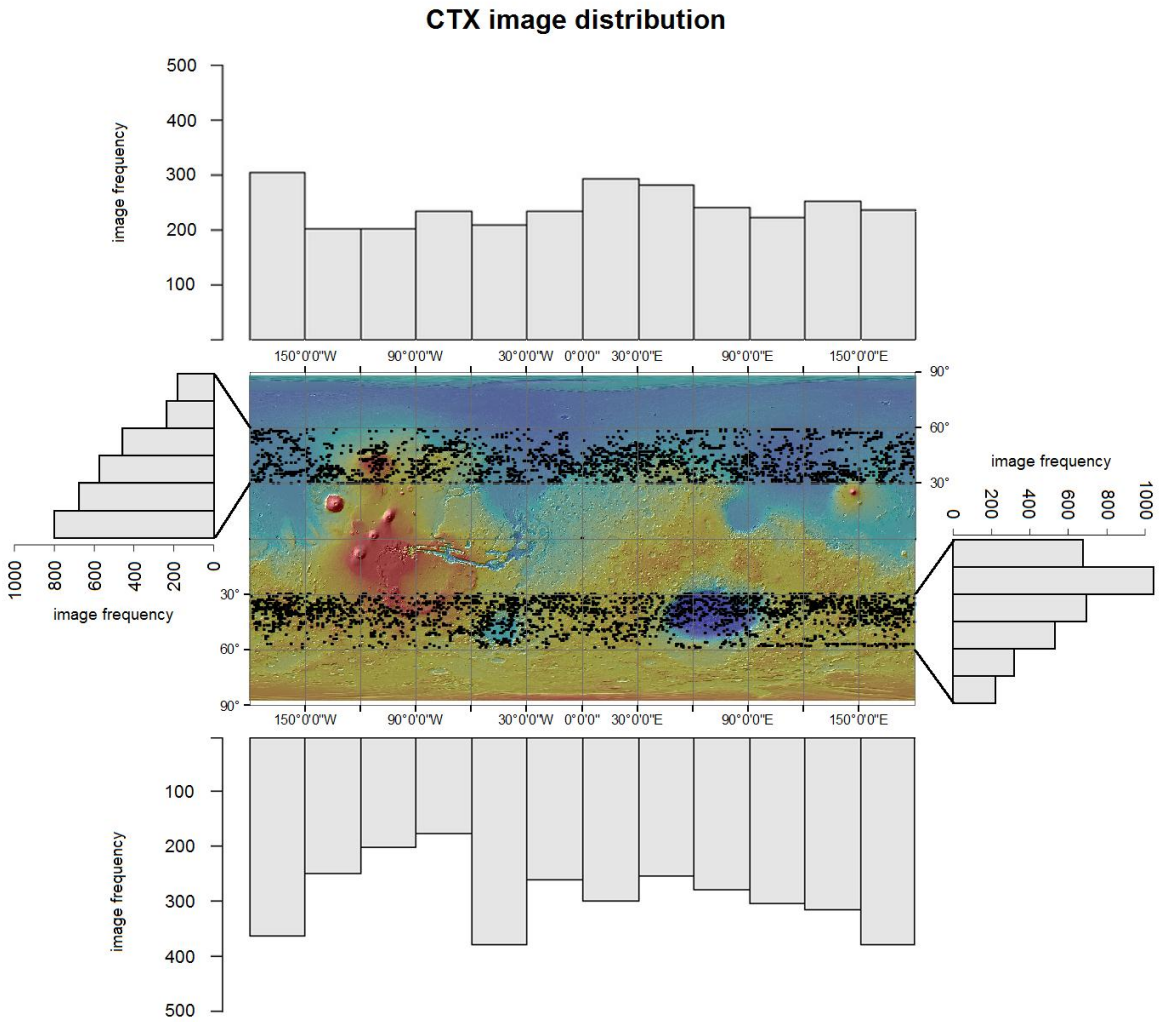

Fig. 3: A composite diagram showing the plotted distribution of the initial mid-latitude CTX image sample set (purple dots overlaid on a colourized MOLA elevation grid) and the frequency of images plotted in north and south hemispheric histograms with 30 degree longitudinal bin size and 5 degree latitudinal bin size. Both sets of histograms show considerable volatility, particularly in the southern hemisphere. Some areas have particularly high image concentrations while others are somewhat sparser. Bin totals in the north have a standard deviation of 34.18, while in the south the standard deviation is 128.4.

longitudinal distribution was plotted first as it was felt that this aspect was more likely to register human-induced statistical bias. Latitudinal distributions were also plotted, for although a strong equatorward bias was expected for the latitudinal distributions (on account of the higher area lying between adjacent lower latitudes as opposed to

higher latitudes), and thus less useful initial observations were expected, any informed quantification of spatial bias would be incomplete without a consideration of both aspects.

Histograms (showing the density of images in 30 degree and 5 degree bins for longitude and latitude respectively) were produced for the longitudinal and latitudinal ranges of each hemisphere's mid latitudes (Figure 3). The standard deviation (Std. Dev.) of the bin totals in each hemisphere were then calculated to give a measure of 'volatility', which we use as a surrogate for bias.

The histograms show a certain amount of bin size inhomogeneity, particularly in the longitudinal ranges. Image density also varies by latitude. However, this conforms strongly (with the exception of the range between 30 and 35 degrees south) to what was expected in light of decreasing surface area towards the poles. On the whole, volatility appears less pronounced in the north than in the south (standard deviations of 34.18 and 128.4 respectively), but in both cases there is definite bias, the apparent tendency being for images to cluster around topographically complex areas or features of geological significance, e.g. Argyre Planitia between 30 and 60 degrees west in the southern hemisphere.

B4.3. Discussion of bias mitigation

Mitigation of the spatial bias in image distribution proved difficult. Numerous techniques were explored and a great deal of time was invested in finding a satisfactory solution. However, minimising spatial volatility whilst optimising temporal coverage resulted in the removal of large numbers of images – so many that the survey was in danger of becoming unrepresentative. Therefore, it was eventually decided to simply accept the existing levels of bias in image distribution and perform an inclusive survey using all the available data, thus simultaneously eliminating the possibility of creating or augmenting what existing bias there was and maximising the areal coverage of the survey by including all the available data.

Chapter 2:
An inventory and population-scale analysis of martian glacier-like forms

1. Introduction

In recent years, the acquisition of very high-resolution images of the martian surface has resulted in various aspects of Mars' landscape coming under increased scrutiny. The result of this is that our understanding of the geological processes which operate at and near the martian surface have become more fully developed. One suite of landforms that has received particular attention is that associated with the presence of, and processes relating to, water ice. Indeed, it is widely held that Mars' recent geological past has been dominated by the action of ice-rich processes (e.g. Kargel, 2004; Baker et al., 2010). Many of these landforms and landscape elements share visible characteristics with terrestrial glaciers (e.g., Marchant and head, 2003; Head et al., 2005; Forget, 2006). The general appearance of these features strongly suggests down-slope flow and deformation, including indicators such as lobate structures, extensional troughs, compressional ridges, and, in many cases, elongated lateral and terminal ridges. Observations of such characteristics have led to the application of the term viscous flow feature or 'VFF' (Milliken et al., 2003). Milliken et al. (2003) defined VFFs as exhibiting: "primary or secondary lobate features of the material (typically in alcoves), lineations on the surface (both parallel and transverse to the slope on which the material flows), compressional ridges or extensional troughs, ridges at the flow front or base of the slope, or other general evidence that the material flowed around or over obstacles such as craters or mounds".

We consider the term 'viscous flow feature', and thus 'VFF', to be a suitable morphological descriptor for the full range of features discussed in this chapter. We therefore utilise this term henceforth as an umbrella term for all glacial-type formations exhibiting evidence of viscous flow. Although Milliken et al. (2003) referred to "metres-thick" deposits of ice, and work has subsequently been presented by other parties (e.g. Holt et al., 2008; Plaut et al., 2009) which suggests that some VFFs have mass depths greatly in excess of this, Milliken et al. (2003) included no requirement of depth in their identification criteria and the term 'viscous flow feature' itself makes no reference to depth, therefore we maintain it as being an appropriate descriptor in this context.

Squyres and Carr (1986) hypothesised that some large scale VFFs, commonly referred to as lobate debris aprons (LDAs), formed through the relaxation of topography underlain by an ice-saturated crust. Indeed, recent results from the Mars Reconnaissance Orbiter (MRO) shallow radar (SHARAD) instrument show that LDAs exhibit properties consistent with a dominantly water ice composition beneath a relatively thin dry surface (Holt et al., 2008; Plaut et al., 2009). Squyres and Carr (1986) and Squyres et al. (1992) also observed that VFFs occurred primarily between 30° and 60° in both hemispheres, with forms appearing to be notably less well developed at latitudes above 55°. Later work supported these observations, and VFFs of various lengths have been described almost exclusively within Mars' mid-latitudes (Milliken et al., 2003; Head et al., 2010). Milliken et al. (2003) conducted a global survey of VFF distribution utilising 13,000 Mars Orbiter Camera (MOC) images. Of these images, 146 included one or more VFFs, almost all of which were located in the mid-latitudes, with the maximum frequency of occurrence lying on the 40° line of latitude in both hemispheres. This distribution is consistent with prevailing theories relating the origin of VFFs to Mars' climatic history which postulate that increased rotational obliquity as recently as ~5 x 10^6 years before present (Touma and Wisdom, 1993) permitted the equatorward migration of moisture from Mars' polar caps, allowing the accumulation (and subsequent flow) of water ice in Mars' mid-latitudes (Head et al., 2003; Forget et al., 2006; Schon et al., 2009). Climate modelling by Fanale et al. (1986) suggested that water ice from this past epoch could remain stable in the mid-latitudes under Mars' current climatic regime if shielded by dust or regolith. The findings of Holt et al. (2008) and Plaut et al. (2009) from SHARAD data have corroborated this hypothesis, raising the possibility that smaller scale VFFs may also contain water ice beneath a thin (0.5 – 10 m), 'dry' regolith layer.

The broadly-defined VFF suite of landforms (see above) includes many variations in morphology and apparent landscape association (e.g. Head et al., 2010). The morphologically distinctive sub-types of VFF include 'lineated valley fill' (LVF), broad and often extensive 'lobate debris aprons' (LDA), and smaller alcove-fed 'glacier-like forms' (GLFs) (e.g. Li et al., 2005; Holt et al., 2008; Morgan et al., 2009; Plaut et al., 2009. Baker et al., 2010; Head et al., 2010; Hubbard et al., 2011) (Figure 1). It should be noted that GLFs were originally termed 'glacier-like flows' by Arfstrom and

Hartmann (2005). However, Hubbard et al. (2011) amended the term to ‘glacier-like form’ on the grounds that: (i) actual motion had not yet been measured, (ii) supplementary (basal) motion components had not yet been ruled out, and (iii) the term ‘flow’ can refer to either a feature or a process. Herein, we also use the term GLF to mean ‘glacier-like form’.

Although the exact composition of icy deposits remains unconfirmed, all three sub-types of VFF (i.e., LVF, LDA and GLF) appear to be composed of a similar material and observations suggest the existence of close inter-relationships. For example, LVF is commonly interpreted to be the product of convergent LDAs, which themselves seem often to be fed by the lower-order alcove GLFs (Figure 1[a]) (Head et al., 2010). GLFs in particular are visually and contextually very similar to terrestrial valley glaciers, having a broad, topographically constrained upper basin that appears to feed material in a down-slope direction into a tongue that is often bordered by raised, moraine-like ridges (Arfstrom and Hartmann, 2005) (Figure 1 [b]). Such moraine-like ridges may be the result of activity more recent than that responsible for the emplacement of higher-order LDAs and LVF (Baker et al., 2010). These and other similarities suggest that GLFs may be of particular value in explaining the origins and processes associated with all types of martian VFF, as it is these valley-glacier-like forms to which terrestrial glacial analogues can be most directly compared. However, direct comparisons with terrestrial analogues are somewhat complicated by the environmental differences between Earth and Mars (e.g. Pelletier et al., 2009).

At present neither the mass-balance relations nor the mechanisms by which VFFs flow are well understood. However, modelling by Milliken et al. (2003) showed that a ~10 m thick layer of ice could produce the observed deformation landforms under present and past martian conditions within the time permitted by current age estimates (10^5 – 10^7 years), while an even thicker deposit would deform faster (Milliken et al., 2003).

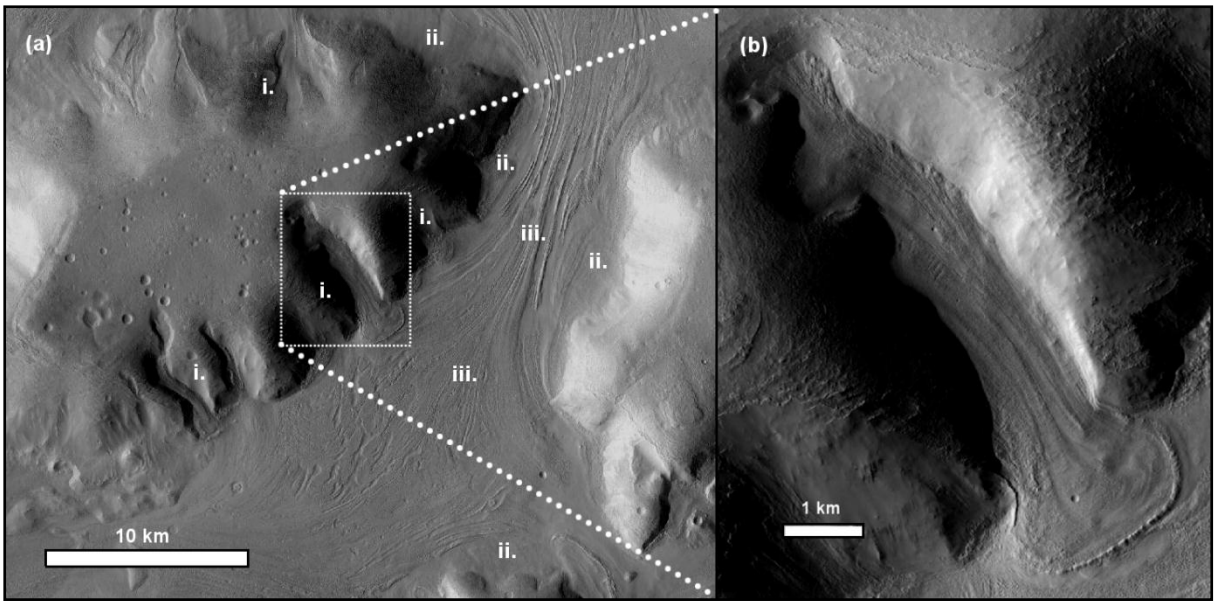

Fig. 1: VFFs in 'fretted terrain' (term first used by Sharp, 1973) in Protonilus Mensae - Mars' northern mid-latitudes (CTX image P22_009455_2214_XN_41N305W). (a) the three dominant sub-classifications of VFF in context. i: low-order glacier-like forms (GLFs); ii: elongated rampart-like lobate debris aprons (LDA); iii: the distinctive, often apparently non-directional lineated valley fill (LVF). Pronounced ridges can be seen along the middle of the LVF, running parallel to the valley walls and suggesting the convergence of opposing LDA. (b) An exploded close-up of a particularly well defined example of a GLF. Note that all images are oriented north-up and that the light source in both cases is from the left.

On Earth, temperature and precipitation (along with the presence of a land base) exert the dominant controls on the global distribution of flowing glacier ice. These factors are in turn mediated by inter-related geographical variables including, most importantly, latitude and altitude. In a global context, ice accumulates at the lowest elevations towards the poles, where air temperatures are coldest. As ambient air temperatures increase towards the equator, the elevation at which permanent ice masses occur generally increases, with a superimposed precipitation effect (Sugden and John, 1990). This dependence on elevation initiates a regime of mass-balance and ice movement whereby ice accumulation above a threshold altitude (termed the equilibrium line altitude, or 'ELA') is broadly matched by annual flow through the ELA and ice loss below the ELA. This ELA is dynamic and its exact location varies to reflect changes in climate. The short-term ELA, for any given year, coincides with the position of the snowline visible on a glacier at the end of the melt season or dry season. The snow deposits remaining above the ELA represent mass accumulation;

i.e. snow that has survived the melt season and will remain (after being buried beneath any snow that falls in the ensuing winter) into the next year. The overall shape of an ice mass is predominantly determined and subsequently maintained by the transfer of ice from this accumulation area into the ablation area. How this mass-balance regime operates has a strong influence on how a glacier flows – steeper mass-change gradients generally enhancing flow. However, no firm evidence currently exists relating to the spatial expression of accumulation and ablation at the surface of martian VFFs - where atmospheric temperatures are ubiquitously and perennially below the freezing point of water. Thus, to date, no ELA has been identified on the surface of Mars.

The absence of an identifiable accumulation area on martian GLFs makes it difficult to predict or explain the distribution of these forms – which are overwhelmingly located in the mid-latitude regions of both hemispheres. Even if Mars' observed landscapes of apparently flowing ice (LVF, LDAs and GLFs) represent only the remnants of one or more larger ice masses that have since down-wasted, as some have argued (e.g. Dickson et al., 2008; Madeleine et al., 2009), these deposits appear to have experienced flow in the period since a hypothesised martian glacial maximum. However, the driving forces behind this flow remain poorly understood. In particular, it is unclear whether there was (or is still) a mass-balance-type regime in operation, or whether VFFs owe their flow-like appearance only to viscous creep on sloping surfaces.

The aim of this chapter is to contribute to ongoing investigations surrounding the poorly-understood mechanisms of GLF origin and evolution by (i) extending the spatial coverage and resolution of Milliken et al.'s (2003) survey, and (ii) resolving a more detailed picture (now facilitated by the availability of high-resolution, wide-angle CTX camera data) of where and how GLFs occur in these latitudinal ranges. Specific objectives of this research are to (i) provide a high spatial resolution survey of individual GLF locations, (ii) provide an inventory of morphometric data for all individually-surveyed GLFs, and (iii) describe the spatial variation in GLF concentration and morphometry with respect to the likely controlling variables of latitude, elevation and relief. We also provide the community with an accompanying online database of location and morphometric data relating to each of the 1309 GLFs

identified in this study (available online at: http://www.sciencedirect.com/science/journal/00191035/217/1).

2. Methods

2.1. Survey of GLF distribution

Milliken et al. (2003) previously performed a survey of 13,000 high-resolution (~1.5 - 6m / pixel) MOC images. These 13,000 images yielded 146 that contained VFF-type landforms (Milliken et al., 2003). However, the narrow field of view (0.4°) of these images meant that a lower proportion of Mars' surface was observed than it is now possible to survey using recent, wider-angle (5.7° field of view) imagery from the Context Camera (CTX) mounted on the MRO spacecraft. These images are relatively high spatial resolution (6m/pixel) and typically have a swath width of ~30 km.

The areas lying between 30º and 60º latitude (north and south) surveyed by Milliken et al. (2003) were expanded (by 5º in both directions) for this survey in order to minimize the likelihood of omitting outlying GLFs that may have been missed in Milliken et al.'s (2003) survey. Thus, the regions of interest (ROIs) investigated herein lie between 25º and 65º in both hemispheres. At the time of the survey, 8,058 CTX images were available that had been targeted within these ROIs (Figure 2).

2.2. Criteria for identifying GLFs

A set of physical criteria was devised to allow the efficient and repeatable identification of GLFs. These criteria were adapted and refined from those used by Milliken et al. (2003) to identify VFFs. Milliken identified primary and secondary lobate structures as being important indicators of flow, along with surface lineations (both parallel and transverse to the direction of movement), compressional ridges, extensional troughs, ridges at the flow front or slope base, or other general evidence of mass flow around or over obstacles. The criteria used in the survey presented

here were also informed (with a view to facilitating detailed analogue-based research) by the morphology and contextual characteristics of terrestrial glaciers. Thus, to be classified as a GLF in this survey, a feature was required to comply with all of the following conditions:

A GLF must:

i) be surrounded and constrained by higher topography and show general evidence of flow over or around obstacles.
ii) be distinct from the surrounding landscape, exhibiting a texture or colour different from adjacent terrains.
iii) display surface foliation indicative of down-slope flow; e.g. compressional / extensional ridges, surface lineations or arcuate surface morphologies or surface crevassing.
iv) have a length to width ratio > 1 (i.e. be longer than it is wide), and thus be distinct from the apron-like LDA class of feature.
v) have either a discernable 'head' or a discernable 'terminus' indicating a compositional boundary or process threshold.
vi) appear to contain a volume of ice (or some other viscous substance), having a relatively flat 'valley fill' surface (Figure 1b), thus differentiating it from an assemblage of post-glacial type landforms.

A selection of well-formed GLFs are shown at Figure 3.

2.3. Morphometric database

The 8,058 CTX images located within the ROI (Figure 2) were inspected by eye using the criteria listed in Section 2.2. Each image was viewed online using the 'Mars Image Explorer' interface hosted by Arizona State University. This facilitated efficient image inspection and GLF identification. Where GLFs were identified, JMARS software was used to view the relevant images in a projected, georeferenced format,

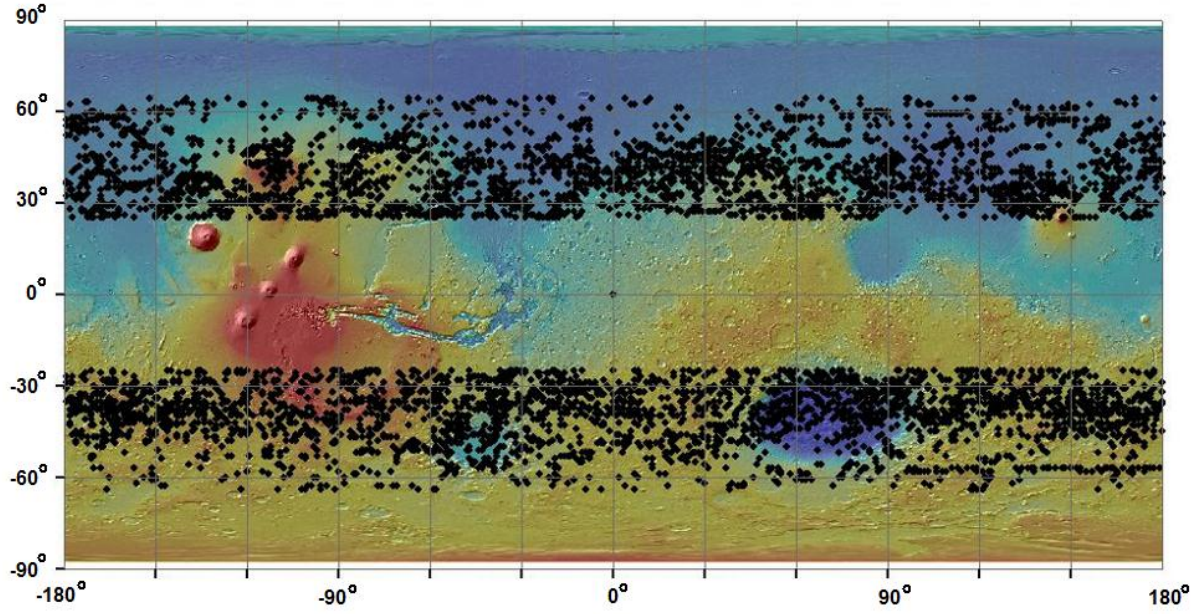

Fig. 2: Mars global map showing the locations of all 8,058 CTX images used in this survey (Section 2). Positions are plotted using the central targeting co-ordinates of each image. This map gives an indication of CTX image coverage in Mars' mid-latitudes (25º-65º north and south) at the time of this survey.

permitting the manual extraction of precise geographical information for each GLF. The information thus extracted included the co-ordinates (to 4 decimal places) of each GLF's head, terminus, true left mid-point and true right mid-point. By 'true left' and true right' we refer to what would appear to be the 'left' and 'right' of a feature if one were to stand at the headwall and look down-feature. The mid-point is exactly that: the halfway point between the head and the terminus.

Care was taken to avoid double counting GLFs that appeared in more than one image (i.e. repeat or stereo coverage). This was made easier by JMARS' facility for uploading and overlaying multiple CTX image stamps on a Mars geographic information system (GIS). These co-ordinate data were used to calculate the simple length and width of each GLF (as the crow flies from head to terminus or true left to true right respectively), as well as the dominant orientation (the true bearing from head to terminus of each GLF calculated using a 'great circle' function) of each individual feature. In addition, it was possible to estimate a simplified area for each GLF by multiplying its length by its mid-channel width.

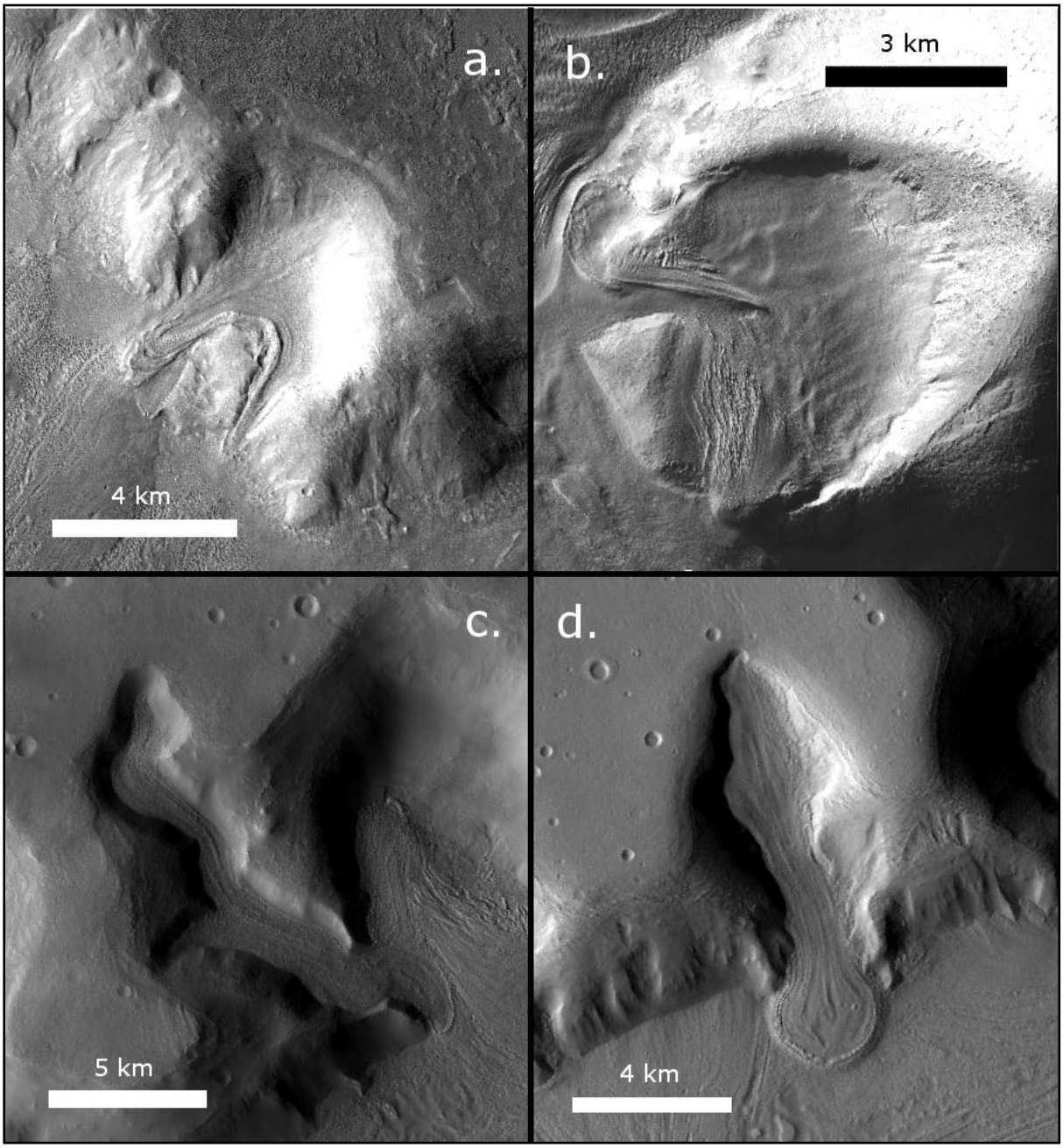

Fig. 3: Montage of four CTX image details showing various well-developed GLFs: a) A double-tongued GLF situated in eastern Deuteronilus Mensae and featured in CTX image P20_008770_2240_XN_44N322W; b) A GLF located in Eastern Hellas and featured in CTX image P02_001727_1391_XN_40S257W; c) A convergent GLF located in Coloe Fossae and featured in CTX image P02_001768_2160_XI_36N303W; d) A GLF which displays striking similarity to a terrestrial piedmont glacier. This example is located in Protonilus Mensae and features in CTX image P22_009653_2224_XN_42N309W. Note that in all cases images are oriented north-up and illumination is from the left (west).

2.4. Geographic controls

To investigate the controls responsible for observed GLF distributions, a range of environmental parameters was quantified and recorded for the immediate area surrounding each identified feature. Once this had been carried out for each GLF, it was possible to analyse the distribution of GLFs relative to variation in these potential control parameters.

While sampling the absolute elevation of a point on any given GLF is straightforward, extracting an approximation of local relief required a slightly more involved approach. In order to determine both characteristics for each identified GLF, elevation data were extracted from an areal buffer of 5 km radius around the centre head of each feature (Figure 4). These buffer zones were scaled at 5 km on the grounds that this would provide sufficient cover to extend beyond the confines of the GLF in question (mean GLF channel width was calculated at 1.3 km), encompassing the key properties of the immediate surrounding area but without extending too far and thus skewing the data with unrelated topography. The head, rather than the centre, of each GLF was selected as the key point for this analysis as it is likely (based on the assumption that GLFs have flowed downhill from an uppermost 'source' area) that it is the environmental characteristics of the upper source area that are of most importance in the formation of GLFs.

Descriptive statistics for the MOLA elevation data embedded within all pixels falling within these 5 km radius buffers were extracted for each GLF. Elevation was calculated for each GLF as a mean of its respective buffer's collected MOLA values and relief could be approximated by calculating the standard deviation (std. dev.) of these values. The statistics extracted in this way included (for each initial point and its surrounding buffer) the minimum elevation, the maximum elevation, the mean elevation, and the std. dev. of elevation values.

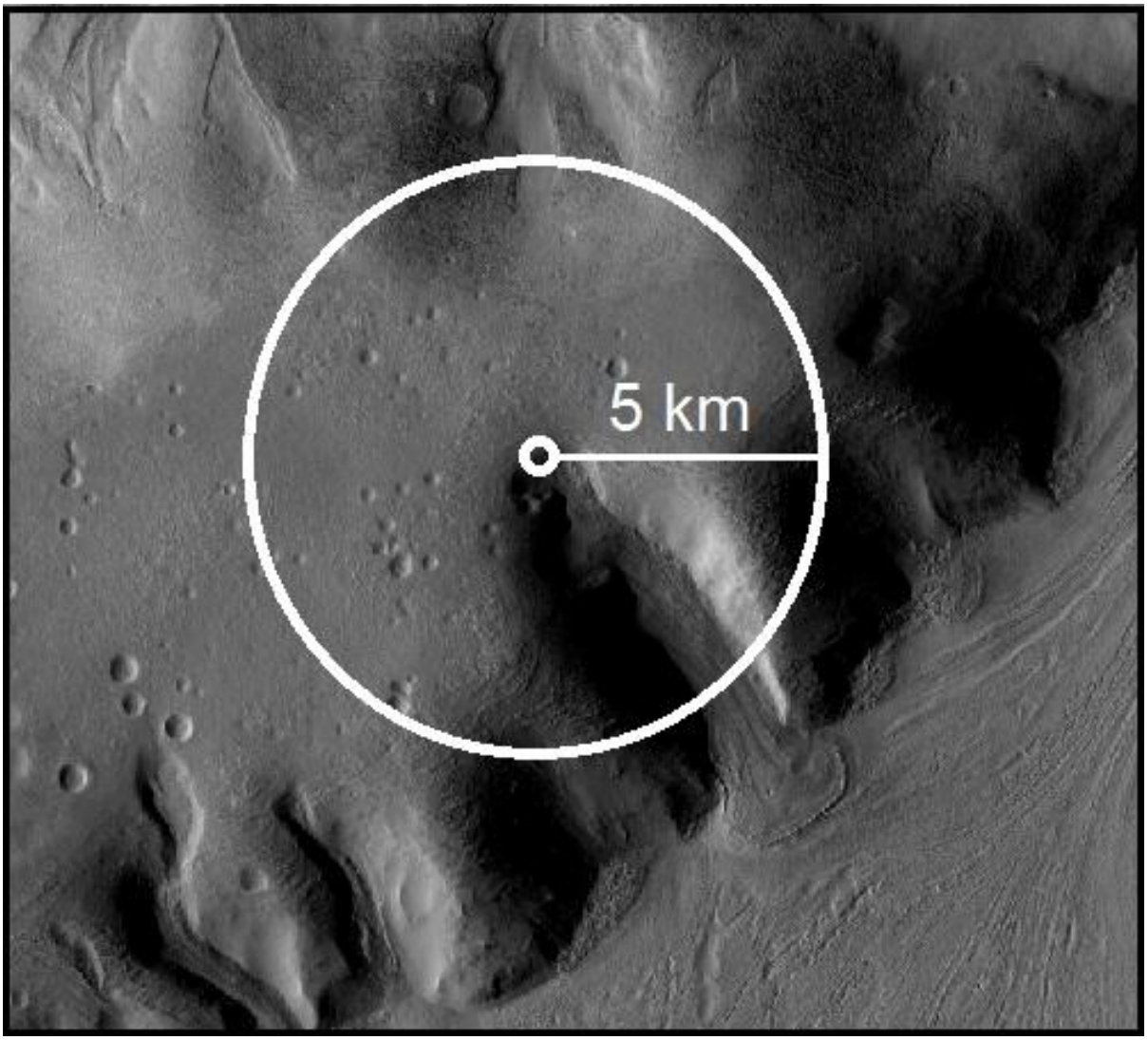

Fig. 4: An example of a "5 km radius buffer" such as those described in Section 2.4. "Buffers" such as this were generated around the heads of every GLF in the database and Arc GIS software was used to extract data on elevation and relief from each buffer and for every GLF. This figure shows a scene from CTX image P22_009455_2214_XN_41N305W. The image is oriented north up and illumination is from the left of frame.

2.5. Analysis of local geographical variables

Histograms were produced describing GLF numbers as a function of the geographic variables measured both for all GLFs and for each hemisphere separately. Basic descriptive statistics including mean, std. dev., skewness and kurtosis were then calculated for each histogram, thus quantifying the nature of the spread of GLFs relative to each geographic variable. Skewness gives an indication of the asymmetry of distributions, with negative values indicating a skew (or longer 'tail') to the left, and a positive value indicating the converse. Kurtosis provides a statistical indication of the 'peakedness' of a distribution, higher kurtosis indicating that more of the variance in a distribution is the result of infrequent, extreme deviations.

Compass rose diagrams were also plotted to illustrate GLF orientation, again on global and hemispheric scales, and equivalent angular descriptive statistics were extracted. All of these data are available from the accompanying online database (http://www.sciencedirect.com/science/journal/00191035/217/1).

2.6. Mars' mid-latitude 'hypsometry'

MOLA data, resized to 10 pixels/degree for each hemisphere, were used to create histograms showing elevation by sector (a surrogate for absolute hypsometry) for the study ROIs. This allowed GLF numbers, plotted by elevation, to be compared with the relative map-projected areas corresponding to given elevational ranges available within the ROIs. Note, that by using map-projected 1 degree x 1 degree sectors (see above) and not 'real world' area-defined sectors a certain amount of skew will be introduced into the results of this analysis. This method was chosen as all the available data sources could be fit easily into this slightly simplified analytical framework. We however argue that using this simplified framework will not overly affect the usefulness or credibility of any results it is the relative distributive frequencies, not the absolute frequencies, of GLF concentration and elevation distribution with which we are concerned.

Direct quantitative comparison of sectorized elevation and GLF count was facilitated by normalising both counts (GLF and surface area) and expressing the ratio of normalised GLF count to normalised sectorised elevation as an index of the relative prevalence of GLFs within each elevation bin. Thus, an elevation bin containing the same fraction of GLFs and of total surface area within the ROI would have an 'elevation index' of 1. If the fractional representation of GLFs is lower than that of sectorised elevation then the index will be <1, and vice versa.

It should be noted here that the elevation data used to generate the sectorised elevation curves was not vetted to account for variable CTX coverage. Elevation data were included from all areas within the ROIs regardless of CTX image coverage. Some regions exist in both hemispheres where CTX coverage is sparse (for example many parts of the lowland plains north of the martian dichotomy boundary) (Figure 2). It is therefore possible that a bias may exist where GLF population distribution is compared to ROI sectorised elevation.

3. Results

3.1. GLF distribution

Of the 8058 CTX images inspected, 771 (9.6%) were found to contain one or more GLFs. Of these GLF-positive images, 372 (54.3%) were located in the northern hemisphere and 399 (45.7%) were located in the southern hemisphere. In total, 1309 individual GLFs were observed, 727 (55.5%) in the northern hemisphere, and 582 (44.5%) in the southern hemisphere. The spatial distribution of these GLFs is highly clustered (Figure 5), and particularly so in the northern hemisphere, where the often-complex highland terrain of the dichotomy boundary is intersected by the large lowland plains of Utopia Planitia, Arcadia Planitia and Acidalia Planitia (Figure 5 and Figure 6). High GLF concentrations are observed in areas of rough topography such as Phlegra Montes, Acheron Fossae, and the western Tempe Terra area (Figure 5 and Figure 6). These locales contain 56, 29 and 64 GLFs respectively, constituting 7.7%, 4.0% and 8.8% of the northern hemispheric total. However, the most densely clustered northern mid-latitude populations were observed along the dichotomy

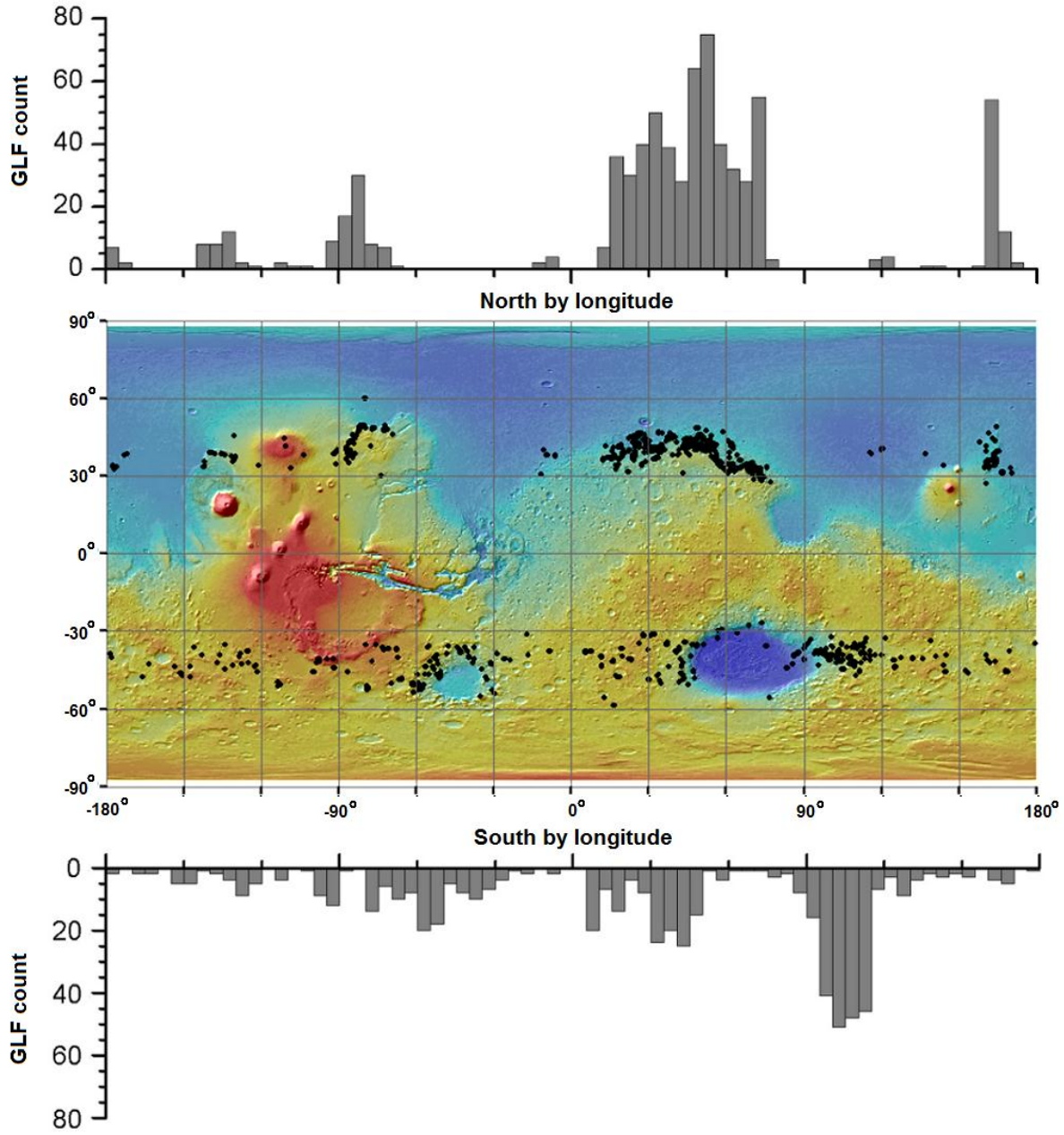

Fig. 5: Mars global map showing the mid-latitude distribution of glacier-like forms (GLFs). 1309 GLFs were identified globally. 727 were located in the northern hemisphere and 582 were located in the southern hemisphere. Histograms are displayed above and below the distribution map showing concentration of GLFs per 5º longitude. GLF locations are plotted on a MOLA hillshade projection.

boundary in the so-called 'fretted terrains' (Sharp, 1973) of Deuteronilus Mensae, Protonilus Mensae and the Nili Fossae region located north-west of Isidis Planitia

(Figure 5 and Figure 6). This contiguous zone featured 527 individual GLFs, constituting 72.5% of the northern hemispheric total (Figure 5). In contrast, the lowland plains contain virtually no GLFs, although isolated examples are occasionally present within large craters (Figure 5).

Notable GLF clustering was also observed in the southern hemisphere. High concentrations of GLFs were identified throughout the north-western rim of the Argyre Planitia impact basin (~65 GLFs / 11.2% of the southern total), in the cratered terrains of eastern Terra Sirenum (~35 GLFs / 6%) and in the regions east (~186 GLFs / 32%) and west (~60 GLFs / 10.3%) of the Hellas impact basin (Figure 5 and Figure 6). The most densely populated of these regions is that of eastern Hellas.

Observation of these surveyed distributions alone shows that clustered GLF populations appear to favour the middle latitudes (centred around ~40º north and south) and areas of high relief. This is investigated further below.

3.2. GLF morphometry

Histograms showing GLF numbers plotted as a function of length, width, elongation (length divided by width) and area (length multiplied by width) are shown in Figure 7. Basic descriptive statistics (mean; std. dev.; skewness and kurtosis) for each of these properties (plus orientation) are presented in Table 1. Student ‘t’ test results indicating the statistical inter-hemispheric similarity of the descriptive data shown in Table 1 is presented in Table 2. As can be seen in Table 1, overall GLF dimensions have remarkably similar mean values in both hemispheres. The ‘P’ values in Table 2 show that this similarity is statistically significant at a threshold significance of 99% for length, width and area.

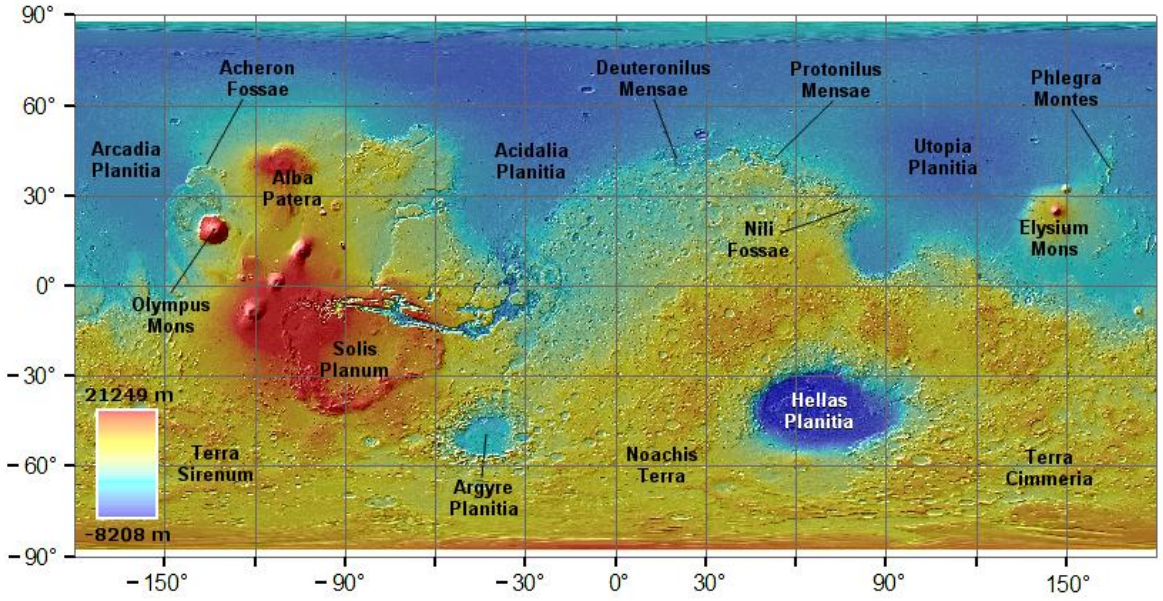

Fig. 6: A map of Mars with major landmarks and key regions annotated. Place names are marked on a MOLA digital elevation model displayed as a colour ramp.

3.2.1. GLF length

Mean GLF length is 4.91 km and 4.35 km in the northern and southern hemispheres respectively. The manner in which length values vary around the mean are also similar in the two hemispheres, with the std. dev. values of 3.42 km and 3.28 km and similar values for skewness and kurtosis for the two regions (Figure 7 and Table 1).

3.2.2. GLF width

In contrast to GLF length, inter-hemispheric comparison of GLF width reveals some variation. Although mean widths are statistically indistinguishable for the two hemispheres (1.26 km in the north and 1.34 km in the south), the variation in widths is greater in the north (std. dev. = 1.45 km) than in the south (std. dev. = 0.956 km). The north also displays higher skewness and kurtosis than the south (Figure 7 and Table 1).

3.2.3. GLF area

GLF area (Figure 7 and Table 1) shows broad similarities in all descriptive properties in both hemispheres.

3.2.4. GLF orientation

GLF orientation shows a polarised distribution (Figure 8 and Table 1). In the northern hemisphere GLFs are predominantly orientated NNE, the mean bearing from head to

Table 1: Basic descriptive statistics of GLF morphometry, including length, width, simplified area and orientation. See also plots at Fig. 5. All values are given to within 3 significant figures.

ROI	GLF Char.	Mean	St. dev.	Skewness	Kurtosis
All	Length (km)	4.66	3.37	3.29	18.4
	Width (km)	1.27	0.928	3.37	17.4
	Elongation	4.19	2.98	9.62	192
	Area (km^2)	7.61	13.4	6.25	54.5
	Orientation (º)	146	117	-	-
North	Length (km)	4.91	3.42	3.14	16.3
	Width (km)	1.26	1.45	13.9	279
	Elongation	4.51	2.32	1.62	5.43
	Area (km^2)	7.86	14.3	5.86	43.3
	Orientation (º)	26.6	106	-	-
South	Length (km)	4.35	3.28	3.56	22.2
	Width (km)	1.34	0.965	2.94	13.4
	Elongation	3.79	3.6	11.9	207
	Area (km^2)	7.54	13.4	6.97	71
	Orientation (º)	173	73.2	-	-

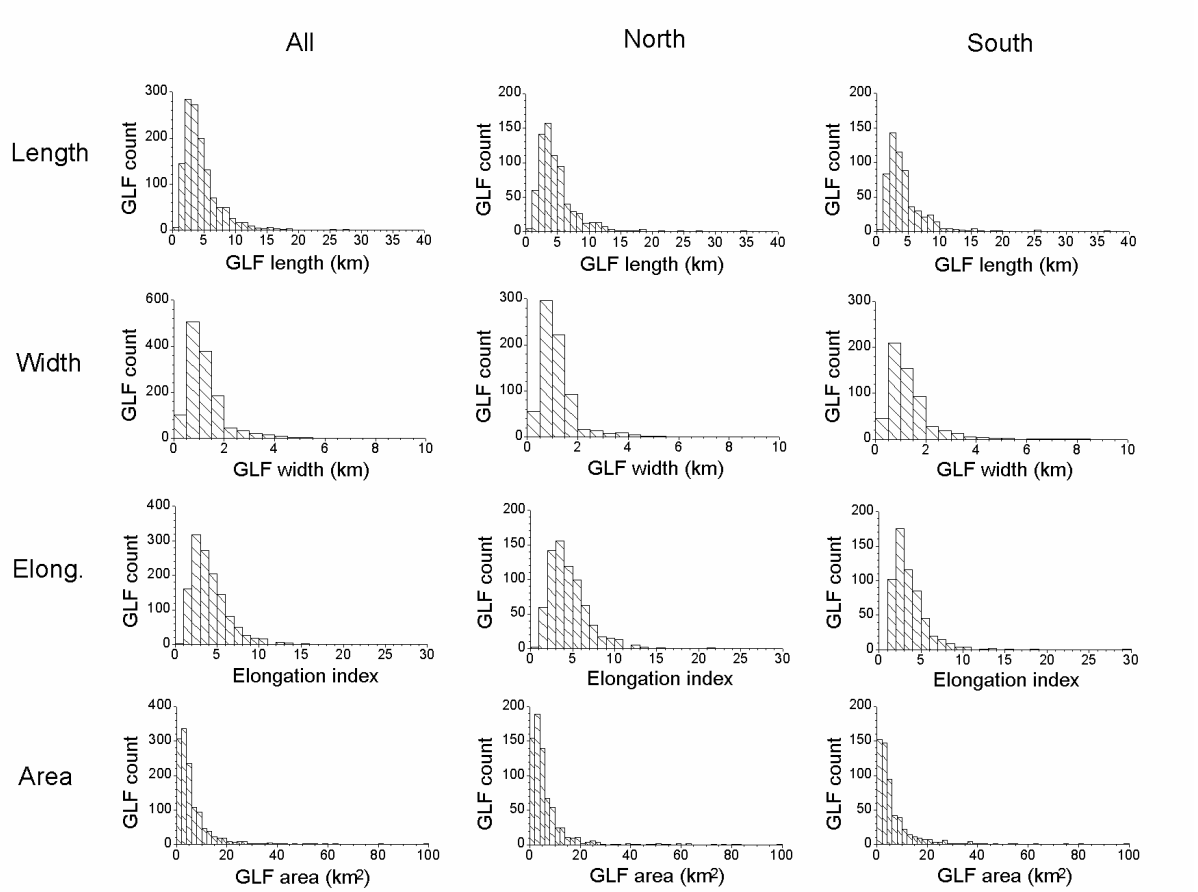

Fig. 7: Tabulated histograms showing distribution of GLF populations relative to measured length, measured width, calculated elongation (length / width) and simple area (length multiplied by width). Distributions are shown for Mars' global GLF population and for each hemispheric population separately.

Table 2: The statistical similarity (between the northern and southern hemispheres) of certain GLF properties. 'P' is calculated using a 2-sample 't test'. Those properties and P values highlighted in bold text are found to be statistically similar at a confidence interval of 99%.

GLF property	P value
Longitude	0.000
Latitude	0.000
Length	**0.003**
Width	**0.274**
Area	**0.683**
Elongation index	0.000

terminus being 26.6º, whereas in the southern hemisphere mean orientation is south, or SSE, at 173.1º (Table 1). These results indicate a strong preference for a poleward orientation in both hemispheres, with an additional slight bias towards an easterly aspect in both hemispheres. It is also interesting to note that, although the poleward bias is a strong one in both hemispheres, the northern mid-latitudes contain a comparatively high proportion of GLFs that break with the trend and face south, whereas in the southern mid-latitudes the poleward bias is more dominant (Figure 8). This explains the global mean's tendency to the south (146.6º) which would otherwise be surprising given the fact that the northern mid-latitudes host the larger of the two hemisphere's GLF populations. Std. dev. of orientation is, as one would expect from this observation, higher in the northern hemisphere (105.6º) than in the southern hemisphere (73.2º).

3.3. Local geographic parameters

As with GLF morphometry (Section 3.2. above), histograms of GLF population were plotted showing GLF distribution relative to the geographic parameters latitude,

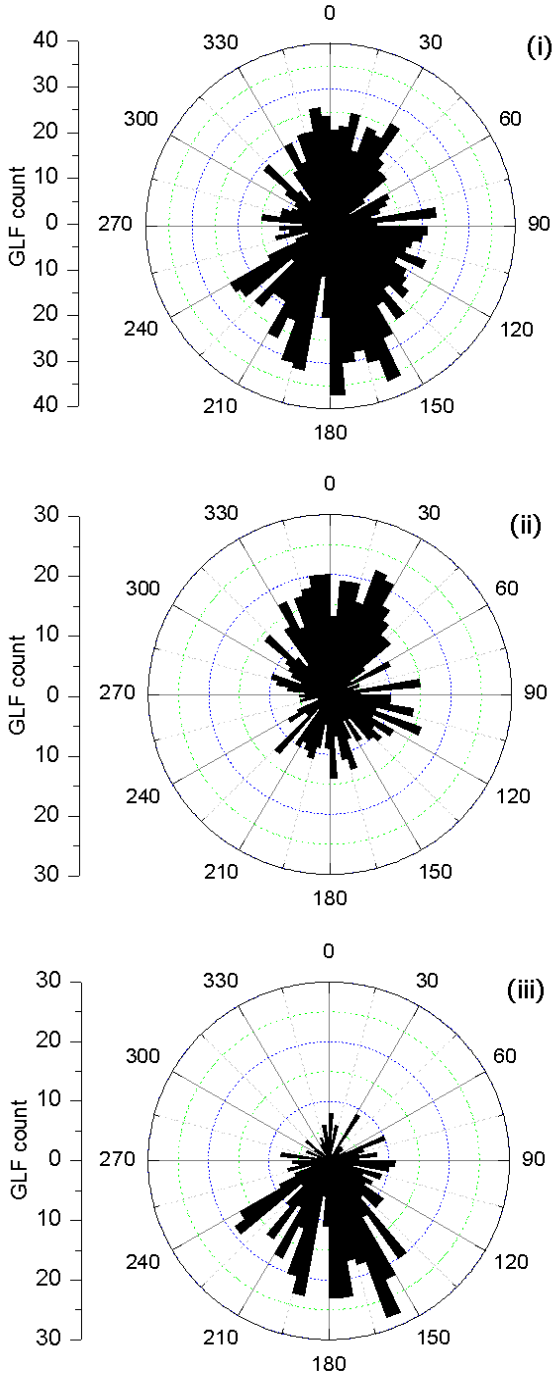

Fig. 8: Compass-rose diagrams showing GLF population distribution by orientation (to within 5º bins). Global population orientations are shown at (i), northern hemisphere orientations at (ii) and southern hemisphere orientations at (iii). A generalised polarisation of orientations is apparent with GLFs in both the northern and southern hemispheres tending toward a polar aspect. Interestingly, a slight easterly bias is apparent in both the northern and the southern plots.

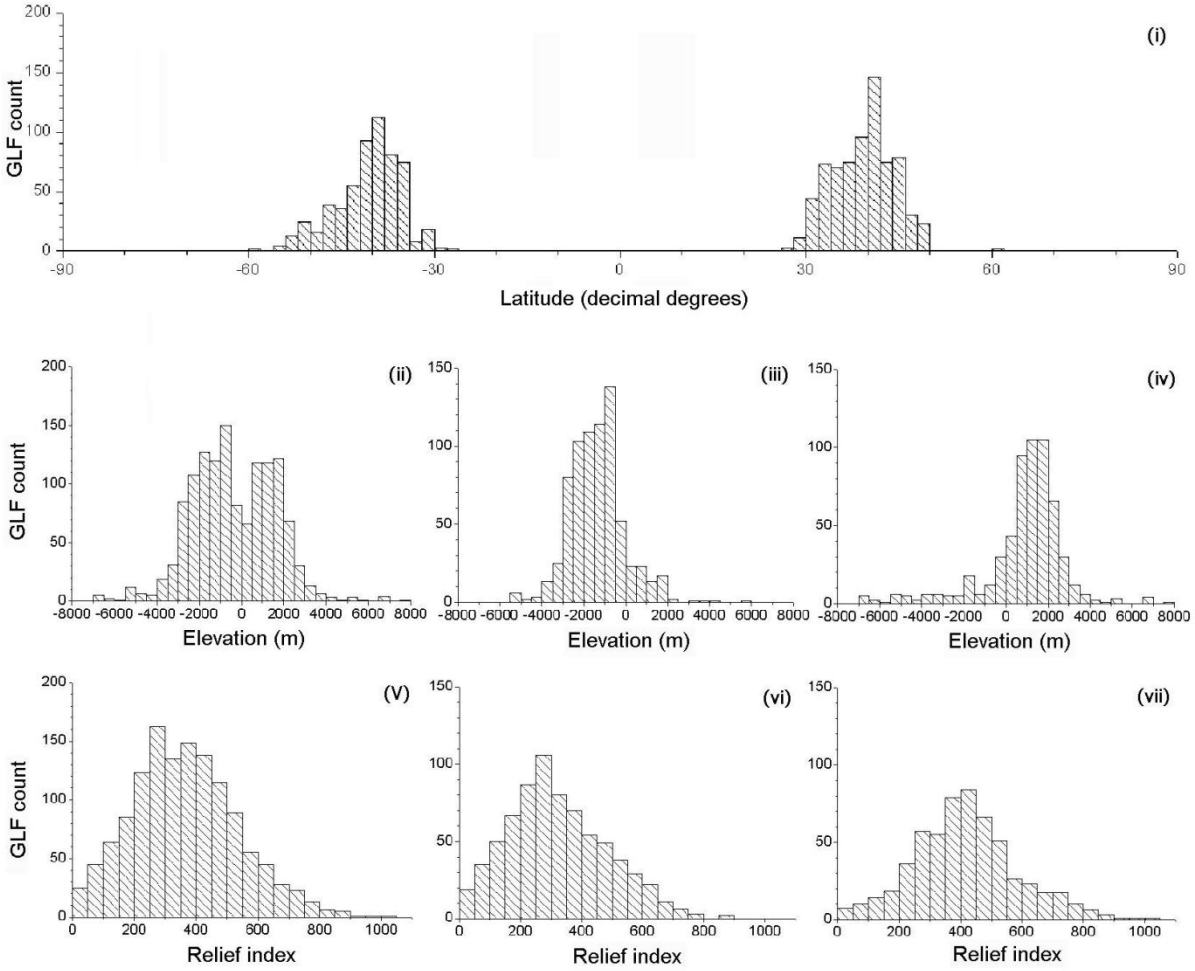

Fig. 9: Histograms showing distribution of GLF population relative to global latitude (i) (in 2º bins); global elevation (ii); northern hemispheric elevation (iii); southern hemispheric elevation (iv); global relief (v); northern hemispheric relief (vi); and southern hemispheric relief (vii).

elevation and relief (a proxy index from the std. dev. around mean elevation; Section 2.4) (Figure 9 and Table 3).

3.3.1. Latitude

GLF distribution is similar in both hemispheres with a mean latitude of 39.3º (std. dev. = 4.9º) in the north and 40.7º (std. dev. = 5.3º) in the south. Skewness in both hemispheres (0.068 in the northern hemisphere and -0.582 in the southern hemisphere) suggests a bias towards the pole, with the 'tail' of the histogram trending towards higher latitudes in both cases (Table 3). This skew is considerably

Table 3: Basic descriptive statistics of GLF distribution relative to latitude, elevation and relief (std. dev. of local elevation values). See also histograms at Fig. 7. All values are given to within 3 significant figures.

ROI	Parameter	Mean	St. dev.	Skewness	Kurtosis
All	Latitude (º)	-	-	-	-
	Elevation (m)	-366	1954	0.049	0.387
	Relief (m)	364	171	0.413	0.108
North	Latitude (º)	39.3	4.94	0.0682	0.0249
	Elevation (m)	-1366	1292	0.592	2.37
	Relief (m)	323	161	0.489	-0.074
South	Latitude (º)	-40.7	5.27	-0.582	0.270
	Elevation (m)	885	1922	-1.28	3.89
	Relief (m)	417	168	0.347	0.447

more pronounced in the south than in the north. Kurtosis is low in both hemispheres: 0.025 in the north and 0.270 in the south, describing a 'centralised' distribution in both cases.

3.3.2. Elevation

Mean GLF elevations in the northern and southern hemispheres were -1366.3 m and +884.7 m respectively (relative to Mars datum) (Table 3), a difference of > 2000 m. Both distributions are highly centralised with std. dev. values of only 1291.6 m in the north and 1921.9 m in the south (Figure 9). Skewness (north and south being calculated at 0.592 and -1.283 respectively) and kurtosis (calculated as 2.374 and 3.887) values for both hemispheres are also relatively low (Table 3). So, in both hemispheres GLF distribution shows a marked preference for (and strong

centralisation around) a certain range of elevations, although this range differs considerably in each hemisphere.

Considering GLF distribution in relation to the sectorised elevation of the ROIs (Section 2.6.) yields an apparent contrast between the two hemispheres (Figure 10). Figure 10(i) indicates that the sectorised elevations of the two hemisphere's ROIs are markedly different, with land surface in the northern hemisphere clustering around an elevation of ~ -4000 m and land surface in the southern hemisphere clustering around an elevation of ~ (+) 2000 m. However, comparison of the equivalent GLF elevation histograms with these sectorised elevation distributions (Figure 10[ii]) reveals that, while the distributions of both GLF and land surface coincide in the southern hemisphere, they do not in the north. Here, GLFs are strongly shifted towards higher elevations, occurring predominantly in the range -3000 to -500 m (whereas the modal land surface elevation range occurs at -4500 to -3500 m). This effect is clearly illustrated by a plot of the ratio of the normalised GLF data to the normalised surface-area data against elevation (Figure 10[iii]). While this ratio remains fairly close to 1 across most elevation bands in the southern hemisphere, it deviates in the northern hemisphere towards large positive values in the elevation range -2000 to 0 m (peaking at a value of 7 in the -1000 to -500 m bin).

3.3.3. Relief

The GLF relief index has a mean value of 323 (std. dev. = 161) in the northern hemisphere and 417 (std. dev. = 168) in the southern hemisphere (Table 3). This suggests that GLFs occur in areas of optimum (i.e. neither maximum or minimum) relief in both hemispheres, although both are slightly different (with the higher of the two being in the southern hemisphere). The southern hemispheric population also shows a more Gaussian peaked distribution with a kurtosis of 0.447 compared to the northern hemisphere population's kurtosis of -0.074. The northern population also has a slightly larger skewness of 0.489 compared to 0.374 in the south.

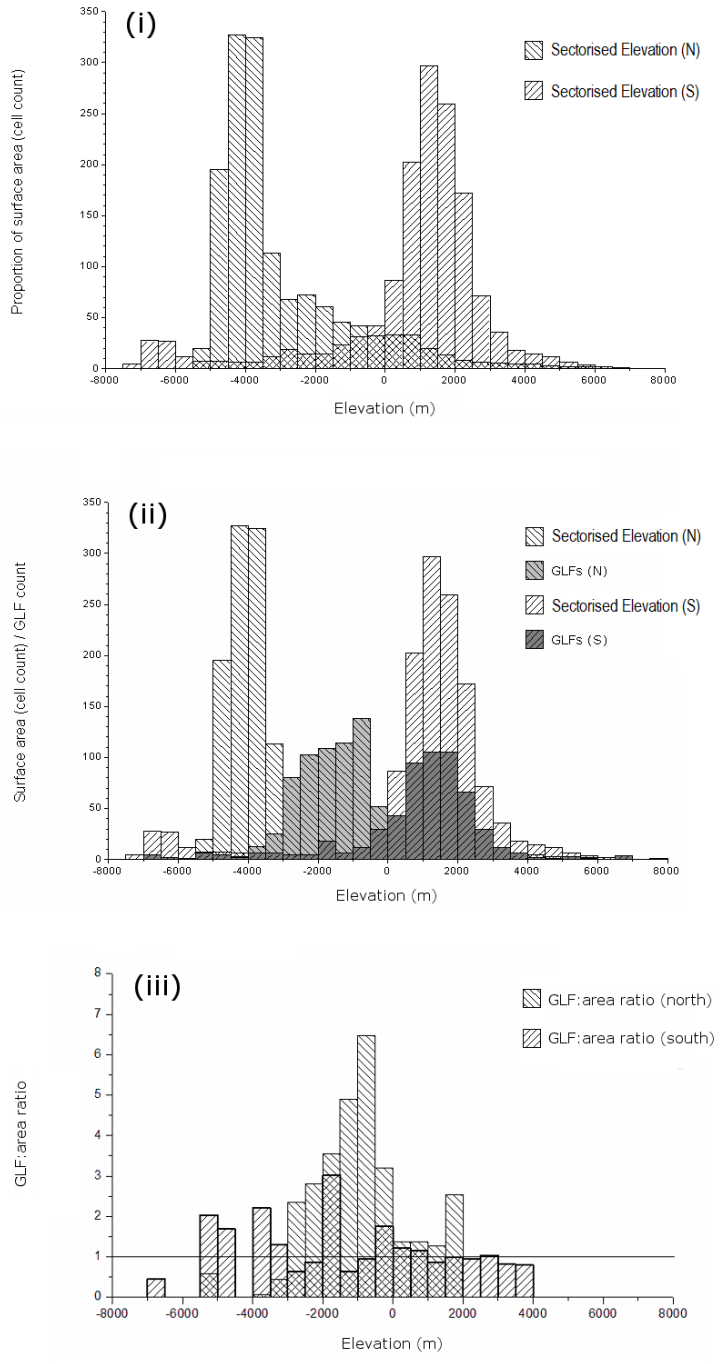

Fig. 10: (i) Sectorised elevation curves for the surveyed ROIs (25º - 65º north and south). Both plots (overlaid) are based on MOLA data, re-scaled to a resolution of 10 pixels/degree, and show the proportion of the map-projected land surface in each ROI to fall within set 500 m elevation bins. (ii) Comparison of GLF distribution by elevation to the sectorised elevation curves of both mid-latitude ROIs. As can be seen, the bimodal nature of both data series show similarities. GLF distribution relative to elevation is split, with the northern GLF population trending toward the lower elevations that are heavily represented in the northern mid-latitude sectorised elevation curve. (continued on next page…..)

Fig. 10 (cont): (iii) A comparison of GLF:area ratio (area as a proportion of ROI 'hypsometry') in the northern and southern hemispheres. A value of '1' in each column represents a GLF population proportional to the percentage of surface area characterised by a given elevational range. Values in > 1 represent elevational ranges where GLFs are over-represented, while values of < 1 denote elevational ranges where GLFs are under-represented. As can be seen from the overlaid plots – the GLF population in the southern hemisphere is distributed relatively proportionately relative to elevation by area. In the northern hemisphere however, GLFs are under-represented at elevations < -3000 m (elevation relative to Mars datum), and heavily over-represented at elevations between -3000 m and 0 m.

4. Interpretation of results

4.1. GLF morphometry

The striking similarity of GLF morphometries in the northern and the southern hemispheres (Table 1 and Figure 7) suggests that all GLFs share a common composition and that they form and evolve in a similar fashion. Mean length, width and area are statistically similar at a confidence interval of 99% in both hemispheres despite topography being highly variable. The main difference appears to be that GLF width is (slightly) more variable in the northern ROI than in the south: with std. dev., skewness and kurtosis all being higher in the northern than in the southern hemisphere. As the mean values are still broadly similar - and the distributions visible in Figure 7 closely resemble each other - this does not give grounds to infer that a fundamentally different process is in operation. Rather, perhaps, the nature of the underlying terrain exercises some control, for example the tendency of GLFs in the southern hemisphere to occur in craters compared to the butte and mesa landscape of the northern hemisphere's fretted terrains (for example Figure 1).

Regarding orientation, the pronounced preference for a poleward aspect for the majority of GLFs in both hemispheres (Figure 8) is consistent with observations made in previous studies of VFFs within craters at a more local scale (Berman et al., 2009). However, this study reveals the global dominance of this pattern, indicating that it is highly unlikely that the observed trend results from localised factors. This preference for a poleward aspect is similar to glacier emplacement on Earth where

persistent ice accumulation and survival are more likely in pole-facing alcoves where insolation is lower (e.g. Unwin, 1972). This correspondence between Earth and Mars supports the interpretation of GLFs, and by extension associated VFFs, as being glacier-like in nature. It also lends credence to arguments that GLFs grow and flow under a similar regime (sensitive to processes of accumulation and ablation and the balance between the two) to that of their terrestrial counterparts. However, it is important to note that this does not necessarily imply that the modes of accumulation and ablation that operate on Earth and Mars are at all similar. Current GLF distributions on Mars reflect not only where ice accumulated, but also where it has survived in the face of a changing planetary climate. Therefore, patterns of current GLF orientation cannot be used as evidence of any orientational preference in initial mass emplacement or, by extension, any specific mode of ice precipitation.

An interesting feature of the observed pattern of GLF orientations is the bias in both hemispheres toward an easterly aspect (Figure 8 and Table 1). In the northern hemisphere, mean GLF orientation is 26.6º, while in the south the mean is 173.1º. Conway et al. (2011) revealed a similar eastward bias in the orientation of gullies situated in the walls of craters in Terra Cimmeria and Noachis Terra. The authors attributed these gullies to de-stabilisation of the mid-latitude icy mantle terrain, indicating a possible link to GLFs and other VFFs as was also suggested by Milliken et al. (2003) for VFFs and gullies and by Christensen (2003) for 'snowpacks' and gullies. These studies suggest that liquid water may have incised the gullies as ice or snow deposits melted at some point during Mars' recent geological history. However, no explanations have yet been presented for the apparent eastward bias in either gully orientation or VFF orientation.

4.2. GLF population relative to local geographic parameters

4.2.1. Latitude

The distribution of GLFs relative to latitude shows a strong clustering of hemispheric populations around ~40º latitude (39.3º in the northern hemisphere and -40.7º in the southern hemisphere) (Figure 8 and Table 2). These population clusters correspond

very closely to each other and the std. dev. of population around these values is low, indicating that latitude exerts a very strong control on GLF population.

Interestingly, both populations, although highly clustered by latitude, do exhibit statistical skewness towards the pole, with GLF population in both cases falling more gradually towards higher latitudes than towards the equator. This is not as apparent in the north, where there is a gap in GLF population between 50º and 60º latitude (Figure 9 [i]), but outlying GLFs in craters at latitudes between 60º and 63º north suggest that environmental conditions are still suitable for GLF formation, implying a non-climatic control in this 'empty zone'. We interpret this hiatus in terms of the dichotomy boundary, which has effectively 'cropped' GLF population, elevation and relief north of the boundary being so low as to have suppressed GLF formation (or potentially inhibited GLF preservation). It is therefore tempting to suggest that if regional topography were not split in such a fashion then a skew such as that visible in the south would also be seen here.

GLF population may increase with distance from the pole as the icy mantling deposit described by Kreslavsky and Head (2000; 2002) gradually de-stabilises with increasing proximity to the equator (Conway et al., 2011). The mean or 'optimal' latitudes of 39.3º and -40.7º (in the north and south respectively) could then represent effective thresholds whereby climate has de-stabilised ground ice to the point where it flows most readily, departure from this threshold latitude in a poleward direction leading to increased stability of the mantling material, while equatorward proximity induces more rapid ice de-stabilisation and ablation.

The evidence would appear to suggest that the dependence of GLF distribution upon latitude is to a large extent the result of conditions and factors in play during initial GLF formation. GLF concentration manifestly increases with distance from the poles (up until an observed threshold as discussed above), which represents a break from the terrestrial norm, which sees the abundance of glacial ice generally decreasing in tandem with latitude. Terrestrial analogy suggests that on Mars too, which has a broadly similar climatic regime if not entirely similar conditions, ice should be less likely to survive at lower latitudes. As the converse is (to an extent) true, we propose

that the signal in these results originates predominantly in GLF formation and to a lesser extent in GLF preservation.

4.2.2. Elevation

The highly clustered distribution of GLFs relative to elevation in both hemispheres (Figure 9) suggests a preference for certain altitudinal ranges, indicating that as well as latitude, elevation exerts an important control over where and how GLFs form (or where GLFs have survived). However, GLFs are clustered around different altitudinal ranges in the two hemispheres (Figure 10[ii]).

Inspection of the plot showing GLF population as a normalised proportion of sectorised elevation (Figure 10[iii]) shows that in the southern ROI, where GLF population relative to elevation corresponds comparatively well to sectorised elevation (and elevations are almost ubiquitously in excess of -3000 m), GLFs are quite evenly represented (proportionally) relative to the available land surface within each elevational band. In the northern ROI, however, GLFs are under-represented in elevational bands below ~ -3000 m, and markedly over-represented in those lying between -3000 m and 0 m (Mars datum). One possible explanation for the observed pattern in both hemispheres is that a threshold elevation exists, below which GLF formation does not occur, or at least GLF formation is strongly suppressed (some outlying examples have been mapped in lower-lying areas such as in craters north of the martian dichotomy boundary and in the Hellas basin). Our evidence reveals that this threshold lies at ~ -3000 m. Another factor is that a large percentage of the landsurface in Mars' northern hemisphere where elevation is below -3000 m lies northwards of the dichotomy boundary (Figure 6). These low-lying surfaces have very low relief, thus GLF flow could be retarded.

These observations contribute to the case for martian GLFs having been sensitive to a mass balance regime that is in some ways similar to that which exists on Earth; elevation-related factors apparently exerting an important influence on the emplacement and (possibly) the flow of ice.

It must be clearly stated in this case that the pattern of GLF distribution pertaining to elevation could also very possibly be due to variable GLF preservation rather than initial formation. GLFs may have existed above and below the observed elevation thresholds but have subsequently ablated or been otherwise destroyed. However, despite this uncertainty, the sensitivity of GLF distribution to elevation seems clear and the ~ -3000 m threshold seems key.

4.2.3. Relief

The distribution of GLF populations relative to relief shows a preference for mid-range values and strong clustering about the mean in both hemispheres. However, skewness in both hemispheric population distributions indicate that GLFs are preferentially located in 'moderately' rough topography. A higher mean in the southern ROI (417 units in the south compared to 323 units in the north) indicates that GLFs occupy rougher terrain in the south. This may be due to the preponderance of GLFs that are situated on crater walls in the south. In the north, the heads of many GLFs are situated at or near the top of a cliff or at the edge of a raised plateau. Southern GLFs often originate part-way up crater rims, the incline of the basin extending farther above the upper reaches of the GLF in question. Thus the immediate area adjacent to the GLF's head would have a higher relief than were it to co-incide with the edge of a plateau.

These distributions imply that a link exists between GLF distribution and relief: GLFs favouring moderate relief areas and neither flat nor precipitous terrain. Since relief does not correlate with elevation (Figure 11) any relationship between GLF distribution and relief is real and not a by-product of elevation. This suggests that GLFs are produced by gravity-induced creep, the propensity of accumulated ice to flow being at least partially a function of local slope.

This hypothesis necessitates the existence of an upper and lower relief threshold beyond which GLF-type flow does not occur. This is easy to imagine for low-relief areas where channelized, gravity-induced flow is unlikely under associated extremely low shear stresses. It is more difficult to explain for high-relief surfaces. In

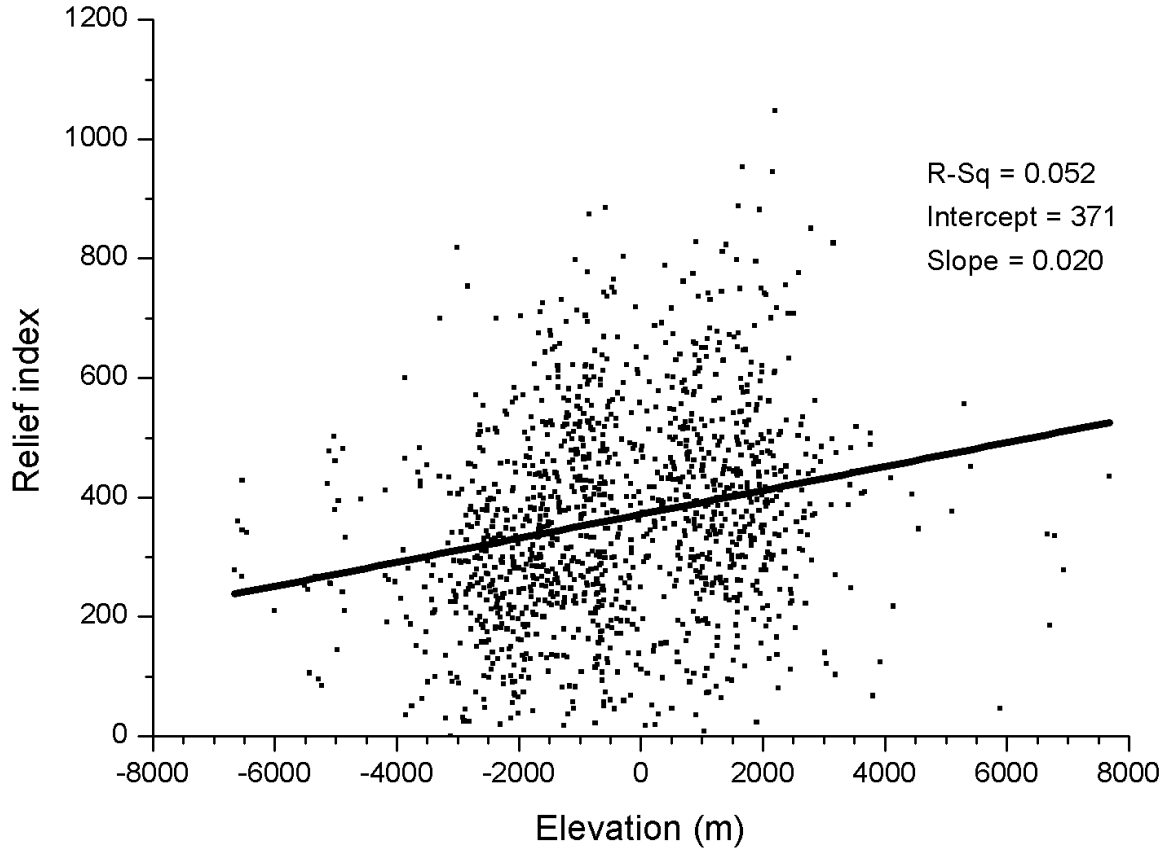

Fig. 11: A scatterplot showing the relationship between elevation and relief on an individual GLF basis. The Pearson's 'R', intercept and slope of the regression (plotted as a line) are all marked on the graph, showing a very weak correlation. This infers that elevation and relief, on a localised scale, are very weakly related, reducing the risk of co-linearity when GLF distribution relative to each independent variable is investigated.

such areas perhaps icy material has simply weathered away through sublimation enhanced by exposure, or has broken away in the fashion of rock-fall debris, gradients being too high to permit gradual, viscous flow. This hypothesis dovetails once again into the issue of GLF formation opposed to GLF preservation and would benefit from further research.

5. Conclusions

Visual analysis of 8058 CTX images revealed the presence of 1309 GLFs on the surface of Mars. Analyses performed on the distribution of these GLFs indicate that they have developed through the interplay of various factors.

GLFs mapped across Mars' mid-latitudes share broadly similar morphometries suggesting a common composition and evolutionary history (Figure 6 and Table 1). At the largest scale, latitude appears to exert the strongest, 'first order' control over GLF distribution. Their strong preference for certain latitudes, and the statistical skewness of these populations toward the poles, coupled with the predominantly poleward orientation of most individual GLFs on a global scale, strongly suggests a sensitivity to climate and insolation, as previously proposed on the basis of local and regional studies. At a local scale, the siting of GLFs appears to be closely controlled by elevation. Thus elevation may be considered to exert a 'second-order' control, with the optimal elevation around which GLFs cluster in each hemisphere (GLFs show a strong preference for a tight range in both ROIs) varying between the north and the south. However, inspection of each ROI's sectorised elevation distribution and the distribution of GLFs relative to the spread of available elevations suggests that on a planetary scale GLFs occur most readily above an altitude of ~ -3000 m. This suggests that ice only accumulates (or has merely only survived) above this elevation, indicating that quasi-mass-balance conditions either are, or perhaps were, in operation. However, subdued relief in low-lying areas may also have been a factor in suppressing GLF flow and formation.

The fact that the highest density of GLFs occurs in the middle elevations and GLFs are not statistically over-represented at the highest (Figure 10) contrasts the terrestrial scenario. This may be due to Mars' exceptionally broad hypsometry and the characteristics of Mars' atmospheric stratigraphy.

Finally, relief appears to play an important, perhaps 'third-order' control that is independent of elevation, GLFs occurring predominantly in areas of moderate relief.

The extent to which present-day GLF distribution has been affected by processes of ice removal and preservation since a hypothesised last glacial event is difficult to ascertain, particularly given the gaps in current understanding of GLF composition. Terrestrial glaciers exhibit great variety in their debris content and / or their surface debris load, and this variable debris component can have a profound effect on ablation rates and thus long-term ice survival (e.g. Nakawo and Young, 1981; Benn and Evans 1998, p. 72; Hindmarsh et al., 1998). Equivalent diversity in material properties almost certainly exists on Mars. It may be, therefore, that GLF preservation and thus present-day distribution are also partly affected by composition. Little direct information is available on GLF composition, and although the morphometric analyses performed during this research indicate some degree of uniformity, further research aimed at improving our understanding of this issue could be of great value. A detailed inspection of the landscapes in the vicinity of and immediately adjacent to current GLFs could be of particular benefit, perhaps yielding evidence of mass deposition and thus former ice-borne debris loads, as well as perhaps expanded extents of former GLFs which could enhance our understanding of where and how ice has survived and where it has not.

We suggest that GLFs presently occur where icy material, preferentially distributed within well-defined latitudinal and elevational ranges, has undergone local, gravity-induced flow and deformation in response to local relief. It could well be that adjacent areas of similar elevation and latitude, but of lower relief, house substantial ice reservoirs, but such deposits have not (yet) undergone flow and thus are not apparent as GLFs. Indeed, the widespread presence in these latitude bands of texturally distinct surface 'mantle' terrains believed to represent ice-dust mixtures (Mustard et al., 2001; Milliken et al., 2003; Head et al., 2003) suggests this is likely the case.

Martian GLFs therefore may not exhibit accumulation areas or ablation areas as exist on Earth, except perhaps where they flow downhill sufficiently to cross an elevational threshold which may lie at ~ -3000 m, beyond which the survival of any single GLF will be compromised by climatic factors (see Section 4.2.3).

C. Preface to Chapter 3

C1. Introduction to Chapter 3

A population-wide survey of Mars' GLFs was designed and conducted as described in Chapter 2 and its associated Preface. This survey characterised the distribution of GLFs and investigated the relationship of that distribution to various geographical variables. The next logical step was to reduce the scope of observation and investigate GLFs in more detail in an attempt to better understand their fundamental glaciological behaviour.

Chapter 3 (Published as a conference poster [Souness and Hubbard, 2012]) describes an investigation into intra-GLF strain and flow regimes, informed specifically by the identification of crevasse patterns on martian GLFs and the subsequent interpretation of those patterns through the use of Earth analogues. Crevasses provide a striking visual record of the response of GLF mass to variations in local strain rates, highlighting the conditions under which GLF mass flows and strain rates vary.

This Preface to Chapter 3 describes the methods which were adopted during the initial population-wide GLF survey (Preface to Chapter 2) in order both to identify and record the range of landforms that occur in an intra-GLF context, thereby facilitating later studies of smaller-scale GLF morphologies and flow mechanisms (such as the study described in Chapter 3).

C2. Mapping GLF morphology

As the CTX survey described in Chapter 2 (and the Preface to Chapter 2) involved inspecting, classifying and locating each and every GLF in Mars' mid-latitudes (within the coverage of the CTX imager at the time of survey design), full use of that opportunity was made to gather morphological observations. Thus, a prospective checklist of specific morphological characteristics to be identified during the survey

was first compiled. These criteria were designed to yield information on GLF flow history, fluvial activity or landscape modification, all of which are presently areas where our understanding of Mars' GLFs and associated VFFs is extremely limited.

Other factors taken into consideration include the nature of the imagery (panchromatic, two-dimensional, medium-resolution [6 m / pixel]) and how this would impact on feature identification. Items added to the checklist therefore focussed on larger features such as moraine-like structures, crevasses and fracture fields and some possible meltwater features, leaving the targeted high-resolution analysis of specific areas, prospectively selected on their merit as exhibiting particular characteristics, for the final stage of the project.

C2.1. The morphological checklist

This checklist is interpretive, not quantitative, and represents an observational guide, not a list of exclusive criteria.

The morphological characteristics included on the checklist were:

- Stratification.

- Evidence of cyclic activity (e.g. regularly spaced morphologies or textures apparently related to flow which may indicate an element of periodicity).

- An apparent 'ice margin' (or margin where the nature of the dominant sub-surface or intra-granular material appears to change abruptly).

- Lateral moraine-like structures.

- Medial-moraine-like structures, signifying the convergence of multiple flow units or some other flow inhomogeneity.

- Terminal moraine-like structures.

- The GLF's terminus exhibits a composite ridge-type complex.

- The GLF exhibits several 'nested' terminal moraine-like ridges / structures.

- Overlapping moraine–like structures (as evidence of multiple phases of glaciation leading to the over-riding of older landforms by subsequent ice flow and the superimposition of younger deposits atop older material).

- Intra-GLF crevassing.

- Morphologies indicative of meltwater activity either on the GLF or in immediate association with the GLF.

- Widespread or localised patches of 'fluting' or apparently flow-related raised structures on the GLF surface.

- Widespread or localised patches of 'fluting' or apparently flow-related raised structures immediately out-with the boundaries of the GLF.

- Morphologies indicative of spatially variable rates of intra-GLF flow, such as crevasses, shear zones or surface deformation patterns.

Clearly, the criteria for the visual identification of these characteristics are somewhat subjective, involving a degree of operator variability. Therefore, precise identification criteria or classification guidelines / constraints were not devised. Rather, the surveyor looked for general indications or qualitative evidence that the features or processes in question were present, an approach consistent with those employed in other classificatory publications previously published on the subject of Martian glacial geomorphology (e.g. Head et al., 2010).

Chapter 3:

Crevassing on martian glacier-like forms

1. Introduction

Increasingly abundant high spatial resolution imagery of Mars' surface has, over recent decades, permitted the scientific community as a whole to study the surface of The Red Planet at ever-escalating levels of detail. This enhanced availability of remotely sensed data was dramatically augmented in 2006 with the arrival in Mars' orbit of the Mars Reconnaissance Orbiter (MRO).

Amongst the many areas of martian research to benefit from advances in satellite imaging is the study of near-surface ice and the various landforms that are arguably attributable to glacial processes. A particularly striking expression of glacial activity on Mars are the glacier-like forms (GLFs) which have been described by various parties (e.g. Marchant and Head, 2003; Head et al., 2005; Forget, 2006), but most recently by Hubbard et al. (2011), Souness and Hubbard (2012) and Souness et al. (2012) (see also Chapter 1, Section 3.2.3). These GLFs are found almost exclusively in Mars' mid-latitudes (e.g. Milliken et al., 2003; Souness et al., 2012 [also Chapter 2, this volume]) and are similar (both in appearance and in apparent geomorphological context) to terrestrial valley glaciers. On Mars they constitute a low-order mass source area for what Head et al. (2010) have described as being integrated glacial landsystems (Chapter 1, Figure 7).

The overall appearance and general morphology of GLFs strongly suggest that they have been, and perhaps still are, subject to viscous flow, resulting in a spatially variable regime of stress and strain throughout their mass extent. As yet, the factors responsible for initiating and sustaining this flow have been only tentatively investigated. Studies of GLF morphometry and distribution relative to various geographical parameters do, however, suggest a sensitivity to elevation and local relief (Souness et al., 2012 [Chapter 2, this volume]), although little is known about the distribution of strain within individual GLFs. Changes occur too slowly for repeat imaging to detect any motion and the current impossibility of field observation precludes small-scale measurement of GLF motion and /or change in-situ. This gap in our understanding of how martian glacial processes operate has thus far been an impediment to the scientific community's understanding of various associated and potentially important issues, such as the extent to which liquid water is (or has been)

present in the martian cryosphere during geologically recent times, and whether flow in GLFs is affected by mass-balance-related factors (such as accumulation at higher elevations) or simply by local relief and gravity-induced creep.

1.1. Crevassing on martian GLFs

The increased availability of high-spatial resolution imagery from satellite-borne platforms (such as those mentioned above) has enabled interested parties to identify and map not only middle to large-scale features (such as GLFs and associated components of Mars' integrated glacial landsystems) but also the smaller-scale landforms and textures found on, and in conjunction with, GLFs. Examples of these smaller-scale landforms include moraine-like ridges (as described by Arfstrom and Hartman, 2005), polygonal surface patterning (e.g. Mangold 2005; Burr et al., 2005; Soare et al., 2008; Levy et al., 2010) and topography associated with localised mass movement such as landforms formed through processes of compression and extension. The surface expression of the latter strain-related activity varies from chevron-like compression ridges, flow-transverse mounds and furrows, to fissures and sharply-defined troughs of varying dimensions and arrangement. Some supra-GLF fissures such as those mentioned above are strikingly similar in appearance to the crevasses which are commonly observed on Earth's glaciers and which, in this terrestrial context, are synonymous with the flow of ice.

1.2. Crevassing on Earth's glaciers

Flow within terrestrial glaciers is predominantly initiated by gravity but also affected and enhanced by the accumulation of snow and ice at higher altitudes. The weight of this accumulated mass causes ductile flow within the bulk ice which subsequently occurs throughout a glacier's mass, subject to local variations in velocity and vector vector (i.e. material moving at a given speed and in a specific known direction). Changes in velocity occur systematically according to position within a glacier. Where high velocity (and thus strain) results in local strain rates that exceed the brittle failure point of the glacier's mass, fracture occurs. Thus, the observable

patterning of fractures (crevasses) in glacier ice on Earth relates directly to local variations in ice flow and associated strain rates, providing a visual record of an individual glacier's strain regime (Hambrey and Lawson, 2000; Cuffey and Patterson, 2010). This relationship has led to crevasses on Earth's glaciers being described as "the writings in a glacier's history book" (Herzfeld et al., 2001).

Examples of crevasse patterns commonly observed on the surface of ice masses on Earth (Figure 1) include: 1: complex crevasse patterning in areas where ice flows over a bedrock protuberance or sudden increase in gradient (generally known as an 'icefall'), initiating fracture through local surface extension (Figure 1, a); 2: linear crevasses which extend from the valley walls toward the middle of the channel in an up-valley direction (Figure 1, b), normally explained by simple extensional shear caused by friction along the valley walls and the resultant retardation of ice flow in these lateral zones relative to mid-channel flow; 3: longitudinal crevasses aligned parallel to direction of flow (often observed at a glacier's snout) and generally understood as being the result of lateral ice extension in zones of longitudinal compression (e.g. where a glacier flows against a bedrock protuberance [Figure 1, a.], the bed slope shallows or the basal ice layers flow across a zone of enhanced basal drag caused perhaps by a change in geology or, in the case of polythermal glaciers, localised 'freezing-on' of the ice to the substrate); 4: arcuate, mid-channel crevasses which are concave in the direction of flow and which usually form as a result of local acceleration of the ice which causes extensional stresses (Figure 1, c) (These vary laterally and systematically across the width of a glacier); 5: long, linear crevasses (often known as 'bergschrunds') that extend transversely across the upper-reach of a glacier (often immediately adjacent to the headwall) (Figure 1, d), caused by the flow of basally 'lubricated' ice away from stationary or 'cold-based' ice at higher elevations, and the separation of a glacier from its rock headwall.

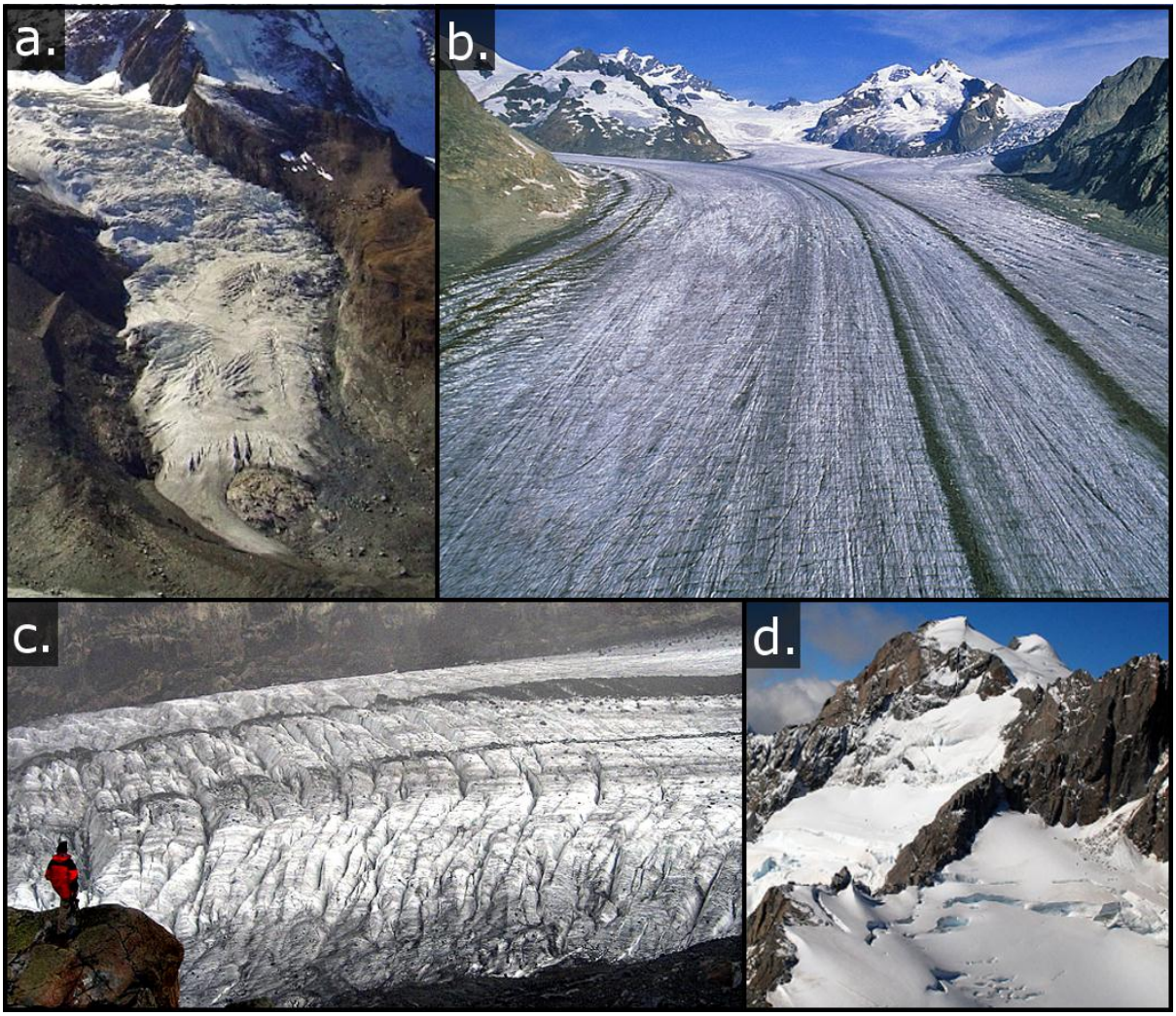

Fig. 1: A montage of images illustrating various manifestations of crevassing on terrestrial glaciers (all images from www.swisseduc.ch/glaciers). 'a.' depicts Breithorngletscher in the Swiss Alps, which exhibits both an 'icefall' (where local acceleration and ice extension due to a steepening in the basal gradient has caused extensive crevassing) and longitudinal crevasses at the glacier's snout (in this case caused by compression where the ice is flowing against a bedrock protuberance). 'b.' shows the Grosseraletsch Glacier in Switzerland which in this picture features transverse crevasses extending from the valley walls on both sides of the imaged scene (direction of flow is towards the camera). These crevasses point slightly up-valley, and are caused by lateral shear where higher friction against the bedrock of the valley sides slows the ice down. 'c.' shows arcuate crevasses on the glacier Vadret Pers, also in the Swiss Alps (direction of flow is to the left of the scene). Here, acceleration on the lip of an icefall has caused arcuate fracturing, oriented concave side down-stream. 'd.' is an image of the upper reaches of Franz Josef glacier in New Zealand, featuring well-defined bergschrunds in the foreground of the scene.

1.3. Justification

As discussed in Section 1.2., mapping and evaluating the overall distribution, orientation and geometry of crevasses on Earth can help us to better understand the particulars of flow within any given glacier. In addition the response of an ice mass to strain is, to a large extent, also a function of that ice mass' precise rheology and composition. The examination and mapping of crevasse patterns also has the potential to provide information on the physical make-up and internal structure of a glacier. Extending this analytical method to martian GLFs could enhance our understanding of GLF flow dynamics and GLF composition. This could, by extension, provide insight into the emplacement history of martian ice deposits and thus geologically recent climate changes on Mars.

2. Aims and objectives

The work described in this chapter aims to report upon the hitherto unreported occurrence of crevasses within the previously surveyed population of GLFs (as surveyed by Souness et al. [2012], Chapter 2 this volume). We also aim to explore the diversity of crevasse patterning and associated morphologies observed in this population. By doing so, and by applying the terrestrial analogue of crevasse formation, we intend to further develop the scientific community's understanding of GLF composition, flow and initial emplacement.

Our specific objectives are: (a.) To compile a database of parent images and precise feature co-ordinates detailing the location of GLFs which exhibit clear surface crevassing; (b.) To conduct an analysis of the distribution of these crevassed GLFs relative to the overall GLF population (discussed in Chapter 2) in order to ascertain if crevassing occurs preferentially within certain geographically specific niches; (c.) To describe and analyse the various crevasse patterns which occur on GLF surfaces; (d.) To apply the terrestrial model of crevasse formation, draw comparisons where appropriate and develop new hypotheses on the spatial variability of GLF strain networks and flow regimes.

3. Methods

3.1. Survey

The survey made by Souness et al. (2012) (also Chapter 2 of this thesis) resulted in the identification of 1309 individual GLFs, all of which were located and mapped precisely using JMars martian GIS software. During this survey attention was paid to the characteristics of individual GLFs (Preface to Chapter 3). Those which displayed fracture patterns similar to terrestrial crevasses were highlighted. These selected GLFs were re-visited and examined. A database of these crevassed GLFs (complete with co-ordinates describing the position and morphometric characteristics of each GLF in question) was collated and is presented within this volume in table format (see Appendix 2). The positions of crevassed GLFs were also mapped using ArcMap software, facilitating visual analysis of crevasse patterning and distribution.

3.2. Interpretation and analysis of martian crevasse case studies

GLF examples exhibiting i) particularly well-defined crevasse fields and ii) varied patterns within those fields, were selected and the parent image downloaded to permit efficient and detailed inspection and landform interpretation.

Images featuring exceptional examples of crevassing were projected using the ArcMap GIS package and geomorphological maps were constructed highlighting visible surface structures and textures which would facilitate easy comparison with Earth analogues. The criteria used in landform identification and mapping are shown in Table 1.

Following the inspection, mapping and general characterisation of the crevasse patterns observed on the selected GLFs, the available body of literature on terrestrial crevassing (and its relationship to the flow and deformation of glacier ice on Earth) was consulted. Various authoritive texts on the deformation of glacier ice and how this manifests as surface crevassing are available (e.g. Cuffey and Paterson, 2010; Lawson and Hambrey, 2000). Using the terrestrially-derived model of crevasse

Table 1: A list of the landform classes (left-hand column) which were observed and mapped in the mapping efforts described in Section 3.2. The second column outlines the visual criteria used in the identification of each surface type or feature class. Some possible ms-interpretations or sources of confusion or error in landform identification and interpretation are given in the third column, whilst the right-hand column outlines the significance of each feature or surface class and how its identification might help observers to develop our understanding of martian GLFs, how they formed, how they flow and how they contribute to the shaping of Mars' surface.

Feature	Identification criteria	Possible interpretation errors	Significance
GLF area	The actual body of a GLF; this area should be enclosed by topography for the majority of its length and appear relatively flat, suggesting that this valley or enclosed space is filled by a non-bedrock mass (i.e. ice). The surface should show evidence of flow, either in the form of transverse deformation patters such as ridges, fractures or chevrons, or linear structures suggestive of flow direction. It may also be delineated by marginal structures similar to terrestrial moraines and have a recognisable source area and/or terminus.	Many different deposits can be confused with or mis-interpreted as GLFs. For example, lava flows, debris fans and dust-filled valleys can exhibit structures similar to those common to GLFs. This issue of equifinality is a problem in GLF mapping, especially as GLFs, despite being composed of a distinctive substance (a mixture of ice and regolith of unknown proportions) are universally buried beneath a layer of martian dust and rock which is hard to distinguish from the surrounding area.	GLFs themselves, as bodies of accumulated ice, constitute compelling evidence of geologically recent and profound climate change on Mars. Studying their morphology and mechanisms of evolution could provide valuable insight into planetary climate change and the ways in which water exists, behaves and contributes to the evolution of the martian environment.

Flow-parallel lineations	Linear, flow-parallel intra-GLF structures with positive relief (possibly analogous to medial moraines observed on Earth's glaciers).	As the precise mechanisms of mass accumulation and flow initiation are unknown, it is possible, although in most cases unlikely, that flow-transverse structures may be confused with flow-parallel structures.	These lineations give an indication of mass-movement pathways and local flow vectors, showing from whence mass has come and to where it is being transferred.
Flow-transverse lineations	Linear structures with positive or negative relief that are arranged roughly transverse to the apparent direction of flow (for example chevrons or compression ridges). These can be straight, arcuate or variably contorted.	As above, flow-transverse lineations could potentially be confused locally with flow-parallel lineations.	Structures with a flow-transverse habit can, through their overall form and contortion patterns, provide an indication of local flow rates and the distribution of stresses within the flowing substrate.
Crevasses	An opening or fracture with a roughly linear form (i.e not simply a roughly-circular hole), located on the surface of a GLF and orientated in any direction.	In certain light or contrast conditions, or where candidate features are closely spaced, it is possible to confuse positive and negative relief. Thus linear ridges could, in certain circumstances, be inaccurately interpreted as crevasses.	Crevasses will provide insight into where GLF mass is deforming or flowing at a rate beyond that which its ductile properties or crystalline structure is able to cope. Thus, an improved picture of local-scale variations in GLF strain regimes can be built, along with a better understanding of GLF composition.

Crevasse traces	Faint, short lineations of a form and orientation consistent with terrestrial crevassing but with poorly pronounced relief, suggesting a sealed, filled or annealed crevasse.	A range of possible alternative interpretations exist for crevasse traces, such as simple flow-transverse lineations, local compression ridges, small open crevasses or even surficial meltwater channels.	Crevasse traces can, as is the case for crevasses themselves, indicate variations in local strain rates. However, they can also show where and how flow rates and or GLF mass has changed in character spatially and temporally, once open crevasses having closed due to the agency of some factor.
Possible crevasse-fill ridges	Narrow, linear ridges with positive relief situated adjacent to the GLF surface or on the GLF where ice deposits appear to be thin and texturing suggests extensive mass wasting. They should be located and arranged in a manner reminiscent of terrestrial crevasses.	It is possible that the crevasse-fill ridge interpretation could mistakenly be applied to moraine-like ridges (MLRs) or particularly narrow and closely-spaced compression ridges / flow-transverse lineations.	Crevasse-fill ridges could indicate areas where crevasses once existed in thicker ice and possibly extended all the way to the GLF bed, allowing either basal or surface debris to enter and fill the crevasse. When the ice ablated a ridge of these deposits remained, preserving the imprint of the crevasse. These provide insight into past ice structures and give an indication of the properties of basal and / or surficial debris properties.

Moraine-like ridges (MLRs)	Long (several Km) ridges of material, often raised substantially (> 100 m) above the surrounding / adjacent VFF surface and with widths often in excess of 500 m (Arfstrom and Hartmann., 2004). MLRs are often seen running parallel to and at the margins of VFF, and are often arranged in an arcuate manner at the terminus of individual flow units.	MLRs are very distinctive and confusion with any particular alternative feature is unlikely, especially as all martian landform designations are purely descriptive. However, Bedforms or streamlined bedrock protuberances could assume similar forms, as could compression ridges at the snout of a GLF, so care should be taken.	MLRs likely mark the former terminal position of GLFs and may testify to the ability of GLFs to transport and perhaps even erode material from the immediate area
Impact craters	Impact craters are simply the sunken, negative relief hollows left in a surface that has been struck by a meteoroid. They are usually roughly circular, but can be distorted by mass movement within the impacted substrate, partially obscured by adjacent mass deposition or, in the case of craters inicy masses, degraded by sublimation or mass wasting.	Impact craters are usually easy to identify and distinguish from the surrounding surface. However, due to distortion and surface degradation in the underlying, impacted surface, cases occur where this is not the case. Therefore many craters may be missed. Also, as icy masses flow and distort, it is known for roughly circular formations to occur in surfaces by means other than meteoroid impact. These can even be recessed features if ice composition varies locally, resulting in	Impact craters can be useful indicators of local flow or mass deformation. Where craters have been distorted or stretched, they provide a record of local strain. Also, where they have been superposed upon another feature or partially concealed beneath a deposit they give a record of successive events and landform histories. Also, over larger areas, the relative density of cratering can provide ameans of relative surface dating through ‘crater counting’.

		variable ablation rates. So, there are opportunities for flow-related morphologies to mistakenly be classified as craters.

formation (as a function of variable englacial strain) inferences were drawn about the spatial variability of strain rates and, thus, flow velocities within martian GLFs.

3.3. Conducting a statistical analysis of crevassed GLF distribution

Using the geographical attributes of the crevassed GLFs (gathered during the investigations outlined in Chapter 2), it was possible to investigate the distribution of crevassed GLFs (according to latitude, elevation and relief) relative to that of the generalized GLF population. It was then possible to compare the overall distributions of crevassed GLFs (plotted according to gradations within the variables discussed above) with those of the similarly binned overall population. Thereafter, just as overall population distribution was analysed relative to Mars' mid-latitude hypsometry in Section 2.6, Chapter 2, crevassed GLF population (again binned according to latitude, elevation and relief) was plotted as a normalised proportion of the overall GLF population corresponding to each bin. This gives an indication of whether crevassed GLFs are proportionately represented throughout the overall GLF population's 'domain' (as defined by latitude, elevation and relief) or whether anomalously high / low concentrations occur. To do this, the count of crevassed GLFs for each bin was worked out as a percentage of the total crevassed GLF population, or 'normalised'. The same was done for the number of GLFs from the overall GLF population that fell into each bin. Finally, the number of crevassed GLFs was calculated as a normalised ratio of overall GLFs:

$$\frac{\%\ \text{crevassed GLFs}}{\%\ \text{overall GLFs}}$$

Where crevassed GLF/Overall GLF ratio was <1, crevassed GLFs are under-represented, possibly suggesting that conditions (as defined by the relevant geographical variable : latitude, elevation or relief) are unsuitable or sub-optimal for crevasse formation. Where crevassed GLF/Overall GLF ratio is exactly 1, crevassed GLFs are represented exactly proportional to the overall GLF population. Thus, naturally, where the crevassed GLF/Overall GLF ratio is >1, crevassed GLFs are over-represented, possibly suggesting that conditions within this environmental niche are conducive to, or optimal for, crevasse formation.

4. Results

4.1. Survey results

4.1.1. Mapped geographical distribution

In total, from an overall population of 1309 GLFs, 64 individual examples (4.98% of the total population) were identified which displayed crevasses. Of these 64 examples, 37 (57.8%) were located in the northern mid-latitudes and 27 (42.2%) were located in the southern mid-latitudes. This hemispheric weighting is similar to that observed in the wider GLF population (55.5% located in the northern mid-latitudes and 44.5% in the southern mid-latitudes).

Inspection of the distribution of crevassed GLFs, mapped in Figure 2, shows crevassed GLFs clustering in certain areas (Figure 2). However, the precise areas in which these population highs occur vary slightly from those observed in the overall population distribution (Figure 4, Chapter 2).

In the northern mid-latitudes the zones most densely populated with crevassed GLFs are, as per the wider population described in Chapter 2 (Section 3.1), Protonilus Mensae and Deuteronilus Mensae. Clustering also seems to occur locally, crevassed GLFs often occurring in small groups on the same butte and feeding into the same LDA. Several examples of this can be seen in Figure 2b. which details an area of Deuternonilus Mensae. Notably, crevassed GLFs are not well represented in

other areas of the northern mid-latitudes which in the earlier survey of general GLF population distribution also hosted dense population clusters (Section 3.1, Chapter 2). For example, concentrations of crevassed GLFs might have been expected in Acheron Fossae, Tempe terra and Phlegra Montes (Figure 4, Chapter 2). However, only isolated examples occur in these areas (Figure 2).

In the southern mid-latitudes, the largest clustering of crevassed GLFs occurs in the mountainous terrains of northwest Argyre Planitia, with other smaller concentrations visible in Noachis Terra and in a crater (name unknown) to the west-northwest of Hellas Planitia. Although northwest Argyre Planitia does host a notable concentration of GLFs in the previously discussed population-wide survey (Chapter 2), the distribution of crevassed GLFs in Mars' southern mid-latitudes is otherwise quite different to the distribution of GLFs more generally. For example, in the population-wide survey, the most concentrated population of GLFs in Mars' southern mid-latitudes lies in Eastern Hellas (identified as containing approximately 32% of the southern hemispheric total of GLFs) (Chapter 2, Figure 4). This area is, however, only sparsely populated by crevassed GLFs.

4.1.2. Results from the statistical analysis of crevassed GLF distribution

The distribution of crevassed GLFs was investigated firstly with respect to variable latitude, elevation, and relief (as per this chapter, Section 3.3, and Chapter 2, Section 2.5). Secondly, the distribution of crevassed GLFs was analysed relative to the overall distribution of GLFs more generally in an attempt to ascertain if there were any geographically-defined population niches in which crevassed GLFs were most commonly observed.

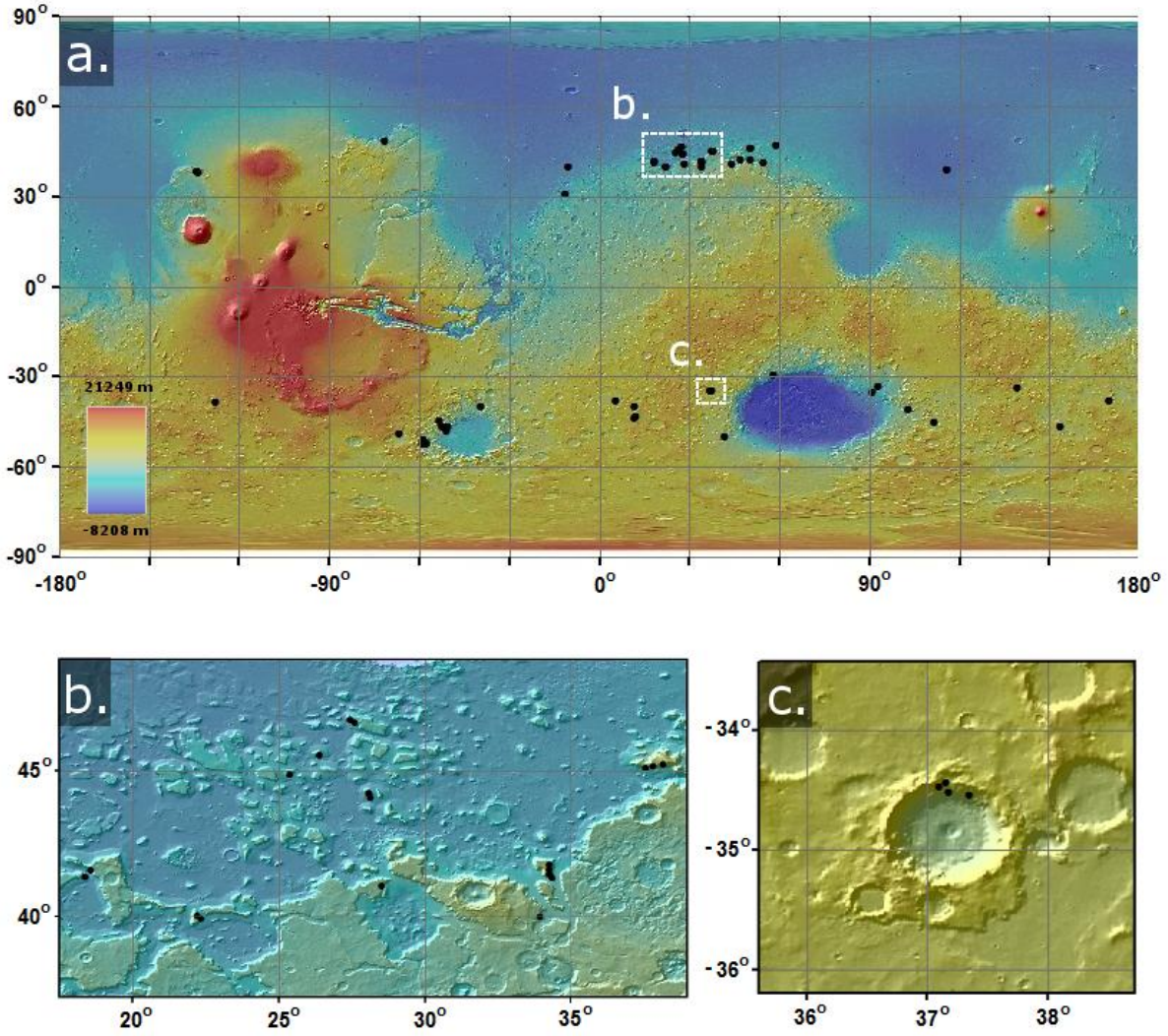

Figure 2: Maps depicting the distribution of crevassed GLFs in Mars' mid-latitudes. These maps are based on a colour-ramped MOLA digital elevation model with a hillshade effect applied to provide an impression of relief. (a.) shows the overall distribution of crevassed GLFs, with 64 cases occurring globally. 37 of these are located in the northern mid-latitudes and 27 are located in the southern mid latitudes. Where populations are too densely clustered to resolve effectively in (a.), expansions are provided at (b.) and (c.), the areas covered being illustrated in (a.) by white dashed boxes. (b.) shows detail of eastern Deuteronilus Mensae and western Protonilus Mensae, where the highest concentration of crevassed GLFs occurs. (c.) shows an expansion of an un-named crater to the west of the Hellas Planitia impact basin where a particularly clustered group of crevassed GLFs occurs.

The distributions of crevassed GLFs (alongside the distribution of GLFs more generally, for comparison) relative to latitude, elevation and relief, are shown in Figures 3, 4, and 5. Summary data for these distributions are shown in Tables 2 and

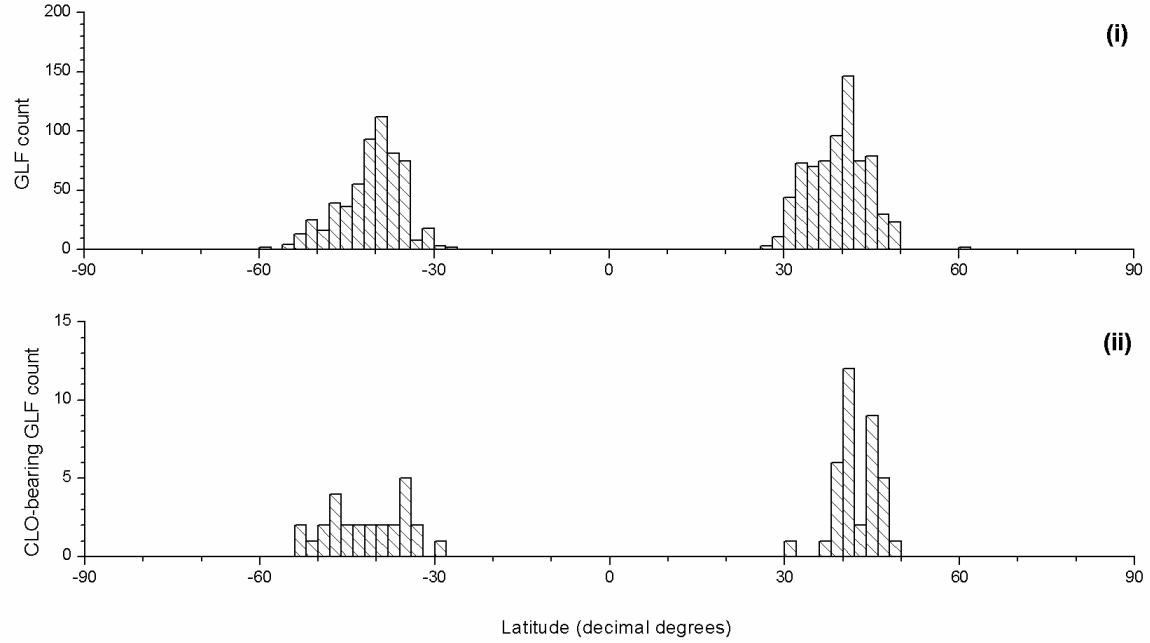

Figure 3: Bar charts showing the distribution of both the general GLF population and of the crevassed GLF population relative to latitude. Overall general GLF distribution is shown at (i). Crevassed GLF distribution is shown at (ii).

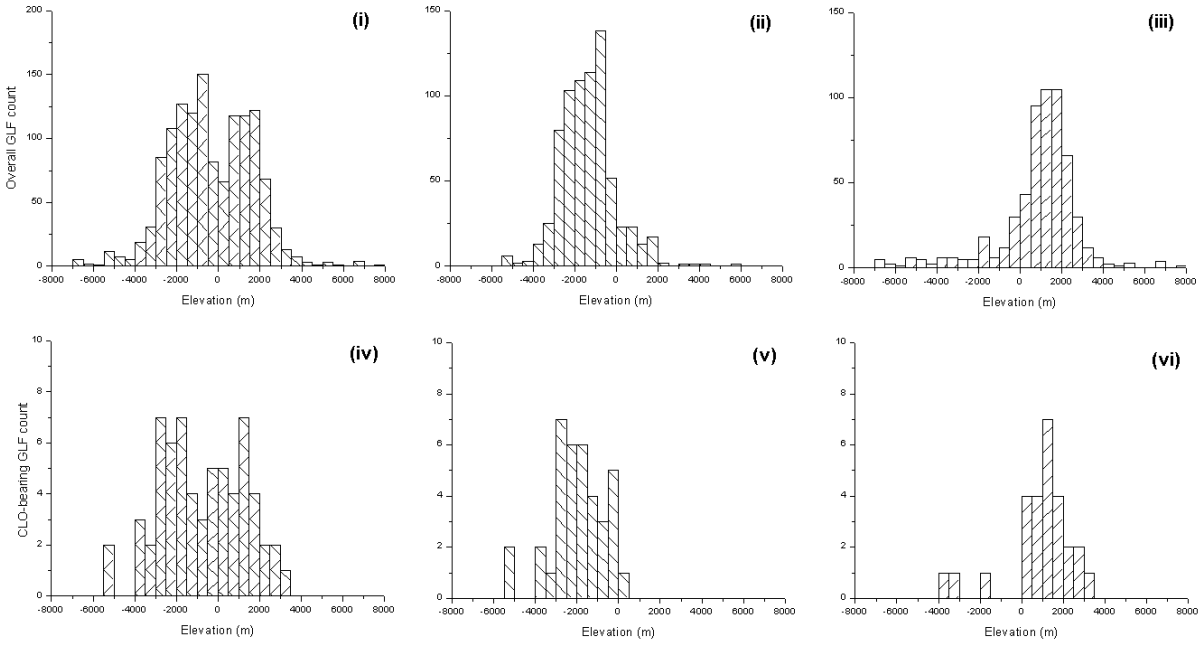

Figure 4: This collection of plots show the distribution of general GLFs and crevassed GLFs relative to elevation. Overall GLF population distribution is shown globally, for the northern mid-latitudes and for the southern mid-latitudes at (i), (ii) and (iii) respectively. Crevassed GLF population distribution is similarly shown at (iv), (v) and (vi)

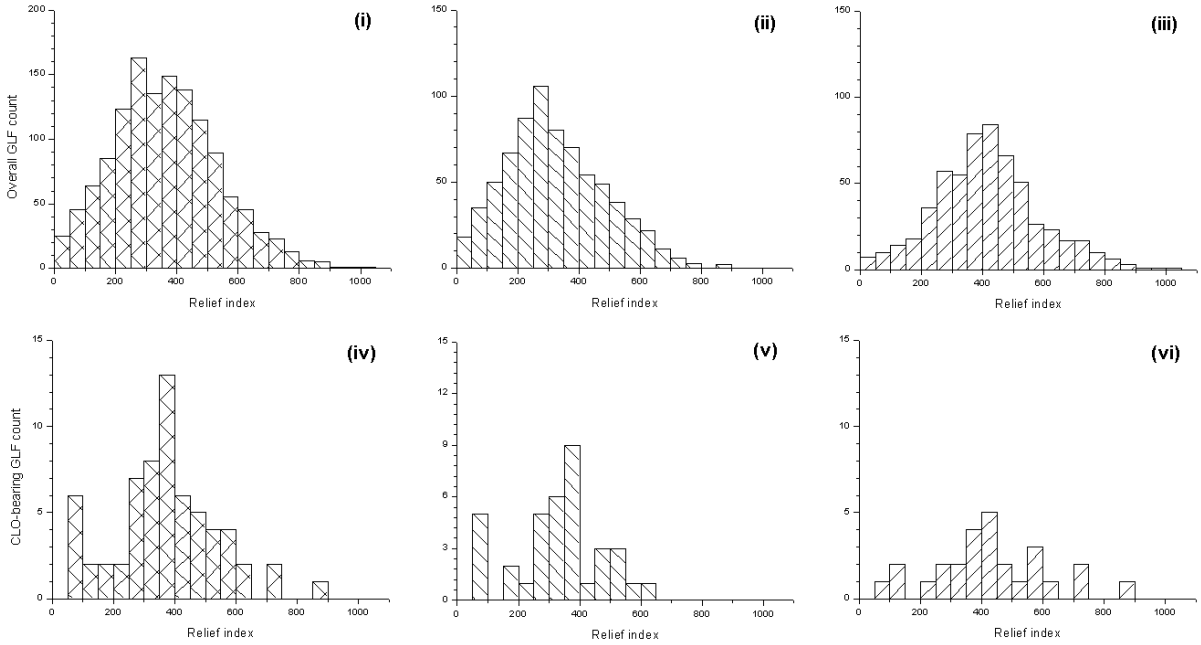

Figure 5: Bar charts showing the distribution of GLFs generally [(i), (ii) and (iii)], and of crevassed GLFs [(iv), (v) and (vi)] relative to local relief (Std. Dev. of elevation values [see Chapter 2, Section 2.4]). The distribution of the general GLF population relative to relief is shown globally, for the northern mid-latitudes, and for the southern mid-latitudes at (i), (ii) and (iii) respectively. The distribution of crevassed GLFs relative to relief is similarly shown in (iv), (v), and (vi).

3. The data in these tables show some differences between the distribution of crevassed GLFs and the wider population.

4.1.2.1. Latitude

With respect to latitude, crevassed GLFs in the northern mid-latitudes appear to be clustered around a mean of 42.3º, slightly higher than the general population mean in this area (39.3º) (Tables 2 and 3). The southern mid-latitude populations however are more closely matched, crevassed GLFs clustering around -41.6º whilst the overall population of GLFs are distributed around a mean latitude of -40.7. Comparing the standard deviation (st. dev.) of the latitude-dependent populations around their respective means shows that the distribution of crevassed GLFs varies

Table 2: Basic descriptive statistics of (general) GLF distribution relative to latitude, elevation and relief (std. dev. of local elevation values). All values are given to within 3 significant figures (see Figures 3.i, 4.i, 4.ii, 4.iii, 5.i, 5.ii and 5.iii).

ROI	Parameter	Mean	St. dev.	Skewness	Kurtosis
All	Latitude (º)	-	-	-	-
	Elevation (m)	-366	1954	0.049	0.387
	Relief (m)	364	171	0.413	0.108
North	Latitude (º)	39.3	4.94	0.0682	0.0249
	Elevation (m)	-1366	1292	0.592	2.37
	Relief (m)	323	161	0.489	-0.074
South	Latitude (º)	-40.7	5.27	-0.582	0.270
	Elevation (m)	885	1922	-1.28	3.89
	Relief (m)	417	168	0.347	0.447

less (statistically) around the mean in the northern mid-latitudes than the overall population (Tables 2 and 3). In the southern mid-latitudes however, the opposite is true.

Skewness values are not strikingly different between the populations, although the crevassed GLF population in the northern ROI is slightly skewed toward lower latitudes whilst the general GLF population skews slightly towards the pole. A more pronounced difference exists between the two populations when we compare kurtosis values. In both mid-latitude ROIs kurtosis is considerably higher for the

crevassed GLF population than for the general population; 1.86 compared to 0.0249 in the northern ROI and -1.16 compared to 0.270 in the southern ROI. From this we

Table 3: Basic descriptive statistics of crevassed GLF distribution relative to latitude, elevation and relief (std. dev. of local elevation values). All values are given to within 3 significant figures (see Figures 3.ii, 4.iv, 4.v, 4.vi, 5.iv, 5.v and 5.vi).

ROI	Parameter	Mean	St. dev.	Skewness	Kurtosis
All	Latitude (º)	-	-	-	-
	Elevation (m)	-777	1994	0.023	-0.712
	Relief (m)	371	166	0.331	0.626
North	Latitude (º)	42.3	3.5	-0.796	1.86
	Elevation (m)	-1983	1247	-0.541	0.432
	Relief (m)	332	134	-0.21	-0.181
South	Latitude (º)	-41.6	6.63	-0.03	-1.16
	Elevation (m)	876	1604	-1.4	2.61
	Relief (m)	425	187	0.287	0.366

can infer a more distributed population, variation being more the result of infrequent, extreme deviations in the case of crevassed GLFs than for the more general population, which is more 'Gaussian' by comparison.

4.1.2.2. Elevation

Some striking differences are immediately apparent when comparisons are made between the general GLF and crevassed GLF distributions relative to elevation (Tables 2 and 3). Firstly, the global mean values are quite different. The mean global elevation of crevassed GLF distribution is -777 m, compared to only -366 m in the general population. Thus, overall, crevassed GLFs would appear to occur more often

at lower elevations. Inspection of the hemisphere-specific populations supports this observation in the northern ROI where crevassed GLFs are centred around a mean elevation of -1983 m compared to -1366 m in the general population. The data from the southern ROI does not show such a striking dis-similarity, however crevassed GLFs are still observed to cluster around a mean elevation that is lower than that of the general population, albeit only by ~10 m (876 m compared to 885 m). Std. dev. data for the three population sets are broadly similar between the crevassed suite and the general population (Tables 2 and 3). The statistical skewness of the population distributions relative to elevation are also comparable, although the data for the northern ROI reveal a bias toward lower elevations in the crevassed population which is not present in the general population. Kurtosis shows higher incidence of 'extreme' deviations in the crevassed population on a global scale, however a lower incidence is apparent when populations are viewed at a hemispheric level where distribution appears to be more statistically centralised in the case of crevassed GLFs.

4.1.2.3. Relief

Minimal variation is apparent between the distributions of the two populations relative to relief (Tables 2 and 3). The mean values, both at a global and at a hemispheric scale, show little difference between the general and the crevassed populations. Std. dev. is also similar, as are measurements of skewness. Only kurtosis shows any obvious variation, and then only at the global scale, where variation in the distribution of crevassed GLFs appears to be more attributable to infrequent, extreme values than is the case in the general population, the distribution of which appears to be more 'Gaussian'.

4.1.2.4. Crevassed GLFs/General GLFs as a normalised ratio

The population of crevassed GLFs (again binned according to variations in latitude, elevation and relief) was plotted as a normalised proportion of the overall GLF

population (see Section 3.3). These plots, corresponding to latitude, elevation and relief, both globally and hemispherically, are shown in Figure 6.

Relative to latitude, the normalised plot for Mars' southern mid-latitudes shows that crevassed GLFs are over-represented at the lower and higher of the latitudinal ranges occupied by the wider GLF population. In the mid-ranges, i.e. around the overall population's mean latitude of 41°, crevassed GLFs are under-represented. In the northern mid-latitudes the situation is slightly different. crevassed GLFs are strongly under-represented at lower latitudes and over-represented at higher latitudes. Around the northern-hemispheric mean (again ~40°) crevassed GLFs are slightly over-represented, however, this over-representation is minor compared to that of the higher latitudes. It is worth noting here that in the northern hemisphere, these higher latitudes correspond to lower elevations, being to the north of the martian global dichotomy boundary (see Chapter 1, Figure 1, or Chapter 2, Figure 5).

Relative to elevation, the normalised distribution of crevassed GLFs shows pronounced visual skewness (Figure 6). At both a global and at a hemispheric scale, crevassed GLFs are consistently over-represented at lower elevations, and then heterogeneously represented at middle and higher elevations.

Relative to relief, crevassed GLFs are, for the most part, heterogeneously represented as a normalised proportion of the overall population, with no major skewness apparent in the plots (Figure 6). However, in both the northern mid-latitudes and in the southern mid-latitudes respectively, large outlying over-representations occur in the lower relief and higher relief zones respectively.

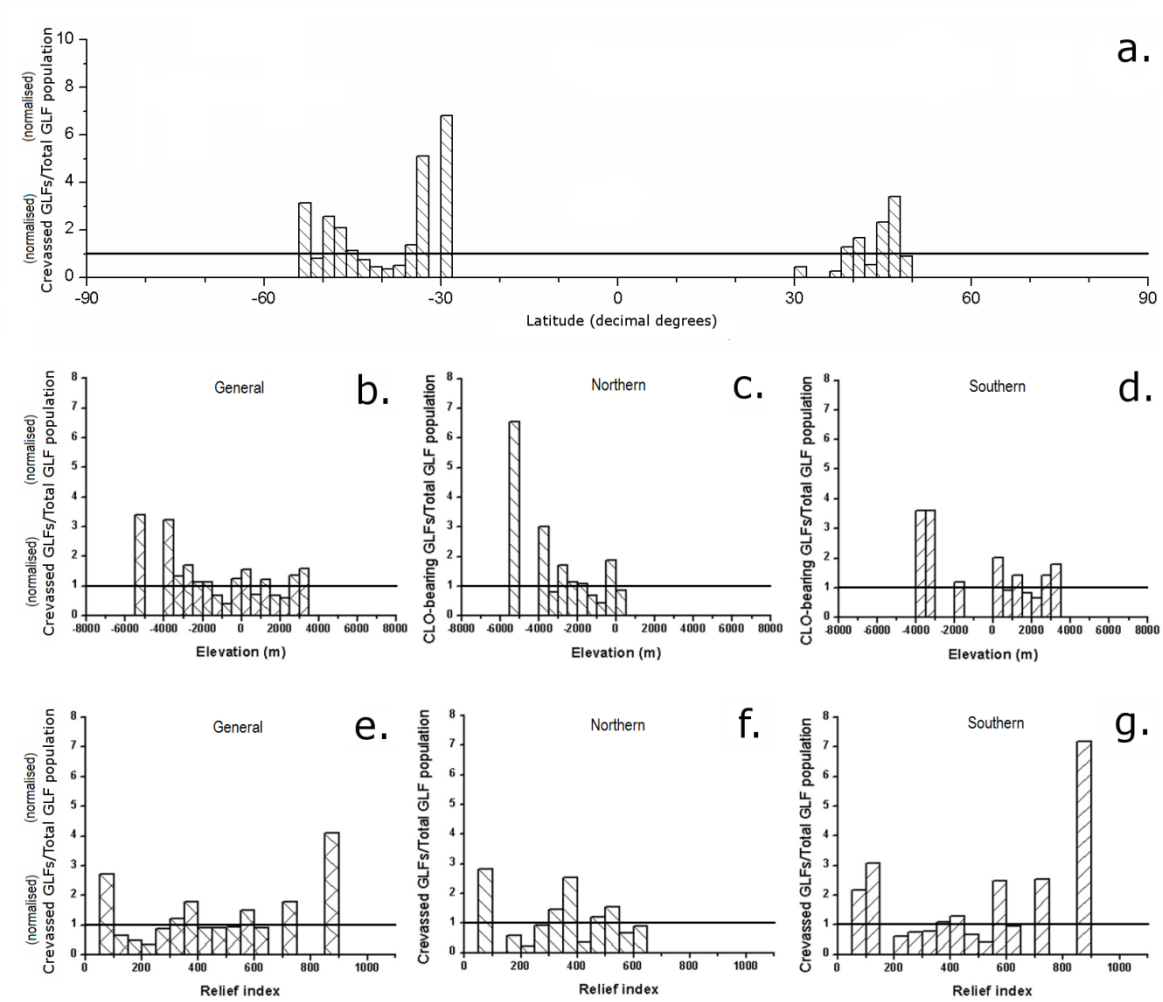

Figure 6: Bar charts showing the distribution of the crevassed GLF population (relative to latitude, elevation and relief) as a normalised proportion (see Section 3.3) of the more general population. 'i)' shows the normalised crevassed population relative to latitude, both globally and hemispherically. 'ii)', 'iii)' and 'iv)' show crevassed GLFs (normalised) distributed relative to elevation at a global, northern mid-latitude and southern mid-latitude scale respectively. 'v)', 'vi)' and 'vii)' show the same, only in these latter cases normalised distribution is plotted relative to relief.

4.2. Intra-GLF crevasse patterns

Close examination of the 64 crevassed GLFs discussed above (and mapped in Figure 2) led to the identification of several distinct and recurring crevasse pattern types, similar to patterns recognised and well-understood in terrestrial examples of

crevassing. These patterns are described below along with a short interpretation, and each with reference to a specific example and accompanying figures.

The first manifestation of crevasses observed on GLFs, and possibly one of the most striking, is illustrated by the GLF shown in Example 1 (Figures 7 and 8). This pattern comprises a dense cluster of transverse linear crevasses located on an abrupt increase in slope (see 3D view in Figure 7a). In the case of Example 1 (Figures 7 and 8), this abrupt increase in slope is located just down-flow of the point at which the featured GLF appears to flow out of a cirque-like alcove.

Crevasses were also occasionally observed along the flanks of certain GLFs. A clear case of this (Example 2) is shown in Figure 9 'b.' (see also Figure 10). These lateral crevasses are linear, and in the case of Example 2 (Figure 9 'b.') are located along the featured GLF's western flank. These crevasses point slightly up-valley and progressively rotate down-slope towards a more transverse alignment (Figure 9 'b.' and Figure 10).

The third example of observed crevasse patterning is also shown in Figure 9 ('c.'). These crevasses are orientated longitudinally and are located near the featured GLF's terminus, in a region where the GLF appears to spread laterally to form a broad piedmont lobe (Figure 9 'a.' and 'c.', and Figure 10). These crevasses are located along the approximate centreline of the GLF and are orientated parallel to the orientation of the valley and orthogonal to a series of major compressional ridges (Figure 10).

Next, we observed arcuate crevassing. This pattern is very infrequently observed on Mars, but is shown clearly by Example 4 (featured in Figures 11 and 12). Here, the featured GLF appears to comprise two side-by-side flow units, each of which exhibits a set of nested arcuate crevasses. The common boundary of each flow unit also appears to form the boundary between the two sets of crevasses, both of which are orientated concavely down-feature (Figure 11 'b.' and Figure 12). The emplacement of these crevasses is unusual, corresponding to no obvious topographic or contextual peculiarities or features which might have precipitated their formation. We

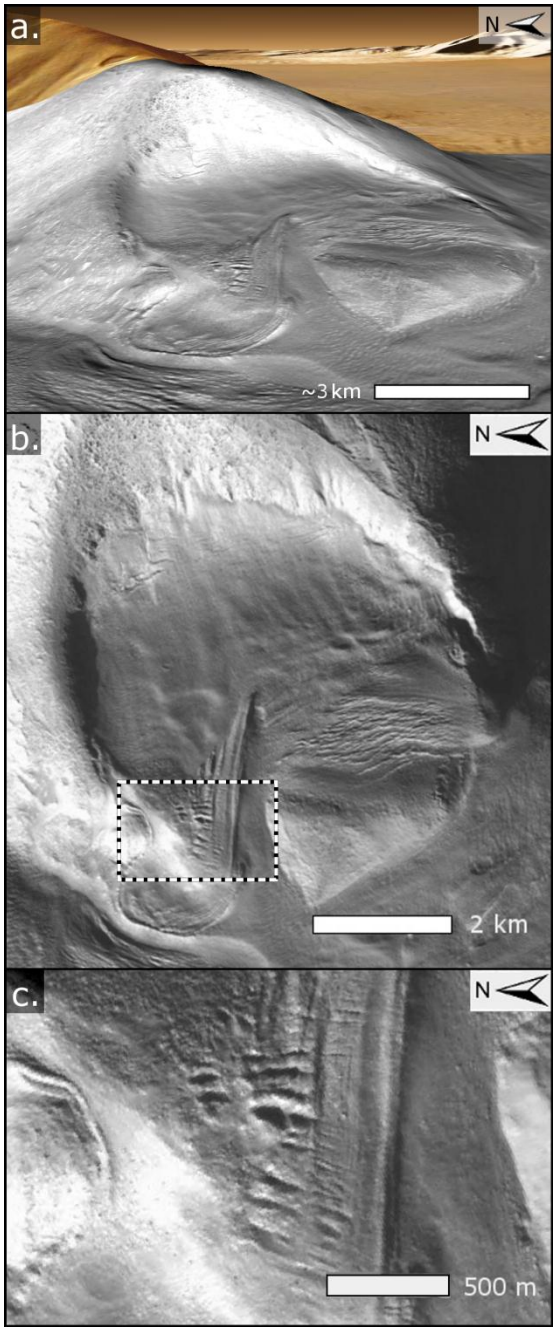

Figure 7: Crevassed GLF Example 1, located in eastern Hellas in Mars' southern mid-latitudes (CTX image: B20_017616_1391_XI_40S257W). This GLF features transverse linear crevasses, some of which are up to 50 m wide and 200 m long. A 3D perspective from the west is shown in 'a.' (Google Mars™), a plan view showing the crevasses in context is shown in 'b.', and an expansion of the dashed box in 'b.' is shown in 'c.'. In this case, crevasses appear to have formed where the GLF flows over a bedrock lip and out of a cirque-like alcove (see 'a.') (note that in 'a.', 'b.' and 'c.', illumination is from the west [bottom] of the scene). Here, increasing gradient has resulted in strong longitudinal extension, causing transverse brittle fracture and crevassing, strikingly similar to an icefall on Earth.

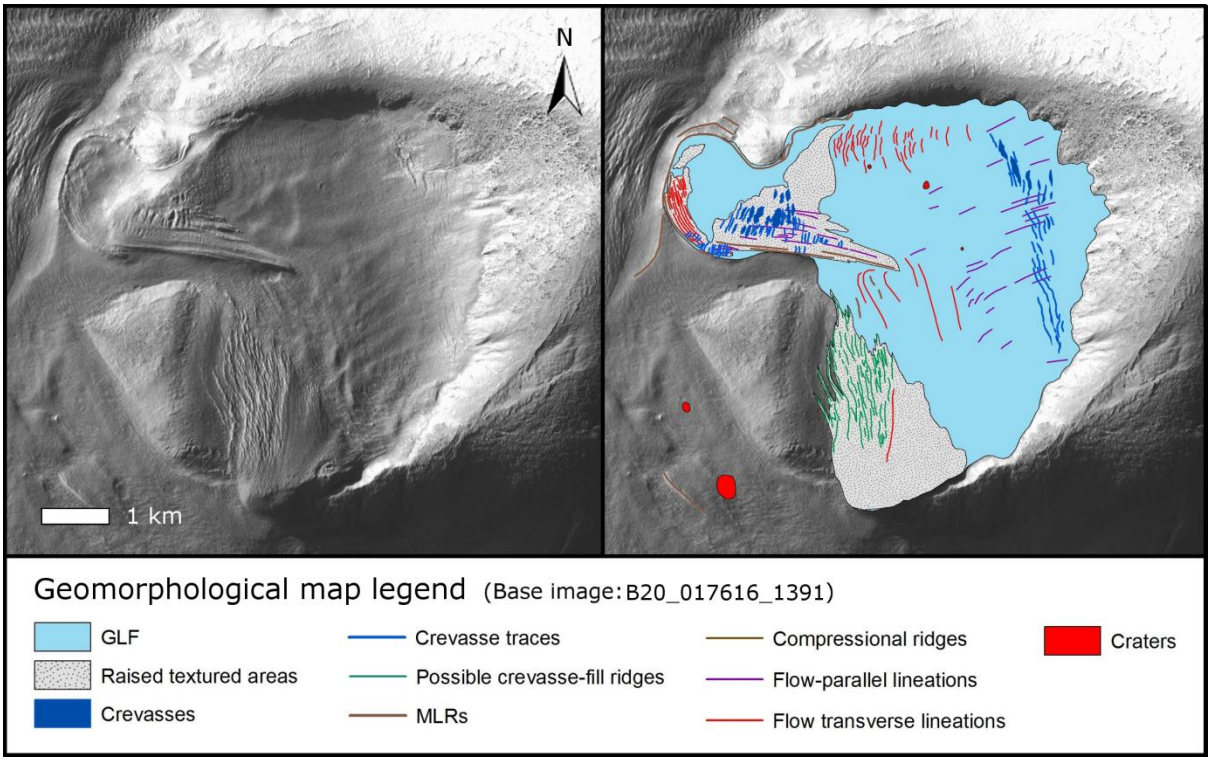

Figure 8: A geomorphological map of the crevassed GLF featured in Example 1 (Figure 7), based on CTX image: B20_017616_1391_XI_40S257W. The raw image is shown on the left and the mapped interpretation is shown on the right. This map highlights the crevasses described for Example 1 (located in the upper left of the frame) in the context of other supra-GLF morphologies such as flow-transverse lineations, flow-parallel lineations, areas of raised texture and what appear to be crevasse-fill ridges to the south of the GLF. Note also the crevasses at the GLF's headwall (right of frame). These are similar to terrestrial bergschrunds, and are discussed at Example 6.

therefore extracted an elevation transect using MOLA data (processed using ITT ENVI and Origin Pro statistical analysis software) in order to better understand the location of these crevasses in relation to local topography. The resultant profile is shown in Figure 11 'c.'. It demonstrates no apparent increase or decrease of surface gradient coincident with the crevassed area.

In Example 5 (Figures 13 and 14) another pattern of parallel, linear crevasses is shown. These are similar in their configuration to those discussed in Example 2, but in this instance they occur away from the valley wall and towards the middle of the feature. Rather than extending away from the valley sides, these crevasses occur directly down-feature from a small 'spur' or protuberance in the valley's western wall.

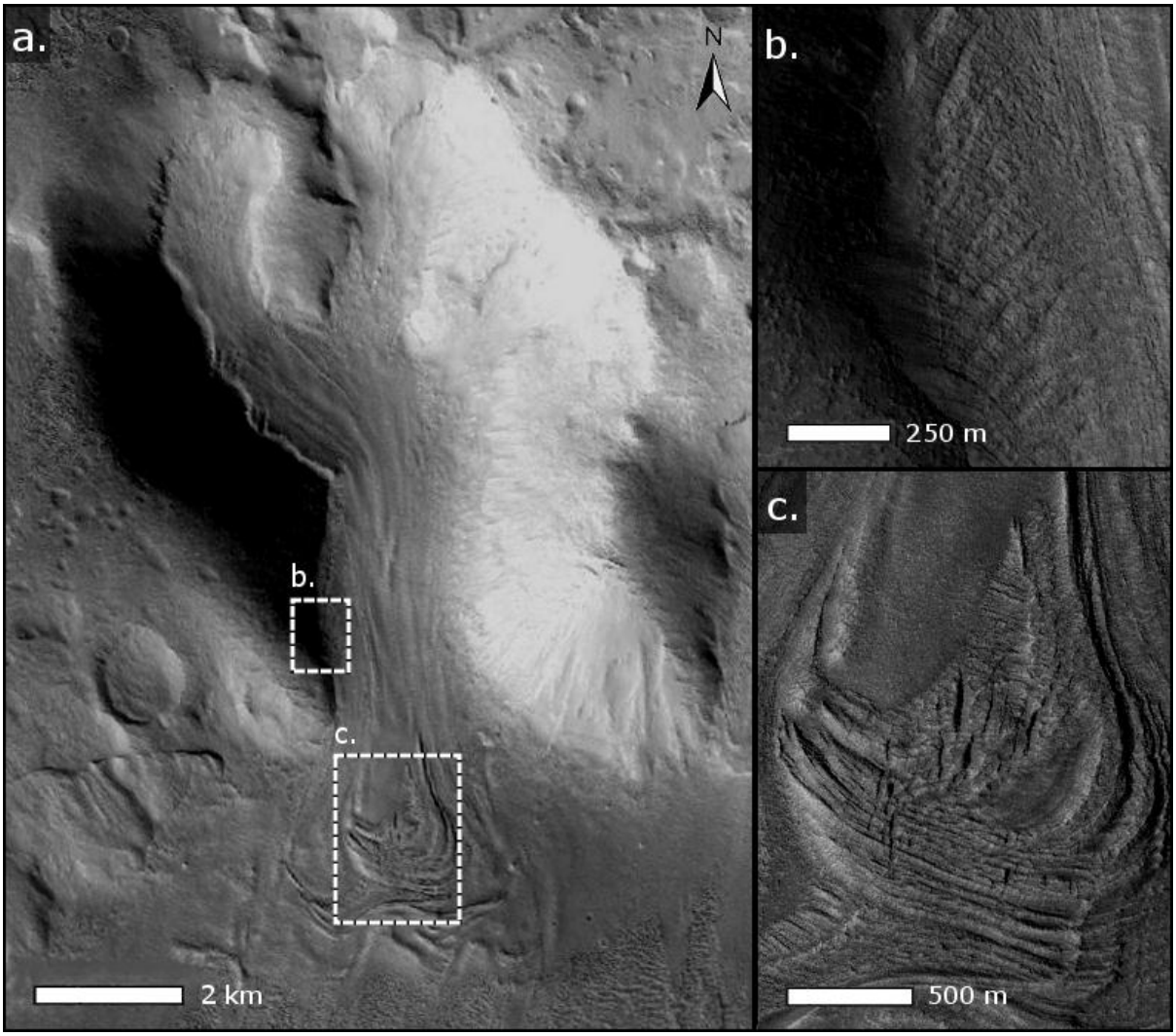

Figure 9. Images detailing two distinctive crevasse fields on a single GLF located in western Protonilus Mensae in Mars' northern mid-latitudes. We show the GLF in its topographic context in 'a' (CTX image P14_006476_2258_XI_45N322W). Note that the direction of flow is from north to south and that illumination is from the west (left). Crevasses are observed along the GLF's western margin (Example 2) and near the GLF's terminus (Example 3). These are highlighted by the dashed boxes in 'a.' and are expanded in 'b.' and 'c.'. Linear crevasses (Example 2) extending up-feature and away from the western valley wall are shown at 'b.'. These crevasses also appear to rotate in a down-feature direction. This pattern is consistent with longitudinal strain in a zone of shear, and the observed tendency to rotate is consistent with similar crevasses on terrestrial glaciers where rotation is caused by gradients in ice flow velocity. Longitudinal crevasses near the GLF's terminus are shown at 'c.'. The latter run parallel to the axis of the GLF and are aligned orthogonal to a series of intense compressional ridges ('c.' is a detail from the High Resolution Imaging Science Experiment [HiRISE] camera image ESP_017130_2255). The crevasses at 'c.' (Example 3) suggest longitudinal compression and consequent transverse extension, rifts opening up approximately perpendicular to the primary direction of extensional strain, as is often observed on Earth.

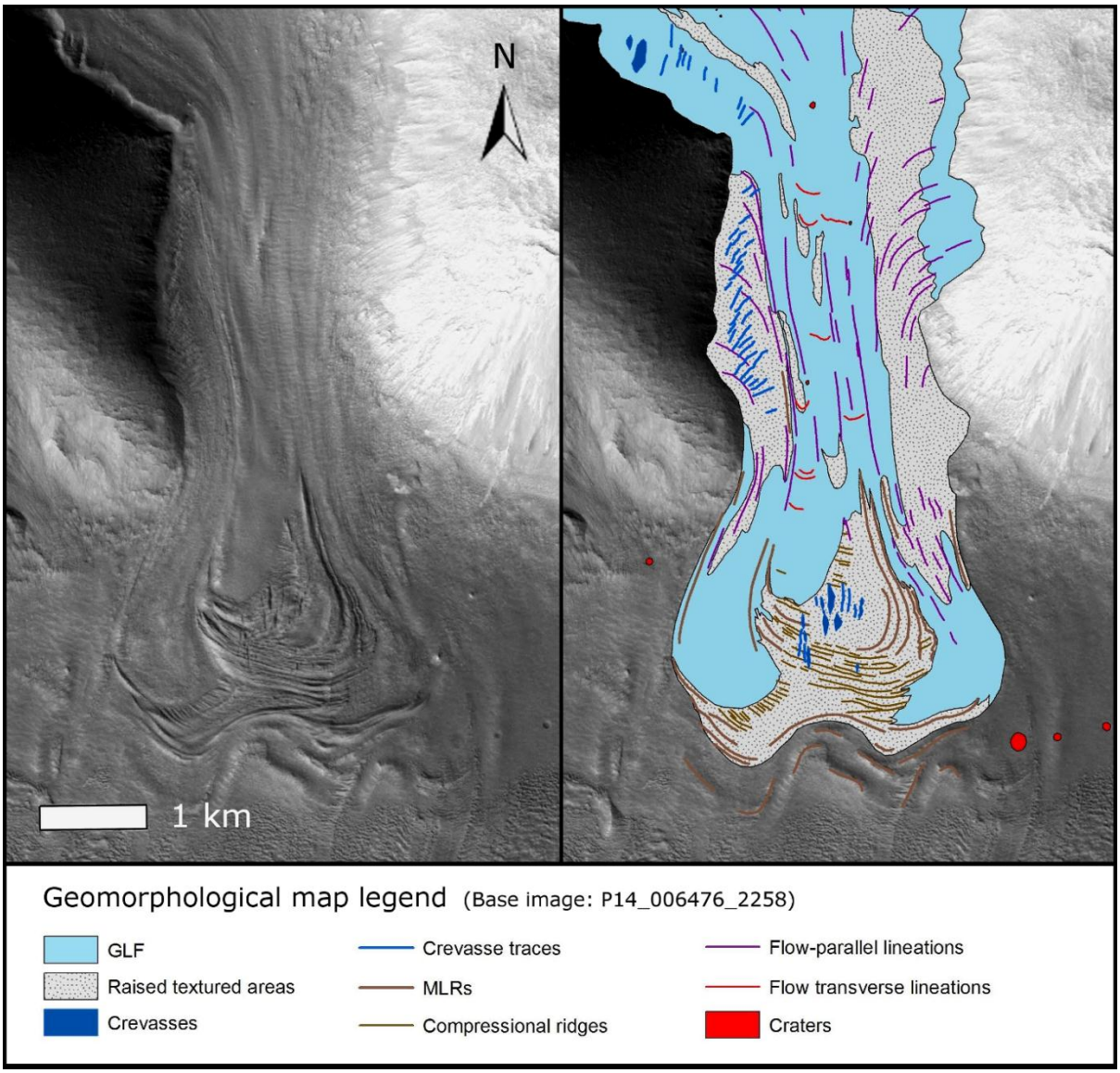

Figure 10: A geomorphological map of the crevassed GLF featured in Figure 8, based on CTX image: P14_006476_2258_XI_45N322W. The raw image is shown on the left and the mapped interpretation is shown on the right. This map highlights the crevasses described for Examples 2 (located to the left of the mapped frame) and 3 (located towards the bottom of the mapped frame) in the context of other supra-GLF morphologies. This GLF appears to be highly deformed towards it lower regions, featuring many well-defined MLRs which, together with flow-transverse and flow-parallel lineations, and areas of raised texture, appear to delineate at least three distinct units of flowing mass.

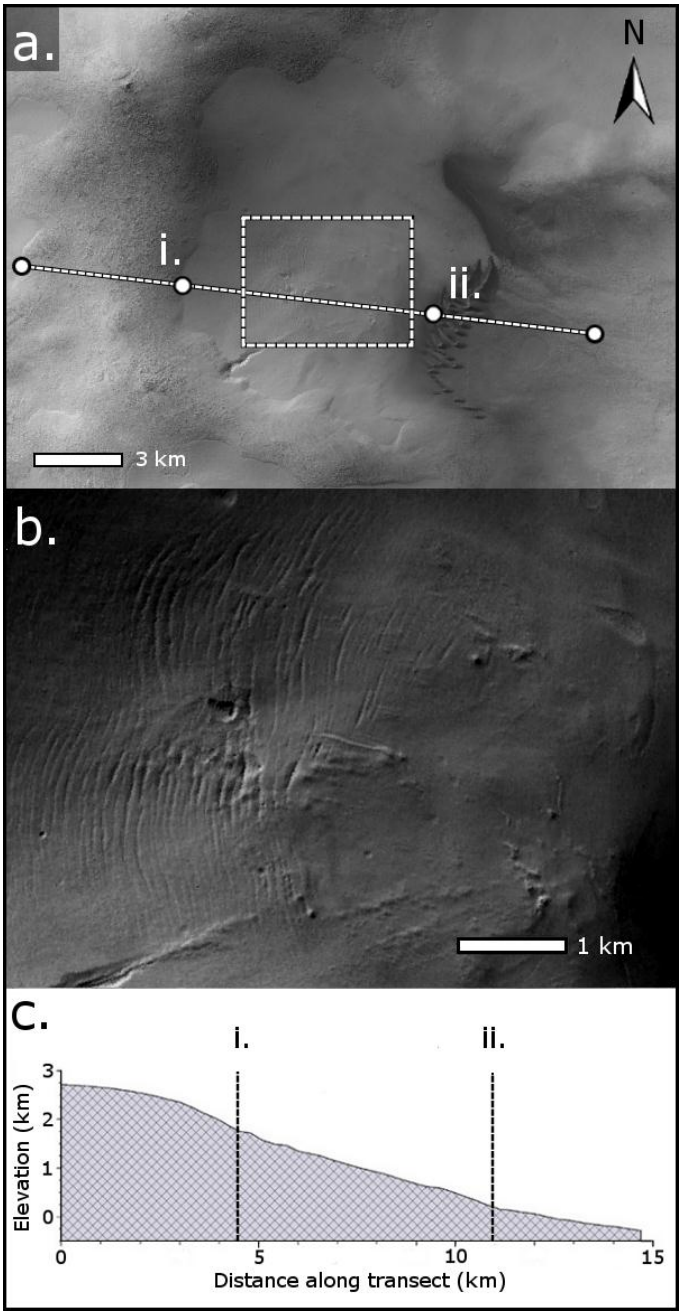

Figure 11: (Example 4) Two sets of arcuate crevasses identified on a GLF located in north western Argyre Planitia in Mars' southern mid-latitudes (CTX image P14_006638_1307_XI_49S051W). The complete GLF is shown in 'a.' (direction of flow is from west to east and illumination is from the west), and the crevasse fields are outlined in the dashed box in 'a.' and expanded in image 'b.'. The dashed line in 'a.' denotes the location of the elevation profile shown in 'c.'. This profile was extracted using imagery draped across a mars orbiter laser altimeter (MOLA) digital elevation model in the ITT ENVI image analysis package. In 'a.' and 'c.' the GLF's headwall and terminus are marked as i. and ii. This profile in 'c.' does not show any apparent increase in gradient corresponding with the location of the crevasse field, raising the possibility of a local decrease in basal friction. This GLF is #4 (southern mid-latitudes) in the supporting online inventory.

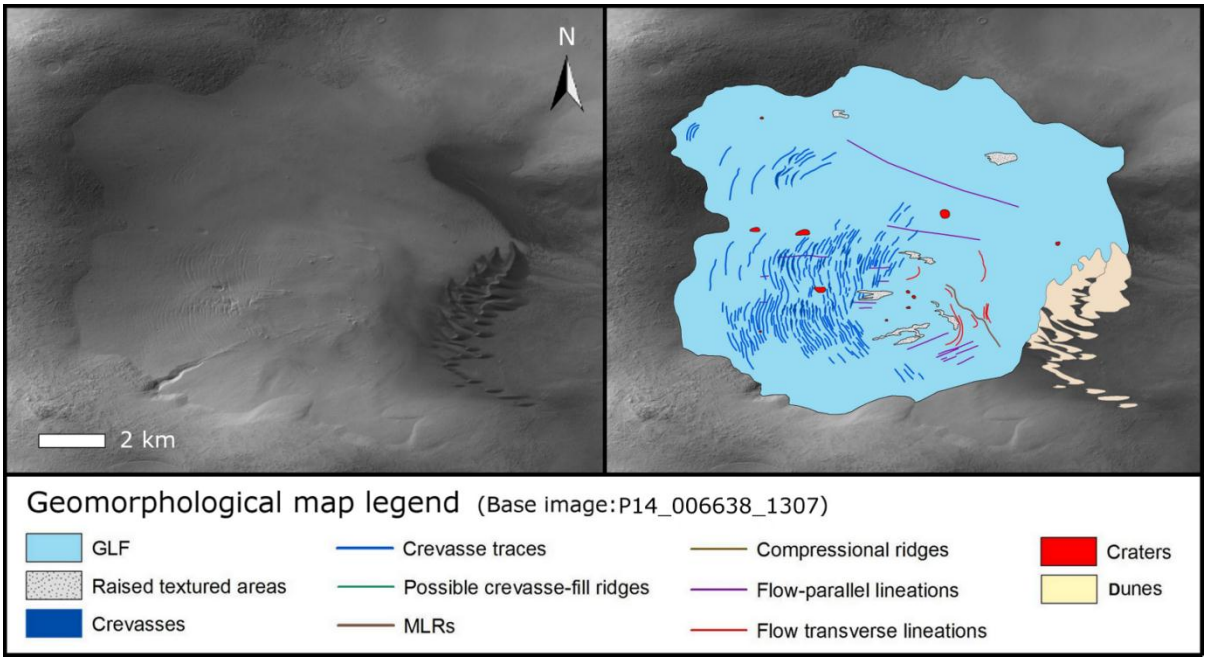

Figure 12: A geomorphological map of the crevassed GLF featured in Example 4 (Figure 10), based on CTX image P14_006638_1307_XI_49S051W. The raw image is shown on the left and the mapped interpretation is shown on the right. This map highlights the crevasses in the context of other supra-GLF morphologies, including dunes that have built up against the terminus of the GLF.

This spur separates the main channel (to the east) from what resembles a small cirque to the west. This gives the impression of a medial zone between two separate flows, the crevasses occupying the 'suture' zone (Glasser and Scambos, 2008) between them. Similarly to the crevasse patterning featured in Example 2, the crevasses featured here in Example 5 are oriented transverse to the apparent direction of flow and point slightly up-feature. They also appear to rotate slightly in a down-flow direction with increasing proximity to the GLF's terminus.

Closer inspection of the crevasses featured in Example 5 (Figures 13 and 14) reveals fine ridges nestled in the vertex of the fractures. In one or two cases, these ridges are actually higher than the crevasse walls, resulting in a feature with positive relief rather than a negative relief crevasse (Figure 13 'c.'). This could indicate long-term wasting of the surrounding GLF's surface.

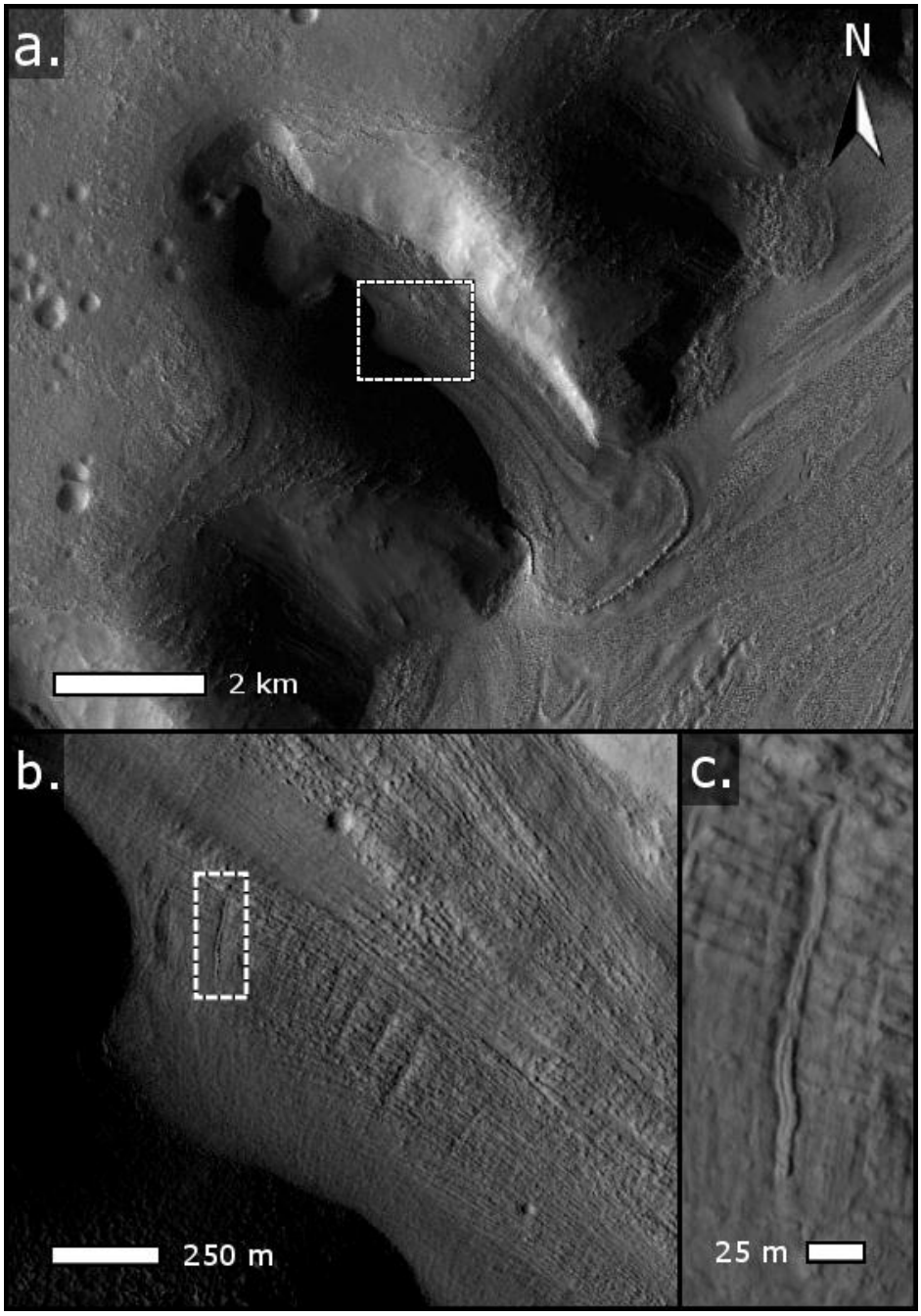

Figure 13: (Example 5) Transverse crevasses on a GLF located in Protonilus Mensae (CTX image P01_001570_2213_XI_41N305W). The entire GLF is shown in 'a.' (flow is from north west to south east and illumination is from the west), with the hatched box expanded in 'b.'. The crevasses extending down the GLF in 'b.' are arranged similarly to those shown in Figure 8 b., although those shown here occur a substantial distance away from the GLF's margin, apparently forming down-flow of a confluence area. Closer inspection of individual crevasses, expanded in 'c.' (HiRISE image PSP_009455_2215) shows some to be raised ridge instead of the usual crack-like opening. This is strikingly similar to 'crevasse-fill ridges' on Earth where former crevasses have advected down-glacier and melted out. This GLF is #11 (northern mid-latitudes) in the supporting online inventory.

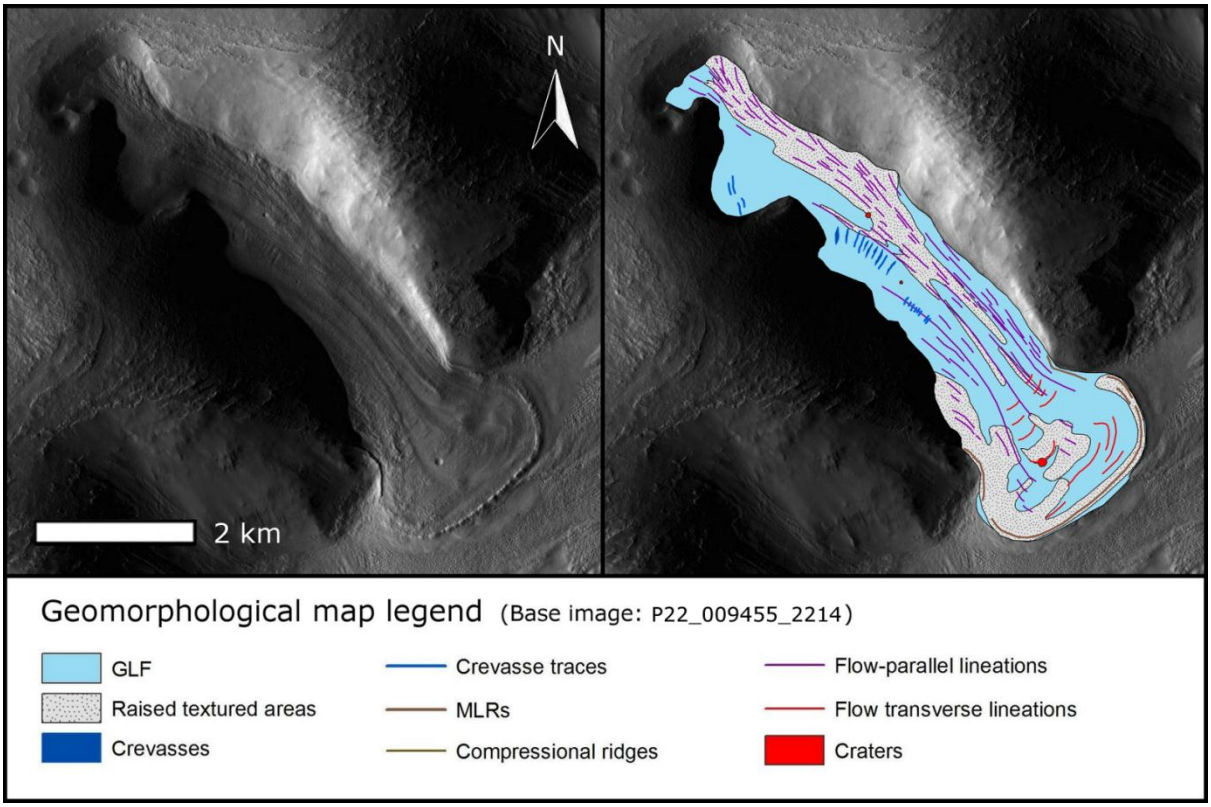

Figure 14: A geomorphological map of the crevassed GLF featured in Example 5 (Figure 13), based on CTX image P22_009455_2214. The raw image is shown on the left and the mapped interpretation is shown on the right.

The final (and most common) crevasse pattern identified consists of linearly concurrent fractures which run parallel to the headwall of many GLFs. These are clearly visible on the GLF featured in Example 6 (Figure 15), and also on the GLF shown in Example 1 (Figures 7 and 8). These fractures are aligned approximately 90° to the apparent direction of flow and appear to be very localised, occurring only proximally to the steep adjacent bedrock (or, in some cases, dust-covered) headwall. These fractures are strongly reminiscent of terrestrial bergschrunds.

5. Discussion

5.1. Visual analysis of mapped geographical distribution

The first thing to become apparent upon inspection of crevassed GLF population distribution is the relative scarcity of these features. In an overall global GLF

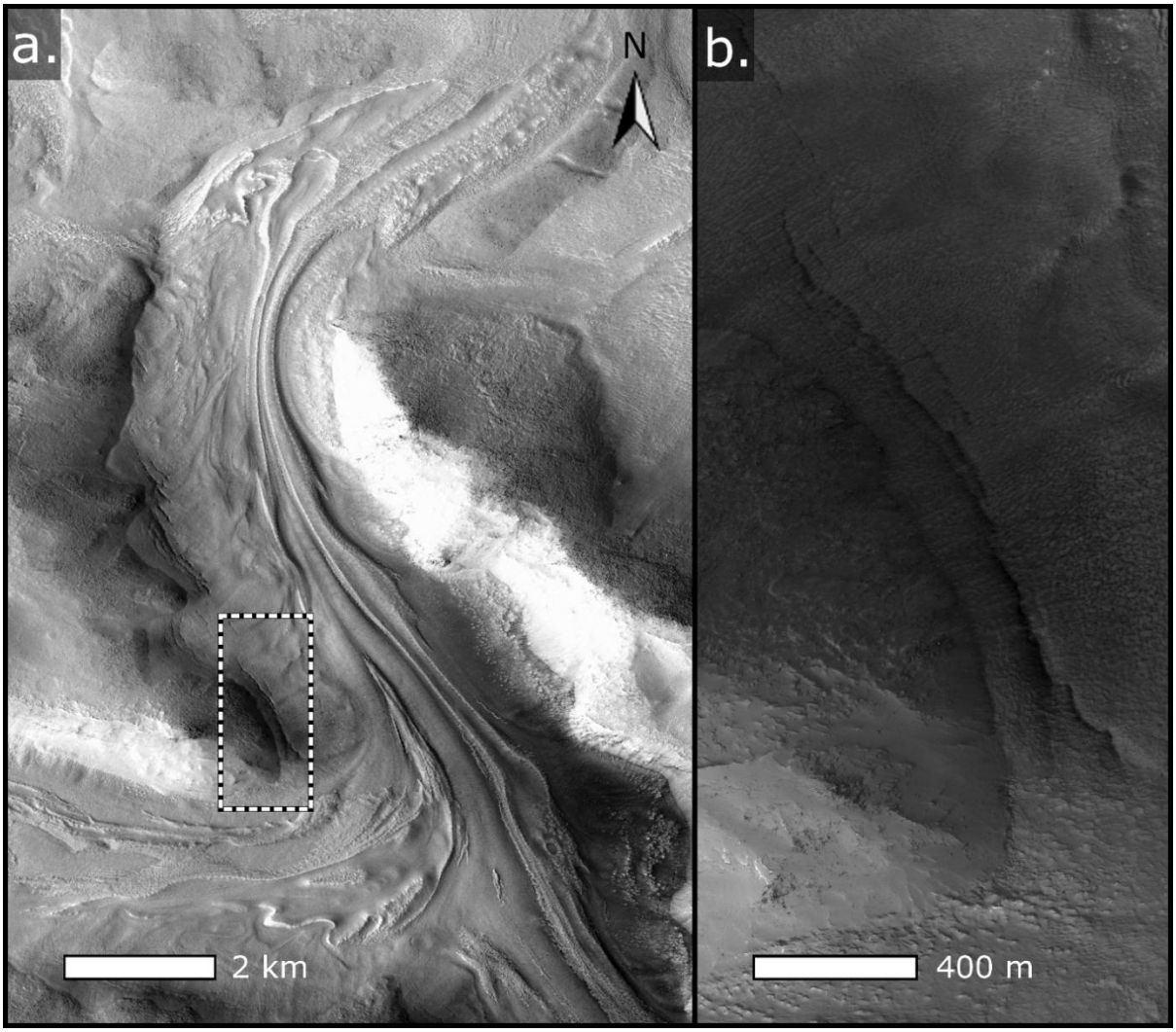

Figure 15: (Example 6) Linear crevasses located on a large GLF on the southern rim of Moreaux Crater in Protonilus Mensae. Illumination is from the west (left) and the dominant direction of flow is from the south to the north. 'a.' shows the crevasses in their overall context (CTX image P17_007491_2211_XI_41N315W). These crevasses are arranged parallel to a headwall (although this is actually parallel to the lay of the valley, and thus constitutes a valley side-wall, this also appears to be a source area judging by the associated morphologies, and thus constitutes a 'headwall'), and strongly resemble the bergschrunds often seen in similar contexts on Earth's glaciers (See also Figure 1 'd.' for comparison). A detailed view is shown at 'b.' (HiRISE image ESP_022101_2210).

population numbering 1309 (Souness et al., 2012 [see also Chapter 2, this volume]) only 64 examples (~5%) were found to exhibit surface crevassing. This suggests either that the prevailing conditions in Mars' mid-latitudes, through some process of mechanical inhibition, generally preclude the possibility of surface crevassing on flowing ice, or, that crevasses in the wider population have been de-activated and

subsequently erased or annealed through a process of ice deflation and / or viscous relaxation (Pathare et al., 2005) respectively. That is to say that the GLFs which are identified as exhibiting crevasses in Figure 2 are either mechanically or compositionally exceptional in some way (possibly due to their environmental context) or they are all that remains of a previously more widely crevassed population.

The population of 64 crevassed GLFs is split unequally between the two hemispheres, with 37 (57.8%) located in the northern mid-latitudes and 27 (42.2%) located in the southern mid-latitudes. This uneven split between north and south is similar to the hemispheric division in the wider GLF population, where 55.5% were located in the northern mid-latitudes and 44.5% were located in the southern mid-latitudes. We therefore interpret the bias of crevassed GLFs towards the northern mid-latitudes as simply being a manifestation of that hemisphere's denser overall population.

The intra-hemispheric distribution of crevassed GLFs is less easy to account for. The overall population in the northern and southern mid-latitudes are clustered in numerous distinct and, in most cases, non-contiguous areas. In the northern mid-latitudes the highest concentration of general (i.e. predominantly non-crevassed) GLFs is located in Protonilus Mensae and Deuteronilus Mensae. These adjacent regions are followed by Acheron Fossae, Tempe Terra and Phlegra Montes. In the southern mid-latitudes the highest concentration by far is found in Eastern Hellas. The distribution of crevassed GLF population concentrations might be expected to mirror these configurations. However, as can be see in Figure 2, this is not the case. The virtual absence of crevassed GLFs in most areas out-with Protonilus and Deuteronilus Mensae in the northern mid-latitudes and the concentration in the southern mid-latitudes' Argyre Planitia (as opposed to eastern Hellas) shows that crevassed GLFs do not simply constitute a homogeneously distributed proportion of the wider population. They occur in discrete communities and, potentially, under specific environmental conditions different to those under which most GLFs in the wider population appear to prevail. Inspection of the results from the statistical analysis of crevassed GLF distribution (compared to that of the wider population)

offers some insight into what those specific environmental conditions might be (Section 5.2).

5.2 Statistical analysis of distribution

The statistical distribution of crevassed GLFs according to latitude, elevation and relief, compared to that of GLFs more generally, shows some unique characteristics (see Section 4.1.2). These are discussed below in reference to the three primary geographical variables.

5.2.1. Latitude

Both hemispheric populations of crevassed GLFs cluster around approximately the same mean latitude as the more general GLF population in each region. This suggests that, similarly to the overall GLF population, the distribution of crevassed GLFs is to some extent determined by latitude. However, the manner in which this latitudinal control applies may be different, as suggested by the varying Std. Dev. of crevassed GLFs around their respective hemispheric means. In the northern mid-latitudes, Std. Dev. is less for crevassed GLFs than for the wider population, but in the southern mid-latitudes it is greater, suggesting that crevassed GLFs are distributed very differently according to latitude, albeit centred around approximately the same mean as the wider populations. The St. Dev. in the southern mid-latitudes is particularly high, suggesting a comparatively non-centralised distribution.

Skewness does not give much indication of dis-similarity in this case, although higher kurtosis in the crevassed GLF populations supports a more distributed, locally-specific and non-gaussian distribution than in the wider population. Inspection of the normalised plot of crevassed GLF representation by latitude (Figure 6) offers some additional insight. Here, direct evidence can be seen of the crevassed population's preference for higher and lower, or 'extreme' latitudes within each hemisphere's mid-latitude GLF domain. In the southern hemisphere this is very pronounced, crevassed GLFs being very obviously over-represented at the marginal

latitudes where GLFs more broadly ought to be ‘unstable’ and thus more sparsely represented. In the northern mid-latitudes this is also true, with an over-representation in the higher latitudes, but less so at lower latitudes. This complexity in the northern mid-latitudes could be due to the influence exerted by the pronounced division in topography offered by the martian dichotomy boundary, latitudinally-dependent elevation complicating the statistical signal in this case.

5.2.2. Elevation

The universally lower mean values of the crevassed GLF distribution (relative to elevation) compared to those of the broader population immediately suggest an environmental preference in the distribution of the former. This interpretation is reinforced by the inter-population similarity of std. dev. statistics, which suggest that we are not seeing a broad scattering of crevassed GLFs across a portion of the broader population’s elevational domain, but a concentration around a specific and distinct elevational range. Skewness and Kurtosis are also broadly similar at all levels between the two population sets.

Inspection of the normalised ratio plot of GLF distribution according to elevation (Figure 5) reinforces the observations made from numerical data alone (above), clearly showing a strong and consistent over-representation of crevassed GLFs at lower elevations at both a global and at a hemispheric level. This indicates that, much as was observed in the distributions relative to latitude, crevassing is more likely to occur in GLFs situated in the marginal zones of the wider population’s domain, in the case of elevation specifically at lower elevations. This preference for lower elevations may be in some way related to atmospheric density or temperature.

5.2.3. Relief

Minimal statistical variation between the distribution of crevassed GLFs compared with that of the wider population suggests that crevassed GLFs do not occur preferentially under any specific relief, or rather they do not occupy any specific

niche within the relief domain spanned by the wider GLF population. The normalised plots in Figure 6 [‘v)’, ‘vi)’ and ‘vii)’] do not refute this hypothesis. Over-representations do occur in the lower and higher relief values of the northern and southern mid-latitudes respectively, however these do not appear to conform to any pattern and thus we interpret them as being statistical outliers.

5.2.4 Summary of statistical analysis of distribution

The statistical distributions discussed above indicate that crevassed GLFs are clustered preferentially around lower elevations and in latitudinal zones at the fringes of the overall population’s range. This suggests a bias towards areas where environmental conditions are comparatively extreme. We therefore suggest that crevassing occurs most readily in areas where GLFs are less stable. Environmental extremes could, under different conditions, lead to enhanced susceptibility to fracture within the GLF mass or to enhanced flow and thus increased strain within GLFs. Examples of such extremes are very low temperatures or, conversely, higher atmospheric density and higher temperatures. Exposure to lower temperatures could lower the brittle failure point of the ice and increase a GLF’s susceptibility to fracture. Where GLFs experience higher temperatures (for example at lower latitudes or at lower elevations) flow velocities might be higher, thus subjecting the ice to increased strain rates and thus increasing the likelihood of crevasse formation.

5.3. Discussion of intra-GLF crevasse patterns.

Inspection of the figures described in Section 4.2. reveals several distinctive crevassing patterns strikingly similar to those which commonly occur on Earth’s glaciers. The examples outlined in Section 4.2. are recalled below complete with an interpretation of what each pattern may reveal about the mechanisms of glacial flow on Mars.

In Example 1 (Figures 7 and 8) highly localised, linear crevasses were observed on a GLF’s surface at exactly the point where the GLF in question appeared to flow over

a steepened section. In this context, these crevasses indicate strong longitudinal extension, which is known to initiate crevassing of this kind on terrestrial glaciers. We therefore interpret the martian crevasses in Example 1 as being the result of ice acceleration where the GLF passes over a cirque lip and moves down a steeper slope, forming what is effectively a martian icefall (see also Figure 1).

The crevasse pattern observed in Example 2 (Figures 9 and 10) consisted of linear, transverse crevasses which extend up-flow and away from the valley wall. Crevasses such as these are common on Earth's glaciers, where this configuration indicates the presence of extensional lateral shear caused by friction between the flowing ice and the valley walls. This is in accordance with a general increase in longitudinal ice velocity away from the valley-sides and towards the GLF's centreline. The crevasses in this example (2) were also observed to rotate in a down-flow direction with increased proximity to the GLF's terminus. This is also frequently seen on terrestrial glaciers, where it is known to result from the gradual deceleration of ice flow towards the glacier's terminus (e.g. Hambrey, 1994). Both characteristics, (crevasses oriented transversely and with a down-flow rotational characteristic) indicate a transverse velocity gradient similar to terrestrial glaciers and a transverse channel geometry that deepens towards the centreline, similar to terrestrial glaciers which are typically parabolic in cross-section.

Example 3 is situated on the GLF previously observed for Example 2 (Figures 9 and 10), but in this case Example 3 shows longitudinal crevasses located on the GLF's terminus. These crevasses, situated roughly in the centre of the GLF and oriented parallel to the lay of the valley, would on Earth be interpreted as forming as the result of rapid lateral extension, possibly associated with the spreading of a piedmont lobe (e.g. Fleischer and Sales, 1972) or with longitudinal compression. The latter could be caused by flow against a raised protuberance or an increase in basal friction which, on Earth, is often associated with the transition from a 'wet-based' sub-glacial environment (where liquid water plays an important role) to a 'cold-based' environment where the glacier is frozen-on to the substrate (e.g. Sugden and John, 1990). The incidence of these longitudinal crevasses on a martian GLF indicates either that the GLF in question has a heterogeneous basal environment or, that it has a material viscosity low enough that when it leaves the confines of the valley

walls it undergoes lateral extension and generates sufficient englacial strain to exceed the ice's extensional strain threshold and thus cause longitudinal crevassing.

Figures 11 and 12 detail the crevasse patterning described under Example 4 (Section 4.2). In this case the crevasses are arranged in a nested, arcuate series, concave side down-flow. On Earth, an arcuate pattern such as this reflects local ice acceleration and extension combined with lateral drag (Hambrey and Lawson, 2000). This might be expected to co-incide with increased gradient or a reduction in local basal friction. Inspection of Figure 11 'c.' reveals no clear topographic control in this case. Although it should be noted that the topographic profile in Figure 11 'c.' is a surface profile only, and does not show basal topography, the absence of any obvious steepening in surface gradient raises the possibility that the longitudinal acceleration inferred from Example 4 may be the result of reduced basal traction. On Earth, a very common cause for locally reduced basal traction is increased sub-glacial meltwater activity (e.g. Sundal et al., 2011). While there is no independent evidence for such a control at Example 4, several glacial and proglacial landforms associated with a GLF located near Hellas Planitia have been interpreted in terms of a change in basal thermal regime (Hubbard et al., 2011). Although such thermal changes are unlikely under present-day conditions, they may have been possible in the past when thicker ice more effectively insulated the ice-bed interface from cold atmospheric temperatures. Thus, from the crevasse patterning observed in Example 4 (Figures 11 and 12) we can infer that martian GLFs may, under certain environmental conditions, experience (or have experienced in the past) polythermal basal conditions resulting in heterogeneous basal traction and thus spatially variable flow rates.

The crevasses in Example 5 (Figures 13 and 14) were described as being similar in overall layout to those in Example 2 (Figures 9 and 10). They were also observed to rotate down-flow, much as do those in Example 2. Therefore we interpret the former as also being the result of lateral shear caused either by marginal friction or transversely variable flow rates. However, a major difference exists between the two examples in that the crevasses in Example 5 do not occur along the featured GLF's valley walls. Instead they occur towards the middle of the channel, directly down-flow of a valley wall spur, which forms a minor bifurcation, with a small cirque-like alcove

to the west (true right) of the channel and the main body of the valley extending up-flow to the other side. We therefore suggest that these crevasses are again the result of lateral shear, but that this shear is caused by the convergence of two separate flowing ice masses, the smaller (that emerging from the cirque-like alcove) being the slower-moving of the two, resulting in pronounced lateral shear in the confluence zone that has caused the ice surface to fracture in a manner similar to that in Example 2 (Figures 9 and 10). This leads us to infer that GLFs have, in some cases, multiple source areas, and that differential flow between the confluences of these source areas can lead to lateral shear in the main body of the flow. This increases the variety of deformation structures, both lateral and longitudinal, that one might expect to observe within GLFs.

Finally, Example 6 contains linear, laterally consecutive but generally non-contiguous crevasses that run parallel to the featured GLF's headwall (Figure 15). These were compared to bergschrunds that are frequently observed on terrestrial glaciers. On Earth, bergschrunds are typically the highest-elevated crevasses on a glacier, occurring where the ice in the upper-reaches of a glacier has moved down-slope and away from its headwall, opening a long and usually broken crack which is almost stationary and is oriented at right-angles to the prevailing direction of flow (Mair and Kuhn, 1994). On Earth these often extend to the bedrock. The existence of these crevasses on GLFs suggests that motion in GLFs occurs, or has occurred, all the way from the terminus of the GLF to its headwall. From the fact that these bergschrund-like crevasses are visible at all, we can also infer that on the GLFs that exhibit them, no processes of accumulation operate at higher elevations. Otherwise, these crevasses would surely have been filled or obscured.

Other observations and inferences about GLF evolution can be drawn from the general appearance of the crevasses observed in all 6 examples. For example, close inspection of some of the crevasses in Example 5 (Figure 13) revealed raised ridges rather than recessed crevasses (Figure 13 'b.'), strikingly similar to 'crevasse-fill ridges' on Earth. On Earth, crevasse-fill ridges represent former crevasses that have advected down-glacier and melted out, resulting in surface ridges formed around debris that had fallen, or was injected, into the original crevasse when it was open. These martian ridges, combined with the apparent absence of currently-active

crevasses up-flow of them, indicate that at least some martian crevasses are now relict. They also indicate that GLF surfaces have generally lowered over time, most probably by ice sublimation, although intermittent melting cannot be discounted.

The crevasse-fill ridges in Example 5 (Figure 13) likely represent the product of pronounced ice deflation or degradation. However, not all crevasses observed on GLFs exhibit evidence of such advanced wasting. Some examples appear 'subdued', exhibiting rounded edges (e.g. Example 2 [Figure 9 'b.'] and Example 4 [Figure 11]) which indicate slight degradation. Other examples however appear sharp and fresh (e.g. Example 3 [Figure 9 'c.']), suggesting minimal deflation of the surrounding ice since crevasse formation. We interpret this range of preservation states as being evidence that crevasses have been forming and degrading on martian GLFs for a prolonged period of time. Indeed, in some cases, they may still be forming or at least be undergoing alteration through continued flow under present-day conditions.

6. Conclusions

Crevassing has been observed on a small proportion of Mars' mid-latitude GLF population. These crevassed GLFs are widely distributed but in some cases show a tendency to cluster in specific areas. These population centres are not always spatially coincident with those of the wider GLF population, suggesting that crevassing occurs more readily on GLFs under specific environmental conditions. Statistical analyses of crevassed GLF distributions, compared to those of GLFs in the wider population, indicate that these conditions may exist within the lower elevations and at the latitudinal fringes of Mars' GLF domain. Therefore we suggest that crevassing on GLFs occurs in conjunction with, and indicates, the physical destabilisation of GLF ice, either at extremely low temperatures which lower the brittle failure threshold of the ice, or at lower elevations and higher temperatures which may foster higher flow velocities and thus higher englacial strain rates.

The crevasses caused by this destabilisation occur in numerous intra-GLF contexts and assume various patterns in their manifestation, many of which mirror crevasse

patterns common on terrestrial glaciers. Using the variety of crevasse patterns documented on Earth as an analogue, and applying the well-understood relationship between these terrestrial examples and terrestrial glacial flow and strain mechanisms, we infer that strain rates within GLFs respond, or responded to: (i) variable bed slope (Figures 7 and 8); (ii) lateral drag at shear margins (e.g. along valley sides or where two or more ice flow units converge) (Figures 9, 10, 13 and 14) and; (iii) possibly spatially-variable friction at the ice-bed interface (Figures 11 and 12). We also observe evidence to suggest that: (iv) flow occurs, or occurred, throughout some GLFs, extending in some cases as far up-channel as the GLF headwall (Example 6 [Figure 15]); (v) that GLF surfaces have lowered over time, most likely by sublimation but also possibly by occasional melting; (vi) and finally that crevasses have been forming in GLFs over a prolonged period of time and may, in some cases, continue to form under present-day conditions.

D. Preface to Chapter 4

D1. Introduction to Chapter 4

This chapter (now 'in press' [Souness and Hubbard*, in press*] in the Journal Icarus), which takes the form of a paper currently submitted to Icarus, draws upon results and conclusions of work presented in previous chapters to develop our understanding of an issue that is central to martian cryospheric and climatic reconstruction, namely the quest to improve our knowledge of the extents and volumes of Mars' former ice masses. These 'historic' ice masses are believed to have been substantially larger than those observed on Mars under present-day conditions (Head et al., 2003; Dickson et al., 2008). We re-visit geomorphological interpretations made by Dickson et al. (2008) and test the hypotheses formulated therein. In this way, Chapter 4 demonstrates how the work presented in this thesis thus far has expanded the scientific community's understanding of martian glaciation, and how approaching martian issues from a terrestrial glaciological perspective can enhance our understanding of Mars' surface evolution.

D2. Reconstructing the extents of Mars' last glacial maximum

In the extensive body of terrestrial glaciological literature relict landforms are frequently used to reconstruct the extents and depths of former ice masses and, although this technique is not easily transferred to Mars (due to the impossibility of direct field access and the enigmatic appearance of many of the landforms and textures observed in Mars' glaciated regions) attempts have been made in previously published literature to apply the same principles to extrapolating thicknesses for Mars' historic last martian glacial maximum ice masses (Dickson et al., 2008).

D3. Contributions to Mars glacial science

In previous chapters of this thesis we have: provided a broad overview of the current state of knowledge of martian glaciation; identified the areas most in need of investigation by specialists of a more geomorphological background; conducted a detailed survey of the distribution of GLFs within Mars' mid-latitudes; built a detailed inventory of GLF locations and morphometries; characterised the geographical contexts in which they are found; identified and mapped the occurrence of surface crevassing on GLFs, and drawn comparisons between crevassing on terrestrial glaciers and the crevasse patterns observed on martian GLFs, further developing our understanding of flow patterns and strain regimes within Mars' GLFs.

In Chapter 4 we apply what has been learnt during the previous studies listed above, re-interpreting evidence for what has been described by Dixon et al. (2008) as a glacial trim-line, or 'highstand' datum for palaeo-ice sheet thickness. In Chapter 4 we revisit the landform evidence and explore the possibility that previous parties have misinterpreted the feature in question as a highstand datum.

If validated or accepted by the broader scientific community, this contribution will have an impact on future efforts to reconstruct Mars' glacial past, developing our understanding of the range of relict glacial features as indicators of past cryospheric process. If, however, the interpretations proposed in Chapter 4 are refuted, this work will at least serve to encourage more rigorous consideration of the available evidence in future interpretive studies.

Chapter 4:

An alternative interpretation of an Amazonian glacial highstand in eastern Protonilus Mensae, Mars: Observations from catchment and feature-scale flow mapping using data from the CTX and HiRISE imaging systems.

1. Introduction

1.1. Mars' integrated glacial landsystems

Landforms of glacial origin have been observed and mapped in both mid-latitude regions of present-day Mars (e.g. Squyres 1978; Squyres 1979; Milliken et al., 2003; Souness et al., 2012). This ice appears to have flowed in recent geological times (e.g. Forget, 2006; Head et al., 2005; Marchant and Head, 2003), leading to the formation of what Head et al. (2010) describe as 'integrated glacial landsystems'. These ice deposits are possibly the remnants of a larger glacial ice mass that formed during a past martian ice age (Head et al., 2003). This martian ice age is thought to have occurred under climatic conditions markedly different from those that prevail on present-day Mars. The transition from this past climatic regime to that of the present-day is believed to have been driven by shifts in the obliquity and eccentricity of Mars' orbital rotation (Read and Lewis, 2004; Ward, 1992), the most recent and substantial example of which is thought to have occurred approximately 5×10^6 years bp (Touma and Wisdom, 1993).

Investigations using high-resolution imagery have shown that flowing ice on Mars often forms integrated patterns, representing mass transportation which begins in multiple discrete cirque-like alcoves and converges before commonly traveling for considerable distances down-valley (Dickson et al., 2008). These landsystems are composed of several distinctive flow-induced features, including glacier-like forms (GLFs [Hubbard et al., 2011; Souness et al., 2012]), lobate debris aprons (LDA), and lineated valley-fill (LVF) (Squyres, 1978, 1979; Lucchitta, 1981). GLFs represent the first-order component of this glacial system, originating in small valleys or cirque-like alcoves, whilst LDA (broad, rampart-like flows) are often formed where multiple adjacent GLFs converge, or icy material originates from a long escarpment. Where opposing LDA converge or coalesce, complex flow patterns and contortions are often observed; this surface being known as LVF (Squyres, 1978, 1979; Lucchitta, 1981).

The surface patterning produced by ice flow within these systems is diverse and complicated, exhibiting many textures without obvious counterparts on Earth. As

such, flow histories are often difficult to extrapolate and the mechanisms of ice flow are still poorly understood.

1.2. Ice loss since the last martian glacial maximum

Although substantial areas of present-day Mars' mid-latitudes are characterized by glacial features and the action of flowing ice (e.g. Milliken et al., 2003; Souness et al., 2012; Squyres, 1978) (see Section 1.1.), flow in these observed formations does not appear to have been affected by recent mass accumulation and input (such as occurs in Earth's glaciers) but of viscous creep induced by local relief and gravity (Souness et al., 2012). This fact, along with evidence from various other observations (e.g. raised glacial trimlines [Dickson et.al., 2008; 2010] and the degraded remains of tropical mountain glaciers [Head and Marchant., 2003]), points to these icy flow features being the degraded remnants of a once much larger ice deposit which is thought to have existed under previously warmer conditions on Mars, perhaps associated with a shift in orbital obliquity. However, the precise extent and volume of this hypothesized last martian glacial maximum (henceforth 'LMGM') ice mass is still unknown.

Some estimates of possible down-wasting and ice mass loss between the LMGM and the present day have been made. Dickson et al. (2008) proposed a minimum surface deflation of ~920 m, suggesting that Mars' mid-latitudes once hosted ice deposits with a thickness > 1 km. These calculations were based on the identification of what are thought to be 'trimlines' and glacial highstands observed in the Protonilus Mensae region of Mars' northern mid-latitudes (Dickson et al., 2008), a well as in craters in Phlegra Montes (Dickson et al., 2010).

Protonilus Mensae is part of the dichotomy boundary (which separates Mars' raised southern highlands from its northern lowlands) and is topographically complex, characterized by long, incised valleys and 'fretted terrain' consisting of isolated buttes separated by wide mesas (Sharp, 1973). Protonilus Mensae, along with the similar and neighbouring regions of Deuteronilus Mensae and Coloe Fossae, also contains a very high proportion of Mars' GLFs and associated glacial features (e.g.

Souness et al., 2012). Therefore, care must be taken in the interpretation of what is a very complex, varied, and often somewhat ambiguous assemblage of landforms.

1.3. Existing hypotheses on the directionality of historic ice flow in Protonilus Mensae

Dickson et al. (2008) interpreted an ice mass located in a large cirque-like alcove in eastern Protonilus Mensae (this cirque-like alcove is henceforth referred to as 'Protonilus Mensae 1' [PM1]) as having flowed into that alcove rather than out of it (Figure 1). Although the authors of that work described mass sourcing and subsequent flow patterns for the Protonilus Mensae area as generally being characterised by "accumulation…in fretted valleys, in alcoves along the bounding scarp, and in alcoves surrounding the massifs, with flow extending away from these regions into local lows…", they invoke a different history for PM1, suggesting that, in this specific case, mass flowed into an alcove instead of out from it. This interpretation was based on the identification of a loop-like ridge which encompasses a lobe of icy material and which, when viewed in planform, is oriented into the PM1 alcove, rather than out of it as is normally the case (Figure 1). Dickson et al. (2008) attribute the positive relief of this loop-like ridge of material to compressive forces and local folding resulting from the inward flow of material abutting the alcove's walls.

Dickson et al (2008) correlated the elevation of this lobate compressional feature with other glacial deposits and apparent trimlines elsewhere in the area, extrapolating a contour line at an elevation of ~800 m. The 800 m high suggested terminus of this hypothetically invasive ice tongue, is currently raised well above the ice surface of the adjacent valley floor and has been proposed as representing the elevation of an LMGM high-stand and a datum for estimations of post-LMGM ice loss on a regional scale (Dickson et al., 2008). This interpretation has been well received and widely adopted (e.g. Dickson et al., 2010; Parsons et al., 2011; Pearce et al., 2011; Soare et al., 2012; Head, 2012). However, a case exists for re-evaluating the use of deposits in cirque-like alcove PM1 as evidence for this glacial reconstruction in the light of i): the complexity of the terrain in this locality; ii): the locally ambiguous

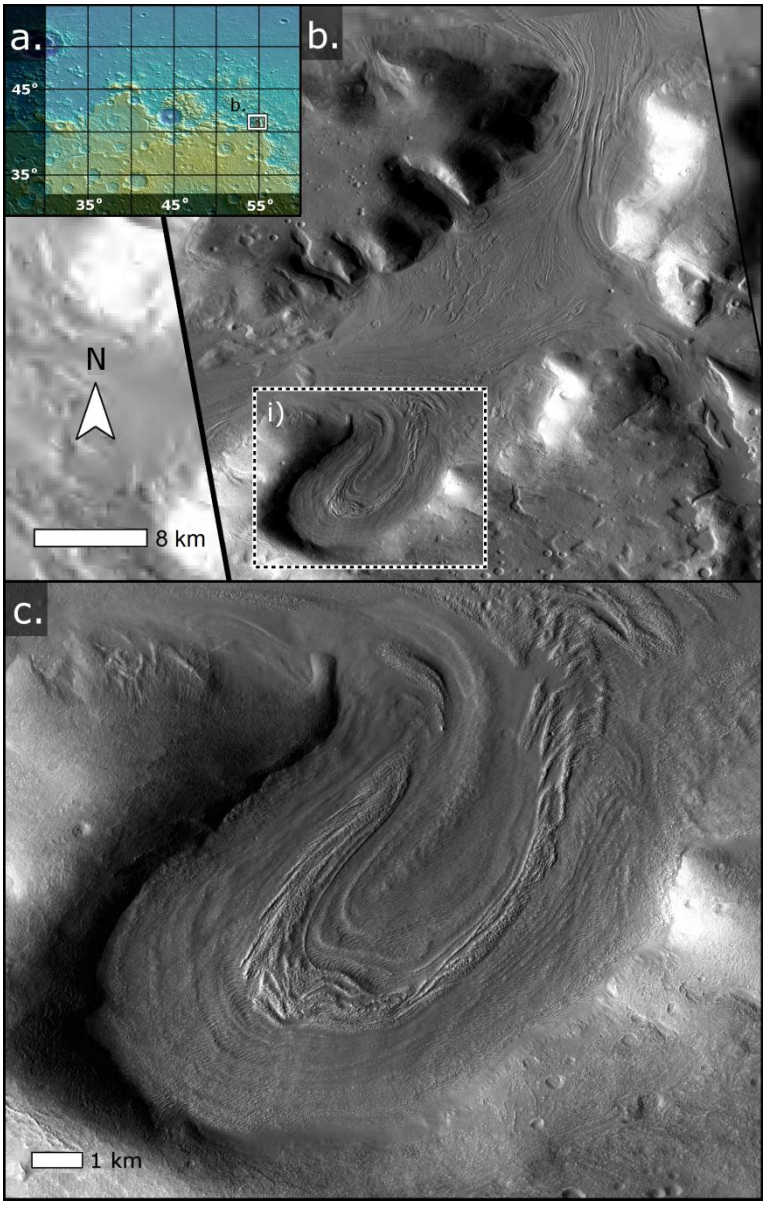

Fig. 1: A diagram illustrating the location and detail of the cirque-like alcove PM1. The map inset in the upper left (a.) shows Protonilus Mensae: an area of the 'fretted terrains' in Mars' northern mid-latitudes. This context map is gridded in decimal degrees and has been shaded using Mars Orbiter Laser Altimeter (MOLA) elevation data. Blue indicates lower areas whilst yellows denote raised topography. The small white boxed section in inset map 'a.' depicts the area expanded in 'b.'. 'b.' contains CTX image P22_009455_2214_XN_41N305W (georeferenced to a mosaic of Thermal Emission Imaging System (THEMIS) daytime infra-red images). The dashed box section 'i)' indicates cirque-like alcove PM1. This dashed box is expanded in 'c.' which shows a detailed view of the PM1 feature. Both 'a.', 'b.' and 'c.' are oriented north-up and illumination in 'b.' and 'c.' is from the west.

nature of morphologies observed on the surface of ice flows in this area, iii): the rarity (on Earth at least) of ice invasion into a cirque (or, in the case of Mars, a cirque-like alcove), especially one with a poleward aspect which, according to both the terrestrial and martian models of glaciation, would increase PM1's suitability for ice accumulation / preservation and, thus reducing the likelihood that it would have been vacant of ice during a glacial event, make it less likely to be susceptible to invasive flow.

In this paper we conduct a re-examination of the site based on the morphological evidence of historical flow patterns at the cirque-like alcove PM1, and raise the possibility of an alternative interpretation to that offered by Dickson et al. (2008) for morphologies within the PM1 alcove.

2. Significance of study

The issues addressed by our investigation are important because the possible mis-interpretation of such a widely-cited LMGM datum could (although other evidence for massive martian glaciation does exist [e.g. Madeleine et al., 2009]) have implications for the interpretation of similar features elsewhere, as well as for the accuracy of subsequent attempts to model Mars' LMGM ice volumes. Mis-interpretation of PM1 could potentially also have an impact on efforts to understand and reconstruct Mars' recent Amazonian climate, both during, and since, the LMGM, as well as having implications for reconstructions of how much H_2O existed, and presently exists, in Mars' cryosphere.

3. Study site

3.1. Location

The flow feature PM1 (Figure 1) is located at Mars grid reference: 54.55 lon, 40.80 lat (decimal degrees). It is oriented approximately northeast (looking outward from its headwall) and forms the southern edge of an enclosed glacial catchment in eastern

Protonilus Mensae (Figure 1). Protonilus Mensae lies in Mars' northern hemisphere on the dichotomy boundary between the longitudes of ~ 37º - 55º east.

The catchment in which PM1 is situated appears to be filled with icy material that has flowed from multiple sources. Numerous GLFs occupy the walls of the catchment's escarpments (several of which form the southeast face of a raised butte, typical of those which characterize the 'fretted terrains' [Sharp, 1973] in this area). These GLFs appear to contribute a substantial proportion (although by no means all) of the icy material that has historically flowed into this catchment. This mass then merges into a number of LDAs which appear to flow away from their accumulation areas before finally converging as a complex LVF in the catchment's centre. A portion of this contorted material appears to be leaving the catchment by flowing through two narrow topographic channels, one of which lies to the north of the basin and the other to the west.

3.2. Description

Flow feature PM1 (Figure 1) is ~ 6.5 km wide and ~ 11.8 km long, giving it an area of ~ 76.2 km^2. It fills a broad, amphitheatre-shaped cirque-like alcove on the southern wall of the catchment and is distinctive for the wide, "loop-like lobe" (Dickson et al., 2008) of raised material that can be seen to occupy its floor. This lobe is aligned parallel to and at an approximately uniform distance (radially) of some 2,300 m (from the alcove's valley walls and headwall. In fact the lobe is slightly further from the headwall than the valley walls, and the width of the peripheral surface decreases towards the PM1 alcove's entrance, but the overall appearance is of a relatively even spacing. This loop-like lobe of material encloses a tongue-shaped area of smoothed appearance that gives the overall impression of an invasive ice body that has flowed into the alcove, as interpreted by Dickson et al. (2008).

Note that the topography of the feature PM1 is typical of a terrestrial cirque or a cirque-like alcove observed on Mars in that the mass occupying the valley floor slopes downhill away from the headwall (Figure 2). Thus, the loop-like lobe identified by Dickson et al. (2008) now appears to have flowed uphill (Figure 2). Those authors

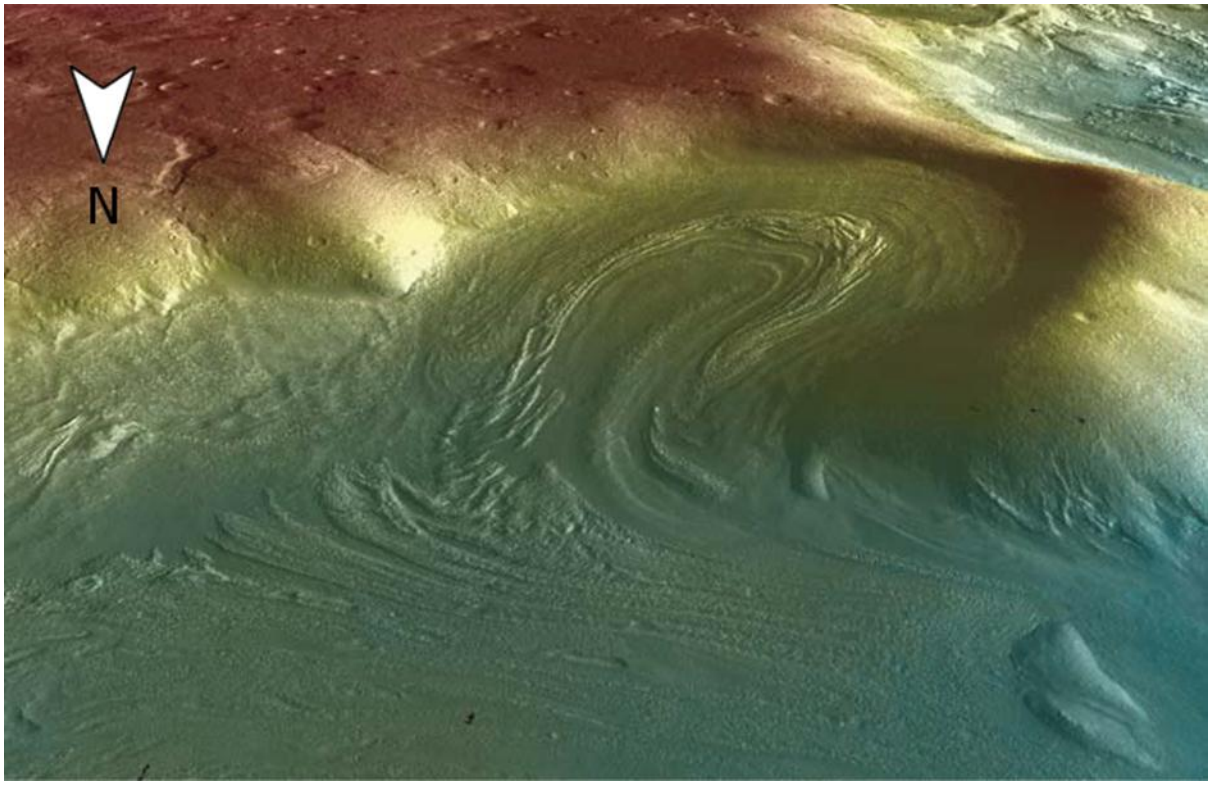

Fig. 2: A perspective view of the PM1 alcove (adapted from Dickson et al., 2008) showing the local topography shaded on a colorized ramp constructed using data from the High resolution Stereo Camera. No vertical exaggeration was applied in the construction of this perspective view (Dickson et al., 2008). This image looks approximately southwards.

do not suggest this to be the case, rather the lobe in question flowed into the alcove during a past glacial event when the ice in the valley floor was significantly more elevated than it is today, flow at that time having been of a conventional down-slope character. In this paper we evaluate the glacial and geomorphological evidence for this 'invasive flow' interpretation.

4. Methods

4.1. Image sources

We utilise Context Camera (CTX) (~ 6 m per pixel resolution) and High Resolution Imaging Science Experiment (HiRISE) camera (~ 30 cm per pixel resolution) imagery

to examine, map and interpret the evidence for the directionality of geologically-recent flow within the ice deposits located at PM1 (see Section 3).

4.2. Ice flow mapping

Images were initially viewed using the Mars Image Explorer (MIE) interface, hosted by Arizona State University (ASU) (viewer.mars.asu.edu). These data were subsequently downloaded from the MIE and from the HiRISE website (hirise.lpl.arizona.edu/amazitisi.php), before being uploaded into ESRI's ArcMap 9.3 geographic information system (GIS) program. In ArcMap, the images were georeferenced to the 128 pixels per degree Mars Orbiter Laser Altimeter (MOLA) gridded digital elevation model (DEM) and the 256 pixels per degree global mosaic of Thermal Emission Imaging System (THEMIS) daytime infra-red images. This raster dataset was then used to build geomorphological maps.

4.2.1. Interpretation of PM1 surface textures and landforms

The geomorphological maps of PM1 were drawn from interpretations made through manual inspection. These interpretations were informed using terrestrial glaciological principles and published literature as a source of analogs.

Extrapolating spatial variations in historical strain vectors from interpretations based solely on visual inspection is difficult, and the results are invariably subject to a degree of uncertainty. This uncertainty stems predominantly from subjectivity and human error (an inescapable component of manual inspection), and (on Mars) from the fact that so little is known about the mechanisms responsible for the formation and subsequent alteration of the flowing ice masses in question. In Table 1, we present the various classifications applied to the maps discussed in Section 5, including the significance of each classification and some of the possible issues associated with their accurate interpretation.

Table 1:

Feature	Identification criteria	Possible interpretation errors	Significance
Glacial material	The actual body of a glacial mass; this area should appear relatively flat, suggesting that this valley or enclosed space is filled by a non-bedrock mass (i.e. ice). The surface should show evidence of flow, either in the form of transverse deformation patterns such as ridges, fractures or chevrons, or linear structures suggestive of flow direction. It may also be delineated by marginal structures similar to terrestrial moraines and have a recognisable source area and/or terminus.	Many different deposits can be confused with or mis-interpreted as glacial material. For example, lava flows, debris fans and dust-filled valleys can exhibit structures similar to those common to glaciers. This issue of equifinality is a problem in mapping, especially as glacial material on Mars is almost universally buried beneath a layer of dust and rock which is hard to distinguish from the surrounding area.	Classifying and mapping the extent of subdued glacial material defines the boundaries of active ice flow.
Subdued glacial surfaces	Areas of a glacial mass exhibiting a surface texture more 'subdued' than the norm, i.e. smoother areas with lower roughness and a less pitted or contorted appearance.	This interpretation is purely based on appearance, and ascribes no process-related or genetic history. Therefore interpretation is purely subjective and less prone to error. However, at ice margins, care should be taken to avoid 'overlap' with non-ice terrain.	Differences in surface texture can indicate differences in flow or mass re-working history. Therefore, mapping 'subdued' surfaces could help to build a more detailed map and a richer set of data from which to extrapolate flow history.
Non-ice terrain	Exposed bedrock, or surfaces of a non-glacial origin.	Ascertaining surface composition can be difficult (see above). Therefore care should be taken not to confuse non-ice terrain with glacial material or subdued glacial material.	As with glacial material, classifying and mapping the extent of non-ice terrain helps to define the boundaries of historically or presently active ice flow.
Raised, textured areas	Raised textured areas are defined in this study as areas within (or adjacent to) a glacial mass which are raised above the surrounding ice, displaying a markedly different surface texture indicative of some	The term 'Raised, textured areas' does not include any direct reference to origin or mechanical evolution. Therefore, the only likely issue with interpretation would be mistaking a sunken hollow for	Raised, textured areas most likely indicate either areas where ice ablation has been retarded through some mechanism, possibly due to variable debris cover or to a variation in composition.

	mechanical process in operation or of a local difference in composition.	a raised feature on account of image inversion. Therefore great care must be taken to be properly aware of the angle of illumination, especially when using monochrome imagery. There is also a descriptive similarity to moraine-like ridges (MLRs). However, we describe MLRs as being long, narrow and linear. 'Raised, textured areas need not be any of these things.	Where they occur therefore likely reflects patterns of deformation and thus localized flow, making raised, textured areas useful indicators of mass transportation pathways.
Flow-parallel lineations	Linear, flow-parallel structures with positive relief (possibly analogous to medial moraines observed on Earth's glaciers).	As the precise mechanisms of mass accumulation and flow initiation are unknown, it is possible, although in most cases unlikely, that flow-transverse structures may be confused with flow-parallel structures.	These lineations give an indication of mass-movement pathways and local flow vectors, showing from whence mass has come and to where it is being transferred.
Flow-transverse lineations	Linear structures with positive or negative relief that are arranged roughly transverse to the apparent direction of flow (for example chevrons or compression ridges). These can be straight, arcuate or variably contorted.	As above, flow-transverse lineations could potentially be confused locally with flow-parallel lineations.	Structures with a flow-transverse habit can, through their overall form and contortion patterns, provide an indication of local flow rates and the distribution of stresses within the flowing substrate.
Pits and troughs	Enclosed depressions or sunken areas on the surface of the glacial mass. Pits and troughs can be of any size or shape and can be either isolated or interlinked.	The terms 'pit' and 'trough' are purely descriptive and infer no directionality or mechanism of formation. Therefore the only real danger in interpretation is in avoiding 'image inversion' as described above for 'raised, textured areas'.	'Pits and troughs' most likely indicate areas where ice mass has preferentially ablated, possibly due to reduced debris cover or a variation in composition. Where they occur therefore likely reflects patterns of deformation and thus local flow, making them useful indicators of mass transportation pathways.
Moraine-like ridges (MLRs)	Long (several Km) and comparatively narrow ridges of material, often raised substantially (> 100 m) above the surrounding / adjacent VFF surface and with widths	MLRs are very distinctive and confusion with any particular alternative feature is unlikely, especially as all Martian landform designations are purely descriptive. However,	MLRs likely mark the former terminal position of GLFs and may testify to the ability of GLFs to transport and perhaps even erode material from the immediate area

	often in excess of 500 m (Arfstrom and Hartmann., 2004). MLRs are often seen running parallel to and at the margins of VFF, and are often arranged in an arcuate manner at the terminus of individual flow units.	bedforms or streamlined bedrock protuberances could assume similar forms, as could compression ridges at the snout of a GLF, so care should be taken.	
Streamlined mounds	Small (100s of m in length and 10s of m in width), elongated 'mounds' exhibiting a 'mound and tail' morphology with a wider and steeper 'stoss' end towards the headwall of the valley and a narrower 'lee' end tail pointing down-slope and out of the valley. These streamlined mounds not only protrude above the surrounding icy surface, but appear 'lumpy' and compositionally different. They also often occur in dense clusters.	Streamlined mounds could potentially be confused with short, broken sections of MLRs or other flow-transverse or flow-parallel lineations. This risk is reduced by the fact that streamlined mounds regularly occur in clustered groups, often 'texturing' large areas of the ice surface, whereas the other mentioned formations do not generally do this. Also, Streamlined mounds are much smaller than MLRs or most other lineations.	Streamlined mounds may represent the surface expression of flow-related deformation within the icy material. Therefore, their orientation could reflect the historical or contemporary direction of flow within that ice mass.
Impact craters	Impact craters are simply the sunken, negative relief hollows left in a surface that has been struck by a meteoroid. They are usually roughly circular, but can be distorted by mass movement within the impacted substrate, partially obscured by adjacent mass deposition or, in the case of craters in icy masses, degraded by sublimation or mass wasting.	Impact craters are usually easy to identify and distinguish from the surrounding surface. However, due to distortion and surface degradation in the underlying, impacted surface, cases occur where this is not the case. Therefore many craters may be missed. Also, as icy masses flow and distort, it is known for roughly circular formations to occur in surfaces by means other than meteoroid impact. These can even be recessed features if ice composition varies locally, resulting in variable ablation rates. So, there are opportunities for flow-related morphologies to mistakenly be classified as craters.	Impact craters can be useful indicators of local flow or mass deformation. Where craters have been distorted or stretched, they provide a record of local strain. Also, where they have been superposed upon another feature or partially concealed beneath a deposit they give a record of successive events and landform histories. Also, over larger areas, the relative density of cratering can provide a means of relative surface dating through 'crater counting'.

5. Results

5.1. Feature-scale geomorphological mapping

PM1 displays three distinct surface types (see Figure 3 for a geomorphological map, complete with a legend describing the mapped formations). These are characterized here as: a) glacial material; b) subdued glacial surfaces, and; c) raised, textured areas (refer to Table 1 for descriptions and classificatory details on these surfaces). These three surfaces are associated with numerous smaller-scale formations, including: d) a suite of flow-parallel and flow-transverse lineations; e) pits and troughs; f) moraine like ridges (MLRs [as per Arfstrom and Hartmann, 2005]); g) degraded (and in some cases distorted) craters, and; h) widely-distributed small-scale flow-parallel streamlined mounds (Figure 4), similar to the 'mound-and-tail terrain' described by Hubbard et al (2011) (see Table 1 for more details).

The division of PM1's surface into three textural types reveals a horseshoe-shaped band of raised, textured ground running around the amphitheatre, lying approximately 2,300 m distal from the headwall and, on its concave side, enclosing a central, lobe-shaped area of subdued glacial material. This is the 'loop-like lobe' described by Dickson et al. (2008), which we here classify under 'raised, textured surfaces'. Along the centreline of this enclosed lobe lies a second area of raised and somewhat textured terrain which, combined with the principal band of textured surface (above), gives PM1 a concentric appearance.

This concentric surface is associated with a sequence of MLRs that, for the most part, run parallel to, and are nested on both sides of the principal loop-like lobe of raised and textured material (above). However, at the open, valley-ward (northern) end of PM1, these MLRs assume a different spatial layout, defining two separate lobes that protrude from each opposing side of the PM1 alcove, specifically from the space enclosed between the alcove's valley walls and the loop-like lobe of raised material (Figure 5). These lobes extend away from the PM1 alcove towards the catchment's main valley floor. The easternmost of these lobes is particularly well-defined (Figure 5) and in this case, beyond the last well-defined MLR, arcuate chevron-like formations (flow transverse lineations [Table 1]) occur intermittently but

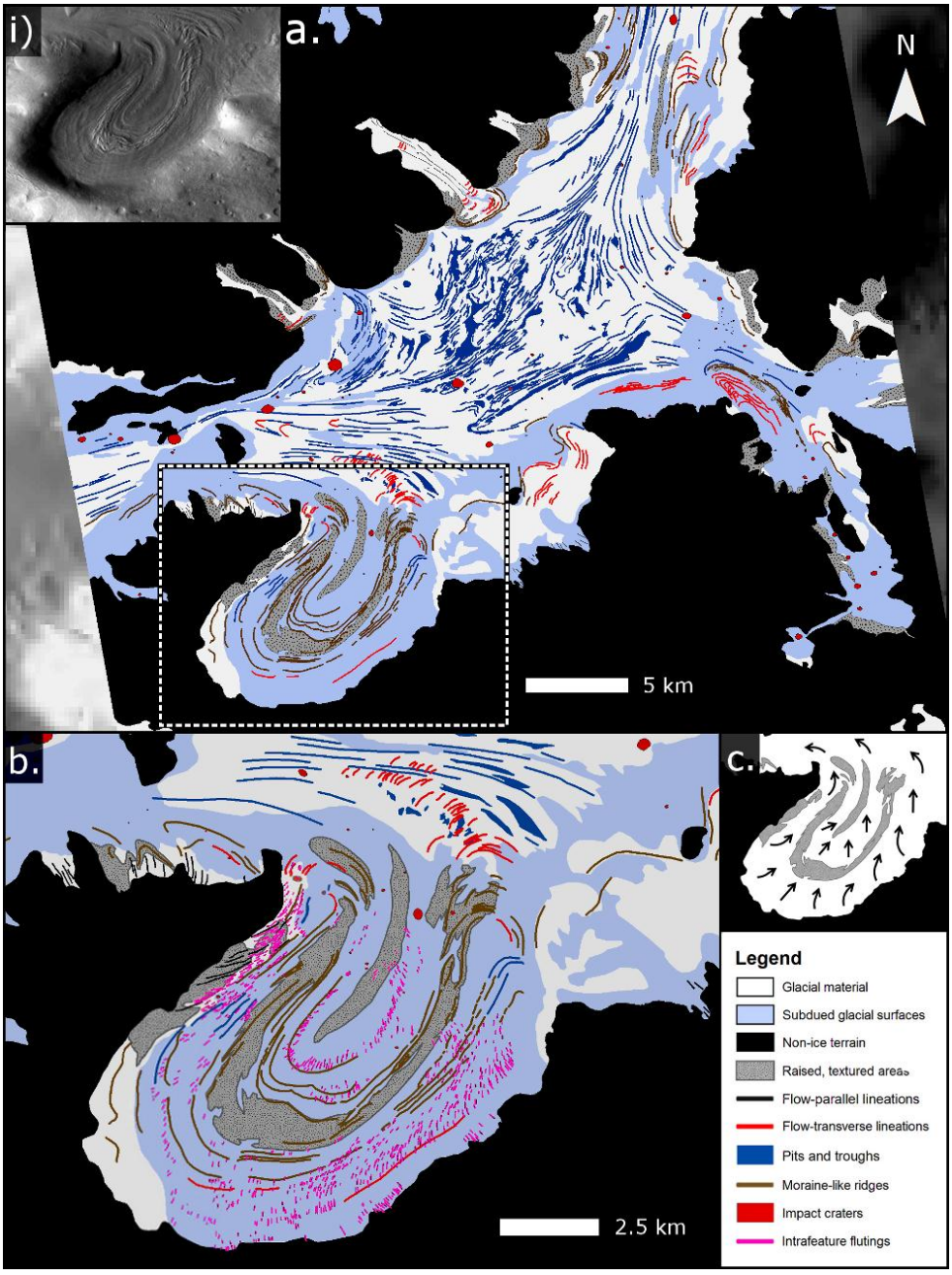

Fig. 3: Geomorphological maps showing the landform and surface texture assemblages observed and classified on the surface of PM1 and its parent catchment. 'a.' shows landforms and surfaces classified at a catchment scale, accompanied by a context image (CTX image P22_009455_2214_XN_41N305W) in 'i)'. 'b.' shows an exploded detail of the PM1 alcove (identified in 'a.' by a dashed box). In 'b.', smaller landforms have been classified and mapped (namely the small-scale streamlined mounds shown in Figure 4). At the time of writing this manuscript only two HiRISE images were available for this locality which did not overlap excessively. Thus mapping of smaller-scale features was only possible within the area covered by these images (ESP_018725_2215 and PSP_001834_2215). The extent of these images is shown in Figure 4a. 'c.' contains a diagram depicting likely mass flow directions, extrapolated from the landforms and textures mapped in 'a.' and 'b.'.

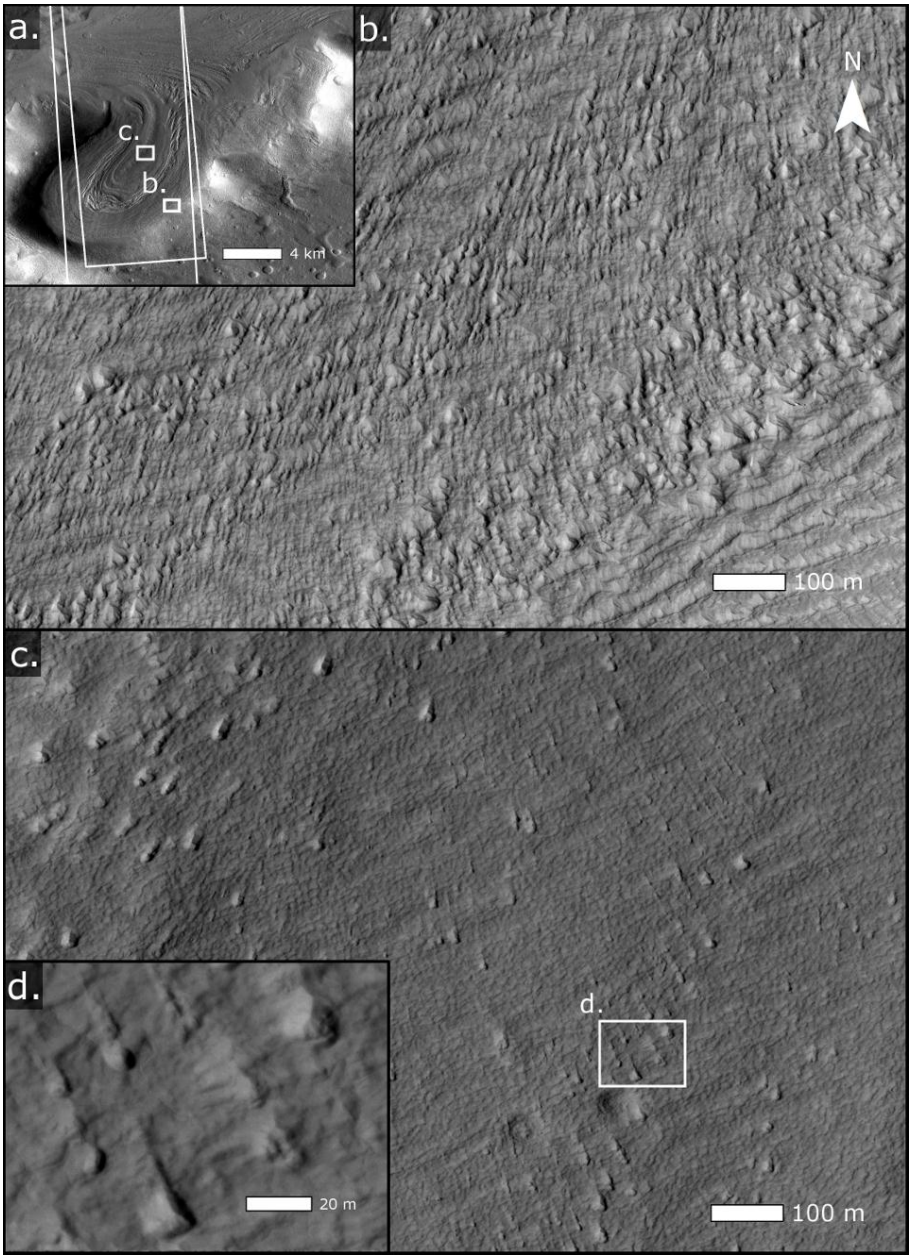

Fig. 4: Images depicting the small-scale streamlined mounds which are observed on the surface of the flow feature PM1 (see Section 5.1.). 'a.' shows a section of CTX image P22_009455_2214_XN_41N305W and describes the local context of the enlarged sections 'b.' and 'c.', the locations of which are shown in 'a.' by small white boxed areas. 'a' also shows the extent of HiRISE images ESP_018725_2215 and PSP_001834_2215, which cover only a portion of the scene (the larger, slightly oblique white boxes). The enlargements of 'b.' and 'c.' are sections of HiRISE image ESP_018725_2215_RED, as is 'd.', which shows a close-up of the 'mound-and-tail' morphology of several streamlined mounds located in 'c.'. These are located within PM1's central, enclosed lobe. Note the stoss and lee morphology of the mounds in 'd.', which indicates flow to the NNW of the frame. The areal footprint of the HiRISE image used is depicted in 'a.' by the large, slightly oblique white box. 'd.'. All images are oriented north-up and illumination is from the west.

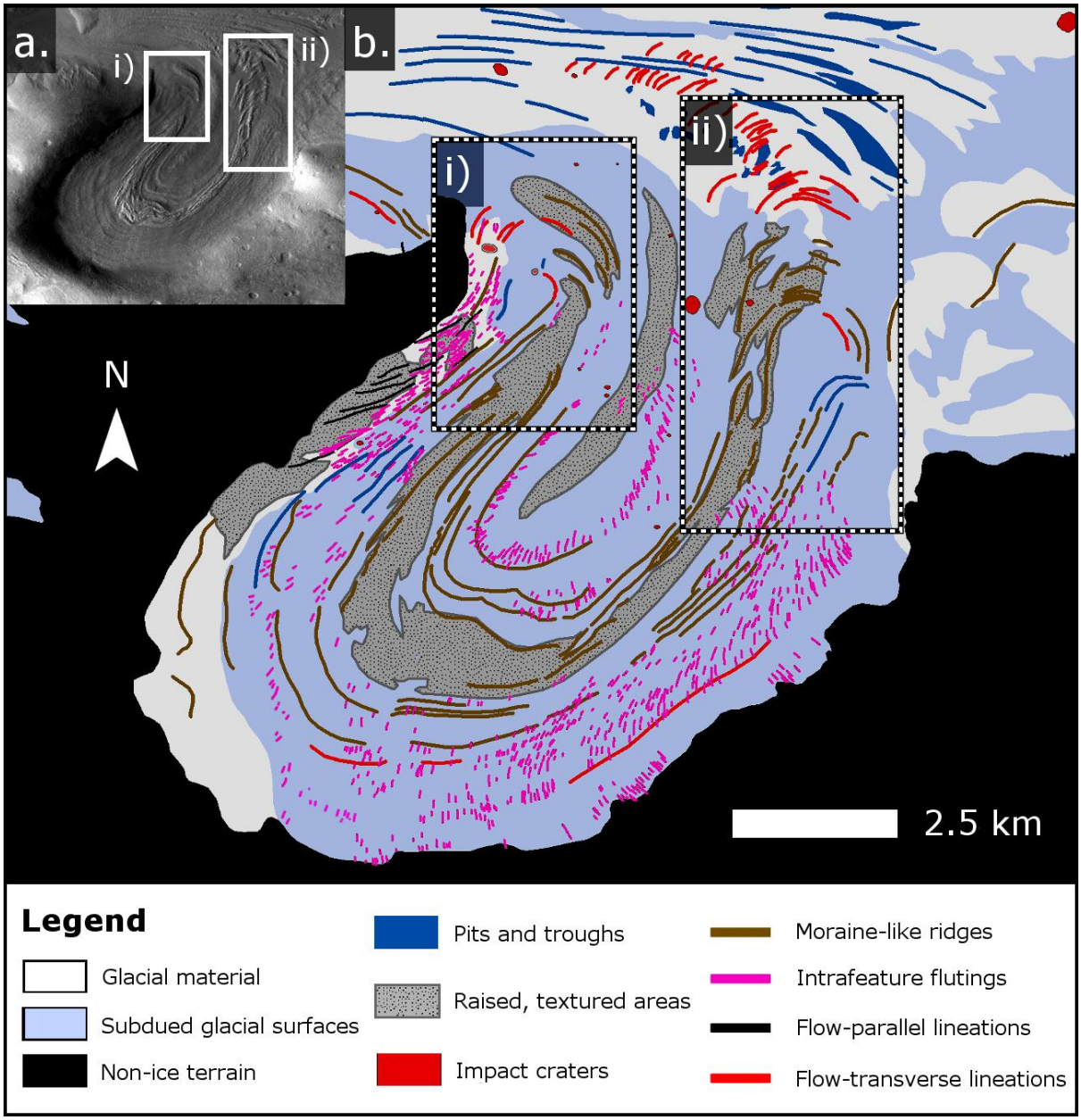

Fig. 5: These diagrams highlight the two lobes that protrude from each opposing side of the PM1 alcove. 'a.' shows a detail of the PM1 alcove featured in CTX image P22_009455_2214_XN_41N305W. 'b.' shows a geomorphological map of the PM1 alcove (also featured in Figure 3b). The extruding portion of each lobe is highlighted in both 'a.' and 'b.' by rectangular boxes labelled 'i)' and 'ii)', corresponding to the western and eastern lobes respectively. In 'a.' these boxes are solid white for clarity, whereas in 'b.' the boxes are dashed. The highlighted lobes protrude from the space enclosed between the alcove's valley walls and the horseshoe-shaped band of raised material (see the attached legend), and are delineated by moraine-like ridges (MLRs) and arcuately-shaped flow-transverse lineations. These are depicted in brown and red respectively.

with diminishing clarity in a northward and then westward direction, at which point the two separate lobes begin to converge. The western lobe is less well-defined, therefore a detailed illustration is provided for clarity at Figure 6.

Where the eastern and western lobes converge the central part of PM1's surface, enclosed by the 'loop-like lobe', appears to almost 'pinch out', giving this central portion (the apparently 'invasive' lobe discussed above) a teardrop-like shape, the tailing end of which gradually diminishes in diameter and points progressively westwards with distance (northward) from the centre of the PM1 alcove. Those MLRs and chevrons located on the eastern side of the PM1 alcove were identified in earlier work by Dickson et al. (2008). However those to the west (Figure 6) were not.

The small-scale 'streamlined mounds' (Figure 4) mapped within PM1 (Figures 3b, 5 and 6) exhibit a complex layout. Within the headwall and valley-wall-proximal zone of subdued glacial material, the mounds appear to originate from the valley sides (with the steeper stoss-side being proximal to the valley wall), proceeding down-slope towards the central portion of PM1, enclosed by the loop-like lobe of raised terrain. As the mounds approach this raised area they gradually begin to change orientation, assuming a trajectory aligned less adjacent, and more parallel, to the valley walls. In the south-eastern half of PM1 this turn is to the right (the mounds rotating clockwise) (figures 3b, 4 and 5b), whereas in the north-western half of PM1 the turn is to the left (the mounds rotating anti-clockwise) (figures 3b, 4 and 5b, and Figure 6). In both cases, the mounds propagate down-slope, flanking the enclosed area and intervening loop-like lobe, their narrower, lee-ends, pointing towards the alcove entrance and the two apparently outbound lobes which emerge proximal to the opposing valley sides (see above and Figure 5). Note that in all of these observed instances, streamlined mounds are oriented with their wider and steeper 'stoss' ends located at the uphill (Figure 2), valley-wall end (Figure 4).

The development of streamlined mounds within PM1's central enclosed lobe is less widespread and less well defined than on the headwall proximal surface. However, those that could be mapped, (located predominantly on the headwall-proximal edge of the lobe, but with some examples located towards the central raised mass and in the intervening space [Figures 4 and 5]) are arranged roughly adjacent to the loop-

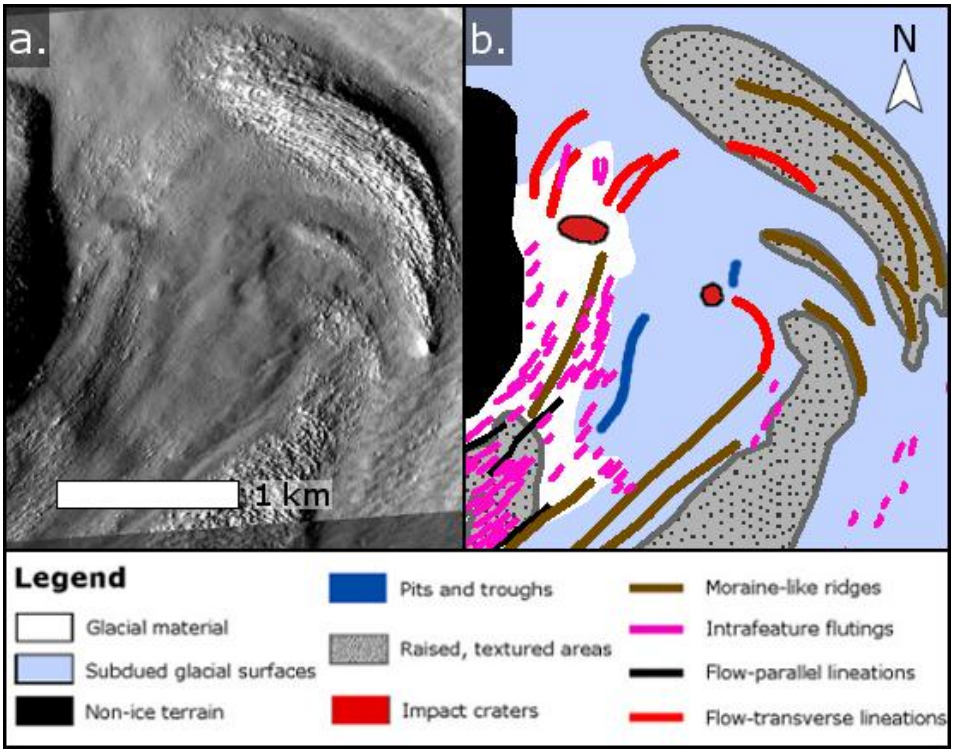

Fig. 6: A detailed view of the 'western lobe' complex, illustrated both by the original monochrome from HiRISE image PSP_001834_2215 (a.) and as a geomorphological map (b.) in which the various components of the 'lobe' are delineated. The area shown corresponds approximately to ('i') in Figure 5.b. Note that illumination in 'a.' is from the left.

like lobe's margin, appearing to converge towards the raised and textured area in the centre of the lobe before turning towards a more flow-parallel orientation in the direction of the alcove opening (Figures 3b and 5b). Again, the stoss sides of the observed mounds are consistently at the uphill, valley-wall-proximal end of each formation (Figure 4).

It is interesting to note that these raised streamlined mounds, observed across PM1, appear 'lumpy' in some cases (e.g. Figure 4d).

5.2. Local catchment-scale flow mapping

Surface structures were mapped for the wider catchment centred to the north east of the PM1 alcove, as shown in Figure 3. Through inspection of these mapped features

and textures and the extrapolation of apparent spatial associations, it was possible to construct an interpretive map of historical mass transportation pathways. The distribution of raised moraine-like ridges (MLRs), elongated pits and troughs, and in some cases deformed craters, provided indicators for past flow vectors, especially where flow could be traced directly from the terminus of a GLF or similar mass-source alcove (e.g. PM1).

Overall, it appears that mass was historically sourced in several individual sub-catchments, the ice from each originating within or adjacent to one or more GLFs or LDAs. Here, proximal to mass source alcoves, the surface expression of each flow unit is generally broad and laterally extensive. However, these mass surfaces can be traced away from the source area where they gradually become laterally constricted, resulting in a considerable reduction in surface area and the production of clear lateral surface structures (Figure 7). Clear examples are visible in the north west of the catchment and along the southern flank, including the area proximal to and apparently extending directly from alcove PM1.

The map in Figure 7, coloured to indicate mass sourced from various individual sub-catchments, indicates that ice originating in the PM1 alcove can be traced northwards before making a sharp turn to the west (following local gradients) where it merges with neighbouring ice flows, is compressed into a narrow band of material, and is extruded from the wider catchment system through the topographic channel to the west.

6. Discussion

6.1. Feature-scale geomorphological mapping

Small-scale streamlined mounds were observed and mapped within PM1. These mounds displayed a ‘stoss and lee’ morphology, with the steeper and wider ends all occurring at the uphill (see Figure 2), valley-wall-proximal end of the features. They also appeared ‘lumpy’, suggesting that they may be potentially compositionally distinctive from the adjacent glacial surfaces. This is impossible to prove, however

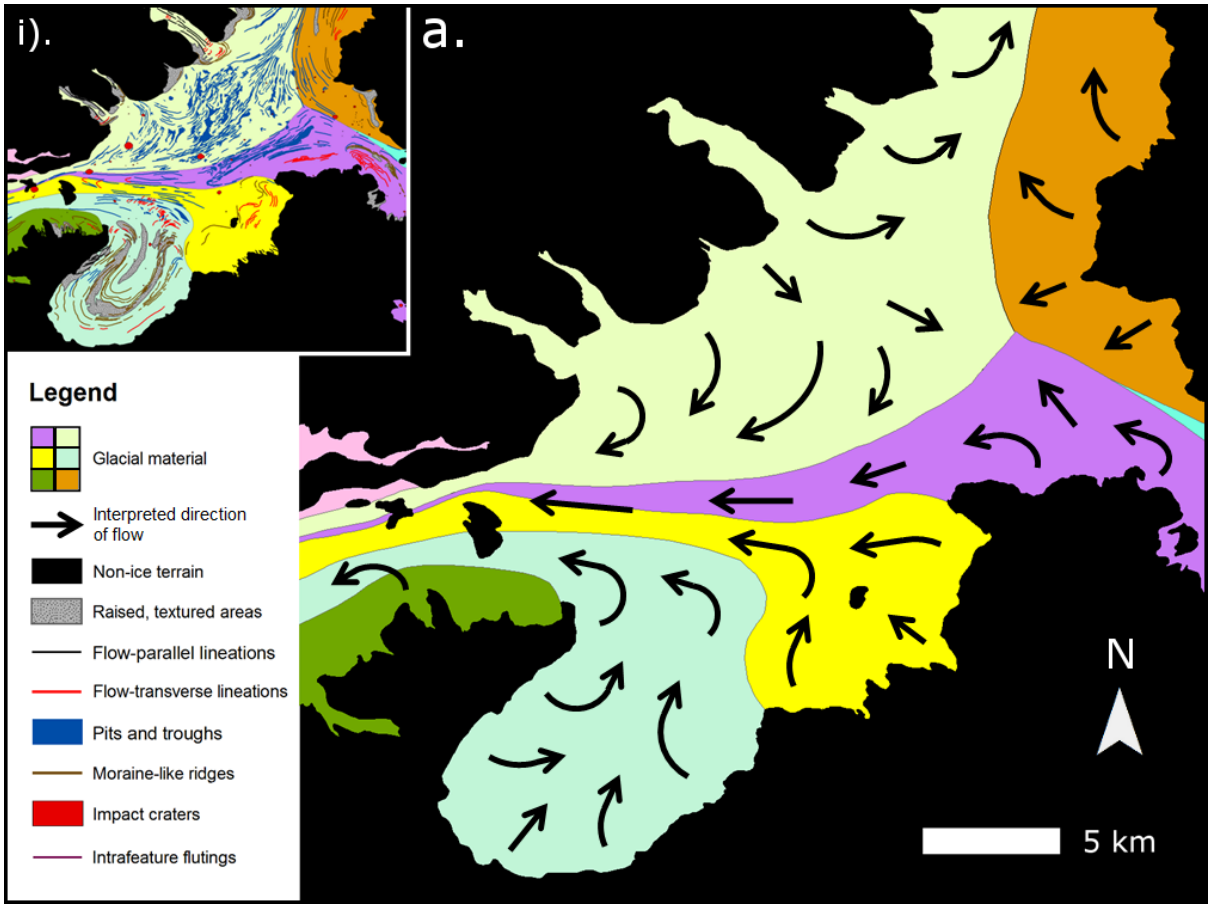

Fig. 7: A diagram showing a catchment-scale mass flow map of PM1 and the immediate area. Flow patterns and directions (shown by arrows of equal thickness), extrapolated from previous geomorphlogical mapping (see Figures 3, 5 and 6), are shown in 'a.'. Note that arrows of differing lengths do not infer variable flow velocity. Only flow direction is indicated. Individual and distinct flow units have been delineated and separately colourized to aid in the interpretation of local flow characteristics. A similarly colourized map with mapped landforms and surface textures is shown in the inset 'i)' for reference.

their 'raised' morphology could also be interpreted as evidence of a unique (or at least different) composition that has made them more resistant to erosion or deflation than other adjacent glacial material. Their morphology is very similar to that of the 'mound-and-tail formations' observed and described on a GLF in eastern Hellas by Hubbard et al. (2011). These authors compared the mound-and-tail forms to terrestrial drumlins which have a similar stoss and lee morphology. On Earth, drumlins are classified as being depositional bedforms of subglacial origin. In the

case of PM1 we interpret the streamlined mounds as being supraglacial features, so the drumlin analog is valuable only in that it links a stoss-and-lee morphology, such as is observed, to directionalized mass movement. Invoking this comparison implicitly infers that the morphology and orientation of these streamlined mounds is a record of flow direction, although the assumed supraglacial situation of the mounds at PM1 is at odds with the drumlin interpretation. Another phenomenon that has been well recorded on terrestrial glaciers and which offers a possible process analog that accommodates a supraglacial interpretation is longitudinal foliation. Longitudinal foliation occurs on the surface of glaciers (Figure 8) and is, by definition, caused by ice flow and deformation (e.g. Hambrey, 1975). This deformation can, through the folding and re-organization of adjacent ice layers (with different compositional characteristics), create flow-parallel streaks or relief features similar to those observed on the surface of PM1 (Figure 4). Longitudinal foliation streaks can be compositionally distinct due to variable bubble content (Hambrey, 1975), but have also been observed to include amounts of lithic debris sourced from the glaciers' bed (e.g. Glasser et al., 1998). The raised nature of PM1's streamlined mounds, and their often 'lumpy' appearance (noted in Section 5.1), are consistent with spatially variable surface composition, and could be explained by either variable ice characteristics or heterogeneous debris content. We therefore suggest that substantive evidence exists to support the longitudinal foliation analog and therefore interpret the mounds observed on PM1 as being a product of ice flow and deformation. Consequently, we take their orientation as being indicative of local motion with an outward, down-slope directional component. This interpretation is based primarily on the observation that the wider stoss sides of the observed mounds are in all cases located at the uphill, valley-wall-proximal end of the features. Examples of 'wide upstream and narrowing downstream' planar morphologies, associated with flow and occurring in supraglacial textures and morphologies, other than the drumlin analog, can also be found in the terrestrial glaciological literature. For example, 'glacial flowstripes' have been observed in terrestrial glacierized catchments by Glasser and Gudmundsson (2012). These authors collate a number of descriptions for these terrestrial formations, which have been attributed various names in a number of publications. Fahnestock et al. (2000) describe 'flow stripes' as "surface topographic ridges…. with metre-scale relief, hundreds of metres to km in width, (and) tens to hundreds of km in length". Campbell et al. (2008) again describe 'flow stripes' as "surface undulations with

Fig. 8: An image of longitudinal foliation on the surface of the glacier Comfortlessbreen in NW Spitzbergen, Svalbard, Norway (from the 'glaciers online' resource at http://www.swisseduc.ch/glaciers/glossary/foliation-en.html). The foliation manifests as relatively small-scale, closely-spaced linear relief features caused by the shear or compression of discontinuous layers of coarse bubbly, coarse clear and fine-grained ice. This flow-parallel patterning is similar to the streamlined mounds observed on PM1 (Figure 4), particularly the closely-packed example of streamlined mounds shown in Figure 4b. The direction of glacier flow is towards the camera. Photo by M.J. Hambrey, 1978.

kilometre-scale spacing and metre-scale relief". These formations are consistently characterised as being 'curvilinear' (e.g. Casassa and Brecher, 1993; Casassa et al., 1991; Wuite and Jezek, 2009), and they are recognised as generally being aligned parallel to flow. One interpretation of their inception (where flowing masses converge) also places a broader, 'stoss' end in the upstream position (Glasser and Gudmundsson, 2012).

Our interpretation of outbound flow in PM1, based partly on the orientation of the observed streamlined mounds, is supported by the pattern observed in the overall layout of those mounds (See Figure 3b, Figure 5 and Figure 6) which in both the centrally enclosed and peripheral arc sections of the PM1 alcove shows convergence from both sides of the alcove and subsequent outward (northward) flow (Figures 5 and 6). Therefore we propose that the location and orientation of the observed PM1 mounds, both in the valley-wall-proximal arc of subdued terrain and within the enclosed central lobe (Figure 4) (see Section 5.1.), indicate that mass was universally sourced from the PM1 alcove's periphery, most likely from the valley walls and alcove headwall, and that this mass flowed towards, and ultimately converged in, the valley centre.

It should be noted that these streamlined mounds are observed only on the mapped 'subdued glacial surfaces', and not on the adjacent 'raised and textured areas' mapped in Figures 3 and 5. One such raised, textured area is the loop-like lobe originally identified by Dickson et al (2008), and interpreted by those authors as being a compressional feature caused by the collision and subsequent folding / deformation of two mass units. We agree with the interpretation of this feature as being the result of mass compression, and suggest that any spraglacial formations or internal foliation within the pre-existing material would almost certainly have been destroyed or obscured by compressive forces such as those inferred by Dickson et al. (2008). Thus, if we are to accept this morphological interpretation, it is not surprising that streamlined mounds are absent from the raised, textured areas.

Unfortunately, due to their small size, it was only possible to map the distribution of streamlined mounds using the high resolution imagery provided by the HiRISE camera. As there were only two HiRISE images available for this location at the time this manuscript was prepared the streamlined mounds mapped in Figures 3, 5 and 6 are confined to these imaged areas and thus appear to occur only in the central portion of the PM1 alcove. However, the fact that these mounds appear across the area of subdued glacial surfaces captured in HiRISE images implies that, were the rest of PM1 to be imaged at as high a resolution, streamlined mounds would be observed there as well.

Further to the streamlined mounds discussed above, two distinctively convex lobes of material were observed to extrude from the two opposing ends of PM1's north-facing open end (see Figures 5 and 6). These are evidenced by the presence of various arcuate chevrons and MLRs in the geomorphological record (Figure 5 'i)' and 5 'ii)' and Figure 6) which suggest the expulsion of mass. The more easterly of these were also identified by Dickson et al. (2008), and their interpretation of outward flow in this case is consistent with our own. In fact, this outward-facing, convex down-slope morphology not only suggests outward flow, but in this context it actively precludes the possibility of inbound flow. This observation, combined with those summarized above, suggests that flow within (and immediately adjacent to) the PM1 alcove was of a conventional outbound type. The westward propagation of the eastern outbound lobe series and its eventual encroachment upon the more westerly lobe (Figure 5 'i)' and Figure 6) also 'cuts off' the loop-like central formation from the rest of the (northern) catchment. This makes it exceptionally difficult to reconcile this central loop-like formation with mass influx from the north as the two contending flow vectors at hand are at almost right angles to each other. A consistently outbound flow direction would seem more likely.

A final meso-scale feature to discuss here is the longitudinal strip of 'raised textured area' observed and mapped (Figures 4 and 5) running roughly north – south and enclosed within the previously described loop-like lobe. Formation of the outer loop-like lobe has been attributed to compression and uplift through internal folding and deformation (Dickson et al., 2008), an interpretation we do not refute. This central strip of raised material has not however been described in previous works, however It would appear likely that it too is the result of compressional deformation. If this is the case then the stresses responsible must have been applied inwards from the valley walls, an observation which again is at odds with the 'invasive flow' hypothesis which would almost certainly have resulted in more transverse patterns of compressive faulting or deformation.

6.2. Catchment-scale flow mapping

Catchment-scale mapping of the area also supports the outbound interpretation, highlighting flow pathways for all the mass historically sourced in (and subsequently extruded from) the various sub-catchments in this system, including the PM1 alcove (Figure 7). PM1's mass pathway, thus mapped, compares well with examples from similarly configured glacial catchments on Earth, appearing to leave the PM1 alcove and turn immediately westwards as described above, merging with ices sourced from adjacent GLFs and LDAs and subsequently following the path of least resistance (as defined by the local topographic [see Figure 2] and inferred englacial strain gradients) and exiting the catchment to the west as a much reduced strip of material, compressed through coalescence with mass from several other distinct source areas. The layout of the surface structures used to construct the map shown in figures 3, 5 and 6, and which delineate the various flow units depicted in Figure 7, are wholly incompatible with the invasion of PM1 by mass from the north. The linear, flow parallel structures which so effectively describe mass first exiting PM1 and its adjacent mass source alcoves, and subsequently extruding westwards, are in the latter case at right angles to what would be expected were mass to have travelled from north to south alone.

6.3. Testing the 'inbound flow' hypothesis

According to the hypothesis presented by Dickson et al. (2008) the mass enclosed within cirque-like alcove PM1 in eastern Protonilus Mensae represents glacial ice which flowed into the alcove, rather than out of it, and which has subsequently experienced minimal deflation or wasting since the LMGM, representing a preserved glacial 'highstand'.

On Earth, the main context in which one might expect a glacial cirque to be invaded by ice, rather than being the source area of outbound ice flow, is where an ice sheet overrides an adjacent mountain region, this invasive ice occupying valleys and cirques as it moves through and over the area. This can only happen in cases where, in spite of the presence of an advancing ice sheet, the local climate in the

over-ridden mountain region is still too warm to permit net annual ice accumulation. This is possible where the summit of the overriding ice sheet, or the lowest extent of its accumulation zone, is a considerable distance away from, or at an elevation somewhat higher than, the invaded mountain region, thereby creating a temperature gradient of sufficiently high relief that conditions will be non-glacial at the margins of the ice sheet. An example of just such a mountain range on Earth is the now de-glaciated Khibiny Mountains of the Russian Federation's Kola Peninsula, which the geomorphological record suggests were overridden from the west by the Fennoscandian Ice Sheet during the last ice age (Hättestrand et al., 2007).

According to this model, for a mountain range to be overridden by ice, or for individual cirques within a range to be invaded, it is required that conditions in the locality not be conducive to the accumulation and advance of ice.

It is true that glacial masses have been observed to 'invade' tributary valleys and adjacent alcoves in the McMurdo Dry Valleys in the Transantarctic Mountains (Dickson, 2012, personal communication) and this fact is made relevant by this region's recognised value as a terrestrial Mars analog site. However, in the Dry Valleys, as with any other terrestrial glacierized catchment, invasion of flowing ice occurs only into alcoves where conditions are not already conducive to ice accumulation and thus glaciation is not already established. In the Dry Valleys such non-glacial conditions are widespread. In Protonilus Mensae on Mars however conditions quite manifestly have, in recent geological time, been suitable for the widespread accumulation and subsequent flow of glacial material and no reason has been proposed to suggest why the PM1 alcove should be regarded as an exception to this apparent norm.

We test the hypothesis of Dickson et al. (2008) by considering the evidence available in light of what is known from terrestrial analogs. Table 2 shows a breakdown of what should be discernable from the geomorphological record if the icy mass in PM1 flowed i) into the PM1 alcove, or; ii) out of the PM1 alcove.

As can be seen from the weighting of the evidence, Dickson et al's hypothesis shows weaknesses and room exists for the consideration of an alternative interpretation.

Table 2: Tabulated reasoning testing the 'inbound flow' hypothesis.

i): The inbound model requires that:	Is this observed?
1: Conditions in the proposed invaded area and wider locality are not conducive to the accumulation and advance of ice.	No. Extensive glaciation is observed locally.
2: If PM1 is proposed to be anomalous, then it's geographical setting must be sufficiently unique as to preclude glaciation.	No. PM1 is north-facing and is similarly elevated to adjacent GLFs.
3: The small-scale morphologies observed in PM1 should Indicate inbound flow.	No. Morphologies indicate outbound mass flow.
4: Catchment-scale mapping should provide evidence of a source area and approach pathway for inbound mass.	No. Mapping provides no evidence of mass having approached from the catchment centre.

ii): The outbound flow model requires that:	Is this observed?
1: Conditions in the immediate area and wider catchment appear conducive to ice accumulation and flow.	Yes. Extensive glaciation Is observed locally.
2: The small-scale morphologies in PM1 should indicate outbound flow.	Yes.
3: Catchment-scale mapping shows a possible mass transfer pathway which would remove material from the PM1 alcove and re-distribute it in a manner consistent with conventional glaciation. The alcove and exited the catchment.	Yes. Morphologies suggest that mass from PM1 was extruded from

The morphology of features in the immediate catchment area indicate the presence of an integrated glacial landsystem involving mass input from GLFs in numerous cirque-like alcoves feeding into LDA and subsequently into LVF. Therefore, at the time of the LMGM, conditions in this catchment can be said to have been broadly suitable for the sourcing and subsequent flow of ice, and the morphology of the alcove defined as PM1 gives no reason to suggest that conditions in PM1 were any different from those experienced by any of the adjacent cirque-like alcoves, all of which appear to have produced outbound flow. Indeed, PM1 has a predominantly northerly aspect and is situated at a similar elevation to the adjacent GLFs (Dickson et al., 2008). Studies of GLF distribution and morphometry performed by Souness et al. (2012) showed that in both of Mars' hemispheres, GLFs were predominantly

poleward-facing, suggesting that ice accumulates more readily, or is preferentially preserved, in these areas. Thus, PM1's geographical location and orientation make it a highly favourable location for ice build-up (or preservation) and not for ice-free conditions into which advancing lower-elevation ice would invade. This supports the likelyhood of mass in this alcove having been sourced locally and subsequently extruded in the conventional 'outbound' manner.

Small-scale morphologies also support outbound flow, examples including the orientation and morphology of small streamlined mounds, the directionally arcuate morphology of flanking outbound lobes, the layout of flow structures at the PM1 alcove's entrance which 'cut it off' from the wider catchment's central mesa, and the longitudinal north-south orientation of compressional terrain within the loop-like lobe it's-self which suggests mass inclusion and stress application from the valley walls.

Regarding the suggestion by Dickson et al. (2008) that the apparent elevational correlation (~800 m) between the PM1 loop-like lobe and other possible trimlines and lateral glacial deposits elsewhere in the catchment supports the interpretation of PM1's morphologies as being indicative of a highstand, we propose that an elevational correlation could easily be coincidental and certainly cannot be used to infer direction of flow. Topography and local gradient on the other hand are generally recognised as being reliable indicators of flow direction, and in the case of PM1 (for topography see Figure 2) both of these indicate conventional outbound flow.

7. A new hypothesis

We propose the alternative hypothesis that the loop-like lobe of material that is observed to extend into alcove PM1, and which is interpreted by Dickson et al. (2008) as being an extension of mass from the wider valley floor that has flowed into the PM1 alcove, does not in fact contain evidence of any inbound flow component and results from conventional outbound flow. We propose that this loop-like lobe, which represents the principal line of evidence advanced by Dickson et al. (2008) for inbound flow can be explained by a scenario involving two glacial events. Numerous glacial events have previously been suggested for this region (e.g. Dickson et al.,

2006; Dickson et al., 2008). We propose that the older of these events left a residual deposit that occupied the floor of the PM1 alcove prior to a subsequent re-advance of ice during a more recent stadial event. Evidence of just such intermittent glacial 'pulses' (possibly climatically-driven) has been observed elsewhere in Mars' northern mid-latitudes (e.g. Grindrod and Fawcett, [2011], who observed regularly spaced textural bands oriented transverse to the direction of flow in LDA in Mars' northern hemisphere). During this hypothesized recent stadial, or re-advance, we propose that mass entered the system from the headwall and valley sides (as evidenced by the orientation of small-scale streamlined mounds and the relatively unambiguous morphology of the outbound lobes which enter the catchment system from each side of the PM1 alcove [Section 6.1.], consistent with the interpretations made by Dickson et al., [2008]) and began to converge from three sides on the preserved icy material in the alcove's centre (Figure 9). This convergence caused the compression of both ice units along their shared boundary, resulting in the formation of the obvious loop-like, parabolic lobe of raised, textured material, as well as the various nested MLRs that occupy the area (Figures 3 and 5). This advance of material from three sides compressed the older material towards the centre of the PM1 alcove, resulting in the formation of the raised and slightly textured central strip (Figure 1) which is mapped along the centreline of the enclosed lobe (figures 3 and 5). Mapping and inspection of small-scale streamlined mounds within this centrally enclosed lobe also suggest an outbound flow component existed, or indeed currently exists, here also.

Our interpretation, outlined above, explains the unusual loop-like lobe observed by Dickson et al. (2008). It does, however, depend upon there having been a pre-existing ice mass in the alcove which was subsequently compressed. This requirement is satisfied if the hypotheses of Dickson et al. (2008) are maintained with regards the lateral flanking lobe/s of material (Section 6.1.) which those authors interpret as having formed concurrently with a later, more recent glacial event. This chronology, with which we agree, requires there to have been an earlier glacial event from which the 'older' deposits contained within the loop-like lobe may originate. The relative scarcity of streamlined mounds in the central lobe-shaped area (as discussed in Section 6.1.) could support the hypothesis that this surface is of a

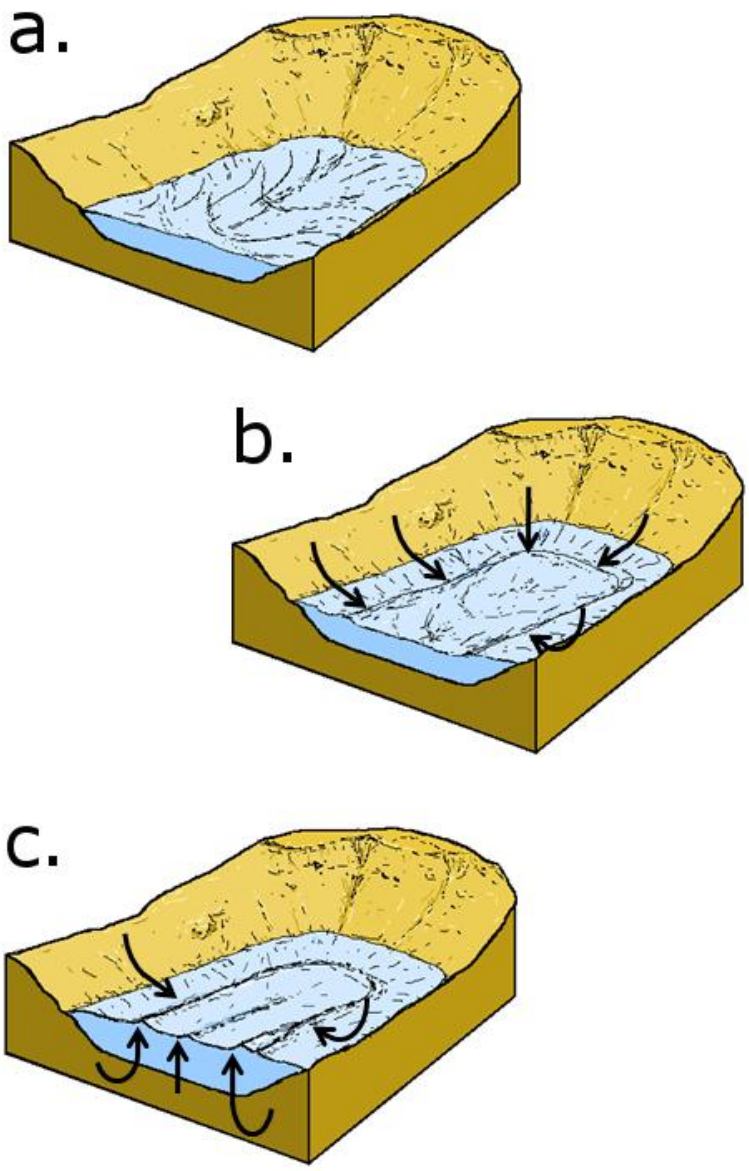

Fig. 9: These diagrams describe the means by which we propose that the unique surface morphologies observed in the cirque-like alcove PM1 were formed. We hypothesise that a body of residual ice survived de-glaciation following the LMGM and occupied the PM1 alcove (a.) at a time prior to a relatively short-lived re-glaciation or 'stadial' event. During this stadial, mass entered the PM1 alcove from all three sides (b.). This mass, converging upon the pre-existing residual ice mass, caused compression and upward extrusion of material at the contact margin, creating the arc-shaped raised and textured area visible today, as well as a series of MLRs.

greater age, smaller-scale landforms such as the streamlined mounds possibly having been erased through prolonged exposure to atmospheric deflation, Aeolian erosion and / or particulate deposition. However it is difficult to date the two surfaces in any absolute fashion.

We propose that the mechanisms of re-advance in this case were identical to those in operation elsewhere, and that only the scale of the cirque-like alcove is unusual - its large size resulting in a unique morphology. We propose that, due to the abnormally large dimensions of the PM1 alcove (when compared to most first-order ice mass source hollows observed in Mars' mid-latitude glacial landsystems, which are generally only 1-2 km in diameter, compared to ~ 6.5 km in the case of PM1), the duration of the re-advance responsible for the mass compression observed was insufficient for enough fresh material to enter the system and force the older remnant ice out into the main catchment valley. This 'truncated re-glaciation' resulted in the partial compression of older deposits rather than their collective expulsion, creating the parabolic plan morphology seen at the present-day.

8. Conclusion

The present-day suite of landforms in and around the cirque-like alcove PM1, observed at a catchment scale, a feature scale and at a small-scale, can be explained by conventional outbound flow activity. A sustained period of anomalously distributed local ice accumulation followed by a period of anomalous flow during a past glacial period would have been required in order for the cirque-fill feature in question to have formed in the manner suggested by Dickson et al. (2008). Room exists for multiple hypotheses at this stage, but we suggest that there is no need to invoke highly unusual and largely unsupported glacial invasion in an otherwise conventionally-configured glacial catchment. The observations presented in this paper suggest that the ice / bedrock contact at the headwall of cirque-like alcove PM1 is perhaps not a preserved glacial highstand, but rather just the upper source area of a localized, and now down-wasted conventional martian glacial system. We

therefore propose that this site may well not represent an effective datum for the reconstruction of previous glacial highstands and subsequent ice volume changes.

Chapter 5:
Discussion

1. This manuscript and the growth of martian cryospheric science

The work contained within this volume constitutes the cumulative product of a concerted research campaign spanning 3 years. This campaign began in September 2009, and although its direction was based on plans laid at that time, it has evolved over the years since. In this discussion we review the scientific climate in which this work was conceived and summarise the results presented in previous chapters, placing them in their broader scientific context. By doing so we aim to collate this work as a cohesive body of literature and highlight the ways in which it contributes to the wider scientific community's ongoing efforts to better understand Mars.

1.1. The way things were

At the outset of this project (in September 2009) the martian science community's understanding of Mars' glacial processes and the range of landforms to be found on Mars (both resulting from or associated with glaciation) was still at a comparatively early stage. Although numerous studies had been undertaken and published describing VFFs (including GLFs, LDA and LVF [for example see Squyres, 1978; 1979; Lucchitta, 1984; Kreslavsky and Head, 2000; 2002; Milliken et al., 2003; Marchant and Head, 2007; Head et al., 2010;]) only a limited number of attempts had been made to extrapolate the mechanical particulars of the formation and subsequent evolution of these glacial landforms (as discussed in Chapter 1 [Section 5] of this volume). Catchment-scale classificatory models had been devised (e.g. Head et al., 2010) and compelling evidence had been presented to suggest that landforms which looked outwardly very much like solid-ice glaciers on Earth were, in fact, also composed predominantly of H_2O ice on Mars (Holt et al., 2008; Plaut et al., 2009). We concluded However (in Chapter 1 [Section 5.2]) that a great deal of work was still to be done, and that a niche existed for contributions from parties versed in terrestrial geomorphology and glaciology. In particular, opportunities existed for work aimed at developing the community's collective understanding in: i) the fields of VFF origins and evolution (Chapter 1, Section 5.2.1); ii) the relationships between VFFs and liquid water (Chapter 1, Section 5.2.2); iii) VFF composition and structure

(Chapter 1, section 5.2.3), and; iv) the mechanisms of VFF flow and the particulars of their mechanical history (Chapter 1, section 5.2.4).

1.1.1. Major research themes in 2009

As stated above, the bulk of available literature on martian glaciation was, in 2009, of a broadly descriptive nature. Therefore at that time, with so little information then available on the material properties and internal structure of Mars' glacial masses, some of the most compelling issues at the forefront of martian cryospheric research were associated with the physical composition of these apparently glacial landforms. At this time the Phoenix lander had only recently arrived on Mars' surface (the Phoenix set down on 25th May, 2008, landing in the circum-polar regions of Mars' northern hemisphere), providing the first opportunity to directly sample the martian sub-surface. A great deal of scientific interest and activity was consequently focussed on that platform's observations of crustal composition and surface regolith ice content (e.g. Keller et al., 2009; Renno et al., 2009). Work on the larger-scale, more visible glacial landforms, including VFFs, was still predominantly descriptive (e.g. Marchant and Head, 2009), and the emphasis lay in classification with an accompanying drive to explain the distribution of apparently icy masses through numerical climatic modelling and reconstruction (e.g. Fastook et al., 2009; Head et al., 2009). Other important work to emerge at this time included the presentation of radar data from the SHARAD instrument which indicated a 'massive' ice composition for VFFs (e.g. Holt et al., 2008; Plaut et al., 2009; Safaeinili et al., 2009). This work was all of a pioneering nature, and enhanced our understanding of the features and issues in question, however very few advances were made regarding our appreciation of how Mars' glacial deposits initially formed (other than the SHARAD data which, by indicating a 'massive' ice structure, suggested deposition through precipitation) and how they have subsequently evolved, precluding any substantial advances in our understanding of how flowing ice has contributed to the shaping of Mars' present-day surface.

1.2. Developments since 2009

During and after 2009 martian research saw renewed interest in the description and classification of the various glacial formations of Mars' mid-latitudes, resulting in the publication by Head et al. (2010) of a set of criteria designed to facilitate the repeatable identification and subsequent analysis of the various glacial-type features or VFFs hitherto observed but not, until that time, fully and collectively recognised as being part of an 'integrated glacial landsystem' (Head et al., 2010). This work firmly established this term into the vocabulary of martian glacial research and, with this recognition of process and glacial genealogy, investigations of a descriptive nature became less prevalent. Emphasis began to move towards improving our collective understanding of how Mars' climate has changed in recent (Amazonian) times, with various works investigating the chronology of change through the identification of climatic events preserved in the landform record (e.g. Dixon et al., 2010; Grindrod and Fawcett, 2011) as well as clues to the nature of these changes, and the conditions which prevailed during and between them. This was attempted through further inspection and analysis of Mars' many varied ice-related landforms (e.g: Feldman et al., 2011; Head et al., 2011; Rutledge and Christensen, 2011), these analyses now being planned and driven from a more causes and mechanisms-based perspective.

One exception to the observation that descriptive studies became less prolific following the publication of Head et al. (2010) is that one of the first in-depth studies addressing the classification and, by use of terrestrial glacial analogues, the explanation of some of the features and textures observed in association with martian GLFs was at this time made by Hubbard et al. (2011). This contribution to the field of martian cryospheric investigation represented one of the first high-profile geomorphological treatments of the martian ice issue conducted from a perspective rooted in terrestrial glaciology. It highlighted the value of contributions from the geographical and glacio-geomorphological community, and also underlined the potential value of terrestrial analogues as a source of comparisons, lending to the possibility of inferring mechanical particulars and internal dynamics for Mars' ice bodies.

1.3. Current investigations and the present state of knowledge

In 2011 the HiRISE imaging system (aboard the MRO) returned repeat images of certain locations on Mars which revealed highly localised, periodic slope events. These were characterised by periodic changes in colour, surface material darkening and then subsequently reverting to its previously lighter tint. This ‘darkening’ gives the outward appearance of being fluvial in nature. With this observation of measureable gully activity, recorded at a very high resolution, the attention of many researchers (who previously had been interested in solid ice bodies and the evolution of these bodies on Mars) became diverted to the possibility of contemporary martian hydrological processes, many speculating that the occurrence of infrequent or seasonal ‘recurring slope lineae’, or areas of intermittent discolouration, could be evidence of liquid water release (e.g: McEwen et al., 2011). By 2012 the argument as to whether these intermittent lineae were of a ‘dry’ or ‘wet’ nature had diverted a great deal of attention away from investigations of Mars’ glaciers and glacial landsystems (e.g: Dickson and Head, 2012; Levy and Fountain, 2012). Therefore, although research into ices and the behaviour of water on Mars, be it in a solid or liquid state, continues to progress, investigations aimed at understanding glacial flows and their mechanical particulars would appear to be experiencing a lull following Head et al.’s (2010) classificatory paper, which would appear to have had the effect of ‘rounding off’ investigations in that vein.

2. Our work

2.1. This thesis as a contribution to martian cryospheric science

As discussed in previous sections, investigations into Mars’ flowing ice bodies appear to have entered a lull phase, with the scientific community’s current understanding of VFFs (including GLFs, LDAs and LVF) having (temporarily?) plateaued with the conclusions that they, in their many forms, are: i) the residue of a once larger ice mass which formed during a past martian glacial event (e.g. Forget et al., 2006; Head et al., 2003); ii) composed primarily of massive water ice (Holt et al.,

2008; Plaut et al., 2009); iii) potentially sensitive to periodic and climatically-driven episodes of growth and / or retreat (e.g. Grindrod and Fawcett, 2011); iv) all formed in a similar way, individually constituting parts of an integrated glacial landsystem (Head et al., 2010); v) a potential record of climatic events and possibly a geomorphological archive of environmental and physical change on Mars (e.g. Dickson et al., 2008; Dickson et al., 2010).

These hypotheses each represent profound advances in our understanding of Mars and its recent environmental history. However, as we have observed, a great deal remains that is unknown about VFFs (see Chapter 1, Section 6). In particular, relatively little has, until now, been done to develop our understanding of the mechanical history and present-day mechanical / physical properties of VFFs. Previous work has been broadly descriptive, but has stopped short of exploring possible mechanisms of growth and subsequent change in any detail, or from a geographical or glaciological perspective. Use of Earth analogues has been relatively limited. This may be due to the previous paucity of researchers engaging with these issues from a background of glacial geomorphology.

The body of research contained within this volume, submitted for evaluation towards acceptance into a doctorate of philosophy, contributes work which addresses the aforementioned shortfall in our understanding of VFFs and other glacial landforms on Mars. The author has trained and worked in the field of glaciology, and has addressed the issues surrounding glaciation in Mars' mid-latitudes from a perspective rooted in the former. Specifically, we have conducted research into the distribution, origins and physical characteristics of 'glacier-like forms (GLFs [Hubbard et al., 2011]) on Mars, the latter being the most similar of all observed VFFs to valley glaciers on Earth - the terrestrial mode of glaciation for which the most extensive body of literature is available and of which we posses the most developed understanding.

2.1.1. Our overall aims at the outset

In Chapter 1 (Section 5.2) we highlighted several particular areas where our understanding of GLFs (and by extension VFFs) was lacking. To summarise here, the main questions highlighted were: i) What factors are responsible for the present-day distribution of GLFs; ii) What mechanism is responsible for driving flow within GLFs; iii) do GLFs adhere to a terrestrial-style mass-balance regime; iv) Are GLFs universally cold-based, or do they (or have they) experience thermally-mixed (polythermal) conditions whereby liquid water plays a role in their mechanical evolution; v) How similar are Mars' GLFs to Earth's glaciers in terms of their internal structure; vi) How similar are Mars' GLFs to Earth's glaciers in terms of their internal strain regimes? Consequently, the aims of this thesis were to:

1: Conduct a detailed survey of GLFs using new CTX imagery with the intention of compiling the most comprehensive inventory and morphometric database of GLFs and their characteristics established to date.

2: Perform an analysis (based on data gathered under objective #1 [see Chapter 2]) of GLF distribution, investigating the possibility of Mars' GLFs operating under a geographically sensitive mass-balance regime similar to that of Earth's glaciers.

3: Gather detailed observations of the physical characteristics of GLFs that might, when viewed from a terrestrial glaciological perspective, lend insight into the mechanical processes by which Mars' GLFs have changed over time and (possibly) played a role in shaping the present-day surface of Mars.

4: Conduct additional opportunistic analyses investigating GLF origins and evolution, based on the data and insights gathered from aim #3.

2.2. The contribution of this thesis

The contribution of this thesis, described by chapter, to addressing these aims (above) is expanded below.

2.2.1. Chapter 1: A review of the literature and the state of the discipline

Chapter 1 of this thesis (published in Progress in Physical Geography [Souness and Hubbard, 2012]) was researched and written with a view to reviewing the existing literature relevant to GLFs, and VFFs more widely on Mars. The specific intention was to open this field of research to physical geographers and researchers with a background in terrestrial geomorphology and glaciology. The chapter summarised the work and advances that had been made thus far in the study of Mars' mid-latitude glacial formations and highlighted various areas where the scientific community's knowledge of these features was still under-developed (Section 2.1. above). Chapter 1 thereby i) built an objective summary of the advances made up to that point in time, and ii) offered a fresh perspective on where the gaps in our understanding lay. In so doing, Chapter 1 may have attracted researchers from new fields of expertise, albeit fields already closely aligned to those which have traditionally been interested in the study of other planetary bodies (e.g. physics and geology). Thus, Chapter 1 has the potential to diversify the range of specialisations at large in the field. This contribution might stand to open new and promising lines of enquiry into the issues at hand, bringing new eyes to bear on some old problems, and hopefully also lead to the identification of some new problems and some interesting new lines of inquiry.

2.2.2. Chapter 2: A survey and population-scale analysis of Mars' mid-latitude GLFs

Chapter 2 presented results of a comprehensive survey of mid-latitude GLF locations and morphometries. Initially, the locations of >1300 individual GLFs were recorded on the basis of visual analysis of >8000 CTX images. Morphometric data were recorded and presented for every GLF, and various descriptive data were sampled using a Mars global GIS, describing the geographical characteristics of the localities in which GLFs are observed. This work is published in 'Icarus', a journal concentrating on Solar System science (Souness et al., 2012). As part of this publication, all data gathered during the initial survey and subsequent morphometric

and geographical analyses was made available to the scientific community as an online resource.

Chapter 2 describes various analyses that were undertaken using the datasets described above. These analyses examined the relationships between GLF spatial concentration and several geographical variables (latitude, elevation and local relief). From the results (described fully in Chapter 2, sections 3 and 4), a number of observations were made on the origins and evolution of GLFs. Specifically, we found that:

1: Mars hosts (at least) 1309 GLFs, 727 of which are found in the northern mid-latitudes and 582 of which are found in the southern mid-latitudes.

2: GLFs mapped across Mars' mid-latitudes share broadly similar morphometries.

3: GLFs show a strong preference for a poleward orientation.

4: At a global scale, latitude appears to exert the strongest, 'first order' control over GLF distribution.

5: At a local scale, the siting of GLFs appears to be closely controlled by elevation with GLFs occurring most readily above an altitude of ~ -3000 m.

6: Relief appears to play an important, 'third-order' control that is independent of elevation, GLFs occurring predominantly in areas of moderate relief.

These observations led us to various conclusions, namely that i) GLFs throughout Mars' mid-latitudes, in both hemispheres, share a common composition and origin; ii) GLFs are sensitive to local climate and insolation; iii) GLFs are very sensitive to elevation and may have formed under a mass-balance regime similar to that which drives glacial accumulation and subsequent flow on Earth.

It was also observed that GLFs on present-day Mars appear to prefer moderate-relief surfaces. This observation suggests that Mars' GLFs are no longer sensitive to

a mass-balance regime, and that this mass-balance mechanism only operated effectively at some time in the past. Under present-day conditions, flowing ice, or ice displaying signs of historic flow, is possibly only observed where local topography has forced viscous creep under the influence of gravity.

Four of the objectives of this thesis (Section 2.1. above) are addressed by, and at least partly satisfied by, the research presented in Chapter 2: i) A comprehensive geographical and morphometric survey of Mars' mid-latitude GLFs and their immediate environments was performed; ii) various analyses were performed using this data, resulting in new insights into the formation and subsequent flow of GLFs, and finally; iii) the survey was used as an opportunity to take notes and compile a morphological record documenting GLF morphologies and various other phenomena observed during the survey.

Achievement of the aims described above has made an important contribution to our understanding of Mars' GLFs. Previously, for instance, assumptions that all VFFs shared a common composition and evolutionary history were based on qualitative observation. Chapter 2 provides the first quantitative evidence for this shared origin, based on the results of the morphometric analysis. The first analysis of GLF location relative to latitude and local topography was also presented. Chapter 2 found that latitude constitutes a first-order control, followed secondly by elevation and thirdly by relief. These findings provide an original and quantitative insight into the factors responsible for GLF's present-day distribution. Previous numerical modelling-based studies had offered explanations for the present-day regional distribution of generic ice bodies (generally coincident with the dissected mantle terrain [Chapter 1, Section 2.1]), including ground ice, but not for that of ice bodies which could potentially still have been active. The conclusions presented in Chapter 2 – that GLFs initially formed under mass-balance conditions, but that these conditions are unlikely to have persisted to the present-day and that GLFs now only exist where local topography has caused flow to occur through gravity-driven viscous creep – offer new and important perspectives on Mars' climatic history and the mechanism of initial ice deposition in Mars' mid-latitudes.

2.2.3. Chapter 3: An analysis of the morphology and distribution of crevasse patterns on GLFs

Chapter 3 uses the data and insights reported in Chapter 2 to inform and effectively target studies of smaller-scale geomorphological phenomena found on and in association with GLFs. This meets the aim described at #4 in Section 2.1. (this Chapter).

Aim #4 (Section 2.1) demands that opportunistic research expand our awareness of GLF origins and evolution. Therefore landforms and morphologies were sought (specifically those which appear to have a counterpart in Earth's glacierised catchments) which, based on comparisons to terrestrial analogues, appear to be indicative of spatial or temporal variations in glacier structure or process. A clear and readily identifiable example of just such an observable phenomenon is surface crevassing.

Crevassing was observed and recorded on numerous GLFs during the initial survey. Chapter 3 was therefore written to provide the first detailed description of these crevasses as they occur on Mars, and offers an interpretation of what their distribution and variable morphologies can tell us about how GLFs flow and decay in Mars' mid-latitudes.

Numerous distinctive crevasse patterns were observed on GLFs, all of which appear to conform to patterns present on Earth's glaciers. This observation represents an important contribution to our understanding of Mars' GLFs. Variations in surface crevasse patterns on terrestrial ice flows are a direct indication of spatial variations in strain rates. The relationship between the two is well understood. Whereas it is easy to quantify and thus understand strain rates on Earth's glaciers, either through field measurement or through remotely sensed observation, this is not the case on Mars as direct access is currently impossible and rates are too low to resolve in satellite imagery. Therefore, mechanical details of GLF flow inferred through the mapping of surface crevassing and comparison to Earth analogues represent the first opportunity of its kind to understand what happens inside GLFs as they flow / flowed in Mars' recent geological past.

Through the comparison of GLF crevasse patterns and terrestrial analogues, it was established that strain rates in GLFs are highly variable, including zones of significant longitudinal extension, lateral extension, and ice-marginal lateral shear. These results also suggest that GLFs have a transverse depth profile similar to terrestrial glaciers, and certain crevasse patterns also indicate that basal friction varies spatially and / or temporally in some GLFs, raising the possibility of liquid water activity at some point in the recent history of certain examples.

Comparison of the spatial distribution of crevassed GLFs with that of the overall population also provided some tentative new insights into how GLF strain rates and flow behaviour varies geographically at a population scale. These analyses indicated that crevassing may occur more frequently in 'environmentally marginal' areas, i.e. at the fringes of the overall GLF population's environmental domain as defined by latitude, elevation and, to a lesser extent, relief.

Finally, observations of numerous examples of crevassing on GLFs revealed a range of preservation states, some being 'sharp' and consequently inferred to be relatively recent, while others were degraded, partially filled, or in some cases even inverted through sublimation and the exhumation of debris deposits which had previously lain at the bottom of the fissure. This range of morphologies likely demonstrates that crevassing has been taking place on GLFs for a very long time, and may even still occur today under contemporary conditions. From this we can infer that, although GLFs may not have accumulated mass for a long time (as implied by results in Chapter 2), they may still be 'active' in that a strain regime still operates, or at least operated relatively recently.

Chapter 3 contributes to the community's collective understanding of Mars' GLFs by providing the first direct observations of variable GLF strain rates, the first map of intra-population morphological heterogeneity and a new perspective on the timing of GLF activity. These observations, including variable strain rates, possible destabilisation of GLFs under environmentally marginal conditions, and the historical legacy of these processes, add valuable detail to our understanding of how GLFs originally formed, their physical make-up and how they continue to develop.

2.2.4. Chapter 4: A re-interpretation of geomorphological evidence for 'invasive' flow in Protonilus Mensae

Chapter 4 presents detailed mapping of flow at a catchment-scale in one particular area of Protonilus Mensae, addressing the research goals identified at aim #4 (Section 2.1.1).

Chapter 4's consideration of catchment-scale flow is framed as part of a wider argument and is accompanied by morphological maps and interpretations of smaller-scale landforms. These include enigmatic 'mound-and-tail' features (as described by Hubbard et al., 2011), arcuate flow morphologies and a range of surface texture types. Together, these research components contribute to the re-interpretation of one particular landscape of flow-related morphologies.

Flow at this location (the GLF is located in Protonilus Mensae at Mars grid reference: 54.55 lon, 40.80 lat [decimal degrees] [Figure 1, Chapter 4]) is directionally ambiguous, and Dickson et al. (2008) interpreted it has having been 'invasive'. This conclusion implies that ice flowed from the wider catchment into a cirque-like alcove, rather than the normal scenario which would be the reverse, with ice flowing outward from such a cirque. On the basis of this 'anomalous flow' interpretation, the authors of that work suggested the site could be used as a datum for historical ice thicknesses, arguing that what would normally be described as the headwall of the feature actually represents a terminal deposit, and thus constitutes the lowest elevation of a former glacial highstand. However, as the morphology of the terrain in the immediate area is complicated, and small-scale GLF surface structures have, until recently, seen so little treatment in the literature by terrestrial glaciologists, there appears to be a strong case for testing this somewhat "counter-intuitive" hypothesis. This case is all the more powerful given the potential importance of this site as a datum for wider regional or planetary-scale reconstructions.

Chapter 4 presents detailed geomorphological maps (created in Arc GIS) of the landscape in question. These maps assisted in the interpretation of local flow, simplifying the form and distribution of various landforms and textures which,

according to the criteria described by Head et al. (2010), are the product of flowing ice.

Having reviewed the full range of local evidence, Chapter 4 collates an argument for flow at the site in question having been of a conventional outbound type. These findings are at odds with those of Dickson et al. (2008). Thus the results of Chapter 4, whilst providing research components of individual worth (e.g. detailed geomorphological maps and descriptions of landforms at various scales), also demonstrate how the study of GLFs, including the investigation and interpretation of both their overall morphology and that of the range of smaller landforms often found in association with GLFs, can have a profound impact on our understanding of other issues relating to the martian environment, both past and present.

Chapter 4 unites the perspectives and experiences gained from Chapters 1, 2 and 3 and brings this collective understanding to bear, through the construction of an integrated methodology, to address a particular issue which has been very visible in the martian glaciology forum for some years (e.g. Dickson et al., 2008; Dickson et al., 2009; Head, 2012). The original interpretation of the landform presented by Dickson et al. (2008), and that Chapter 4 re-considers, has far-reaching implications. Therefore, a re-evaluation of this hypothesis, regardless of its outcome, is of value to the wider scientific community.

Chapter 6:
Further work

1. Thoughts for the future

Although every effort has been made to ensure that the work contained within this thesis was thorough and scientifically sound, there is always room for improvement and certainly also for the development of ideas and the extension of lines of inquiry. This section outlines some of the ways in which the work contained within this thesis might be improved or extended (Section 2).

In addition, with the experience gained during the research, related lines of investigation are proposed that might be of interest in future (Section 3).

2. Critical evaluation

This Section identifies areas where the work contained within this thesis might be improved or developed, and suggests means by which such improvements might be made.

2.1. Chapter 2: A global survey of Mars' GLFs

2.1.1. Subjectivity and human error

One of the biggest problems encountered whilst designing and carrying out the survey discussed in Chapter 2 was the issue of subjectivity and anthropogenic error. Although specific criteria for identifying GLFs were developed and applied in order to maximise repeatability, minimise subjectivity and thus mitigate against its impact on the results, it proved impossible to fully account for the problem. Human error is certainly a factor. Therefore, we propose that it would be beneficial to repeat the survey using an automated technique of some kind whereby the human component was removed and full objectivity could be claimed. However, it is entirely possible that if this were to be done, wholly new forms of error might be introduced.

E-cognition software does exist that might be able to identify and classify landforms of the correct dimensions and relative morphometry. However, this technique would likely identify many similar, but mechanically distinct, formations such as gullies and landslide deposits. Therefore, it is likely that a more complex approach might be required. If, however, such a programme could be augmented with a command line that took into account elevation, local relief and geographical context, and perhaps even surface texture, thus narrowing the search parameters, it might be possible to automatically detect a large proportion of what have, in the survey presented in Chapter 2, been manually classified as GLFs.

A technique such as this would also be of use in that it would permit a far larger number of CTX images (or, indeed, images from other sensors) to be included in the survey. Whereas previously the volume of data used was somewhat restricted by the limitations of the available manpower, an automated method could exploit endless data resources, maximising coverage and thus output.

2.2. Chapter 3: Crevassing on martian glaciers

2.2.1. Higher resolution inspection of open crevasses

During the inspection of martian crevasse fields, several cases were observed in which crevasses were exceptionally deep and wide, but where the available imagery (CTX) was of an insufficient level of detail to resolve the material or deposits within the open crevasse. One such example is located in Eastern Hellas at Mars grid ref: -40.88 lat, 102.57 lon. Requests were submitted for the site in question to be targeted by the HiRISE camera, but unfortunately these images have not yet been acquired. We propose that it would be scientifically beneficial to view the crevasses at this site at a higher resolution, such as that available using HiRISE. This might provide a glimpse of the GLF's internal structure, where one might see stratification or entrained debris. This is perhaps unlikely, but is nonetheless possible. Alternatively, it might be feasible to infer the volume and depth of the crevasse using stereo imagery, providing a minimum thickness for the GLF at that point, and also perhaps a volume for crevasse-fill deposits or a thickness for supra-GLF regolith deposits, the

latter either from direct observation of a dissected exposure at the crevasse lip, or inferred from a calculated volume of crevasse-fill. Reliable thickness estimates for GLFs and depth measurements for supra-GLF dust / regolith deposits do not currently exist.

3. Possibilities for further complementary or associated work

3.1. Extending the work contained in Chapter 2: A global survey of Mars' GLFs

3.1.1. A survey of de-glaciation

The survey described in Chapter 2 of this volume was concerned with GLFs, which are classified as 'active' ice bodies, with an ice content that prevails under Mars' present-day conditions. Therefore, the survey undertaken was one of 'glacierised' landscapes. An interesting and perhaps highly informative extension of this investigation would be to perform a survey of Mars' 'glaciated' or post-glacial landforms, mapping the historical extents of Mars' now decayed ice masses. An investigation of this kind could provide valuable insights into the mechanisms of geologically recent de-glaciation on Mars, and also a 'map' of Mars' past climate. The union of such a dataset with numerical climate models could potentially create the opportunity to chart oscillations in Mars geologically recent climate both spatially and temporally.

A range of landforms exists which it might be possible to map in this manner. These include moraines, various streamlined features, surface texture units with a lineated, 'dissected' or subdued character, meltwater rivulets, trimlines and / or kame terraces. Examples of many such features were observed during the survey described in Chapter 2.

3.2. Developing the methodology associated with Chapter 3 (Crevassing on martian glaciers)

3.2.1. Global surveys and characterisations of other GLF surface morphologies and contextual phenomena

During the survey described in Chapter 2 notes were taken on many distinctive characteristics and morphological phenomena observed on, and in association with, GLFs. It was observations of this kind which facilitated the work conducted in Chapter 3 - describing and classifying the various crevasse patterns observed on Mars' GLFs.

This work on crevassing proved very interesting in that it provided the opportunity to infer particulars of GLF flow mechanisms and how their internal strain distributions vary spatially. This was achieved by reference to basic physical principles and by using crevasses on terrestrial glaciers as analogues. A similar study of other specific formations and phenomena (preferably process-related) identified on Mars' GLFs could prove equally useful to developing our understanding of GLF formation and evolution. Examples of such formations and phenomena are surface polygons, fluting, landforms indicative of meltwater activity, landforms or textures with apparent stratification or apparent periodicity, deformed craters, or any morphologies which indicate spatially heterogeneous flow. A pursuit of any one of these landform or texture types, along similar methodological lines as used in Chapter 3, could prove scientifically valuable and would constitute an original and novel piece of stand-alone research.

3.2.2. Numerical flow modelling and observations of crevassing

As described in Chapter 3, GLF crevassing was observed in a variety of intra-glacial contexts and in a variety of patterns. Through use of Earth analogues possible explanations for these patterns and contexts were suggested, and inferences about GLF flow mechanisms were made. This line of scientific inquiry could be developed through the use of numerical flow modelling. With the 'true' or observed morphology

and placement of crevasses as a target for calibration purposes, numerical simulations of ice flow and fracture could be run using a range of experimental values for martian ice rheology and flow velocity. Through multiple iterations of such a simulation (in an attempt to reconstruct what we see in the various case studies included in Chapter 3) it might be possible to better constrain our knowledge of GLF composition and flow rate.

3.3. Miscellaneous ideas for future research

3.3.1. Investigating supra-GLF debris thickness using thermal emission characteristics

Imagery is available from the thermal emission imaging system (THEMIS), mounted aboard the Mars Odyssey platform, which quantifies the thermal emission characteristics of Mars' surface both at night and during the day. It might be possible to approximate the (relative) depth of dust and regolith deposits on the surface of GLFs and other VFFs from the spatial variability of their thermal inertia. Work of this kind has been done on terrestrial glaciers (e.g. Mihalcea et al., 2008), where remotely-sensed thermal data was used in conjunction with targeted field measurements of debris cover to construct a technique for mapping debris thickness across a glacier using only satellite measurements of night-time thermal emissivity.

Tentative observations of night-time THEMIS imagery targeted in Coloe Fossae has shown a gradation of surface thermal emissivity on the longitudinal profile of larger valley VFFs, as well as a stark difference in the emissivity of surface deposits on smaller cirque-GLFs and adjacent VFFs. This emissive variability suggests variable debris thickness. This would be consistent with the glaciological context observed locally, but the hypothesis has not yet been quantified to any extent. An attempt to do so, and to identify other areas where a similar trend is visible, could prove scientifically valuable, providing insight into whether (and potentially at what rate) Mars' VFFs and GLFs re-work or re-distribute lithic material on Mars' surface.

3.3.2. Prospecting for englacial debris concentrations using SHARAD data

Just as THEMIS data has been suggested as a possible source of data on surface debris concentrations (above), we also propose that particulars of GLF debris content and transportation could be inferred from shallow radar (SHARAD) data.

Where englacial debris content is high (e.g. in the case of medial moraines on a large GLF or VFF) it is possible that a SHARAD track which crosses the area in question might record a variation in basal topography or in the VFF internal dielectric constant, the latter being indicative of (among other things) debris content. No evidence currently exists for VFF debris entrainment, or for the spatial variability of debris content (if indeed VFFs contain any debris). Therefore inspection of selected SHARAD data tracks might provide new, scientifically valuable and novel insights which could feasibly change the way the scientific community thinks about GLFs and other VFFs as a force of landscape change on Mars.

Chapter 7:
Conclusions and final comments

The introduction to this thesis identified several prominent questions that were hitherto un-adressed in the martian cryospheric literature and for which this research project was designed to provide answers. These questions were: i) what forces are responsible for the present-day distribution of GLFs; ii) what can these forms tell us about the nature of Mars' recent climate change and; iii) how do glacier-like forms interact with the martian surface as a means of mass removal and / or deposition?

The research conducted for this thesis produced new and original results and yielded many new perspectives on Mars' glacial landscapes, bringing us closer to answering the questions listed above.

Evidence suggests that Mars' GLFs are all of a common composition and depositional origin, and that they are largely relict but possibly still actively flowing. Our findings lead us to suggest that GLFs were likely deposited under Earth-like mass-balance conditions but that, in the absence of any present-day accumulation processes, they now flow in response to gravity alone. The manner in which they flow and the spatial heterogeneity of the associated strain regimes appears still to be very similar to that which is observed in Earth's glacierised catchments today, i.e. they are subject to the same material physics. This is to be expected, but some measure of confirmation on the issue is still scientifically valuable. Certain characteristics of this flow heterogeneity also imply that liquid water may still be an active component of glacial processes on present-day Mars.

The emergent picture is of Mars' GLFs as being the remains of what were formerly dynamic systems with variable strain regimes and a possible fluvial component that makes it possible that these landforms have played an active and potentially important role in the shaping of Mars' present-day surface. Further research into these forms and their mechanical particulars could prove invaluable to ongoing efforts to better understand planetary climate change (on Mars and on Earth) as well

as the role of liquid water, and thus the likelihood or possibility of life, on Mars, either in the past or in the future.

This thesis presents these findings for inspection and utilisation by the wider research community as an objective attempt to bring terrestrial glaciological perspectives and methods to bear on planetary issues in the hope of strengthening science's collective understanding of the latter.

References

Arfstrom JD (2003) Protalus ramparts and transverse ridge moraines on Mars: Indicators of surface ice depositional processes. *Lunar Planet. Sci.* 34: Abstract 1050.

Arfstrom J and Hartmann WK (2005) Martian flow features, moraine-like ridges, and gullies: Terrestrial analogs and interrelationships. *Icarus* 174: 321-335.

Baker DMH, Head JW and Marchant DR (2010) Flow patterns of lobate debris aprons and lineated valley fill north of Ismeniae Fossae, Mars: Evidence for extensive mid-latitude glaciation in the Late Amazonian. *Icarus* 207: 186–209.

Banerdt WB, Golombek MP and Tanaka KL (1992) Stress and Tectonics on Mars. In: Kieffer BMJHH, Synder CW and Matthews MS (eds) *Mars*. Tucson: Univ. of Arizona Press, 249–297.

Benn, D. I., Evans, D. J. A., 1998. Glaciers and Glaciation. Arnold. London.

Berman DC, Crown DA and Bleamaster LF (2009) Degradation of mid-latitude craters on Mars. *Icarus* 200: 77-95.

Bibring JP, Langevin Y, Gendrin A, Gondet B, Poulet F, Berthe M, Soufflot A, Arvidson R, Mangold N, Mustard J, Drossart P and the OMEGA Team (2005) Mars surface diversity as revealed by the OMEGA/Mars Express observations. *Science* 307: 1576-1581.

Bryson KL, Chevrier V, Sears DWG and Ulrich R (2008) Stability of ice on Mars and the water vapour diurnal cycle: Experimental study of the sublimation of ice through a fine-grained basaltic regolith. *Icarus*, 196(2): 446-458.

Burr DM, Soare RJ, Wan Bun Tseung J, and Emery JP (2005) Young (late Amazonian), near-surface, ground ice features near the equator, Athabasca Valles, Mars. *Icarus,* 178. 56-73.

Carr, M. H., 2001. Mars Global Surveyor observations of Martian fretted terrain. J. Geophys. Res 106 (E10), 23571-23594. Doi: 10 1029/2000JE001316.

Cattermole P (1992) *Mars: The story of the red planet*. London: Chapman and Hall.

Christensen, P. R., 2003. Formation of recent Martian gullies through melting of extensive water-rich snow deposits. Nature 422, 45-48.

Clark RN and McCord TB (1982) Mars residual north polar cap: Earth-based spectroscopic confirmation of water ice as a major constituent and evidence for hydrated minerals. *Journal of Geophys. Res. Solid Earth,* 87(B1). 367-370.

Colaprete A and Jakosky BM (1998) Ice flow and rock glaciers on Mars*. J. Geophys. Res,* 103. 5897-5909.

Conway SJ, Mangold N, Ansan V (2011) Crater shape evolution with latitude in Terra Cimmeria, Mars – implications for climate. LPSC XLII, Houston, TX.

Cuffey KM and Paterson WSB (2010) The physics of Glaciers. Butterworth-Heinmann. Burlington, MA.

DeVincensi DL, Bagby J, Race M and Rummel J (1999) Mars sample quarantine protocol workshop: Proceedings of a workshop held at NASA Ames Research Centre. NASA/CP-1999-208772.

Dickson J, Head JW and Marchant DR (2008) Late Amazonian glaciation at the dichotomy boundary on Mars: Evidence for glacial thickness maxima and multiple glacial phases. *Geology*, 36. 411-414.

Dickson JL, Head JW and Marchant DR (2010) Kilometer-thick ice accumulation and glaciation in the northern mid-latitudes of mars: Evidence for crater-filling events in the late Amazonian at the Phlegra Montes. *Earth and planet. Sci. Lett*., 294: 332-342.

Dickson JL and Head JW (2012) Active-layer drainage without surface erosion: Time-lapse photography of Antarctic slope lineae and implications for the flow of water on Mars. [#1085] LPSC XXXXIII, The Woodlands, Texas.

Dohm JM, Andersen RC, Baker VR, Ferris JC, Rudd LP, Hare TM, Strom RG, Rudd LP, Rice JW, Casavant RR and Scott DH (2000) System of Gigantic Valleys Northwest of Tharsis, Mars' Latent Catastrophic Flooding, Northwest Watershed, and Implications for Northern Plains Ocean. *Geophys. Res. Lett.,* 27(21): 3559-3562.

Dohm JM, Baker VR, Maruyama S and Anderson RC (2007) Traits and evolution of the Tharsis superplume, Mars. In: Yuen DA, Maruyama S, Karato S and Windley BF (eds) *Superplumes: Beyond Plate Tectonics*. Netherlands: Springer.

Dundas CM and Byrne S (2010) Modeling sublimation of ice exposed by new impacts in the Martian mid-latitudes. *Icarus,* 206: 716-728.

Dundas CM and McEwen AS (2010) An assessment of evidence for Pingos on Mars using HiRISE. *Icarus,* 205(1): 244-258.

Fairén AG, Schulze-Makuch D, Rodriguez AP, Fink W, Davila AF, Uceda ER, Furfaro R, Amils R and McKay CP (2009) Evidence for Amazonian acidic liquid water on Mars – a reinterpretation of MER mission results. *Planetary and Space Science*, 57: 276-287.

Fanale FP, Salvail JR, Zent AP and Postawko SE (1986) Global distribution and migration of subsurface ice on Mars. *Icarus*, 67: 1-18.

Farmer CB, Davies DW and LaPorte DD (1976) Mars: Northern summer ice cap – Water vapour observations from Viking 2. *Science,* 194: 1399-1341.

Fassett CI and Head JW (2005) Fluvial sedimentary deposits on Mars: ancient deltas in a crater lake in the Nili Fossae Region. *Geophysical Research Letters*, 32: L14201 (doi:10.1029/2005GL023456).

Fassett CI, Dickson JL, Head JW, Levy JS and Marchant DR (2010) Supraglacial and proglacial valleys on Amazonian Mars. *Icarus,* 208: 86-100.

Fastook JL Head JW Marchant DR and Forget F (2008) Tropical mountain glaciers on Mars: Altitude dependence of ice accumulation, accumulation conditions, formation times, glacier dynamics, and implications for planetary spin-axis/orbital history. *Icarus,* 198 (2): 305-317.

Fastook JL, Head JW, Madeleine JB, Forget F and Marchant DR (2009) Modelling northern mid-latitude glaciation with GCM-driven climate: Focus on Deuteronilus-Protonilus Mensae valleys. [#1144] LPSC XXXX, The Woodlands, Texas.

Feldman WC, Prettyman TH, Maurice S, Lawrence DJ, Pathare A, Milliken RE and Travis BJ (2011) Search for remnant water ice from past glacial climates on Mars: The Mars Odyssey Neutron Spectrometer. [#2420] LPSC XXXXII, The Woodlands, Texas.

Fishbaugh KE and Head JW (2001) Comparison of the north and south polar caps of Mars: New observations from MOLA data and discussion of some outstanding questions. *Icarus,* 154(1): 145-161.

Fleisher PJ and Sales JK (1972) Laboratory models of glacier dynamics. *Geological Society of America Bulletin.* doi: 10.1130/0016-7606(1972)83[905:LMOGD]2.0.CO;2.

Forget F, Haberle RM, Montmessin F, Levrard B and Head JW (2006) Formation of glaciers on Mars by atmospheric precipitation at high obliquity. *Science*, 311: 368-371.

Forget F (2009) The present and past climates of planet Mars. In: Boutron C (ed.) ERCA: From the Human Dimensions of Global Environmental Change to the Observation of the Earth from Space, Vol. 8. *European Physical Journal Conferences*,1. 235-248.

Frey H and Schultz RA (1988) Large impact basins and the mega-impact origin for the crustal dichotomy on Mars. *Geophysical Research Letters*, 15: 229-232.

Glasser, NF, Hambrey, MJ, Crawford, KR, Bennett, MR, and Huddart, D (1998) The structural glaciology of Kongsvegen, Svalbard, and its role in landform genesis. J. of Glaciology 44. 136-148.

Glasser, NF and Scambos, TA (2008) A structural glaciological analysis of the 2002 Larsen B ice shelf collapse. *J. of Glaciology,* 54(184). 3-16.

Glasser, NF, and Gudmundsson, GH (2012) Longitudinal surface structures (flowstripes) on Antarctic glaciers. The Cryosphere 6. 383-391.

Grindrod F and Fawcett SA (2011) Possible climate-related signals in high-resolution topography of lobate debris aprons in Tempe Terra. *Geophys res Lett*. 38. L19201 DOI: 10.1029/2011GL049295.

Hambrey, MJ (1975) Short Notes: The origin of foliation in glaciers: Evidence from some Norwegian examples. J. of Glaciology 14. 181-185.

Hambrey, M. (1994) Glacial Environments. UCL Press. London.

Hambrey, MJ. and Lawson, W. Structural styles and deformation fields in glaciers: a review. In: Maltman, A. J., Hubbard, B. & Hambrey, M. J. (eds) *Deformation of Glacial Materials* (Geological Society, London, Special Publications, 2000).

Hartmann WK and Neukum G (2001) Cratering chronology and the evolution of Mars. In: *Space Science Reviews* 96: 165–194. Netherlands: Kluwer Academic Publishers.

Hartmann WK, Thorsteinsson T and Sigurdsson F (2003) Martian hillside gullies and Icelandic analogs. *Icarus*, 162: 259-277.

Hartmann WK (2005) Martian cratering 8: Isochron refinement and the chronology of Mars. *Icarus,* 74: 294-320.

Hartmann WK and Werner SC (2010) Martian cratering 10. Progress in use of crater counts to interpret geological processes: Examples from two debris aprons. *Earth Planet. Sci. Lett.*, 294: 230-237.

Hättestrand C, Kolka V, and Johansen N (2007) Cirque infills in the Khibiny Mountains, Kola Peninsula, Russia – palaeoglaciological interpretations and modern analogues in East Antarctica. J. of Quaternary Sci. DOI: 10.1002/jqs.1130.

Head JW and Marchant DR (2003) Cold-based mountain glaciers on Mars: Western Arsia Mons. *Geology*, 31: 641-644.

Head JW, Mustard JF, Kreslavsky MA, Milliken RE and Marchant DR (2003) Recent ice ages on Mars. *Nature*, 426: 797-802.

Head JW, Neukem G, Jaumann R, Hiesinger H, Hauber E, Carr M, Masson P, Foing B, Hoffmann H, Kreslavsky M, Werner S, Milkovich S, Van Gasselt S and The HRSC Co-Investigator Team (2005) Tropical to mid-latitude snow and ice accumulation, flow and glaciation on Mars. *Nature*, 434: 346-351.

Head J (2007) The geology of Mars: new insights and outstanding questions. In: Chapman M (ed.) *The Geology of Mars – Evidence from Earth-based Analogs*. Cambridge: Cambridge University Press.

Head JW, Marchant DR, Forget F, Laskar J, Madeleine JB and Fastook JL (2009) Deciphering the late Amazonian climate history of Mars: assessing obliquity

predictions with geological observations and atmospheric general circulation models. [#1349] LPSC XXXX, The Woodlands, Texas.

Head JW, Marchant DR, Dickson JL, Kress AM and Baker DM (2010) Northern mid-latitude glaciation in the Late Amazonian period of Mars: Criteria for the recognition of debris-covered glacier and valley glacier landsystem deposits. *Earth and planetary Science Letters*, 294: 306–320.

Head JW, Mustard JF, Kreslavsky MA, Milliken RE, Marchant DR, Forget F, Schon SC and Levy JS (2011) Mars in the current glacial-interglacial cycle: Exploring an anomalous period in Mars' climate history. [#1315] LPSC XXXXII, The Woodlands, Texas.

Head JW (2012) Masursky Lecture: Mars climate history: A geological perspective. [#2582] LPSC XXXXIII, The Woodlands, Texas.

Herzfeld, U. C., Herzfeld, U. C. and Clarke, G. K. (2001) Analysis of crevasse patterns as indicators of ice dynamics using structural glaciology and geostatistical classification. American Geophysical union, Fall Meeting. Abstract #IP21A-0674.

Hindmarsh, R. C. A., Van Der Wateren, F. M., Verbers, A. L. L. M., 1998. Sublimation of ice through sediment in Beacon Valley, Antarctica. Geografiska Annaler 80. 209-219.

Holt JW, Safaeinili A, Plaut J, Head JW, Phillips RJ, Seu R, Kempf SD, Choudhary P, Young DA, Putzig NE, Biccari D and Gim Y (2008) Radar sounding evidence for buried glaciers in the southern mid-latitudes of Mars. *Science*, 322: 1235-1238.

Howard AD (2003) Tongue ridges and rumpled crater floors in mid-southern-latitude Martian craters. *Lunar Planet. Sci*., 34: Abstract 2073.

Howard AD (2009) Planetary morphodynamics: Scaling and interpreting sedimentary processes from Earth to Mars and Titan. In: Vionnet CA Garcia MH Latrubesse EM

Perillo GME (eds), *River, Coastal and Esturine Morphodynamics.* RCEM 09 Vol 1. 207-216. CRC Press, Boca Raton.

Hubbard B, Milliken RE, Kargel JS, Limaye A and Souness C (2011) Geomorphological characterization and interpretation of a mid-latitude glacier-like form: Hellas Planitia, Mars. *Icarus,* 211: 330-346.

Imbrie J and Imbrie KP (1986) *Ice Ages: Solving the mystery.* USA, Enslow.

Ivanov MA and Head JW (2006) Alba Patera, Mars: Topography, structure, and evolution of a unique late Hesperian-early Amazonian shield volcano. *Journal of Geophysical Research*, 111: E09003.

Jansson K and Glasser NF (2005) Palaeoglaciology of the Welsh sector of the British-Irish Ice Sheet. *Journal of the Geological Society,* 162(1). 25-37.

Johnson CL and Phillips RJ (2005) Evolution of the Tharsis region of Mars: insights from magnetic field observations*. Earth and Planetary Science Letters*, 230: 241-254.

Kadish SJ, Head JW, Barlow NG and Marchant DR (2008) Martian pedestal craters: Marginal sublimation pits implicate a climate-related formation mechanism. *Geophysical Research Letters,* 35: L16104, doi:10.1029/2008GLO34990.

Kargel JS and Strom RG (1992) Ancient Glaciation on Mars. *Geology*, 20: 3-7.

Kargel JS (2004) Mars: A warmer, wetter planet. Springer Praxis Books.

Keller HU, El Maarry MR, Goetz W, Hviid SF, Markiewiez WJ, Hecht M, Madson M, Mellon M, Ming D, Pike WT, Smith P, Staufer U and Zent A (2009) Physical properties of the icy soil at the Phoenix landing site. [#1671] LPSC XXXX, The Woodlands, Texas.

Keiffer HH, Chase SC, Martin TZ, Miner ED and Palluconi FD (1976) Martian North Pole summer temperatures: dirty water ice. *Science,* 194(4271): 1341-1344

Kite ESS, Rafkin SCR, Michaels TI, Dietrich WEE, and Manga M (in press) Valles Marineris chaos, storms and past climate on Mars. *J of Geophys Res.* doi:10.1029/2010JE003792.

Kreslavsky MA and Head JW (2000) Kilometer-scale roughness of Mars' surface: Results from MOLA data analysis. *Journal of Geophysical Research,* 100: 11781-11799.

Kreslavsky MA and Head JW (2002) Mars: Nature and evolution of young latitude-dependent water-ice-rich mantle. *Geophysical research letters,* 29(15). 10.1029/2002GL015392.

Laskar J, Joutel F and Boudin F (1993) Orbital, precessional, and insolation quantities for the Earth from -20 Myr to +10 Myr. *Astronomy and Astrophysics*, 270: 522-533.

Leovy, C (2001) Weather and climate on Mars. *Nature*, 412: 245-249.

Leverington, DW (2012) A volcanic origin for the outflow channels of Mars: Key evidence and major implications. *Geomorphology,* 132: 51-75.

Levrard, B., Forget, F., Montmessin, F., Laskar, J (2004) Recent ice-rich deposits formed at high latitudes on Mars by sublimation of unstable equatorial ice during low obliquity. Nature 431, 1072-1075.

Levrard, B., Forget, F., Montmessin, F., Laskar, J (2007) Recent formation and evolution of northern Martian polar layered deposits as inferred from a Global Climate Model. J. Geophysical. Res (Planets) 112, E06012.

Levy J, Head JW and Marchant DR (2009) Concentric crater fill in Utopia Planitia: History and interaction between glacial “brain terrain” and periglacial mantle processes. *Icarus*, 202: 462-476.

Levy JS, Head JW and Marchant DR (2010) Thermal contraction crack polygons on Mars: A synthesis from HiRISE, Phoenix, and terrestrial analog studies. *Icarus*, 206: 229-252.

Levy JS and Fountain AG (2012) Hydrological characteristics of recurrent slope lineae on Mars based on time-resolved HiRISE analyses and comparisons with fluid flow through an Antarctic terrestrial analog regolith. [#1029] LPSC XXXXIII, The Woodlands, Texas.

Li H, Robinson MS, Jurdy DM (2005) Origin of Martian northern hemisphe mid-latitude lobate debris aprons*. Icarus* 176 (2), 382-394.

Lorenz RD (2009) Power law of dust devil diameters on Mars and Earth*. Icarus,* 203: 683-684.

Lucchitta BK (1981) Mars and Earth: Comparison of cold-climate features. *Icarus,* 45: 264 – 303.

Lucchitta BK (1984) Ice and debris in the fretted terrain, Mars. *Journal of Geophysical Research*, 89: B407 B418, doi: 10.1029/JB089iS02p0B409.

Lucchitta BK, Clow GD, Croft SK, Geissler PE, McEwen AS, Singer RB, Squyres SW and Tanaka KL (1989) Canyon systems on Mars (abstract). *Fourth International Conference on Mars, Tucson*: 36-37.

Madeleine JB, Forget F, Head JW, Levrard B, Montmessin F and Millour E (2009) Amazonian northern mid-latitude glaciations on Mars: A proposed climate scenario. *Icarus*, 203: 390-405.

Mair R and Kuhn M (1994) Temperature and movement measurements at a bergschrund. *Journal of Glaciology,* 40. 561-565.

Malin MC and Edgett KS (2000) Sedimentary rocks of early Mars. *Science*, 290(5498): 1927-1937.

Mangold N (2005) High latitude patterned ground on Mars: Classification, distribution and climatic control. *Icarus,* 174. 336-359.

Marchant DR and Head JW (2003) Tounge-shaped lobes on Mars: Morphology, nomenclature, and relation to rock glacier deposits. *Sixth International Conference on Mars*: 3091.pdf.

Marchant DR and Head JW (2007) Antarctic Dry Valleys: microclimate zonation, variable geomorphic processes, and implications for assessing climate change on mars. *Icarus,* 192: 187-222.

Marchant DR and Head JW (2009) The glacial deposits of the northern mid-latitudes: Remnants of large-scale plateau glaciation. [#2355] LPSC XXXX, The Woodlands, Texas.

McEwen AS, Ojha L, Dundas CM, Mattson SS, Byrne S, Wray JJ, Cull SC, Murchie SL, Thomas N and Gulick VC (2011) Seasonal flows on warm martian slopes. *Science*, 333: 740-743.

Mege D and Masson P (1996) A plume tectonics model for the Tharsis province, Mars. *Planetary and Space Science,* 44: 1499-1546.

Mellon MT and Jakosky BM (1995) The distribution and behaviour of Martian ground ice during past and present epochs. *J. Geophys. Research.* 100. 11,781-11,799.

Mihalcea C, Brock BW, Diolaiuti G, Agata CD, Citterio M, Kirkbride MP, Cutler MEJ and Smiraglia C (2008) Using ASTER satellite and ground-based surface temperature measurements to derive supraglacial debris cover and thickness

patterns on Miage Glacier (Mont Blanc Massif, Italy). *Cold regions Science and Technology.* 52. 341-354.

Milliken RE, Mustard JF and Goldsby DL (2003) Viscous flow features on the surface of Mars: Observations from high-resolution Mars Orbiter Camera (MOC) images. *Journal of Geophysical Research*, 108: No. E6, 5057.

Morgan GA, Head JW and Marchant DR (2009) Lineated valley fill (LVF) and lobate debris aprons (LDA) in the Deuteronilus Mensae northern dichotomy boundary region, Mars: Constraints on the extent, age and episodicity of Amazonian glacial events. *Icarus*, 202: 22-38.

Mustard JF, Cooper CD and Rifkin MK (2001) Evidence for recent climate change on Mars from the identification of youthful near-surface ground ice. *Nature*, 412: 411-414.

Mutch TA, Arvidson RE, Head JW, Jones KL and Saunders RS (1976) *The Geology of Mars*. Princetown, NJ: Princetown University Press.

Nakawo, M., Young, G. J. 1981. Field experiments to determine the effect of a debris layer on ablation of glacier ice. Annals of Glaciology, 2. 85-91.

Page DP, Balme MR and Grady MM (2009) Dating Martian climate change. *Icarus*, 203: 376-389.

Parsons RA, Nimmo F, Miyamoto H (2011) Constraints on martian lobate debris apron evolution and rheology from numerical modelling of ice flow. *Icarus*. 214. 246-257.

Paterson WSB (1981) *The Physics of Glaciers*. New York: Pergamon.

Pathare AV, Paige DA and Turtle E (2005) Viscous relaxation of craters within the Martian south polar layered deposits. *Icarus*, 174(2): 396-418.

Pearce G, Osinski GR, Soare RJ (2011) Intra-crater processes in central Utopia Planitia, Mars. *Icarus*. 212. 86-95.

Pelletier JD Comeau D and Kargel J (2010) Controls on glacial valley spacing on Earth and Mars. *Geomorphology.* 116: 189-201.

Plaut JJ, Safaeinili A, Holt JW, Phillips RJ, Head JW, Sue R, Putzig NE and Frigeri A (2009) Radar evidence for ice in lobate debris aprons in the mid-northern latitudes of Mars. *Geophysical* Research *Letters*, 36, LO2203. Doi:10.1029/2008GL036379.

Read PL and Lewis SR (2004) *The Martian Climate Revisited; Atmosphere and Environment of a Desert Planet.* Chinchester, UK: Springer Praxis Publishing.

Renno NO, Bos BJ, Catling D, Clark BC, Drube L, Fisher D, Goetz W, Hviid SF, Keller HU, Kok JF, Kounaves SP, Leer K, Lemmon M, Madsen MB, Markiewies W, Marshall J, McKay C, Mehta M, Smith M, Smith PH, Stoker C, Young SMM and Zent A (2009) Physical and thermodynamical evidence for liquid water on Mars. [#1440] LPSC XXXX, The Woodlands, Texas.

Rignot E Hallet B and Fountain A (2002) Rock glacier surface motion in Beacon Valley, Antarctica, from synthetic aperture radar interferometry. *Geophysical research Letters, 29,* doi:10.1029/2001GL013494.

Rutledge AM and Christensen PR (2011) Hypsometric analysis of glacial features in the east Hellas basin, Mars: Implications for past climate shifts. [#2124] LPSC XXXXII, The Woodlands, Texas.

Safaeinili A, Holt J, Plaut J, Posiolova L, Philips R, Head JW and Seu R (2009) New radar evidence for glaciers in Mars' Phlegra Montes region. [#1988] LPSC XXXX, The Woodlands, Texas.

Schon SC, Head JW and Milliken RE (2009) A recent ice age on Mars: Evidence for climate oscillations from regional layering in mid-latitude mantling deposits. *Geophysical Research Letters*, 36, L15202, doi:10.1029/2009GL038554.

Scott DH and Carr MH (1978) Geologic map of Mars. *U.S. Geol. Survey Misc. Geol. Inv. Map.*

Searls ML, Mellon MT, Martinez-Alonso S and the HiRISE Team (2008) Slope analysis and ice stability of the mid-latitude dissected terrain on Mars. *Lunar and planetary Science XXXIX*: Abstract. 2376.pdf.

Sharp RP (1973) Mars: Fretted and chaotic terrains. *Journal of Geophysical Research,* 78: 4073-4083.

Shean DE, Head JW and Marchant DR (2005) Origin and evolution of a cold-based tropical mountain glacier on Mars: The Pavonis Mons fan-shaped deposit. *Journal of Geophysical Research-Planets*, 110: Article number: E05001.

Smith MD (2008) Spacecraft observations of the Martian atmosphere. *Annual Review of Earth and Planetary Sciences*, 36: 191-219.

Smrekar SE, McGill GE, Raymond CA and Dimitriau AM (2004) Geologic evolution of the Martian dichotomy in the Ismenious area of Mars and implications for plains magnetization. *Journal of Geophysical research,* 109: E11002.

Soare RJ, Osinski GR and Roehm CL (2008) Thermokarst lakes and ponds on Mars in the very recent (late Amazonian) past. *Earth and Planetary Science Letters,* 272(1-2): 382-393.

Soare RJ and Osinski GR (2009) Stratigraphical evidence of late Amazonian periglaciation and glaciations in the Astapus Colles region of Mars. *Icarus*, 202: 17-21.

Soare RJ, Costard F, Pearce GD, Sejourne A (2012) A re-interpretation of the recent stratigraphical history of Utopia Planitia, Mars: Implications for late-Amazonian periglacial and ice-rich terrain. *Planetary and Space Sci*. 60. 131-139.

Souness CJ, Hubbard B, Milliken RE and Quincey D (2012) An inventory and population-scale analysis of Martian glacier-like forms. *Icarus,* 217: 243 – 255.

Souness CJ and Hubbard B (2012) Mid-latitude glaciation on Mars. *Progress in Physical Geography,* 36. Vol 2. 238-261.

Souness CJ and Hubbard B (2012) Crevasse-Like Openings as Indicators of Flow in Martian Glacier-Like Forms. [#1070]. LPSC XXXXIII, The Woodlands, Texas.

Souness CJ and Hubbard B (in press) An alternative interpretation of an Amazonian glacial highstand in eastern Protonilus Mensae, Mars: Observations from catchment and feature-scale flow mapping using data from the CTX and HiRISE imaging systems. *Icarus.*

Squyres SW (1978) Martian fretted terrain: Flow of erosional debris. *Icarus,* 34: 600-613.

Squyres SW (1979) The distribution of lobate debris aprons and similar flows on Mars. *Journal of Geophysical Research,* 84: 8087-8096.

Squyres SW and Carr MH (1986) Geomorphic evidence for the distribution of ground ice on Mars. *Science,* 213: 249-2253.

Squyres SW (1989) Urey Prize Lecture: Water on Mars. *Icarus,* 79: 229–288.

Sugden DE (1978) Glacial erosion by the Laurentide ice sheet. *Journal of Glaciology,* 20(83). 367-391.

Sugden, D. E., John, B. S., 1990. Glaciers and landscape. Arnold Publishing.

Sundal, A. V., Shepherd, A., Nienow, P., Hanna, E., Palmer, S. and Huybrechts, P. (2011) Melt-induced speed-up of Greenland ice sheet offset by efficient subglacial drainage. Nature, 469. 521-524.

Tanaka KL (1986). The stratigraphy of Mars. Proceedings of the seventeenth Lunar and Planetary Science Conference, 1. *Journal of Geophysical research*, 91 (B13): 139-158.

Touma J and Wisdom J (1993) The chaotic obliquity of Mars. *Science*, 259: 1294-1297.

Turtle EP, Pathare AV, Crown DA, Chuang FC, Hartmann WK, Heinze JC et al (2003) Modelling deformation of lobate debris aprons on Mars by creep of ice-rich permafrost. *American Geophysical Union, Fall Meeting 2003:* Abstract C21C-0830.

Unwin D J (1972) The distribution and orientation of corries in northern Snowdonia, Wales. Transactions of the Institute of British Geographers 58. 85-97.

Van Gasselt S, Hauber E and Neukem G (2010) Lineated valley fill at the Martian dichotomy boundary: Nature and history of degradation. *Journal of Geophysical Research,* 115: E08003.

Ward WR (1992) Long term orbital and spin dynamics of Mars. In: Kieffer HH, Jakosky BM, Snyder CW and Matthews MS (eds.) *Mars*. Tuscon, Arizona: University of Arizona Press.

Washburn AL (1979) *Geocryology: A survey of periglacial processes and environments*, *second edition*. London: Edward Arnold.

Whiteway JA, Komguem L, Dickinson C, Cook C, Illnicki M, Seabrook J, Popovici V, Duck TJ, Davy R, Taylor PA, Pathak J, Fisher D, Carswell AI, Daly M, Hipkin V, Zent AP, Hecht MH, Woot SE, Tamppari LK, Renno N, Moores JE, Lemmon MT, Daerden F and Smith PH (2009) Mars water-ice clouds and precipitation. *Science*, 325: 68-70.

Wilhelms DE and Squyres SW (1984) The Martian hemispheric dichotomy may be due to a giant impact. *Nature*, 309: 138-140.

Wise DU, Golombek MP and McGill GE (1979) Tharsis province of Mars: Geologic sequence, geometry, and a deformation mechanism. *Icarus*, 38: 456-472.

Wise DU, Golombek MP and McGill GE (1979b) Tectonic evolution of Mars. *Journal of Geophysical Research*, 84: 7934-7939.

Zealey WJ (2008) Glacial, periglacial and glacio-volcanic structures on the Echus Plateau, upper Kasei Valles. Planet. *Space Science.* 57: 699–710.

Multimedia references

http://www.mentallandscape.com/C_CatalogMars.htm

National Space Science Data Centre: nssdc.gsfc.nasa.gov

NASA's Mars Exploration Program: marsprogram.jpl.nasa.gov

Appendix 1:

Geomorphological characterisation and interpretation of a mid-latitude glacier-like form: Hellas Planitia, Mars.

B. Hubbard, R. E. Milliken, J. S. Kargel, A Limaye and C. J. Souness

Appendix 2:

Inventory of Crevassed GLFs (Chapter 3)

Appendix 2a:

Crevassed GLFs in Mars' northern mid-latitudes

Appendix 2b:

Crevassed GLFs in Mars' southern mid-latitudes

Icarus 211 (2011) 330–346

Contents lists available at ScienceDirect

Icarus

journal homepage: www.elsevier.com/locate/icarus

Geomorphological characterisation and interpretation of a mid-latitude glacier-like form: Hellas Planitia, Mars

Bryn Hubbard [a,*], Ralph E. Milliken [b], Jeffrey S. Kargel [c], Ajay Limaye [d], Colin Souness [a]

[a] Institute of Geography and Earth Sciences, Aberystwyth University, Aberystwyth, Ceredigion SY23 3DB, UK
[b] Dept. Civil Engineering and Geological Sciences, University of Notre Dame, Notre Dame, IN 46556, USA
[c] Department of Hydrology and Water Resources, University of Arizona, Tucson, AZ 85721, USA
[d] Division of Geological and Planetary Sciences, California Institute of Technology, Pasadena, CA 91125, USA

ARTICLE INFO

Article history:
Received 29 December 2009
Revised 20 October 2010
Accepted 25 October 2010
Available online 10 November 2010

Keywords:
Mars
Mars, Surface
Mars, Polar caps

ABSTRACT

We describe and interpret the surface terrain types associated with a widely-reported ~4 km long, mid-latitude martian viscous flow feature (VFF). The feature is located in the southern hemisphere, on the poleward-facing rim of a ~60 km-diameter crater in eastern Hellas Planitia. High Resolution Imaging Science Experiment (HiRISE) images, analysed in both 2D and 3D, reveal that the upper margin of the feature is bounded by steep (~30°) headwalls, typically some tens of metres high, that are formed from unconsolidated material and characterised by a series of slope–parallel linear incisions. Below these incised headwalls, the feature flows at a general angle of ~10° from a broad upper basin to a confined lower tongue that is bounded by a nested sequence of elongate raised ridges. These characteristics are typical of several VFFs in the region and are strikingly similar to moraine-bounded valley glaciers on Earth, and we sub-classify this feature as a 'glacier-like form' (GLF)[1]. The GLF comprises five distinctive surface terrain types that contrast sharply with surface characteristics outside its bounding moraines. Four of these terrains (scaly terrain, polygonized terrain, linear terrain and mound-and-tail terrain) are located within the GLF's innermost bounding moraine, while the fifth (rectilinear-ridge terrain) is located between its frontal moraines. These terrains are mapped, characterised and associated with possible mechanisms of formation to draw inferences about the GLF's glaciology and glacial history. This analysis suggests that the GLF reached its maximal extent in the geologically-recent past, and that it may have been partially wet-based at that time. Subsequent to this phase, the GLF experienced an extended period of general recession that has been punctuated by several episodes of still-stand or advance. Currently, the GLF's basin appears to be composed of a lower zone that is dominated by an exposed former glacier bed and an upper zone that may still contain a now-degraded and dust-mantled viscous mass, similar to many partially-glacierized basins on Earth.

1. Introduction

Mars exhibits many landscape features that are similar to glacial ice masses and ice-moulded landscapes on Earth (e.g., Kargel and Strom, 1992). In addition to the polar ice caps, numerous ice-mass-like viscous flow features (VFFs) have been identified and characterised in the martian mid-latitudes (e.g., Hartmann et al., 2003; Head et al., 2003; Kargel, 2004; Mahaney et al., 2007; Marchant and Head, 2003; Milliken et al., 2003). These lobate VFFs generally contrast with mid-latitude permafrost debris-flows or landslides in that the latter are generally raised above the surrounding landscape and have notable headwall supply hollows (e.g., van Gasselt et al., 2007). Flow modelling and investigations of crater density indicate that many VFFs, including that investigated herein (e.g., Hartmann, 2005), are probably geologically recent, between ~10^5 and 10^7 years old.

One particular group of VFFs is visually similar in terms of their large-scale geometry and characteristics to valley glaciers on Earth, termed 'glacier like flows' (GLFs) by Arfstrom and Hartmann (2005). Most GLFs accordingly have a broad upper basin that merges gradually with the surrounding topography, and a tongue that is typically confined by raised bounding ridges. Investigations of their surface form also generally indicate that they are 'cold-based' or frozen to their substrate throughout (Head and Marchant,

* Corresponding author.
E-mail address: byh@aber.ac.uk (B. Hubbard).

[1] This terminology contrasts slightly with Hartmann's original usage in that we refer to the feature as a 'form' rather than a 'flow'. This preference is based on several considerations, including that: (i) although inferred, flow has not yet been measured at such features, (ii) supplementary (basal) motion components cannot yet be ruled out, and (iii) the term 'flow' can refer to both a form and a process of ice-mass motion, which could lead to confusion.

0019-1035/$ - see front matter © 2010 Elsevier Inc. All rights reserved.
doi:10.1016/j.icarus.2010.10.021

2003; Shean et al., 2005). However, recent evidence points to the possibility that martian glaciation may, at some period in the past, have been at least partially wet-based. For example, Arfstrom and Hartmann (2005) argued that the distinctive moraine-like ridges bounding several mid-latitude martian VFFs (including that investigated herein) could form by water-lubricated sediment squeezing from beneath the ice, implicitly requiring wet-based glacial conditions. In terms of earlier glaciations, Banks et al. (2009) interpreted the well-known (but undated) network of sinuous and anastomosing ridges in southern Argyre Planitia (~30–55°S) as subglacial eskers, requiring the presence of a large, wet-based ice mass. In an earlier study of the same area, Banks et al. (2008) had already reported the presence of elongate bedforms and large-scale grooves or striations in the rock surface and interpreted these erosional features in terms of wet-based glacial activity, probably of pre-Amazonian age. Many ice masses on Earth are, in fact, neither wholly cold-based nor wholly wet-based but a combination of both. Such *polythermal* ice masses generally have a warm-based interior (where the thick overlying ice provides sufficient insulation for the 0 °C isotherm to rise to intersect the ice-bed interface) and cold-based margins (where the ice is thinner and the 0 °C isotherm is located within the subglacial substrate) (e.g., Paterson, 1994). These countering influences of surface temperature and ice thickness, for example, allow significant regions of the base of the East Antarctic ice sheet to host large lakes (e.g., Siegert, 2000) and even its (significantly thinner) outlet glaciers to have portions of their interior beds that are wet-based (e.g., Hubbard et al., 2004; Robinson, 1984). Moreover, the thermal regime (i.e., temperate, cold, or polythermal) of any given terrestrial ice mass is likely to have changed through time in response to changes in surface temperature and ice thickness. Despite the hypothesised glacial origin attributed to martian GLFs, no study has yet investigated the detailed surface structure of a GLF with the aim of identifying mechanisms of formation, deformation and glacial history – particularly in the light of alternative thermal regimes.

One mid-latitude martian GLF in particular has attracted widespread attention as a type example of a martian glacier or rock glacier: that centred on 38.15°S and 113.16°E (Fig. 1). This feature is located inside the northern (i.e. pole-facing) rim of a 60–70 km diameter crater, centred on ~38.65°S; ~112.98°E, to the east of the Hellas basin. Initially, several investigators noted this feature's glacier-like outline and moraine-like bounding ridges (e.g., Hartmann et al., 2003; Kargel, 2004; Marchant and Head, 2003; Milliken et al., 2003). However, more detailed exploration of the feature's surface characteristics was limited by the (metres to tens of metres per pixel) resolution of the Mars Orbiter Camera images available at the time. Nonetheless, Arfstrom and Hartmann (2005) did note that the feature's lateral ridges appeared to be double-crested, indicating the possibility of separate glacial advances, while Marchant and Head (2003) observed the presence of 'chevron ridges' on the feature's inner surface, compatible with down-slope flow. Furthermore, both Arfstrom and Hartmann (2005) and Hartmann (2005) constrained the age of the feature's surface on the basis of the density-distribution of small (11–16 m diameter) impact craters, concluding that it was geologically recent (and not older than ~10 Ma), consistent with timescales from flow deformation studies (e.g., Milliken et al., 2003; Turtle et al., 2001).

The Mars Reconnaissance Orbiter's (MRO's) High Resolution Imaging Science Experiment (HiRISE) camera has captured this particular GLF in PSP_002320_1415 and PSP_3243_1415. Importantly, these images show (at a resolution of ~0.25 m per pixel) several terrain types that are similar to those associated with small-scale and relatively dynamic valley glaciers on Earth. The images therefore present an excellent opportunity to verify and expand on earlier interpretations of GLFs and to investigate this feature's glacial history on the basis of its structure and associated landforms.

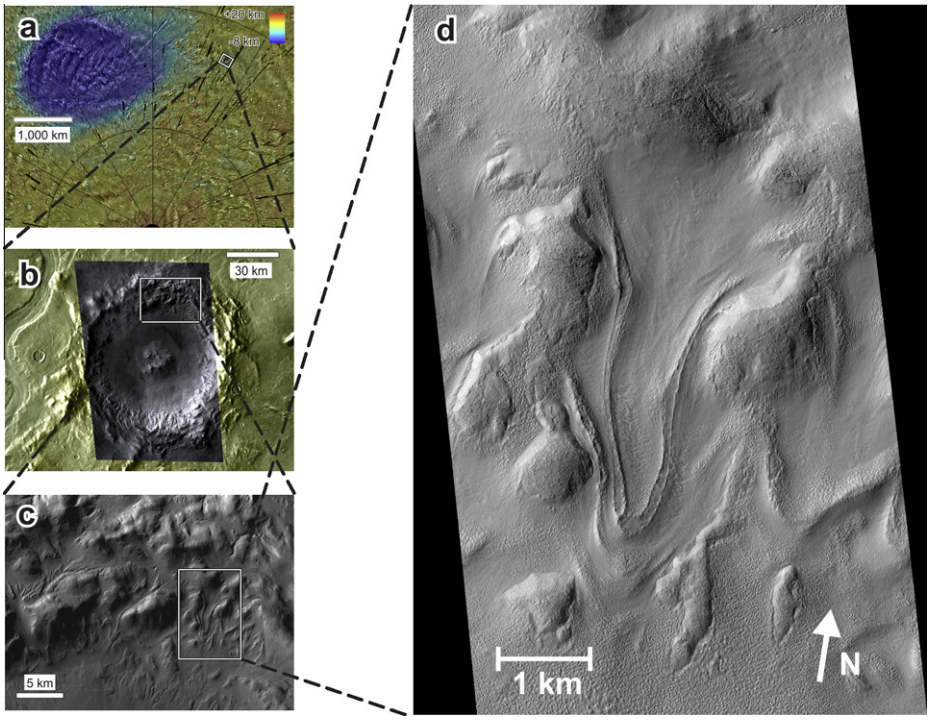

Fig. 1. Location and expansion of the glacier-like form (GLF) investigated herein. (a) Location of the host crater to the east of the Hellas basin illustrated as a MOLA elevation transparency superimposed on a Themis daytime IR mosaic. (b) View of the host crater illustrated as a Context (CTX) image mosaic overlaid on an expansion of (a). (c) Expanded CTX view of the inner northern rim of the host crater wall, illustrating the presence of at least nine GLFs in this vicinity. (d) The GLF investigated herein, illustrated as a section of HiRISE image PSP_002320_1415. The scene is illuminated from the west with the Sun ~23° above the horizon.

2. Methods

In this paper we identify, characterise and map the surface terrain types present on the GLF in PSP_002320_1415 and PSP_3243_1415. Initial terrain identification was carried out by eye and mapping was carried out using the software package ArcGIS. The recording of this GLF in two offset HiRISE images has also allowed us to generate a digital elevation model (DEM) of its surface, permitting characterisation and interpretation on the basis of local relief and slope as well as from planform visual assessment. The DEM was generated using the methods of Kirk et al. (2008). Radiometric calibration, corrections for detector orientation and optical distortions, and mosaicking were carried out using the USGS' Integrated Software for Images and Spectrometers Version 3.0 (Isis 3) software package. We subsequently carried out standard stereogrammetrical techniques using BAE Systems' SOCET SET. Control points distributed across the overlap of the two HiRISE images were used to solve for spacecraft orientation, yielding an RMS discrepancy of ~0.4 pixels (corresponding to a DEM horizontal accuracy of ~0.1 m). However, the minimum attainable horizontal resolution is three HiRISE pixels, so the DEM was gridded at 1 m per pixel. In the vertical, surface elevations were controlled using 202 Mars Orbiter Laser Altimeter (MOLA) data points (125 from individual points and 77 from gridded points). MOLA data have a vertical accuracy of 1 m (Smith et al., 2001), allowing a DEM precision of 0.2 m. Spacecraft jitter unresolved by orientation kernels resulted in slightly larger errors at CCD boundaries, and also in locations where the pixel-matching algorithm was unsuccessful. Such artefacts affected only very local portions of the DEM generated for this study, and were clearly distinguishable on the resulting shaded relief map – allowing their *ad hoc* removal. Thus, no smoothing was performed on any portion of the DEM presented in herein.

3. GLF description

3.1. Physical setting and feature-scale characteristics

The ~4 km long and ~1–2 km wide GLF illustrated in Figs. 1 and 2 is typical of numerous others located on the rim of this particular crater, as revealed by MRO's larger-scale Context Camera (CTX) images (e.g. Fig. 1c). Similar features have also been tentatively identified elsewhere in eastern Hellas (e.g. in CTX image P02_001964_1416_XI_38S247W). Farther afield, a planetary-scale inventory of several thousand CTX images has identified several populations of GLF-like features. These are overwhelmingly located in Mars' mid-latitudes (e.g., Baker et al., 2010). For example, the high-relief areas of Protonilus Mensae and Deuteronilus Mensae feature high numbers of GLFs, often found in association with, or feeding into, larger lobate debris aprons or lineated valley fill (e.g., Morgan et al., 2009). However, as noted earlier by Marchant and Head (2003), these populations tend to cluster into local concentrations, similar to those illustrated in Fig. 1c, implying that correspondingly specific local or regional conditions are required for GLF formation (e.g., Forget et al., 2006) and/or preservation (e.g., Head et al., 2010). Thus, while these features all appear within the mid-latitude dissected mantle terrain (Milliken et al., 2003), which is generally characterised by periglacial surfaces and believed to contain near-surface water ice, they are by no means ubiquitous throughout this terrain type (e.g., Holt et al., 2008; Plaut et al., 2009).

Illustrations of the GLF investigated herein in planform (Fig. 1d) and draped onto its DEM (Fig. 2a) reveal that it extends down-slope at a general angle of ~10° (Fig. 2b) from a broad upper basin to an elongate lower tongue that is enclosed by a sequence of up to four raised bounding ridges. Older and less distinct ridge remnants may additionally be present further from the feature's current basin. In Fig. 3, these ridges are marked onto a geomorphic overlay of the GLF, outlining its prominent features and surface terrains. Interrogation of the DEM indicates that relative relief between the moraines and the GLF surface generally increases down-slope to ~20–30 m towards its terminus (e.g., Fig. 2c). The upper basin grades into the surrounding terrain with no indication of large-scale landscape hollows from which mass could have been eroded by mass-movement processes to supply the lower basin (Fig. 2a). Further, and as reported by Marchant and Head (2003), the surface of the central region of the GLF is characterised by the presence of subdued chevron-type ridges (Fig. 2a), consistent with more rapid surface motion along the GLF's centreline than towards its lateral edges.

Within the innermost bounding moraine, the GLF's surface (Fig. 1d) is of a generally uniform reflectance, similar to the martian surface outside the ridges, indicating ubiquitous debris cover. The inner surface also shows little evidence of wind deflation and/or degradation and is devoid of large impact craters, consistent with larger VFFs identified elsewhere on Mars and calculated to have formed within the last ~0.4 Myr (Head et al., 2003).

3.2. Surface terrain types

The resolution of the HiRISE images has allowed a new assemblage of GLF surface terrain types to be identified and investigated. These terrains contrast markedly with the surface types that predominate outside the immediate vicinity of the GLF. These 'extra-GLF' terrains are dominated by two forms: (i) dust-mantled rocky uplands (Fig. 4a) and (ii) more subdued hilly lowlands (Fig. 4b). Within the GLF's bounding moraines, terrain types change progressively from the feature's headwall to its terminus – commonly grading into each other over distances of some tens to hundreds of metres. We have identified and mapped the distribution of the predominant terrains over the complete surface of the GLF (illustrated in Fig. 3 and summarised in Table 1). Below, we describe these surface terrains sequentially from the head of the GLF to its terminus.

3.2.1. Incised-headwall terrain

Although outside the GLF proper, the feature's upper basin is bounded by a steep (~30°) ribbon of material that is typically some tens of metres wide and covers the equivalent of ~3% of the area of the GLF (Table 1). The headwall is distinctively dissected by multiple, sub-parallel linear troughs that are typically a few metres wide (Fig. 5a) and in all cases aligned parallel to the local slope – even where that local slope changes over some tens of metres. This intensely incised terrain is distinctive from all others identified in the image, including the rocky uplands above it and the surface of the GLF proper below it (Fig. 5a).

3.2.2. Scaly terrain

The uppermost ~36% (Table 1; Fig. 3) of the GLF's basin is composed of tessellating 'scales' that are typically five or six sided and 10–20 m across at their widest point (Fig. 6). Each scale has between one and three raised upslope-facing edges and a body that dips down-slope, resulting in sharply-incised scarps or cracks between adjacent scales. The terrain is gently concave upwards such that its surface slope decreases from $\geqslant 16°$ at the top of its extent to ~12° at its lower margin.

Near the headwalls of the GLF, this scaly terrain is scattered with rounded boulders of lateral dimension $\leqslant$~10 m, the spatial density of which decreases rapidly over a distance of some tens of metres away from the headwall (Fig. 7a). Many of the largest of these

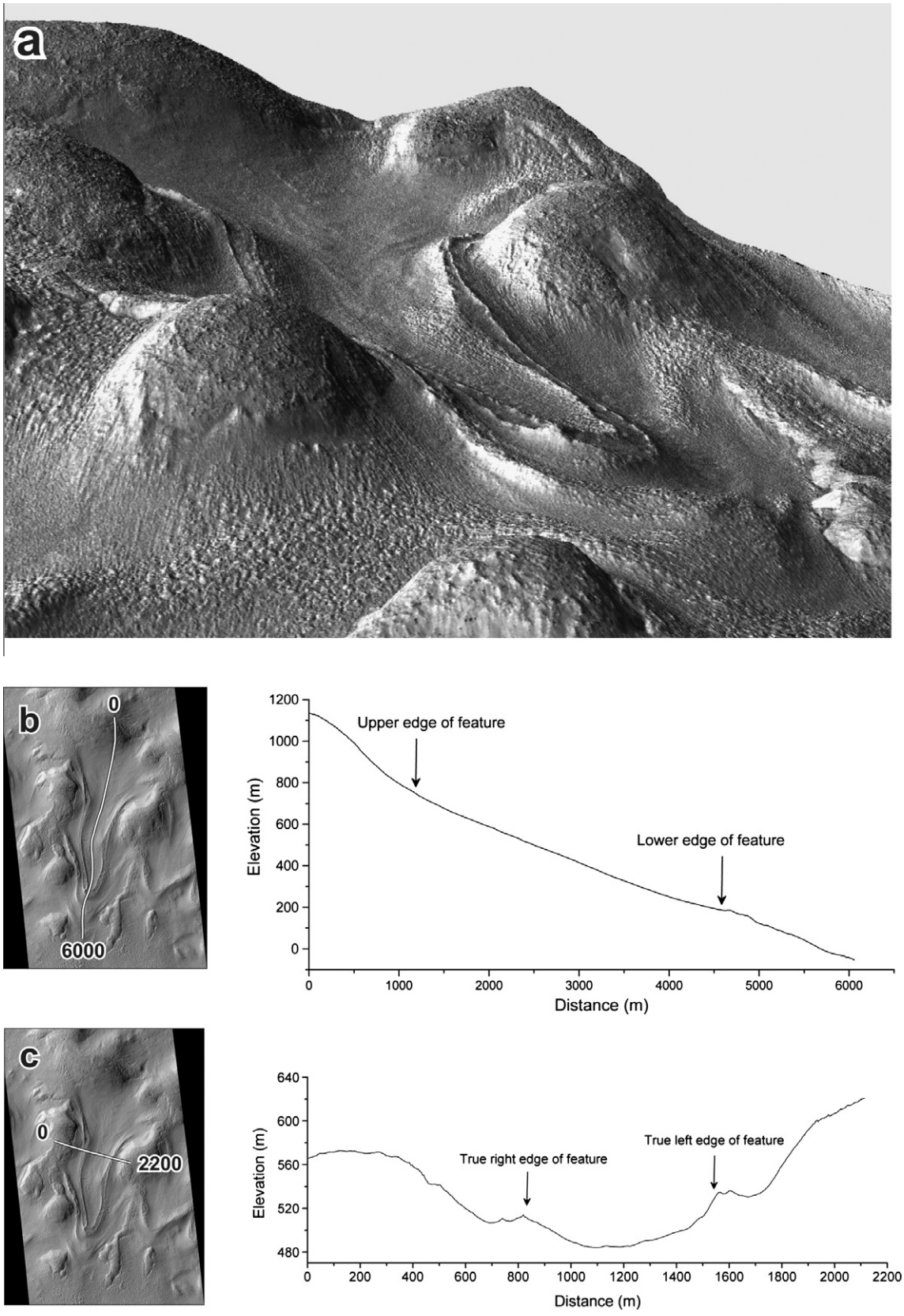

Fig. 2. Three-dimensional representation of the GLF investigated in this study. (a) HiRISE image from Fig. 1d draped over its (6× vertically-exaggerated) surface DEM. (b) Longitudinal profile along the centreline of the GLF. (c) Transverse profile across the GLF. The thumbnails indicate the locations of the transects in Fig. 1d.

boulders are also associated with incised trails that extend upslope from them and which generally narrow to match the width of their associated boulder at the point of contact (Fig. 7b). Trails also become less distinct with distance from the base of the headwall

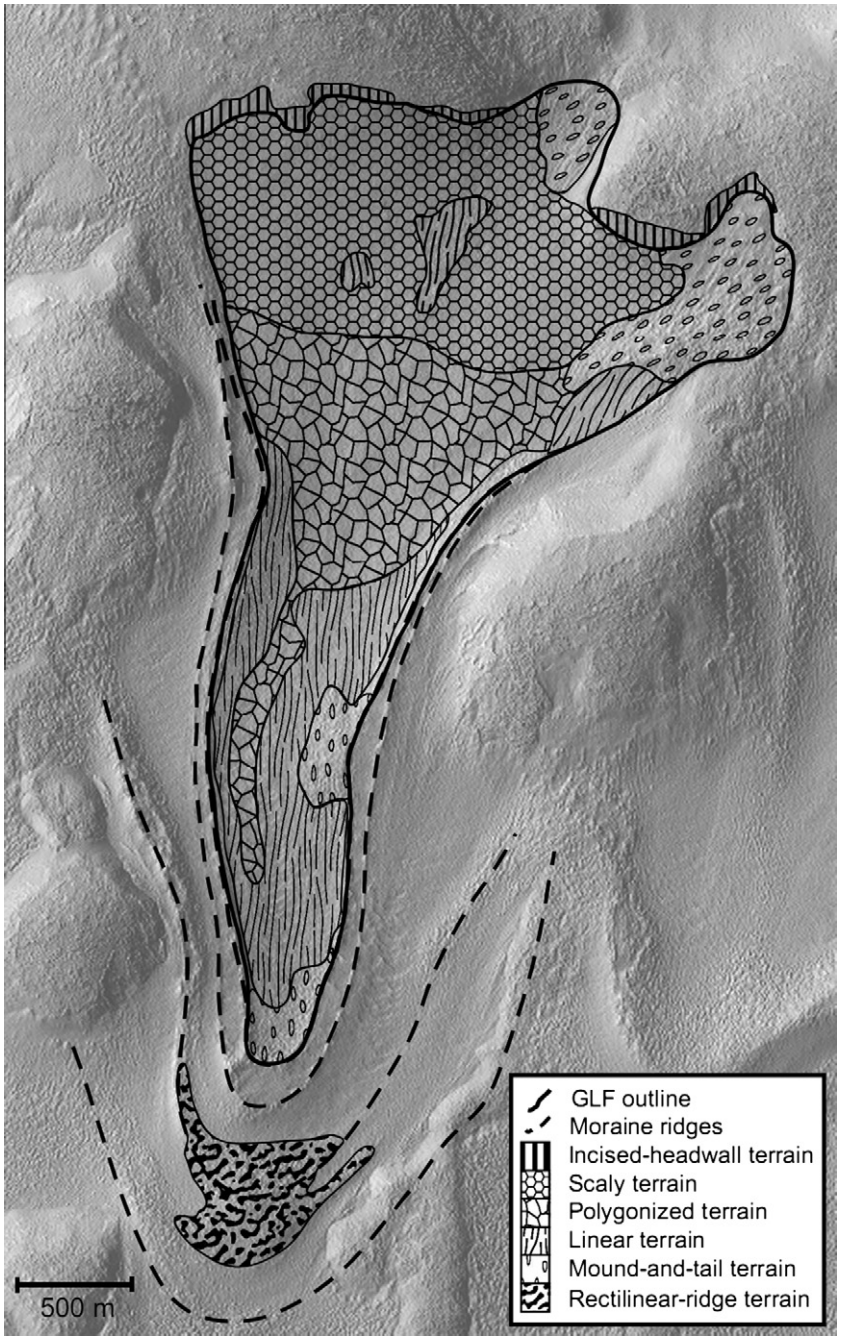

Fig. 3. Geomorphic map of the predominant surface features and terrains overlaid on the HiRISE image from Fig. 1d. Although illustrated here as sharp boundaries, the GLF's surface terrains typically grade into each other over distances of some tens to hundreds of metres.

slope such that there is no evidence of any trails at all beyond ~150 m, despite the presence of several large boulders here.

3.2.3. Polygonized terrain

Progressing down-GLF the scaly terrain merges over a few hundred metres into a terrain of tessellating polygons, each typically 5–10 m across (Fig. 8). This polygonized terrain has a uniform surface slope of ~10° and occupies ~25% of the GLF's surface area (Table 1; Fig. 3), covering much of the lower half of the upper basin and additionally extending as a thin central filament for a further ~1.5 km down-feature. In stark contrast to patterned ground identified elsewhere on Mars, the boundaries of many of this GLF's polygons, particularly further down-feature, are defined by uniformly $\leqslant$~1 m-wide cracks or troughs (Fig. 9a) that are aligned sub-parallel to the local slope (Fig. 9b).

3.2.4. Linear terrain

In the lower half of the GLF, the polygonized terrain gradually merges into a more elongate surface texture (Fig. 10) that accounts for ~22% of the GLF's surface area (Table 1; Fig. 3). The ridges are aligned parallel to the elongation of the GLF, notably bending from NNE–SSW to N–S along the central region of the GLF's tongue (Fig. 11). The ridges are typically some decimetres high (Fig. 10b) and appear to be formed constructively rather than by erosion of the intervening troughs, although some of the surface incisions identified in the polygonized terrain continue for some hundreds

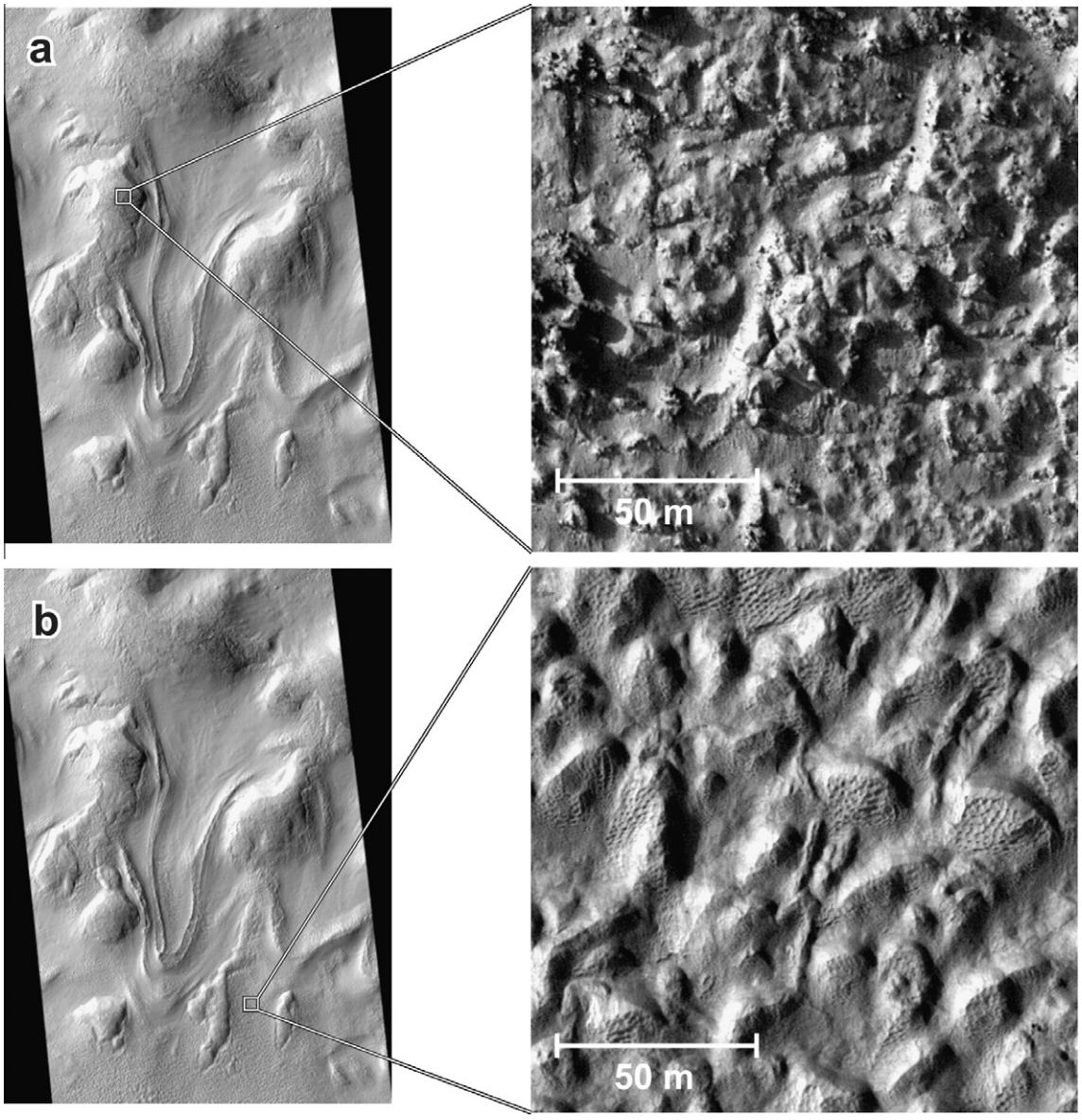

Fig. 4. Typical surface terrain types found outside the GLF investigated in this study. (a) Dust-mantled rocky uplands. (b) Subdued hilly lowlands. Neither of these terrain types is found within the bounding ridges of the GLF under investigation. Note that the ribbon-like feature extending N–S down the centre of (b) is similar to a terrestrial esker, but its interpretation lies outside of the scope of the present investigation. The thumbnails indicate the locations of the expansions in Fig. 1d.

of metres along these troughs. In a few conspicuous cases these channels also cut across the elongate ridges. The width and transverse spacing of the ridges remains constant, at ~5–15 m, throughout this zone. However, the length of individual ridges generally increases, from ~250 m mid-GLF to ~1 km approaching the terminus, yielding elongation ratios (length/width) of ~10–15 and ~100 respectively. Throughout this zone the orientation of the lineations is locally very consistent, being within ~2° of each other, even around the large-scale bend in the GLF. Much of the linear terrain, particularly in up-GLF locations, also exhibits surface cracking although not as strongly as within the polygonized terrain.

3.2.5. Mound-and-tail terrain

The lineations widen and become less distinct as they approach the GLF's terminus, until they break up into a terrain of closely-spaced and elongate mounds, each typically 30–50 m long, 10–30 m across, and 2–4 m high (Fig. 12). These features have a steep upglacier-facing core and a shallow elongate tail. The Hellas Planitia mounds are also geometrically continuous with the lineations that merge into them (Fig. 11), requiring an associated origin. In addition to its occurrence near the GLF's terminus, notable patches of mound-and-tail terrain can also be found elsewhere in the GLF's basin (Fig. 3), in this case above the scaly terrain at the head of the feature and adjacent to the linear terrain along the inside of the GLF's bend. The surface slope of the mound-and-tail terrain is correspondingly variable, from ~8° near the terminus, to ~20° at the head of the GLF. In total, this terrain accounts for ~15% of the surface area of the GLF.

3.2.6. Rectilinear-ridge terrain

Outside the GLF proper, but within its outermost bounding terminal moraine ridge, the surface is composed of a series of ridges, typically of tens of metres across and 2–3 m high (Fig. 13a). These ridges are preferentially elongated in an arc aligned parallel to the GLF's former terminus, covering an area equivalent to ~7% of that of the GLF. Accounting for the general (~4°) dip of this terrain away

Table 1
Summary of the spatial extent and organisation of the surface terrain types characterising the Hellas Planitia GLF investigated in this study. Slopes are averages calculated parallel to the alignment of the GLF.

Feature/terrain type	Area		Slope (°)	Notes
	(km^2)	(%)[a]		
Complete GLF	4.69	100	10	Entire feature excluding incised-headwall terrain and rectilinear-ridge terrain
Scaly terrain	1.67	36	12–16	Present over most of the GLF's upper basin. The scaly terrain's lower boundary merges over ~500 m into the polygonized terrain
Polygonized terrain	1.16	25	10	Present down-GLF of the scaly terrain. The polygonized terrain's lower boundary extends as a thin tongue, and merges over ~500 m, into the linear terrain
Linear terrain	1.03	22	8–12	Predominantly present over most of the GLF's laterally-confined lower tongue. Lineations bend NNE–SSW to N–S, following the GLF's overall shape. Two patches of linear terrain are also present in the GLF's upper basin, bounded by scaly terrain. The lower boundary of the linear terrain merges over ~200 m into the mound-and-tail terrain
Mound-and-tail terrain	0.71	15	8–20	Predominantly present within ~500 m of the terminus of the GLF. Individual forms are aligned parallel to the lineations that merge into them. This area of mound-and-tail terrain terminates abruptly at the innermost bounding latero-terminal moraine. Three less distinctive areas of mound-and-tail terrain are present elsewhere in the basin: one on the true left flank of the GLF's tongue and the other two in the uppermost NE corner of the GLF's basin. These exposures include a range of slopes, depending on location
Incised-headwall terrain	0.14	(3)	30	Present as a narrow ribbon along the headwall of the GLF. The terrain is formed from unconsolidated material that is incised by numerous slope–parallel troughs that terminate abruptly upon intersecting the scaly terrain of the GLF proper
Rectilinear-ridge terrain	0.31	(7)	4	Present inside the outermost arcuate terminal moraine ridge in the forefield of the GLF. The terrain's boundaries merge over some tens of metres into the surrounding extraglacial lowland terrain

[a] Expressed as a percentage of the area of the complete GLF. Percentages in brackets relate to terrain types located outside the GLF proper.

from the GLF, individual ridges are characterised by steep (~12–15°), rectilinear proximal slopes and shallower (~4–8°) and less uniform distal slopes (Fig. 13b).

4. GLF interpretation

4.1. Physical setting and feature-scale characteristics

The GLF's basin-scale characteristics strongly indicate that the feature is the close martian equivalent of a valley glacier, currently either active or relict, comprising an open upland accumulation basin feeding mass to an enclosed lowland tongue. The absence of a notable supply hollow above the basin suggests that the original mass that formed the GLF was largely supplied from the atmosphere or from within the surrounding ground. The latter interpretation is consistent with the geologically-recent release of ice or water from the near-surface of the dissected mantle terrain. Further, the chevron-type ridges present in the middle of the GLF (Fig. 2a) indicate laterally-compressive ductile flow in this zone where its two contributing basins merge. However, in the absence of local mass-balance information it cannot be stated whether mass has been preferentially lost from the lower basin (as is generally the case on Earth), or whether mass has been lost from the entirety of the feature following an earlier phase of accumulation. Figs. 1–3 reveal that at least two of the GLF's bounding ridges extend for >2 km up its lateral margins, strongly indicating that they are not folds or faults associated with tectonic compression. Visually-similar assemblages of bounding latero-terminal moraine ridges are common around debris-transporting glaciers that have recently receded on Earth (e.g., Glasser and Hambrey, 2002; Kruger, 1993). Specifically, each such moraine on Earth indicates the position of either a temporary glacier readvance or a still-stand during a prolonged period of more general recession, reflecting changes in mass balance driven by a corresponding variability in local temperature and/or accumulation (Benn and Evans, 2010). However, about one in 20 glaciers on Earth can advance and retreat periodically (and independently of climatic changes) as a response to internal instabilities that manifest themselves as surge-type behaviour (e.g., Raymond, 1987). The Hellas Planitia GLF shows none of the geomorphic characteristics associated with (terrestrial) surge-type glaciers (e.g., Sharp, 1988), and we do not therefore interpret it as such.

These terrestrial comparisons and mass-balance inferences support and strengthen the conclusions of previous researchers in attributing a fundamentally glacial origin to this feature. We therefore believe that this particular feature can justifiably be referred to as a 'glacier-like form' (GLF), even though it may now be partly or wholly relict and have more in common with a terrestrial rock glacier than a terrestrial (ice-dominated) glacier.

4.2. Surface terrain types

Below, we interpret the GLF's surface terrains, progressing sequentially down-GLF from its head to its terminus.

4.2.1. Incised-headwall terrain

The tens of metres wide ribbon of unconsolidated material bounding the upper margins of the GLF is very similar to ice-marginal moraines on Earth (Fig. 5c), interpreted to have been deposited during progressive recession since the time of maximum recent glacial extent (generally the Little Ice Age; Grove, 1988). This origin is also supported by the relatively sharp boundary between the incised-headwall terrain and the higher-elevation rocky upland terrain (Fig. 5a).

The apparently fresh, slope–parallel troughs in the incised-headwall terrain could result from one or more of several sets of processes, including mass movement (rock-fall), aeolian erosion and fluvial erosion. Formation by dry rock-fall alone is considered unlikely on account of the scale and sharpness of the incisions. The regular spacing of the incisions also suggests that fluid erosion exerts a primary control over their formation. Considering erosion by air and liquid water as the only realistic alternatives, two factors suggest that the latter predominates. First, unconsolidated lateral moraines formed since the Little Ice Age on Earth are commonly scored by similar partially or wholly fluvially-eroded gullies (Fig. 5c). These terrestrial gullies have a similar spacing to the incisions we report on the martian GLF and they are similarly short and straight. Second, the GLF's headwall incisions appear in all instances to run perpendicular to the local slope – changing with slope along the upper boundary of the GLF. While it is clear that water would be expected to behave in this manner it is by no means likely that wind direction could change so consistently at such a local scale. Thus, while we cannot be sure that these incisions are fluvial in origin (and the processes operating to maintain

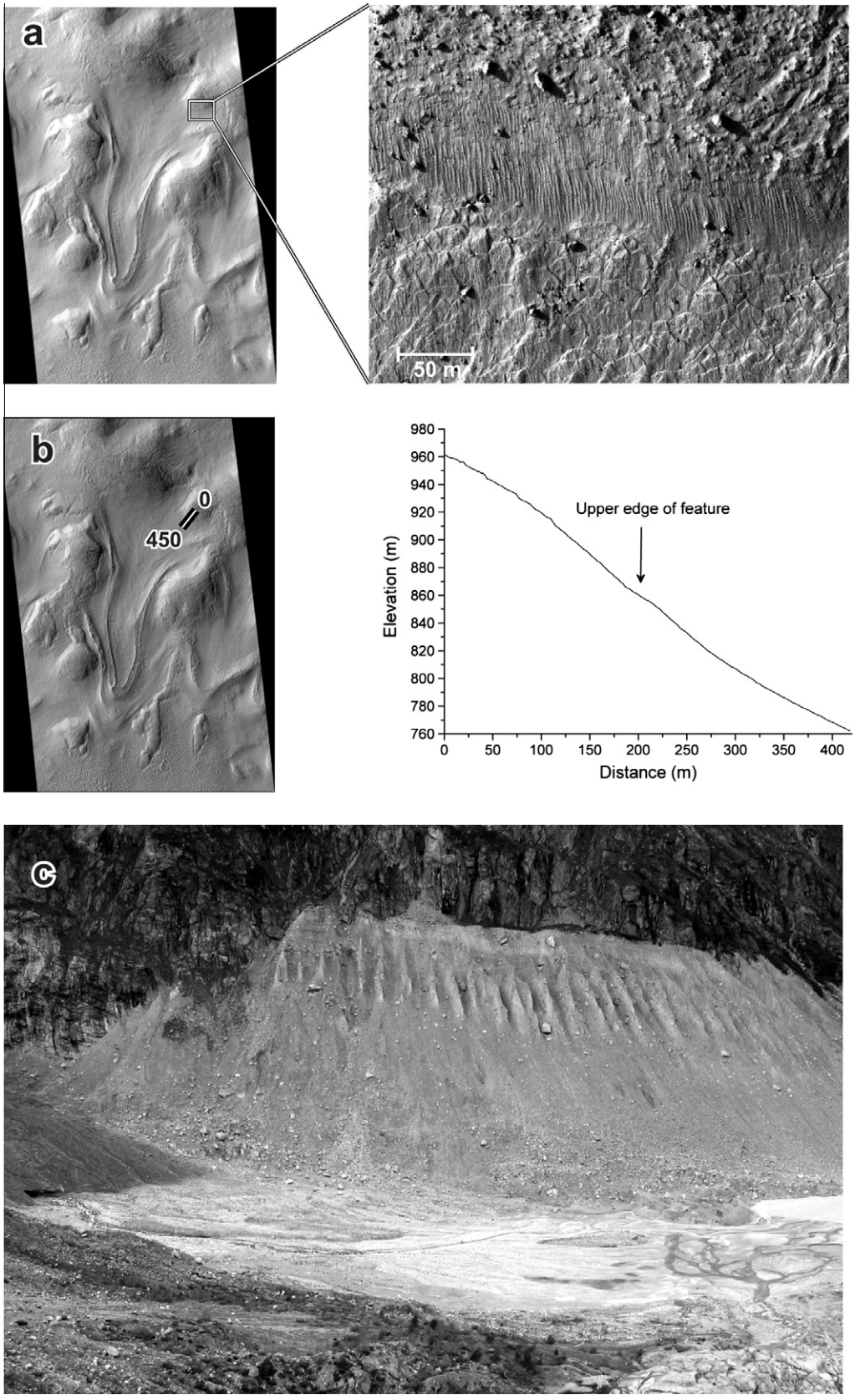

Fig. 5. Incised-headwall terrain. (a) Expanded HiRISE image of slope–parallel incisions located on the headwall of the martian GLF investigated in this study. (b) Longitudinal profile extending from the rocky upland, through the incised-headwall terrain and onto the head of the GLF. The thumbnails indicate the locations of the expansion and surface profile in Fig. 1d. (c) Oblique photograph of fluvial gullies incised into a remnant terrestrial lateral moraine (middle foreground), Glacier de Ferpècle, Switzerland. The current glacier terminus is visible in the middle left side of the image. The gullied moraine is ~50 m high and individual gullies are straight and typically some metres across, similar in form and scale to the incisions in (a). Photograph by Bryn Hubbard.

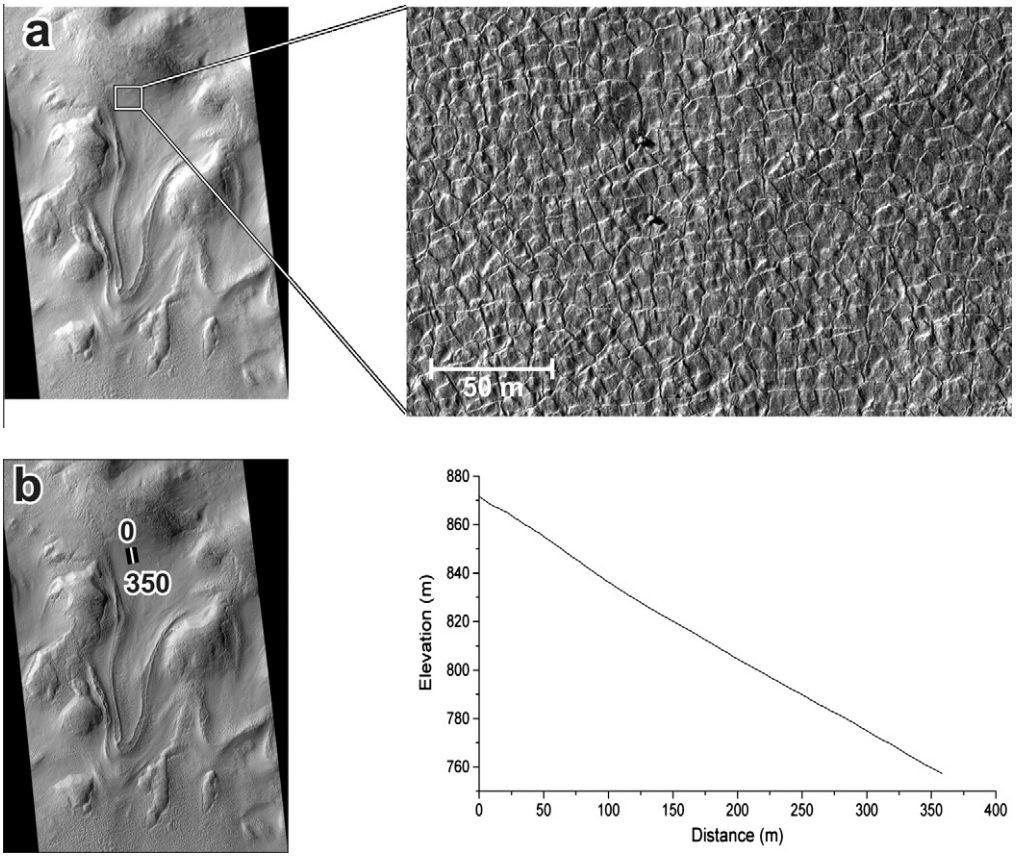

Fig. 6. Scaly terrain. (a) Expanded HiRISE image illustrating scaly terrain located in the uppermost reaches of the martian GLF investigated in this study. Note the presence of two boulders in the centre of the image. (b) Longitudinal profile along a region of scaly terrain. The thumbnails indicate the locations of the expansion and surface profile in Fig. 1d.

them are almost certainly not *exclusively* fluvial), we believe our evidence is more consistent with a fluvial origin than with a solely mass movement or aeolian one.

The well-preserved state of the troughs that characterise the incised-headwall terrain suggests that they were formed in the recent past. Assuming a fluvial origin for these incisions (above), it is quite possible that a geologically-recent source for such water could be near-surface ice (Costard et al., 2002) or surface snow (Christensen, 2006; Clow, 1987). This interpretation is consistent with that made for similar, but generally larger scale, features identified on Mars by, for example, Milliken et al. (2003) and Arfstrom and Hartmann (2005) who associated geologically recent (within the past few million years) gullying with VFFs. More recently, Dickson and Head (2009) presented a broad review of martian gullies and similarly concluded that many of the freshest forms are incised by meltwater generated from near-surface ice emplaced during the most recent high-obliquity cycles. Although these authors could not place an upper age on active gullying, they conclude from gully morphology and the age of gullied materials (e.g., Schon et al., 2009) that the process has probably occurred during the last ~1.25 Myr. Earlier, Malin et al. (2006) tentatively identified gullying within the past decade on the basis of repeat images of two small crater-wall channels (in Terra Sirenium and Centauri Montes), although in neither case could the erosional process involved be definitively identified as fluvial.

4.2.2. Scaly terrain

These cuesta-like shapes are generally similar to thermally cracked periglacial surfaces found on Earth and elsewhere on Mars, although smaller than martian examples hitherto reported (on the basis of generally coarser imagery) (e.g., Mangold, 2005; Mellon, 1997; Mellon et al., 2008). The longitudinal asymmetry in the surface slope of the scales on the Hellas Planitia GLF possibly reflects the additional influence of the ductile deformation of the underlying material in a down-slope direction. If the underlying material were ductile then deformation is most likely in this region of the GLF since the surface slope is steepest here (~12–16°). Like the headwall incisions, this scaly terrain is fresh in appearance, similarly indicating geologically recent (or current) formation or modification.

The roundness, location and spatial density of boulders located on the surface of the scaly terrain indicate that they have rolled off the headwall slope and come to a halt on the lower-angled surface of the GLF proper. Accepting this explanation, the location, orientation and width of the troughs extending up-GLF from the boulders indicate that the rolling motion of larger boulders is able to incise the surface of the scaly terrain to a depth of a few decimetres. We therefore infer that the surface of the scaly terrain is formed of unconsolidated material to a depth of some decimetres, and that it is probably consolidated, and possibly ductile, below this.

4.2.3. Polygonized terrain

The polygonized terrain is similar to periglacial patterned ground identified on both Earth and elsewhere within the dissected mantle terrain on Mars (e.g., Mangold, 2005). This terrain therefore probably represents a lower-angle (~10°) equivalent of the scaly terrain, both being formed by periglacial processes, including frost heave and contraction cracking (French, 2007).

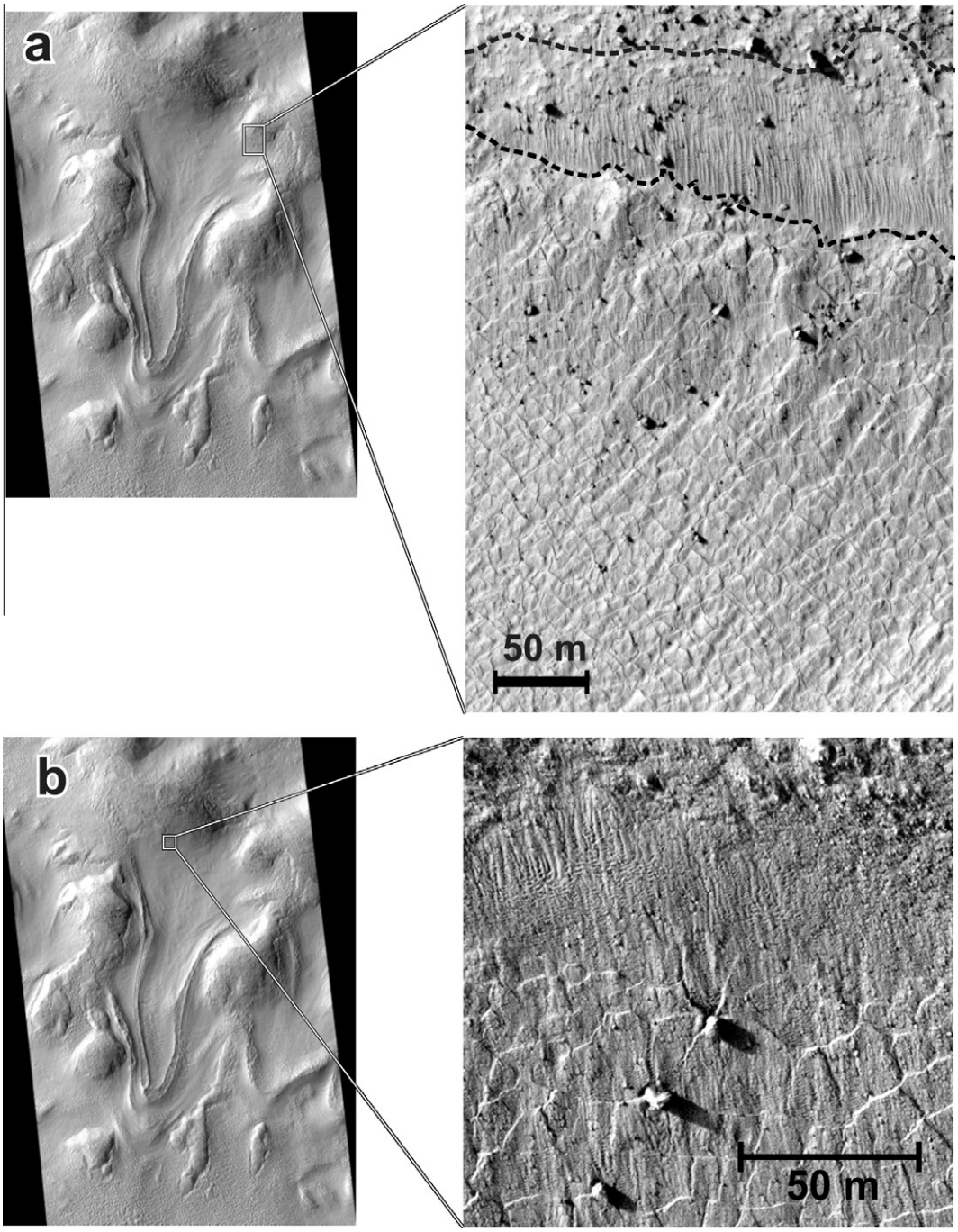

Fig. 7. Expanded HiRISE images of boulders at and below the contact between the incised-headwall terrain and the scaly terrain of the martian GLF investigated in this study. (a) Overview of surface boulders and the three terrains (demarcated by superimposed dashed lines: rocky uplands [top], incised-headwall terrain [centre-top], and scaly terrain [bottom]). Note the decrease in the spatial density of boulders down-GLF of the contact between the incised-headwall terrain and the scaly terrain. (b) Detail illustrating the presence of wide and shallow incised trails extending upslope of boulders lodged in the scaly terrain. The thumbnails indicate the locations of the expansions in Fig. 1d.

While the (approximately) radially-symmetrical cracking that characterises the scaly terrain and the polygonized terrain can be readily explained by periglacial processes, the joining up of these cracks to form extended, slope–parallel segments is more challenging to explain. These distinctive segments do not appear to have a direct analogue either on Earth or elsewhere on Mars. However, Levy et al. (2009) recently compared several instances of freshly-gullied polygonized terrain on Mars with terrestrial analogues from the Antarctic Dry Valleys. These authors concluded that, on Earth, such gullies appear to form from the 'top down' melting of residual snow deposited in incipient cracks and proto-gullies. In the absence of evidence to the contrary, the authors extended this model to the martian features. It is tempting to draw a similar conclusion for the extended incisions we observe in the polygonized terrain on the GLF investigated herein. However, any explanation would also need to account for the relatively short reach of individual incised segments, the absence of a coherent network of segments and the lateral passage of incisions across raised lineations. Such an investigation would require detailed study of these features, possibly including a range of GLFs, and lies beyond the scope of this paper.

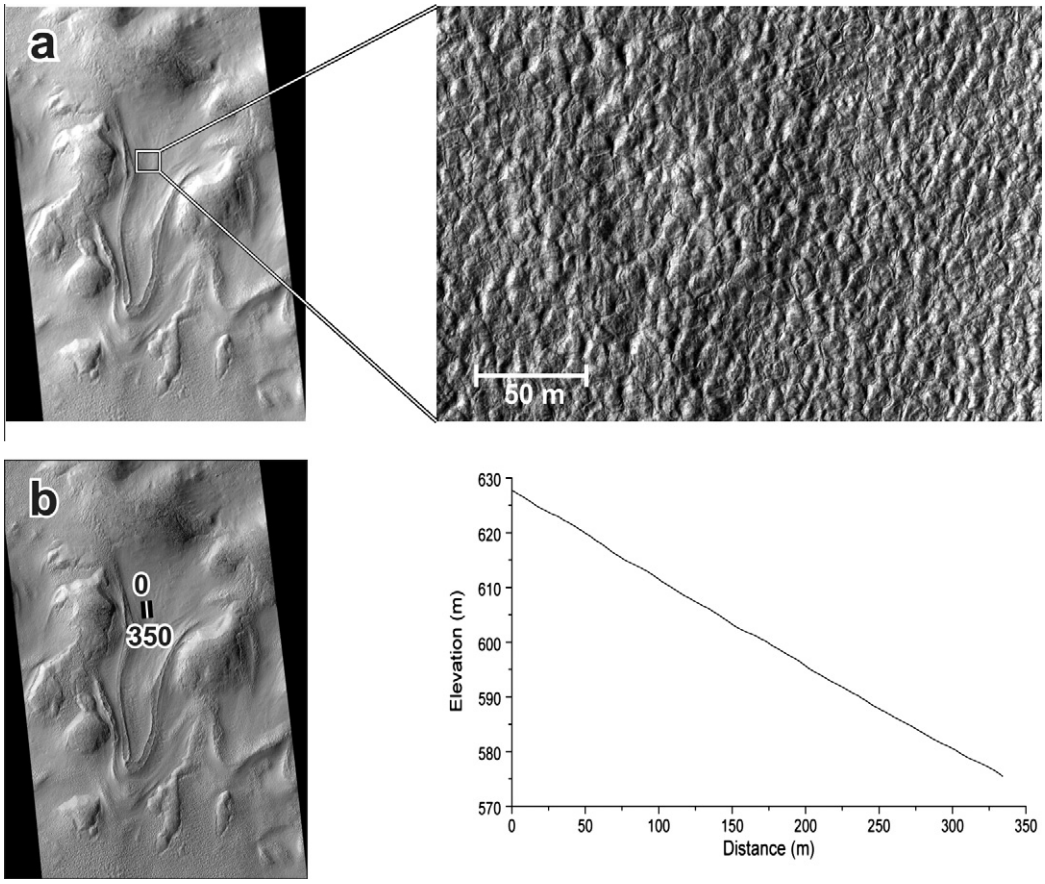

Fig. 8. Polygonized terrain. (a) Expanded HiRISE image illustrating polygonized terrain located in the upper and middle reaches of the martian GLF investigated in this study. (b) Longitudinal profile along a region of polygonized terrain. The thumbnails indicate the locations of the expansion and surface profile in Fig. 1d.

4.2.4. Linear terrain

The linear terrain appears to be broadly similar to three glacier-related features on Earth: (a) supraglacial medial moraines (formed from debris derived from upglacier point sources, or the coalescence of common lateral moraines where tributaries feed into compound glacier basins); (b) supraglacial longitudinal foliation (formed by the differential erosion of layers of ice of differing crystallographic and included bubble compositions); and (c) elongate subglacial bedforms (formed as a result of the interaction of the base of a glacier with its underlying sedimentary substrate). Since the Hellas Planitia GLF basin is geometrically simple with no notable point sources, and the lineations extend across the full width of the feature, these lineations are not interpreted as supraglacial medial moraines. Further, Figs. 10 and 11 reveal three geometrical characteristics of these lineations that mitigate against formation as supraglacial longitudinal ice foliation. First, where an individual lineation terminates upglacier of another, the two are commonly offset laterally. This contrasts with supraglacial longitudinal foliation, which is characterised by a high degree of longitudinal coherence, reflecting their deformation-related evolution. Second, the Hellas Planitia lineations are both wider and more widely-spaced than terrestrial equivalents (both typically decimetres to metres). Third, the lineations on the Hellas Planitia GLF pinch-out towards the terminus, in contrast to terrestrial longitudinal foliation which persists, or is enhanced, longitudinally. We therefore interpret these lineations not as supraglacial features but as elongate subglacial bedforms. Their large scale and absence of boulders marking their up-flow end indicates that they are not flutes. Instead, their spatial coherence, morphometry and fidelity to the flow direction of the GLF (including bending with it along the tongue) indicate that these features are most closely related to (although they are typically shorter than) glacial *megalineations* on Earth (e.g., Clark and Stokes, 2001). Terrestrial megalineations are generally related to fast ice flow which is, in turn, explained by ice-bed lubrication in the presence of basal meltwater (Clark, 1994).

Thus, while we cannot be sure that the lineations on the Hellas Planitia GLF are the small-scale martian equivalent of terrestrial megalineations, they appear to be more similar to these than to alternative terrestrial analogues. If these lineations are martian subglacial bedforms then this strongly implies water-lubricated ice flow at the time of their formation, which (since they extend right to the base of the GLF's lateral moraines) was probably at the GLF's maximum recent extent.

4.2.5. Mound-and-tail terrain

As far as we are aware there is no direct martian or Earth equivalent to the mound-and-tail terrain (Fig. 12). The closest terrestrial equivalents are drumlins, but the scale of the mounds on the Hellas Planitia GLF is several times smaller than that of typical drumlins on Earth. In an analysis of approaching 60,000 terrestrial drumlins, Clark et al. (2009) identified a modal length of 393–441 m and a modal width 173–183 m, while the GLF's mound-and-tail features are typically an order of magnitude smaller than this. Nevertheless, both terrestrial drumlins and the mounds on the surface of the Hellas Planitia GLF have similar shapes, with elongation ratios typically in the range 2.0–2.3. It is also worth noting that the smallest drumlins identified by Clark et al. (2009) were limited by the 5 m spatial resolution of their analysis.

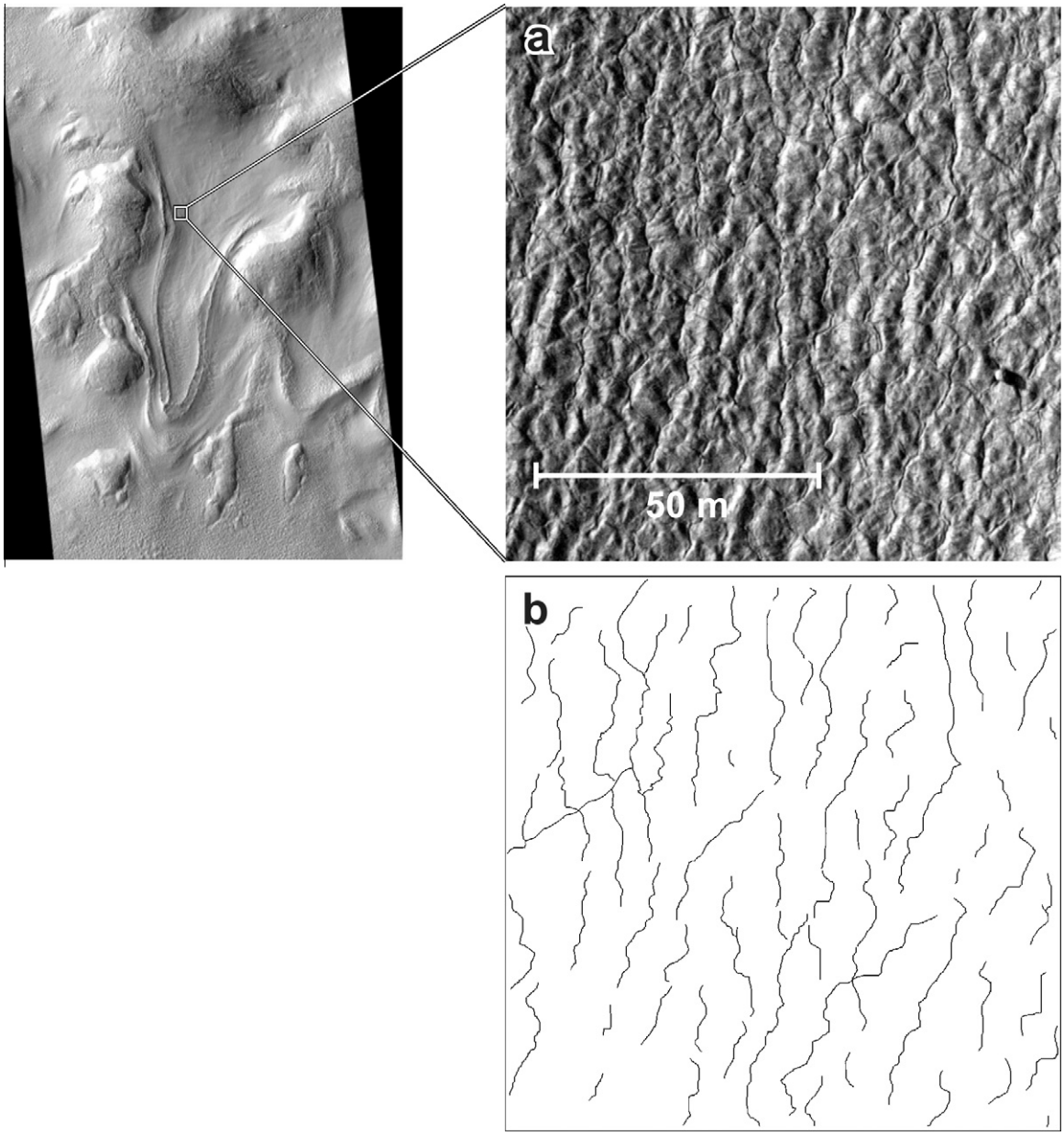

Fig. 9. Extended surface incisions. (a) Expanded HiRISE image illustrating approximately slope–parallel incisions at the boundaries of individual polygons within the polygonized terrain located on the martian GLF investigated in this study. The thumbnail indicates the location of the expansion in Fig. 1d. (b) Trace of the surface incisions illustrated in (a).

It is also important to consider that the GLF's mound-and-tail terrain is geometrically and morphologically continuous with the lineations that merge into them (Fig. 11), requiring an associated origin. Thus, although tentative, the most likely origin consistent with the evidence presented above is that both the lineations and the mound-and-tail forms are streamlined glacial bedforms – the former approximating megalineations and the latter drumlins (but both at a smaller scale than is typical on Earth). On Earth, such elongate bedforms are formed by subglacial sediment moulding and/or deposition beneath wet-based ice masses (Clark, 1994; Menzies, 1979). More specifically, terrestrial drumlins are almost exclusively associated with (a) high pore-water pressures within water-saturated subglacial sediments, and (b) strong longitudinal compression. Both of these conditions are met in the wet-based zone located immediately upglacier of the frozen margin of polythermal glaciers (Patterson and Hooke, 1995).

4.2.6. Rectilinear-ridge terrain

The rectilinear-ridge terrain (Fig. 13a) is similar in shape and appearance to two proglacial moraines on Earth: thrust-block (or push) moraines (Andrews, 1975) and moraine-mound complexes (Hambrey et al., 1997). Thrust-block moraines are formed by the transfer of stress in front of an advancing glacier, resulting in an *en echelon* arrangement of thrust plates that are aligned parallel to the advancing glacier margin and are most effectively (but not exclusively) created in front of frozen glacier margins. Thrust-block moraines are typically tens to hundreds of metres long and metres to tens of metres high, and are commonly characterised by preserved sedimentary structures and low-angle faults (e.g., Fitzsimons, 1997). The rectilinear ridges in front of the Hellas Planitia GLF are orientated similar to thrust-block plates, but they are smaller, being typically only some metres to tens of metres long and some metres high. In contrast, terrestrial moraine mounds are smaller,

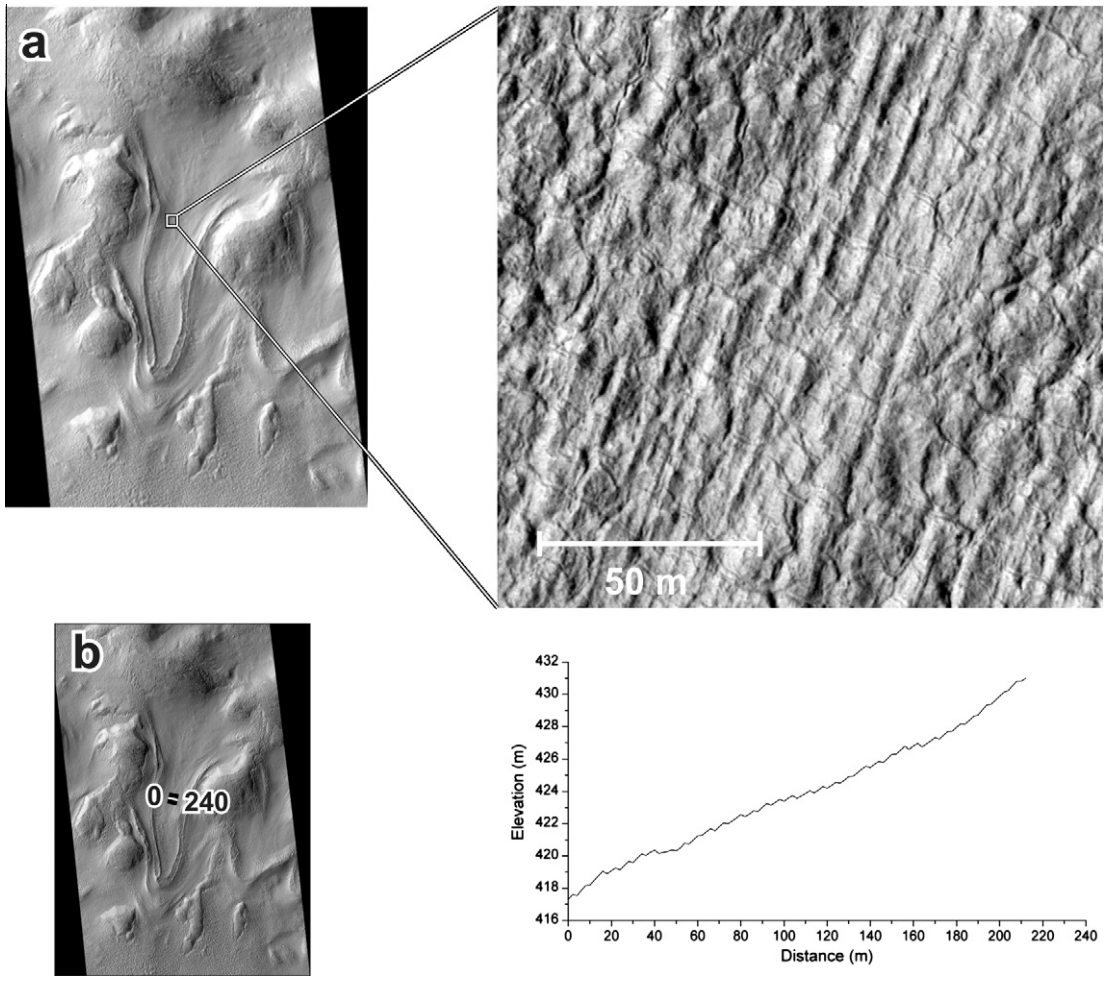

Fig. 10. Linear terrain. (a) Expanded HiRISE image illustrating linear terrain located in the middle and lower reaches of the martian GLF investigated in this study. (b) Transverse profile across a region of linear terrain. Note the regular roughness of the profile as it crosses individual lineations, each some decimetres high. The thumbnails indicate the locations of the expansion and surface profile in Fig. 1d.

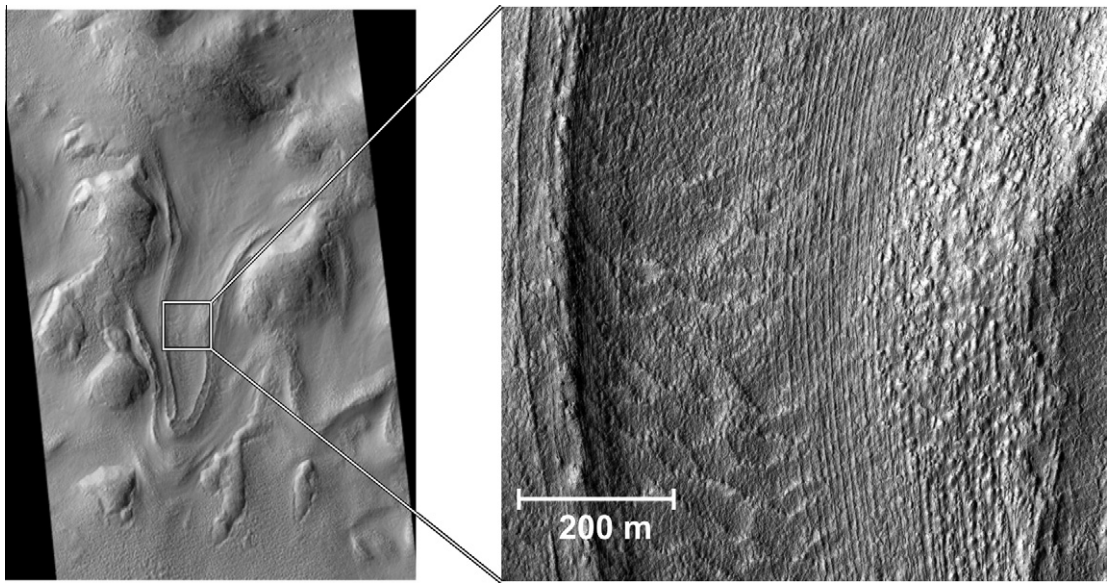

Fig. 11. Expanded HiRISE image illustrating the conformable bend in the linear terrain as it follows the bend in the GLF's tongue from a NNE–SSW orientation (upper image) to a N–S orientation (lower image). Note the geometrical and morphological continuity of the lineations and the mound-and-tail forms in the centre left of the image. The thumbnail indicates the location of the expansion in Fig. 1d.

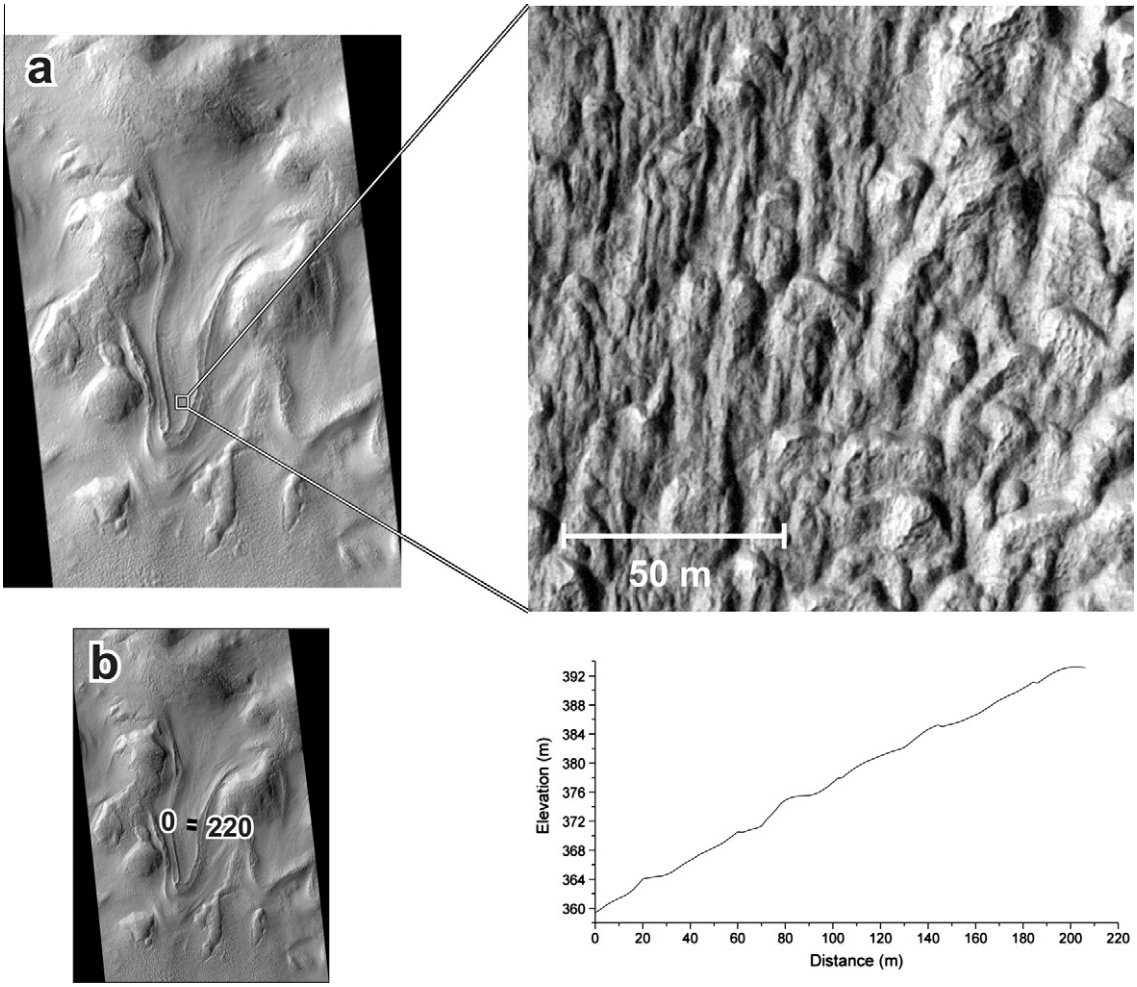

Fig. 12. Mound-and-tail terrain. (a) Expanded HiRISE image illustrating mound-and-tail terrain located predominantly near the terminus of the martian GLF investigated in this study. (b) Transverse profile across a region of mound-and-tail terrain. Note the subdued roughness elements in the profile as it crosses individual mounds, each a few metres high. The thumbnails indicate the locations of the expansion and surface profile in Fig. 1d.

and of a less regular geometrical configuration, than thrust-block moraines (Fig. 13c) – both more consistent with the Hellas Planitia GLF ridges. The possible origins of terrestrial moraine-mound complexes are disputed, but three contender processes – all involving the presence of liquid water – have been proposed: (a) as basal debris thrust up from the glacier bed (Hambrey et al., 1997), (b) as basal crevasse fills (Sharp, 1985), or (c) as ice-contact outwash deposits (Lukas, 2005).

Detailed sedimentological investigations would be required to identify definitively whether the Hellas Planitia rectilinear-ridge terrain is a thrust-block moraine or a moraine-mound complex (or some other, as yet unidentified, form). If it is a thrust-block moraine, then the ridges could have formed under any glacial thermal regime. However, the widespread extent of the terrain is more compatible with cold marginal ice than with warm marginal ice – signifying cold-based or polythermal glacial conditions. If the GLF's ridges are moraine mounds then they probably formed in the presence of warm ice – signifying wet-based or polythermal glacial conditions.

5. Synthesis and conclusions

5.1. Overview

Our detailed interpretation of one of several GLFs located in this region of eastern Hellas Planitia reinforces the existing general interpretation that mid- or low-latitude debris-rich GLFs on Mars have undergone geologically-recent glacial deformation (Head et al., 2003; Milkovich et al., 2006; Milliken et al., 2003). The lowering of this particular flow feature by up to some tens of metres relative to its bounding moraines, allied to the paucity of craters on its surface, indicates dramatic mass loss over the past 10^5–10^6 years. The nested sequence of at least four latero-terminal moraines bounding the feature implies, in the absence of evidence for any internal instability (such as surge-type activity), cyclical or punctuated variations in the processes that have controlled that mass loss.

5.2. GLF surface terrains

Four surface terrain types have been identified within the GLF's bounding moraines. These are, in order extending from the head of the feature to its terminus, scaly terrain (covering ~36% of the GLF's area), polygonized terrain (~25%), linear terrain (~22%), and mound-and-tail terrain (~15%). The remaining ~2% of the GLF's area is composed of indistinguishable sections of the inner slope of its bounding lateral moraine. In the upper basin, the scaly and polygonized terrains are characteristic of periglacial surface forms on Earth, with the former additionally suggesting substrate deformation. In the lower basin, the linear and mound-and-tail terrains are tentatively interpreted as elongate glacier-related bedforms which, if correct, implies water-lubricated basal motion

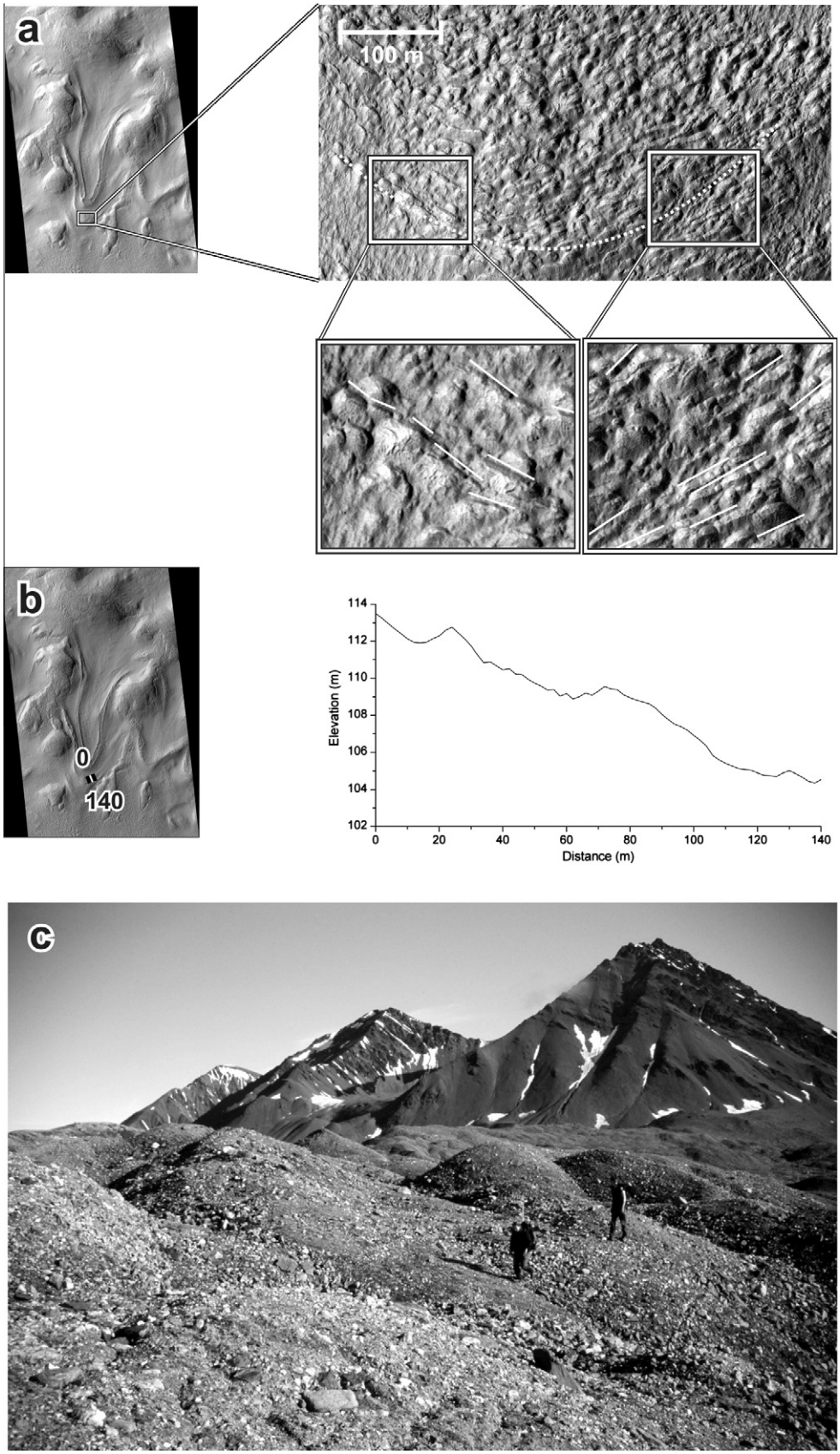

Fig. 13. Rectilinear-ridge terrain. (a) Expanded image (with two further expansions) of rectilinear-ridge terrain located within the outermost bounding ridge of the martian GLF investigated in this study. Individual rectilinear ridge elements are demarcated by superimposed white lines. (b) Longitudinal profile along a region of rectilinear-ridge terrain. The thumbnails indicate the locations of the expansion and surface profile in Fig. 1d. (c) Morphometrically-similar, terrestrial rectilinear moraine mounds located in the forefield of polythermal Austre Lovénbreen, Svalbard. Moraine-mound ridges are aligned parallel to the direction of the photograph, with the upglacier-facing rectilinear faces dipping to the right. Note figures in centre-right for scale. Photograph supplied courtesy M.J. Hambrey.

at the time of their formation. Patches of both linear and mound-and-tail terrain also occur sporadically in the GLF's upper basin.

5.3. Feature-scale interpretation

The surface terrain interpretations presented above are most consistent with a basin from which the (former) glacier has receded completely from its lower reaches (now leaving only exposed bedforms), while glacial material still exists in a degraded state (as dust-covered scaly and polygonized terrains) in the upper basin. This interpretation, however, must be tempered with the understanding that none of these terrains is dated – and they could be currently forming or relict. The images we interpret above also represent only a snapshot of a form that has doubtlessly experienced change, the rate of which remains unknown. Nonetheless, this situation – whereby active ice now occupies only the upper reaches of this GLF's former basin – is similar to almost all present-day glaciers on Earth (e.g., Benn et al., 2005). The presence of exposed bedform patches protruding through the superimposed scaly and/or polygonized terrain in the GLF's upper basin is consistent with this interpretation.

While we lack sufficient information to differentiate confidently between the physical properties of the recently or currently 'active' material in the upper basin and those of the 'residual bed material' in the lower basin, some tentative suggestions may be proposed on the basis of the descriptions and interpretations presented above. First, the surface terrains of the upper basin are sharper and 'fresher' looking than those of the lower basin. This suggests that the upper-basin scales and polygons are currently being formed or maintained, while the lower-basin lineations and mound-and-tail forms may have formed less sharply and/or are no longer being maintained in their original state in the face of current degradation at the martian surface. Indeed, the lineations appear to have been subjected to periglacial cracking since their formation. Second, boulder trails indicate that the surface of the scaly terrain (at least) appears to be formed from a decimetres-thick layer of unconsolidated sediment, possibly underlain by a more solid substrate. Third, the fine scale of the slope–parallel tilting of individual scales in the upper basin suggests that the underlying substrate is actively deforming, or at least deformed, up until the very recent past. All three of these interpretations are consistent with the upper basin being composed of a decimetres-thick mantle of unconsolidated surface dust overlying massive and recently-deformed and/or currently deforming (likely dust-rich) ice. This interpretation would also be consistent with recent radar-based evidence from MRO indicating the presence of near-surface ice within martian mid-latitude lobate debris aprons (e.g., Holt et al., 2008; Plaut et al., 2009). In contrast, the lower basin is characterised by more rounded and less fresh-looking glacial bedforms that show no evidence of recent erosion or deformation. This evidence is consistent with the lower basin material being formed from frozen ground in the absence of a massive, deforming layer of near-surface ice.

5.4. Implications for the thermal regime of GLFs

Two terrain types located in the GLF's lower basin (the linear terrain and mound-and-tail terrain) and one located within its frontal bounding moraines (rectilinear-ridge terrain) are consistent with formation or modification under partially wet-based glacial conditions, probably when the GLF was at its most recent maximum extent. Although alternative mechanisms of formation are possible for these terrains and further investigation is clearly needed, if polythermal conditions did exist in the geologically-recent past then it has important implications for modelling motion processes and interpreting the landform record at similar martian GLFs. In terms of the former, models of GLF motion may need to incorporate lubricated basal motion. In terms of the latter, landscape interpretation may need to account for streamlined depositional bedforms, sliding-related glacial erosion, and perhaps the products of subglacial drainage. While no erosional or drainage-related features have been identified by the present study, erosional grooves have been identified elsewhere on Mars and a broader investigation may now be timely. This could extend to larger martian VFFs which have previously been interpreted as ubiquitously cold-based.

Finally, key characteristics of two of the surface terrains associated with the GLF investigated herein (i.e., the troughs in the incised-headwall terrain and the extended cracks in the polygonized terrain) may have been associated with recent erosion by liquid water. Again, further research is necessary to strengthen or disprove this possibility but, if correct, it implies that surface snow or near-surface ice in and around the GLF's upper basin has melted in the geologically-recent past.

Acknowledgments

We thank the HiRISE team, University of Arizona, and NASA/JPL for their efforts in making the HiRISE image we investigate herein available to the public. We also thank two anonymous reviewers for their helpful comments and Jim Bell for editing. Colin Souness is in receipt of a NERC-funded PhD studentship.

References

Andrews, J.T., 1975. Glacial Systems. Duxbury Press, Massachusetts.
Arfstrom, J., Hartmann, W.K., 2005. Martian flow features, moraine-like ridges, and gullies: Terrestrial analogs and interrelationships. Icarus 174, 321–335.
Baker, D.M.H., Head, J.W., Marchant, D.R., 2010. Flow patterns of lobate debris aprons and lineated valley fill north of Ismeniae Fossae, Mars: Evidence for extensive mid-latitude glaciation in the Late Amazonian. Icarus 207, 186–209.
Banks, M.E. et al., 2008. High Resolution Imaging Science Experiment (HiRISE) observations of glacial and periglacial morphologies in the circum-Argyre Planitia highlands, Mars. J. Geophys. Res. Planets 113, E12015.
Banks, M.E., Lang, N.P., Kargel, J.S., McEwen, A.S., Baker, V.R., Grant, J.A., Pelletier, J.D., Strom, R.G., 2009. An analysis of sinuous ridges in the southern Argyre Planitia, Mars using HiRISE and CTX images and MOLA data. J. Geophys. Res. Planets 114, E09003.
Benn, D.I., Evans, D.J.A., 2010. Glaciers and Glaciation. Hodder Education.
Benn, D.I., Kirkbride, M.P., Owen, L.A., Brazier, V., 2005. Glaciated valley landsystems. In: Evans, D.J.A. (Ed.), Glacial Landsystems. Hodder Arnold, London, pp. 372–406.
Christensen, P.R., 2006. Water at the poles and in permafrost regions of Mars. Elements 2, 151–155.
Clark, C.D., 1994. Large-scale ice-moulding: a discussion of genesis and glaciological significance. Sediment. Geol. 91, 253–268.
Clark, C.D., Stokes, C.R., 2001. Extent and basal characteristics of the M'Clintock Channel Ice Stream. Quatern. Int. 86, 81–101.
Clark, C.D., Hughes, A.L.C., Greenwood, S.L., Spagnolo, M., Ng, F.S.L., 2009. Size and shape characteristics of drumlins, derived from a large sample, and associated scaling laws. Quatern. Sci. Rev. 28, 677–692.
Clow, G.D., 1987. Generation of liquid water on Mars through the melting of a dusty snowpack. Icarus 72, 95–127.
Costard, F., Forget, F., Mangold, N., Peulvast, J.P., 2002. Formation of recent martian debris flows by melting of near-surface ground ice at high obliquity. Science 295, 110–113.
Dickson, J.L., Head, J.W., 2009. The formation and evolution of youthful gullies on Mars: Gullies as the late-stage phase of Mars' most recent ice age. Icarus 204, 63–86.
Fitzsimons, S.J., 1997. Entrainment of glaciomarine sediments and formation of thrust-block moraines at the margin of Sørsdale Glacier, East Antarctica. Earth Surf. Processes Landforms 22, 175–187.
Forget, F., Haberle, R.M., Montmessin, F., Levrard, B., Heads, J.W., 2006. Formation of glaciers on Mars by atmospheric precipitation at high obliquity. Science 311, 368–371.
French, H.M., 2007. The Periglacial Environment. Wiley, London.
Glasser, N.F., Hambrey, M.J., 2002. Sedimentary facies and landform genesis at a temperate outlet glacier: Soler Glacier, North Patagonian Icefield. Sedimentology 49, 43–64.
Grove, J.M., 1988. The Little Ice Age. Methuen, London.
Hambrey, M.J., Huddart, D., Bennett, M.R., Glasser, N.F., 1997. Genesis of 'hummocky moraines' by thrusting in glacier ice: Evidence from Svalbard and Britain. J. Geol. Soc. Lond. 154, 623–632.

Hartmann, W.K., 2005. Martian cratering. 8: Isochron refinement and the chronology of Mars. Icarus 174, 294–320.
Hartmann, W.K., Thorsteinsson, T., Sigurdsson, F., 2003. Martian hillside gullies and Icelandic analogs. Icarus 162, 259–277.
Head, J.W., Marchant, D.R., 2003. Cold-based mountain glaciers on Mars: Western Arsia Mons. Geology 31, 641–644.
Head, J.W., Mustard, J.F., Kreslavsky, M.A., Milliken, R.E., Marchant, D.R., 2003. Recent ice ages on Mars. Nature 426, 797–802.
Head, J.W., Marchant, D.R., Dickson, J.L., Kress, A.M., Baker, D.M., 2010. Northern mid-latitude glaciation in the Late Amazonian period of Mars: Criteria for the recognition of debris-covered glacier and valley glacier landsystem deposits. Earth Planet. Sci. Lett. 294, 306–320.
Holt, J.W., Safaeinili, A., Plaut, J.J., Head, J.W., Phillips, R.J., Seu, R., Kempf, S.D., Choudhary, P., Young, D.A., 2008. Radar sounding evidence for buried glaciers in the southern mid-latitudes of Mars. Science 322, 1235–1238.
Hubbard, A., Lawson, W., Anderson, B., Hubbard, B., Blatter, H., 2004. Evidence for subglacial ponding across Taylor Glacier, Dry Valleys, Antarctica. Ann. Glaciol. 39, 79–84.
Kargel, J.S., 2004. Mars: A Warmer, Wetter Planet. Springer, London.
Kargel, J.S., Strom, R.G., 1992. Ancient glaciation on Mars. Geology 20, 3–7.
Kirk, R.L. et al., 2008. Ultrahigh resolution topographic mapping of Mars with MRO HiRISE stereo images: Meter-scale slopes of candidate Phoenix landing sites. J. Geophys. Res. Planets 113, E00A24.
Kruger, J., 1993. Moraine-ridge formation along a stationary ice front in Iceland. Boreas 22, 101–109.
Levy, J.S., Head, J.W., Marchant, D.R., Dickson, J.L., Morgan, G.A., 2009. Geologically recent gully-polygon relationships on Mars: Insights from the Antarctic Dry Valleys on the roles of permafrost, microclimates, and water sources for surface flow. Icarus 201, 113–126.
Lukas, S., 2005. A test of the englacial thrusting hypothesis of 'hummocky' moraine formation: Case studies from the northwest Highlands, Scotland. Boreas 34, 287–307.
Mahaney, W.C., Miyamoto, H., Dohm, J.M., Baker, V.R., Cabrol, N.A., Grin, E.A., Berman, D.C., 2007. Rock glaciers on Mars: Earth-based clues to Mars' recent paleoclimatic history. Planet. Space Sci. 55, 181–192.
Malin, M.C., Edgett, K.S., Posiolova, L.V., McColley, S.M., Noe Dobrea, E.Z., 2006. Present-day impact cratering rate and contemporary gully activity on Mars. Science 314, 1573–1577.
Mangold, N., 2005. High latitude patterned grounds on Mars: Classification, distribution and climatic control. Icarus 174, 336–359.
Marchant, D.R., Head, J.W., 2003. Tongue-shaped lobes on Mars: Morphology, nomenclature and relation to rock glacier deposits. In: Sixth International Conference on Mars, 3091.pdf.
Mellon, M.T., 1997. Small-scale polygonal features on Mars: Seasonal thermal contraction cracks in permafrost. J. Geophys. Res. Planets 102, 25617–25628.
Mellon, M.T., Arvidson, R.E., Marlow, J.J., Phillips, R.J., Asphaug, E., 2008. Periglacial landforms at the Phoenix landing site and the northern plains of Mars. J. Geophys. Res. Planets 113, E00A23.
Menzies, J., 1979. Review of the literature on the formation and location of drumlins. Earth Sci. Rev. 14, 315–359.
Milkovich, S.M., Head, J.W., Marchant, D.R., 2006. Debris-covered piedmont glaciers along the northwest flank of the Olympus Mons scarp: Evidence for low-latitude ice accumulation during the Late Amazonian of Mars. Icarus 181, 388–407.
Milliken, R.E., Mustard, J.F., Goldsby, D.L., 2003. Viscous flow features on the surface of Mars: Observations from high-resolution Mars Orbiter Camera (MOC) images. J. Geophys. Res. Planets 108, E065057.
Morgan, G.A., Head, J.W., Marchant, D.R., 2009. Lineated valley fill (LVF) and lobate debris aprons (LDA) in the Deuteronilus Mensae northern dichotomy boundary region, Mars: Constraints on the extent, age and episodicity of Amazonian glacial events. Icarus 202, 22–38.
Paterson, W.S.B., 1994. The Physics of Glaciers. Pergamon.
Patterson, C.J., Hooke, R.L., 1995. Physical environment of drumlin formation. J. Glaciol. 41, 30–38.
Plaut, J.J., Safaeinili, A., Holt, J.W., Phillips, R.J., Head, J.W., Seu, R., Putzig, N.E., Frigeri, A., 2009. Radar evidence for ice in lobate debris aprons in the mid-northern latitudes of Mars. Geophys. Res. Lett. 36, L02203.
Raymond, C.F., 1987. How do glaciers surge? A review. J. Geophys. Res. 92 (B9), 9121–9134.
Robinson, P.H., 1984. Ice dynamics and thermal regime of Taylor Glacier, South Victoria Land, Antarctica. J. Glaciol. 30, 153–160.
Schon, S.C., Head, J.W., Fassett, C.I., 2009. Unique chronostratigraphic marker in depositional fan stratigraphy on Mars: Evidence for ca. 1.25 Ma gully activity and surficial meltwater origin. Geology 37, 207–210.
Sharp, M., 1985. "Crevasse-fill" ridges – a landform type characteristic of surging glaciers? Geografiska Annaler 67A, 213–220.
Sharp, M., 1988. Surging glaciers: Behaviour and mechanisms. Prog. Phys. Geography 12, 349–370.
Shean, D.E., Head, J.W., Marchant, D.R., 2005. Origin and evolution of a cold-based tropical mountain glacier on Mars: The Pavonis Mons fan-shaped deposit. J. Geophys. Res. Planets 110, E05001.
Siegert, M.J., 2000. Antarctic subglacial lakes. Earth Sci. Rev. 50, 29–50.
Smith, D.E. et al., 2001. Mars Orbiter Laser Altimeter: Experiment summary after the first year of global mapping of Mars. J. Geophys. Res. 106, 23689–23722.
Turtle, E., Pathare, A.V., Hartmann, W.K., Esquerdo, G., 2001. Investigating creep of ground ice as a cause of crater relaxation in martian high-latitude softened terrain. Lunar Planet. Sci. XXXII. Abstract 2044.
van Gasselt, S., Hauber, E., Neukum, G., 2007. Cold-climate modification of martian landscapes: A case study of a spatulate debris landform in the Hellas Montes Region, Mars. J. Geophys. Res. Planets 112, E09006.

#	Parent image ID	GLF Head lon. (d	GLF Head lat.	GLF Terminus lon. (d	GLF Terminus lat.	Mid-channel true right lon. (de	Mid-channel true right lat.	Mid-channel true left lon. (de
1	P16_007348_2224_XI_42N010W	349.6375	40.0437	349.696	40.0408	349.6633	40.0332	349.6692
2	P13_006201_2100_XN_30N011W	348.6602	30.585	348.5991	30.4649	348.6406	30.5259	348.6438
3	P16_007192_2287_XN_48N071W	288.5635	48.2781	288.6099	48.2708	288.584	48.2664	288.5847
4	P13_006245_2196_XN_39N133W	226.2651	37.9802	226.479	38.0281	226.4307	37.9588	226.4287
5	P21_009251_2184_XN_38N134W	226.1943	38.3902	226.2048	38.4639	226.2117	38.4236	226.187
6	P13_006245_2196_XN_39N133W	226.1182	38.4053	226.1599	38.4695	226.1575	38.4275	226.1411
7	P13_006245_2196_XN_39N133W	225.9507	38.4292	225.9392	38.4656	225.9514	38.4509	225.9312
8	P05_002847_2194_XN_39N244W	116.0425	39.0835	116.1028	39.0813	116.0681	39.0723	116.0679
9	P05_002847_2194_XN_39N244W	116.0361	39.0481	116.0652	39.0547	116.0554	39.0445	116.0525
10	P15_006818_2273_XN_47N301W	58.7725	47.0706	58.8677	47.0398	58.8174	47.0369	58.8267
11	P01_001570_2213_XI_41N305W	54.667	41.3069	54.7622	41.2283	54.7148	41.2586	54.729
12	P22_009653_2224_XN_42N309W	50.5	42.3093	50.5625	42.1643	50.5273	42.2268	50.5439
13	P20_008730_2278_XN_47N309W	50.2568	46.0383	50.3398	46.0132	50.2979	46.0103	50.3044
14	P20_008730_2278_XN_47N309W	50.2542	46.0674	50.3508	46.0659	50.3025	46.0579	50.303
15	P20_008730_2278_XN_47N309W	50.2529	45.9675	50.2043	45.9458	50.2297	45.9578	50.2319
16	P17_007570_2244_XN_44N313W	47.1875	42.3259	47.2075	42.3826	47.2173	42.3611	47.1885
17	P01_001478_2221_XN_42N315W	44.0518	40.7361	44.0659	40.9368	44.0474	40.8308	44.0181
18	B07_012317_2255_XI_45N321W	38.1753	45.2029	38.1938	45.0789	38.1665	45.136	38.2017
19	P17_007689_2259_XI_45N322W	37.7966	45.1319	37.832	45.0716	37.8105	45.0903	37.8384
20	P17_007689_2259_XI_45N322W	37.5474	45.0762	37.4854	45.0298	37.5098	45.0662	37.5242
21	P13_006252_2208_XN_40N325W	34.3469	41.3433	34.4812	41.3323	34.4175	41.3091	34.4136
22	P13_006252_2208_XN_40N325W	34.2739	41.6297	34.4272	41.5696	34.3447	41.5867	34.3545
23	P13_006252_2208_XN_40N325W	34.271	41.7854	34.4448	41.784	34.3784	41.7722	34.375
24	P13_006252_2208_XN_40N325W	34.2583	41.4763	34.4141	41.4954	34.3437	41.4754	34.3413
25	P16_007175_2192_XN_39N325W	33.9453	40.0091	34.002	39.9905	33.9741	39.9866	33.9795
26	P14_006661_2198_XI_39N331W	28.511	41.0464	28.5728	41.0296	28.5388	41.0257	28.5435
27	P01_001373_2242_XN_44N331W	28.1387	44.0767	28.2234	44.0471	28.1829	44.051	28.1843
28	P01_001373_2242_XN_44N331W	28.1006	44.1834	28.2031	44.1834	28.1611	44.1594	28.1543
29	P01_001373_2242_XN_44N331W	28.085	44.2307	28.1714	44.239	28.1353	44.2244	28.1338
30	P16_007162_2263_XN_46N332W	27.5928	46.6338	27.4763	46.5315	27.5203	46.5908	27.5317
31	P16_007162_2263_XN_46N332W	27.429	46.7361	27.3752	46.6978	27.4067	46.7112	27.4148
32	P16_007373_2248_XN_44N333W	26.4055	45.5403	26.4314	45.491	26.4089	45.5105	26.4238
33	P17_007729_2250_XN_45N334W	25.3694	44.8738	25.4099	44.8369	25.3845	44.8462	25.4009
34	P03_002112_2208_XN_40N337W	22.3267	39.9382	22.4082	39.9724	22.374	39.9505	22.3633
35	P03_002112_2208_XN_40N337W	22.2231	40.0525	22.3013	40.0818	22.2812	40.0545	22.2661
36	P17_007782_2219_XN_41N341W	18.5737	41.607	18.5198	41.5747	18.5427	41.5979	18.5496
37	P17_007782_2219_XN_41N341W	18.3875	41.3679	18.4333	41.405	18.4133	41.3831	18.4055

Mid-channel true left lat.	Centre lon. (d	Centre lat.	GLF length (km)	GLF width (km)	GLF area (km sq.)	GLF orientation (deg.)	Buffer min. elevation (m)	Buffer max. elevation (m)
40.0484	349.66675	40.0408	2.66008	0.93986	2.50011	93.68606	-4135	-3141
30.5205	348.62965	30.5232	7.77204	0.35936	2.79293	203.68024	-3861	-3534
48.281	288.5867	48.2737	1.88087	0.8658	1.62846	103.28229	-2431	-1399
37.9881	226.37205	37.97345	10.38555	1.73916	18.06217	74.06926	-196	528
38.4265	226.19955	38.42505	4.39542	1.15974	5.09755	6.3652	-1416	315
38.429	226.13905	38.42825	4.2694	0.76666	3.2732	26.95272	-1454	65
38.4492	225.94495	38.45005	2.22254	0.94305	2.09597	346.10584	-1476	347
39.0943	116.07265	39.0833	2.77739	1.304	3.62173	92.67198	-5918	-4405
39.0513	116.05065	39.0479	1.3954	0.42458	0.59245	73.71014	-5863	-4461
47.0632	58.8201	47.05005	4.25573	1.60345	6.82383	115.36704	-3205	-2811
41.2732	54.7146	41.2659	6.30013	1.07195	6.75343	137.6545	-1304	-62
42.2366	50.53125	42.2317	9.02137	0.93174	8.40554	162.27974	-1502	-524
46.0296	50.2983	46.01995	3.72572	1.17481	4.37699	113.50511	-2111	-877
46.0752	50.3025	46.06655	3.97355	1.0256	4.07527	91.2473	-2179	-1819
45.9478	50.2286	45.9528	2.38005	0.59961	1.4271	237.30638	-2228	-942
42.3723	47.1975	42.3667	3.47299	1.42526	4.94991	14.60332	-1180	-157
40.8132	44.05885	40.822	11.91256	1.6779	19.98805	3.03796	-2723	-2170
45.1404	38.18455	45.1382	7.39024	1.49464	11.04574	173.98597	-1833	334
45.1043	37.8143	45.0973	3.86877	1.43221	5.5409	157.47934	-1250	-150
45.0525	37.5164	45.05935	3.78196	1.01136	3.82494	223.37089	-2765	-923
41.3208	34.41405	41.31495	6.01216	0.71488	4.29797	96.18129	-2442	-1086
41.6106	34.35055	41.59865	7.6719	1.48169	11.36736	117.61526	-2312	-940
41.7923	34.3579	41.78225	7.6817	1.2008	9.22415	90.56103	-2404	-917
41.491	34.3362	41.4832	7.00975	0.93075	6.52435	80.65436	-2285	-934
40.0056	33.97365	39.9961	2.80056	1.15254	3.22776	113.16372	-2092	-1146
41.043	28.5419	41.03435	2.93685	1.04671	3.07401	109.79916	-2406	-1535
44.0654	28.18105	44.0582	4.01151	0.85559	3.43221	115.90542	-3436	-2197
44.1726	28.15185	44.166	4.35669	0.83409	3.63387	89.96428	-3165	-2129
44.2376	28.1282	44.231	3.70199	0.78497	2.90596	82.33333	-3068	-2086
46.5713	27.53455	46.58105	7.69997	1.24561	9.59115	218.093	-2968	-2406
46.6992	27.4021	46.7052	3.15167	0.78376	2.47015	223.94174	-3417	-2460
45.5152	26.41845	45.51285	3.11378	0.67867	2.11324	159.7809	-3348	-2328
44.8574	25.38965	44.8518	2.77114	0.95685	2.65157	142.10103	-3108	-2354
39.969	22.36745	39.95975	4.22143	1.19944	5.06336	61.27611	-3055	-1935
40.0696	22.2622	40.06205	3.94945	1.12704	4.4512	63.88883	-2866	-1762
41.5886	18.54675	41.59325	3.06173	0.6304	1.9301	231.31445	-3376	-1814
41.3936	18.4104	41.38835	2.99727	0.71248	2.13549	42.79091	-3530	-2128

Buffer MEAN elevation (m)	Buffer STD. DEV. of	Elongation
-3818.06	280.976	2.83028
-3751.73	50.4834	21.62772
-1823.57	360.638	2.1724
356.272	97.4383	5.97157
-548.529	530.137	3.79001
-681	456.321	5.5688
-407.266	519.736	2.35676
-5108.06	477.667	2.1299
-5018.95	379.507	3.28657
-3086.21	90.8297	2.65412
-477.133	360.283	5.87726
-728.684	237.557	9.68232
-1690.46	333.255	3.17135
-2065.56	91.7348	3.87436
-1786.54	305.8	3.96936
-471.219	298.797	2.43674
-2484.92	160.727	7.09969
-458.996	563.827	4.94449
-483.07	193.732	2.70125
-1742.5	623.744	3.73947
-1631.16	435.46	8.41004
-1332.87	375.069	5.17781
-1232.9	378.279	6.39718
-1225.6	315.033	7.53125
-1464.86	321.686	2.4299
-1809.52	295.278	2.8058
-2830.31	353.32	4.6886
-2614.28	313.625	5.22327
-2534.34	343.717	4.71609
-2491.35	98.1769	6.18168
-2715.89	298.92	4.02123
-2867.24	369.564	4.58806
-2670.32	256.425	2.89609
-2339.68	379.634	3.51949
-2200.29	378.176	3.50426
-2378.66	515.055	4.85683
-2786.83	456.156	4.20682

#	Parent image ID	GLF Head lon. (d	GLF Head lat.	GLF Terminus lon. (d	GLF Terminus lat.	Mid-channel true right lon. (de	Mid-channel true right lat.	Mid-channel true left lon. (de
1	P16_007389_1406_XN_39S039W	320.6313	-39.7483	320.7053	-39.7883	320.6636	-39.7747	320.6814
2	P16_007429_1331_XN_46S050W	309.4697	-46.4629	309.5405	-46.4429	309.5146	-46.4739	309.5049
3	P04_002603_1328_XN_47S050W	309.312	-47.8235	309.4014	-47.7844	309.3643	-47.8245	309.3418
4	P14_006638_1307_XI_49S051W	307.8496	-46.6306	308.04	-46.6668	307.9453	-46.7175	307.9736
5	P15_006994_1362_XN_43S053W	306.8652	-44.6775	306.8174	-44.7009	306.8325	-44.6726	306.8477
6	P15_006836_1281_XN_51S057W	302.4199	-52.3396	302.8965	-52.6599	302.6045	-52.5437	302.6738
7	P19_008339_1288_XN_51S058W	301.3928	-50.6421	301.3867	-50.5327	301.4058	-50.5925	301.3635
8	P15_006902_1280_XN_52S059W	301.1211	-52.4529	301.3398	-52.5388	301.2246	-52.5222	301.2471
9	P15_006955_1297_XI_50S066W	293.2559	-48.8513	293.0947	-49.2752	293.208	-49.075	293.2266
10	P17_007590_1385_XN_41S127W	232.2786	-38.6411	232.2881	-38.6738	232.2778	-38.6621	232.2913
11	P02_001896_1416_XN_38S190W	169.6392	-37.9148	169.5806	-37.99	169.5815	-37.9329	169.6436
12	P02_001923_1334_XN_46S206W	153.7185	-46.3513	153.7771	-46.3433	153.7534	-46.356	153.75
13	P15_007066_1447_XN_35S220W	139.4126	-33.5025	139.4231	-33.5193	139.4119	-33.5169	139.4248
14	P16_007133_1345_XI_45S248W	111.5884	-45.3142	111.6104	-45.2229	111.6172	-45.2708	111.5898
15	P05_002927_1389_XN_41S257W	102.7117	-40.8472	102.6064	-40.8435	102.6621	-40.8325	102.6606
16	P17_007661_1470_XI_33S267W	92.7922	-33.2781	92.8386	-33.2771	92.8184	-33.2866	92.8186
17	P03_002334_1442_XN_35S268W	91.1779	-35.3048	91.198	-35.3383	91.1821	-35.3255	91.1949
18	B01_010075_1498_XI_30S301W	58.1479	-29.3152	58.1294	-29.3816	58.1328	-29.3445	58.1475
19	P13_006239_1315_XN_48S318W	41.9487	-49.8294	42.0215	-49.8347	41.9878	-49.8469	41.9907
20	P17_007518_1432_XN_36S322W	37.3535	-34.5393	37.3484	-34.5676	37.3469	-34.5515	37.3533
21	P17_007518_1432_XN_36S322W	37.175	-34.5176	37.1628	-34.5501	37.1604	-34.532	37.1736
22	P17_007518_1432_XN_36S322W	37.1562	-34.4383	37.1633	-34.5205	37.1704	-34.4766	37.1821
23	P17_007518_1432_XN_36S322W	37.1018	-34.4788	37.1238	-34.5486	37.1047	-34.5186	37.1138
24	B06_011936_1363_XI_43S347W	12.0806	-43.0857	12.1533	-43.1155	12.1074	-43.1248	12.1211
25	B06_011936_1363_XI_43S347W	11.8965	-43.5071	11.9287	-43.5134	11.9097	-43.5198	11.9121
26	P15_006807_1391_XN_40S348W	11.7432	-40.1035	11.7837	-40.1113	11.7627	-40.1177	11.7681
27	P03_002113_1416_XN_38S354W	5.3921	-37.886	5.4487	-37.9424	5.4104	-37.938	5.4326

Mid-channel true left lat.	Centre lon. (d	Centre lat.	GLF length (km)	GLF width (km)	GLF area (km sq.)	GLF orientation (deg.)	Buffer min. elevation (m)	Buffer max. elevation (m)
-39.749	320.6683	-39.76185	4.12149	1.72572	7.11253	125.14028	119	1207
-46.4444	309.5051	-46.45915	3.12471	1.7928	5.60198	67.73088	373	3674
-47.7849	309.3567	-47.8047	4.24711	2.51226	10.66982	56.96281	681	3285
-46.5857	307.9448	-46.6516	8.03863	7.89637	63.47598	105.54992	687	2755
-44.7049	306.8413	-44.68875	2.44553	2.01877	4.93695	235.43234	-443	1190
-52.4285	302.6582	-52.4861	25.61526	7.27178	186.26864	138.01763	222	1728
-50.5982	301.38975	-50.59535	6.48835	1.627	10.55657	357.97015	2533	4197
-52.4597	301.23045	-52.49095	9.39173	3.79241	35.61732	122.91453	2130	3098
-49.0838	293.1753	-49.0794	25.89332	0.89079	23.06552	193.93052	981	1361
-38.6582	232.28335	-38.66015	1.98743	0.66621	1.32404	167.2209	1864	3199
-37.968	169.6099	-37.95045	5.2314	3.57103	18.68152	211.55104	104	1363
-46.3401	153.7478	-46.34805	2.44401	0.95263	2.32823	78.83409	179	1657
-33.5117	139.41785	-33.5143	1.12285	0.70808	0.79507	152.47829	-56	2029
-45.2722	111.5994	-45.2715	5.48874	1.14592	6.28966	9.63284	1198	2936
-40.8635	102.65905	-40.848	4.72648	1.83864	8.6903	272.62499	-281	2002
-33.2639	92.8154	-33.27525	2.29998	1.3455	3.09462	88.53603	-4464	-2279
-35.3184	91.18795	-35.32195	2.21076	0.74851	1.65479	153.92165	-4313	-3117
-29.3499	58.13865	-29.3472	4.05002	0.82416	3.33787	193.64582	-2440	-472
-49.8176	41.9851	-49.83225	2.80095	1.74019	4.87418	96.46733	-646	407
-34.5535	37.35095	-34.5525	1.69576	0.33416	0.56665	188.44088	-375	1434
-34.5362	37.1689	-34.5341	2.01632	0.69092	1.39312	197.18017	-414	1147
-34.4754	37.15975	-34.476	4.88444	0.57608	2.81384	175.92935	870	1519
-34.5149	37.1128	-34.51675	4.27439	0.49558	2.11832	165.44755	59	1707
-43.0955	12.11695	-43.11015	3.60815	1.83504	6.6211	119.33437	1266	2612
-43.5012	11.9126	-43.5105	1.43365	1.10726	1.58743	105.10846	1035	2542
-40.0984	11.76345	-40.10805	1.8933	1.16984	2.21485	104.14676	-98	457
-37.9104	5.4204	-37.9242	4.26379	1.93739	8.26063	141.64769	230	1417

Buffer MEAN elevation (m)	Buffer STD. DEV. of	Elongation
652.169	296.846	2.38827
1945.65	881.878	1.74292
2232.13	717.191	1.69056
1956.23	594.712	1.01802
224.703	359.594	1.2114
1205.21	345.391	3.52255
3475.33	443.289	3.98791
2700.82	222.054	2.47645
1112.47	74.1077	29.06781
2673.28	365.943	2.98319
781.34	359.728	1.46496
1094.74	417.614	2.56555
1080.08	635.527	1.58576
2044.18	417.385	4.78981
512.241	583.623	2.57063
-3289.31	700.192	1.70939
-3612.95	418.598	2.95353
-1533.03	525.561	4.91411
44.672	334.235	1.60957
668.472	555.987	5.07471
411.307	451.664	2.9183
1178.1	134.29	8.47871
1032.95	434.726	8.62497
1988.97	352.771	1.96625
1886.41	466.043	1.29477
109.873	105.092	1.61843
1086.13	298.088	2.20079